Resistance Spot Welding

of

Advanced High Strength Steels

PROEFSCHRIFT

ter verkrijging van de graad van doctor
aan de Technische Universiteit Delft,
op gezag van de Rector Magnificus prof. ir. K.C.A.M. Luyben;
voorzitter van het College voor Promoties,
in het openbaar te verdedigen op
woensdag 21 oktober 2015 om 12.30 uur.

door

Nick Johannes DEN UIJL

Werktuigbouwkundig ingenieur,
Universiteit Twente, Nederland
geboren te Dordrecht, Nederland.

This dissertation has been approved by the promotor:
Prof. dr. I.M. Richardson

Composition of the doctoral committee:

Rector Magnificus	chairman
Prof. dr. I.M. Richardson	Delft University of Technology, promotor

Independent members:

Prof. dr. ir. J. Sietsma	Delft University of Technology
Prof. dr. R. Boom	Delft University of Technology
Prof. Dr.-Ing. M. Kraska	Fachhochschule Brandenburg – University of Applied Sciences
Prof. dr. ir. R. H. Petrov	Ghent University
Prof. dr. ir. J. Pauwelussen	HAN University of Applied Sciences
Prof. Dr.-Ing. M. Rethmeier	BAM Federal Institute for Materials Research and Testing

Resistance Spot welding of Advanced High Strength Steels
N.J. den Uijl
PhD thesis of Delft University of Technology – with summary in Dutch
ISBN 978-90-824372-0-1

Key words: Welding, Resistance spot welding, Resistance spot welding, Modelling, Post weld hardness, Advanced high strength steels.

Published by Standard Owl Publishing
Printed in The Netherlands.

Contents

Nomenclatura

List of Symbols

$wt\%$	weight percentage	[%]
R_p	yield strength	[MPa]
$A_{80\%}$	formability	[%]
Q	heat	[J]
I	current	[A]
R	electrical resistance	[Ω]
t	time	[s]
t_s	sheet thickness	[mm]
σ_0	static yield stress,	[N/mm^2]
$\Delta\sigma_m$	strain hardening stress increase coefficient	[N/mm^2]
β	large strain hardening coefficient	
Ω	low strain hardening exponent	
ε_0	strain from previous deformation	
n	strain hardening exponent	
σ^*_0	dynamic flow stress coefficient	[N/mm^2]
ΔG_0	activation enthalpy	[J]
m	strain rate behaviour exponent	
k	Boltzmann constant	[J/K]
T	absolute temperature	[K]
ε^*	thermally activated strain rate	
C	strain hardening coefficient	[N/mm^2]
B	pre-strain parameter	
V	voltage	[V]
A	cross section area	[m^2]
ρ	electrical resistivity	[Ωm]
L	distance between two points across which a voltage is applied	[m]
σ	electrical conductivity	[Ω^{-1}m^{-1}]
k	thermal conductivity	[W/mK]
k_l	thermal conductivity by lattice vibrations	[W/mK]
k_e	thermal conductivity by electrons	[W/mK]
q	heat flux	[W/m^2]
D_n	normalised electrode tip electrode	[%]
D_{weld}	weld nugget diameter	[mm]
$D_{electrode}$	electrode tip diameter	[mm]
V_n	normalised weld nugget volume	[%]
V_{weld}	weld nugget volume	[mm^3]
t_s	sheet thickness	[mm]
R^2	coefficient of determination	
t_c	cooling rate at 700 °C	[°C/hr]
$t_{8/5}$	cooling time between 800 and 500 °C	[s]
$H_i(X_j)$	hardness of material constituent (phase)	[HV]
V_i	fraction of constituent (phase) of material	
M_s	martensite start temperature	[°C]
M_{90}	temperature at which 90% of austenite has transformed to martensite	[°C]
A_1	austenite transformation temperature	[°C]

$\rho_{contact}$	contact surface resistance	[μΩm]
σ_{s_soft}	flow stress of the softer material of the two materials in contact	[MPa]
$\rho_{contaminants}$	surface contaminants resistivity	[μΩm]
WZ	weld size (volume)	[m^3]
$\dot{Q}$	heat flow	[J/s]
$\dot{Q}_{net}$	net heat flow	[J/s]
$\dot{Q}_{generated}$	generated heat flow	[J/s]
$\dot{Q}_{lost}$	heat flow lost to surroundings	[J/s]
R_{CSR}	contact surface resistance	[μΩ]
R_{bulk}	bulk resistance	[μΩ]
Λ	latent heat factor	[J/s]

List of Abbreviations

AC	Alternating Current
AHSS	Advanced High Strength Steel
AISI	American Iron and Steel Institute
BIW	Body in White
CCT	Continuous Cooling Transformation
CE	Carbon Equivalence number
CP	Complex Phase
DC	Direct Current
DP	Dual Phase
e.g.	*exempli gratia* (for example)
et al.	*et alii* (and others)
FB	Ferritic Bainitic
GA	GalvAnnealed
GI	GalvanIzed
HAZ	Heat Affected Zone
HDG	Hot Dip Galvanized
HF	Hot Forming
HSLA	High Strength Low Alloy
HV	Vickers Hardness
IIW	International Institute of Welding
LBW	Laser Beam Welding
MS	Martensitic Steel
PAW	Plasma Arc Welding
PWHT	Post Weld Heat Treatment
Q & P	Quenched & Partitioned
RSW	Resistance Spot Welding
SCR	Surface Contaminant Resitivity
TRIP	TRansformation Induced Plasticity
TWIP	TWinning Induced Plasticity
VDEh	*Verein Deutscher Eisenhüttenleute*
WGC	Weld Growth Curve

1. Introduction

In automotive manufacturing two trends at the end of the last millennium have had an important impact. The first was the introduction of advanced high strength steel, the second the availability of dedicated weld modelling software. The introduction of advanced high strength steels enabled automotive manufactures to reduce the mass of the body in white of vehicles and improve safety. The introduction of dedicated weld modelling software enabled improvements in design and reduction in effort (costs and time) for engineering in manufacturing.
Increased strength of advanced high strength steels compared to more conventional high strength steels (e.g. HSLA steels) allows the use of thinner gauges of steel sheets for the body in white, thus leading to a reduction in mass of the construction. Reduced mass is beneficial for several reasons. Reduced mass improves dynamic performance, reduces fuel consumption, decreases exhaust pollution [Wang *et al.*, 2014], and reduces costs.
It reduces costs as steels are priced in tons and though the price of more advanced materials is often higher per ton, the reduction in mass often results in a overall lower price for the construction.
Reduced fuel consumption of itself is a positive effect as fuel prices tend to increase over time, and is therefore beneficial for the consumer. Reduced fuel consumption also has an impact on the emission of green house gasses and nitrogen-oxides, which is desirable form a societal point of view. The European Union has set stringent CO_2-reduction targets (as have others). It has been reported that up to 80% of the CO_2 emissions can be attributed to the in service phase of a vehicle [Campestrini, 2014]. Weight reduction is seen as a key component in CO_2 reduction strategies. It has been estimated that 15-20% of the overall vehicle weight reduction can be gained in the body in white [Lee, 2014].

The reduction in mass of the body in white can also be used by the automotive manufacturer to increase weight in other areas of the vehicles design, for example in electronic systems or driving comfort, thus improving the design of the vehicle without increasing overall mass.
The introduction of dedicated weld modelling software allows for improvements in the design of automotive constructions as it enables the designer to predict the effects of welding processes, such as the introduction of residual stresses after welding, through simulation. Furthermore weld modelling software is useful in engineering of production processes as simulation allows for the prediction of the weldability and determination of optimal process settings. This is conventionally done using experimental methods, which are costly in time and money. Experimental methods also require a lot of material, which increases costs, but also can be a issue in the early stages of engineering of joining processes involving new materials as availability of these materials may be limited in the early stages of development.

Three issues occurred with the introduction of advanced high strength steels. The first concerns the weldability of these materials. Weldability concerns two aspects; manufacturability and performance of the welded joints. The manufacturability concerns the ability to produce joints in mass production. Issues were reported with the resistance spot welding electrode lifetime when welding advanced high strength steels, that were primarily attributed to the increased hardness of these materials compared to more conventional high strength steels. Increased hardness leads to deformation and wear of the electrodes, limiting the number of welds that can be made. This is undesirable because the electrodes will need to be redressed or replaced more often, increasing costs (both because more electrodes are needed and because production times are increased).
The performance of welded joints concerns the behaviour of the welds under mechanical loading. Requirements of the response of welded joints subjected to mechanical loads is governed by standards, both standards set by regulatory bodies (e.g. ISO standards) and standards set by manufacturers. A key requirement of resistance spot welded joints (the

main joining process in automotive manufacturing) is an appropriate weld failure mode. For safety critical applications the desired weld failure mode is full plug failure, that is the weld itself should remain intact under mechanical loading. If the weld remains intact, failure will occur in the surrounding material. Thus the weld, with its complicated metallurgical structure, is not the weakest link, but failure occurs in the unaffected material, that is often much better defined. This is a big advantage in design as the mechanical behaviour of the unaffected material is usually well understood, and can therefore be accurately modelled and the response of the construction can be simulated.
The second issue concerns material data. The results of simulations are very much dependent on the availability of material data. In the case of welding processes material data with respect to temperature variability are especially important. Measuring material data is expensive, especially against temperature. In the case of new materials or materials under development, the availability of sufficient material to measure data is an additional bottleneck. After material data sets have been compiled for resistance spot welding they need to be verified in simulations against experimental data, adding costs and requiring more material (which in the case of new materials or materials under development may be scarce).
The third issue concerns the way modelling software is to be used for engineering purposes. The complexity of welding processes involving process parameters, material data (thermal, mechanical and metallurgical), and environmental influences, makes modelling complicated. Even in the case of dedicated weld modelling software, the fact that models are by definition simplified descriptions of physical phenomena limits the ability of a single software platform to model all aspects of welding operations with a high degree of accuracy. Often weld models have been designed with a specific goal in mind, for instance simulation of the formation of a single weld or series of welds, the residual stresses caused by welding operations, the metallurgical response of a material to welding operations, or a combination of several of these effects. It is impractical, and expensive, to develop a separate weld model for each application, and therefore, it is important for engineering purposes to develop strategies to use available models for a variety of applications. The effectiveness of such strategies, and their value for engineering and scientific research needs to be evaluated and verified against experiments.

Literature not only reported on issues concerning weldability of advanced high strength steels, but also on the perceived causes of weldability problems. In broad terms the issues were attributed to the hardness of the materials, both before and after welding. Before welding the hardness of the materials is suspected to cause welding electrodes to wear and thus decrease electrode lifetime. After welding the hardness of the welds is suspected to cause undesirable weld failure modes. Post weld hardness is an important parameter in resistance spot welding. The idea is that hard microstructures cannot deform sufficiently when subjected to mechanical loads, causing brittle failure in the welds. Therefore in many industrial standards a limit is placed on allowable post weld hardness levels.
Standards in welding form an additional factor in the determination of weldability for materials. For instance a material that will have a high hardness may show consistent full plug failure in tensile tests, but the hardness itself may disqualify the material for use in safety critical applications.

The costs involved with measuring accurate material data suited for simulations of welding and the scarcity of materials to measure data sets in the early stages of material development jusitifies the development of strategies to compile material data sets using available material data for use in simulations of welding of new materials. Such strategies should be based on a sound understanding of the underlying metallurgical principles and be verified against experimental data. Though there are good reasons to develop such strategies little has been published on this subject. There is even little literature available on measured comprehensive material data sets for weld modelling purposes. Most publications use the material data sets available in the material database supplied with the weld modelling software, without a discussion of the variations that can be expected due to the

fact that the material used in the experiments most likely has not been the exact same material that was used to compile the material data set in the supplied database.

Dedicated weld modelling software is used both for research purposes and for engineering of manufacturing processes. Simulations are used in research as support for experimental research and extrapolation of the applicability of these results. The results of simulations have been used to develop guidelines for the application of modern materials, such as advanced high strength steels, in industry. Simulations have also been used to support the development of electrodes. All of these applications are straightforward uses of the capabilities of these tools. Little is reported on the application of these tools outside their direct focus, *e.g.* for investigations into the parameters affecting the electrode lifetime. This is undesirable as opportunities for applications are possibly wasted. Developing strategies for the use of simulation software, outside their primary focus, generates possibilities to save time and costs in research and engineering.

A more comprehensive understanding of the capabilities of simulations, both on material characteristics and process parameters allows for the use of these tools to further support scientific research into the issues concerning weldability. Combining experimental research with the result of simulations, making full use of the capabilities of these tools, adds weight to the effort to tackle the issues concerning weldability of advanced high strength steels.

There are therefore two goals identified for the research reported on in this thesis:

- Identification of the reported issues concerning weldability and an assessment of the problem these issues cause for application of advanced high strength steels.
- Strategies for an effective use of dedicated weld modelling software for research into the weldability of advanced high strength steels.

Issues concerning the application of advanced high strength steels have to do with both the actual performance of welded joints and the standards involved. Strategies for an effective use of simulations include the use of simulations for research to the factors affecting electrode lifetime and prediction of post weld hardness. Finally the research effort is combined to tackle issues concerning the weldability of advanced high strength steels.
For instance because of the focus on post weld hardness in standards it is desirable to be able to predict the post weld hardness of materials. This is especially helpful in the early stages of development of materials (when there is limited material available) and one of the areas where simulation can be beneficial in weldability research. This is one of the research topics where a combination of experiment and simulation adds strength to achieve results.

Weldability is primarily important for the application of materials in industry. Without application there are no clear issue to be identified concerning weldability. Therefore the research reported in this thesis is primarily focussed on materials and process settings used in industry, as well as commercially available weld modelling software.
As such the research reported is primarily of an applied nature. The results serve as a verification of scientific research in an engineering context. The results can not only be used for the the direct goals for which the research was set up and conducted, but can also serve as a verification of the underlying scientific work reported in the literature (on which for instance the weld models used have been based) it also serves as guidance for further steps in more fundamental research.

2. Literature Review

2.1 Advanced High Strength Steels

Steels are commonly classified according to their use and carbon content [Den Ouden & Korevaar, 1992, McGannon, 1971, Young, 1954]. Carbon steels (0 – 0,30 wt% C) are the most important for the structural integrity of an automotive vehicle as they make up the Body in White (BIW). The properties of plain carbon steels depend chiefly on their carbon content and microstructure. In addition to carbon these steels always contain some manganese, silicon, phosphorus and sulphur. Minor amounts of other elements may also be present [McGannon, 1971]. According to the American Iron and Steel Institute (AISI) definition, plain carbon steels may contain up to 1,65 % manganese, 0,60 % silicon and 0,60 % copper in addition to much smaller amounts of other elements [McGannon, 1971]. The main influence of these alloying elements is to increase the strength and toughness as well as the hardenability of the material. The stiffness is practically unaffected [Den Ouden & Korevaar, 1992].
Plain carbon steels, by virtue of their microstructural homogeneity and low carbon content, generally show good formability and weldability, both of great importance in automotive production. However for performance in automotive applications, increased strength is often desired. Strength can be increased by cold working, but this is limited by the chemical composition of the steels. One solution is to increase the amount of alloying elements. Alloy steels may be defined as those which owe their enhanced properties to the presence of one or more special elements or to the larger proportions of elements such as manganese and silicon that are ordinarily present in carbon steel [McGannon, 1971].
Increasing alloying levels increases costs and affects weldability. High Strength Low Alloyed (HSLA) steels were developed to improve strength and toughness of steels, whilst retaining good weldability [Honeycombe & Bhadeshia, 1995]. The earliest of the present-day HSLA steels was the “COR-TEN” brand which was introduced by United States Steel in 1933 [McGannon, 1971]. With the addition of small concentrations (<0,1 wt%) of grain refining elements such as niobium, titanium and vanadium, and also aluminium to steels with 0,03 – 0,08 % C and up to 1,5 wt% Mn, it became possible to produce fine-grained material with yield strengths between 450 and 550 MPa [Honeycombe & Bhadeshia, 1995].
In the automotive industry, legislation on safety and fuel economy has hastened a trend towards the use of higher strength steels for many parts [Honeycombe & Bhadeshia, 1995]. Low alloyed steels, typically containing manganese and silicon, can exhibit both high strength and good formability, if they are first heat treated to produce a matrix of ferrite with islands of martensite [Honeycombe & Bhadeshia, 1995] (see figure 2.1). These steels are referred to as Dual Phase (DP) steels.

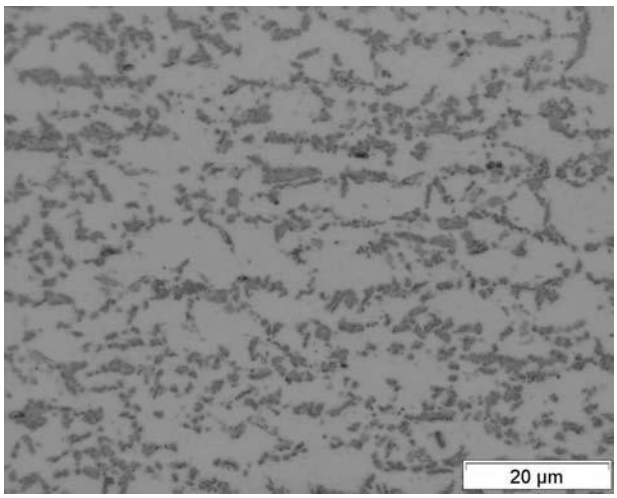

Figure 2.1: Microstructure of a Dual Phase steel [Den Uijl & Anwar, 2005].

The simplest way to achieve a duplex structure is to use intercritical annealing during which the steel is heated to the (α + γ) region between Ac_1, the temperature at which austenite begins to form during heating (with c from the French *chauffant*), and Ac_3, at which the formation of ferrite to austenite is completed during heating (see figure 2.2), and held there to allow small regions of austenite to form in the ferrite. To transform these regions to martensite, subsequent cooling must be very rapid, or the austenite must have a high hardenability (which can be achieved by adding 0,2 – 0,4 wt% Mo to steels containing 1,5 wt% Mn) [Honeycombe & Bhadeshia, 1995, Pickens, 1984].

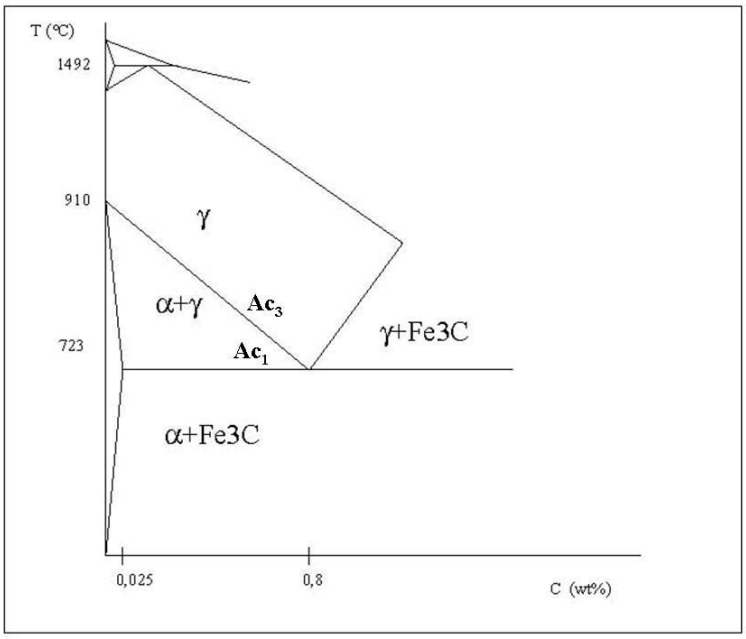

Figure 2.2: Part of the iron carbon (Fe-C) phase diagram [Marchal & Zwetsloot, 2002]

The development of DP steels gave rise to the development of other low alloyed steels with complex microstructures consisting of two or more microstructural phases combining increased levels of strength with reasonable levels of formability. Steels based upon this principle are commonly referred to as Advanced High Strength Steels (AHSS). Figure 2.3 shows the relationship between yield strength (R_p) and formability ($A_{80\%}$) for various automotive steels.
The chemical composition of these steels are chosen with respect to [Pickens, 1984]:

- hardenability,
- tempering properties (*e.g.* resistance to tempering or increased tempering strength due to secondary hardening,
- weldability.

The first two aspects influence the production of the steels. Weldability is important for the application of these steels as they will eventually need to be welded. A key factor to ensure good welding properties is to keep the amount of alloying elements (specifically carbon) as low as possible.
Strength and formability are dependent upon the chemical composition, in combination with the thermo-mechanical treatment of the steels during production. The thermo-mechanical treatment ensures the existence of the complex microstructural composition (as described above for DP steels), which accounts for strength and formability. Strength levels can further be increased by cold working.

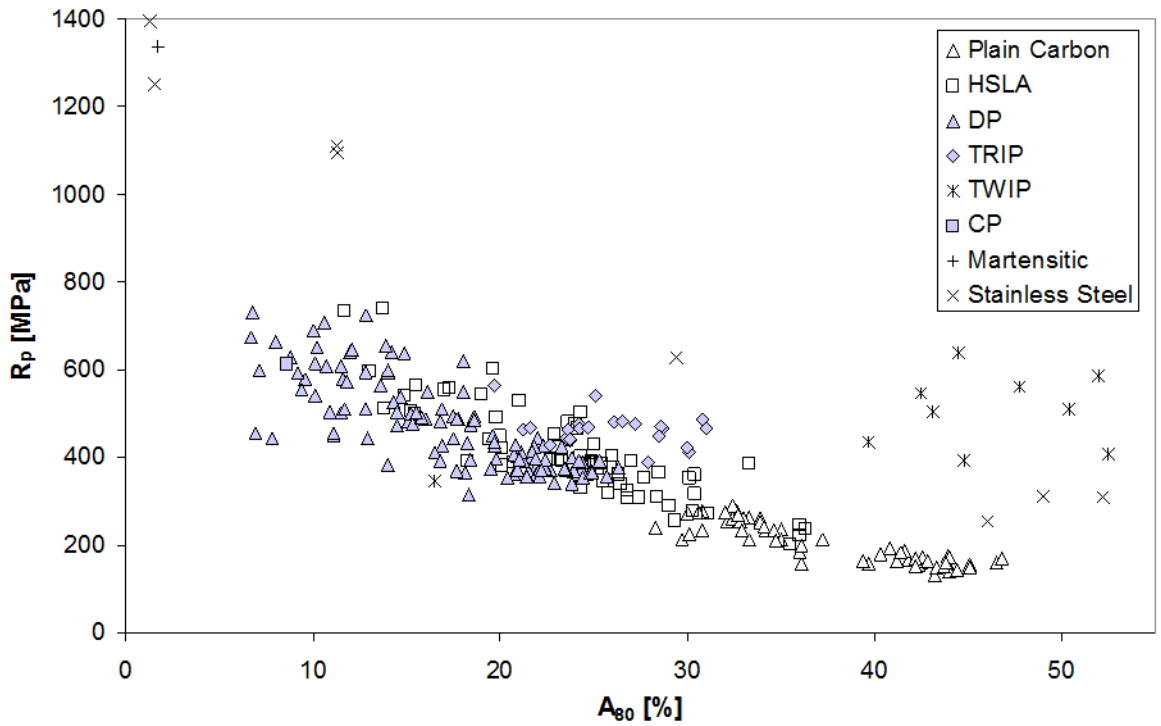

Figure 2.3: The "steel banana" showing the relationship between strength and formability for a wide range of steels used in automotive applications (HSLA: High Strength Low Alloyed Steel, DP: Dual Phase Steel, TRIP: Transformation Induced Plasticity Steel, TWIP: Twinning Induced Plasticity Steel, CP: Complex Phase Steel)
[Den Uijl et al., 2008a].

Production of Transformation Induced Plasticity (TRIP) steels is similar to DP steels, except that an isothermal holding step at a temperature between 300 to 500 ºC is also implemented [Amirthalingam *et al.*, 2005]. The thermal treatment serves to produce a microstructure consisting of ferrite with bainite and austenite. To ensure the occurrence of austenite at room temperature, TRIP steels need to be more highly alloyed than DP steels. Carbon levels are higher and silicon is added to suppress the formation of cementite during transformation to bainite. Thus retained austenite can be stabilized at room temperature.
Increased levels of silicon have a negative effect on the adhesion of zinc during galvanising of steels. To avoid imperfect adhesion of the Zn layer, Si is often replaced by aluminium. Phosphorus is added to aluminium alloyed TRIP steels to increase strength levels. Phosphorus also functions as a ferrite stabiliser, it coarsens the ferrite grain size, raises the ductile to brittle transition temperature, thus leading to decreased fracture toughness [Den Uijl & Smith, 2006].
Phosphorus plays an important role in TRIP steel metallurgy. Its low solubility in iron-carbides significantly retards the formation of cementite, where the diffusion of P away from the carbide becomes the rate determining step. Phosphorus, silicon, and aluminium are the three elements usually adopted in TRIP steel design to ensure that on forming bainite in the overaging step during steel strip production, some austenite is retained. Carbon does not precipitate but rather diffuses across the growth front to austenite. Phosphorus, whilst being a ferrite stabiliser thus indirectly stabilises austenite in TRIP steels [Den Uijl & Smith, 2006].

2.1.1 Coatings

The chemical composition of AHSS is chosen depending upon the coating that is eventually applied, since a thermal treatment is needed to produce the coated steels [Quidor, 2006]. For

automotive applications steel sheet can be uncoated, galvanised (GI) or galvannealed (GA), depending upon the corrosion resistance required for the eventual application of the material. Producing galvannealed steel involves the same steps as producing hot-dip galvanized (HDG) steel. Hot-rolled steel is annealed (*circa* 850 ºC) and coated with a zinc layer by immersion in a molten zinc bath (*circa* 450 ºC). The difference between galvanised and galvannealed steel is that the galvannealed coating contains iron. To make a galvannealed coating the strip is further heated by passing it through a furnace directly after immersion in the zinc bath. By heating to approximately 520-560 °C and keeping the strip at this temperature for a period of time, the zinc coating alloys with iron from the steel by diffusion (see figure 2.4). The required processing time depends on the desired level of alloying (GI or GA). The resulting final product has a coating that is an alloy of predominantly zinc with 8 to 11% iron.

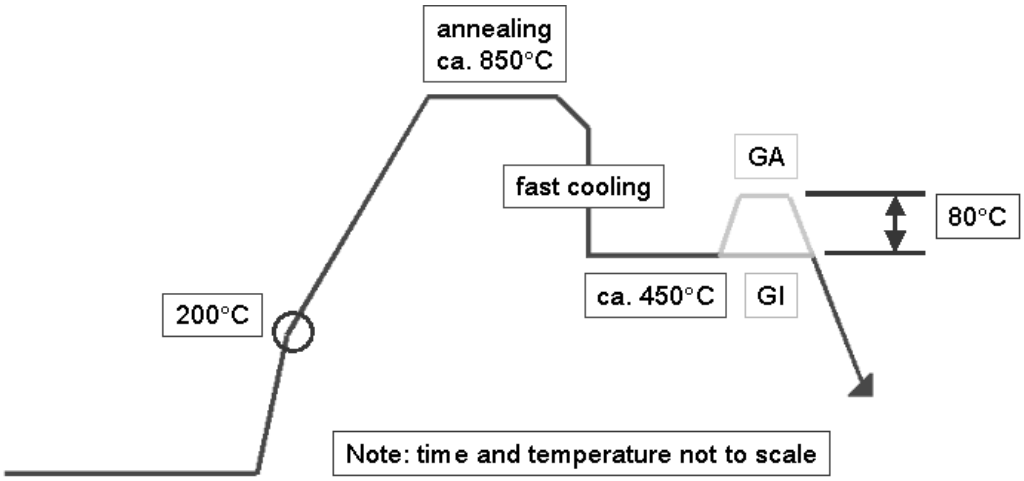

Figure 2.4: Thermal treatment of galvanised and galvanealed TRIP steel [Den Uijl, 2006a].

2.1.2 Mechanical behaviour

The stress strain curves of DP and TRIP steels shows continuous yielding, high tensile strength, low yield to tensile strength ratio and a high uniform and total elongation [Amirthalingam *et al.*, 2005]. In DP steels this behaviour can be attributed to the martensite in the ferrite matrix. As the martensite is formed during the transformation from austenite, it is accompanied by volume expansion. The locally increased volume causes deformation of the ferrite matrix, introducing mobile dislocations at the ferrite/martensite interface, accomodating continuous yielding. The hard martensite increases the ultimate tensile strength [Waterschoot *et al.*, 2002].
In TRIP steels deformation during tensile loading causes the retained austenite to transform to martensite. This transformation is also accompanied by volume expansion, resulting in a localised increase of the strain hardening coefficient. This delays the onset of necking and leads to higher uniform and total elongation [Garcia-Gonzalez, 2005].

2.1.3 Classification

DP and TRIP steels are the AHSS that are the main materials of interest to this thesis. Other kinds of AHSS have been developed, all of them having a microstructure consisting of two or more different phases, of which (at least) one adds strength and hardness to the materials whilst the other(s) provide additional formability (see table 2.1).

Table 2.1: Advanced High Strength Steels

AHSS		**Microstructural composition**
DP	Dual Phase steel	ferrite, martensite [LLewellyn & Hudd 2000]
TRIP	Transformation Induced Plasticity steel	ferrite, bainite, retained austenite [LLewellyn & Hudd 2000]
CP	Complex Phase steel	martensite, pearlite, retained austenite [IISI, 2006]
FB	Ferritic Bainitic steel	ferrite, bainite [IISI, 2006]
MS	Martensitic Steel	martensite, bainite, ferrite [IISI, 2006]
Q&P	Quenching & Partitioning steel	martensite, ferrite, retained austenite. [Wang & Weijun, 2011]

TWinning-Induced Plasticity (TWIP) steels and Hot Forming (HF) steels are sometimes also grouped under the heading AHSS, because they also show improved strength and formability [Auto/Steel Partnership, 2008b]. However they do not have the complicated microstructural composition that sets AHSS apart form HSLA steels. Additionally the chemical composition of TWIP steels, with their high manganese content (17 - 24 %) does not classify them as carbon-steels.
Hot Forming steels (often referred to as Boron steels, though boron is not necessarily part of the chemical composition) have a chemical composition that is much more comparable to that of AHSS. These steels need to be heated into the austenitic temperature region before forming. They are austenitic when formed, ensuring good formability, whilst the subsequent quenching step ensures a martensitic microstructure that gives the final product very high hardness. As their application is completely different from DP and TRIP steels, as well as any of the other steels listed in table 2.1, they can also be considered to be a different class of steels compared to AHSS.
Advanced High Strength Steels are not just classified by their microstructural composition. Depending on application they can be classified according to their chemical composition, the thickness of the material and their mechanical characteristics. The main standard for AHSS in Europe is the so called Euronorm [prEN 10336]. This specifies technical delivery conditions. Manufacturers publish their own product catalogues which specify their materials [CSPIJ, 2008]. Automotive manufacturers have their own standards [GM, 2002] which specify the chemical composition and mechanical characteristics that are demanded. Additionally they may specify surface conditions and some other properties, including microstructural characteristics (typically grain size *et cetera*). Weldability is often not specified in these documents, however automotive manufacturers require certain sets of tests that have to be passed for a material to be accepted, and these include requirements concerning weldability. Efforts are made to standardise these tests within the industry, *e.g.* through the Verein Deutsche Eisenhüttenleute (VDEh) or the WorldAutoSteel platform, which issues appropriate guidelines [WorldAutoSteel, 2009].

2.2 Resistance spot welding

Resistance spot welding (RSW) was invented by Elihu Thomson [Compton, 1939]. The development of the process goes back to 1890 when Thomson filed a patent on a "*Method for Electric Welding*" [Thomson, 1890]. The idea was further developed and in 1909 Thomson filed a patent on "*Electric Welding of Sheet Metal*" [Thomson, 1909].
Nowadays several thousand spotwelded joints are present in cars. The exact number differs between brands and models (see table 2.2) and is dependent on the size of the vehicle and the number of parts that need to be joined in combination and the joining strategy of the manufacturer.

Table 2.2: Number of spotwelds used to assemble the Body in White (B.I.W.) of several brands and models, as presented at conferences. If data is available for updated models (e.g. Ford Fiesta), the data of the latest model are presented here.

Model	*Number of spotwelds*	*[Reference]*
Audi A4 Avant	5061	[Rebele *et al.*, 2008]
Audi A6	5102	[Wilde *et al.*, 2004]
Audi Q5	5580	[Rebele *et al.*, 2008]
Citroën C4	4360	[Perrot *et al*., 2004]
Citroën C5 Berline	4051	[Le Floch & Barbier, 2008]
Citroën C5 Tourer	4282	[Le Floch & Barbier, 2008]
Ford Fiesta 3-Door	3184	[Liesenfelder *et al.*, 2008]
Ford Fiesta 5-Door	3305	[Liesenfelder *et al.*, 2008]
Honda Jazz	2060	[Ito *et al.*, 2008]
Jaguar XJ Saloon	3185	[White, 2006]
Jaguar XK Convertible	2620	[White, 2006]
Jaguar XK Coupe	2620	[White, 2006]
Mercedes SLK	4840	[Trost *et al.*, 2004]
Mini Cabrio	4178	[Brunies *et al.*, 2004]
Mini Hatch	4475	[Brunies *et al.*, 2004]
Nissan Murano	4307	[Saito & Nakamura, 2004]
Nissan Teana	5821	[Michiura *et al.*, 2008]
Opel Insignia	6331	[Heim *et al.*, 2008]
Opel Vectra	4613	[Heim *et al.*, 2008]
Peugeot 307	4434	[Perrot *et al.* 2004]
Peugeot 307 Space Wagon	4764	[Perrot *et al.*, 2002]
Peugeot 407 Sedan	4335	[Bonte & Deren, 2004]
Peugeot 407 Station Wagon	4607	[Bonte & Deren, 2004]
Renault Clio	2916	[Delhommeau & Hoareau 2004]
Renault Laguna Coupe	4379	[Plaideau *et al.*, 2008]
Renault Laguna Hatchback	3998	[Plaideau *et al.*, 2008]
Renault Modus	3746	[Delhommeau & Hoareau 2004]
Renault Twingo	2213	[Delhommeau & Hoareau 2004]
Skoda Octavia 24	4333	[Sekyr, 2004]
Skoda Octavia 34	4771	[Sekyr, 2004]
Skoda Octavia 35	5011	[Sekyr, 2004]
Skoda Superb 451	5051	[Simon & Senkyr, 2008]
Skoda Superb 461	5157	[Simon & Senkyr, 2008]
Volvo V50	3779	[Jonsell *et al.*, 2004]
Volvo XC60	4337	[Lassl, 2008]

For the selection of a joining method for a particular application, many different conditions and aspects are taken into account. Some of the most important are [Janota & Neumann, 2008]:

- the materials used (and their coatings),
- structural aspects (*e.g.* continuous or discontinuous joints),
- accessibility of the joints,
- organisation of the manufacturing operations,
- available workforce and equipment,
- maintenance requirements,
- company customs and routines,
- investments and operation costs [Scotchmer & Chan, 2008].

Whatever the considerations that will lead to the selection of a certain joining process, it is the performance of the joint itself that will be the most important selection criterion. If a joining method is not suitable to achieve the desired performance (concerning strength, fatigue, crash, corrosion, *et cetera*), another process will be selected.
Although the automotive industry has introduced new welding processes to join sheet material (most notably laser beam welding [Ebert, 2006, 2007 & 2008]), resistance spot welding is still a very important welding process [Svensson & Larsson, 2006].

2.2.1 Joule heating

Resistance spot welding is based on Joule's first law that gives an expression for the amount of heat generated by a current flowing through a conductor. The general expression can be stated as [Kearns, 1980; Zhang & Senkara 2006]:

$$Q = I^2 R t, \qquad \text{(Eq. 2.1a)}$$

where Q is the amount of heat generated, I is the current applied through the conductor, R is the resistance of the conductor, and t is the time during which the current is applied.
If the current and/or the resistance is not constant (as they generally will not be), the equation becomes:

$$dQ = I(t)^2 R(t) dt, \qquad \text{(Eq. 2.1b)}$$

Integrating the expression will give the heat generated during a time interval.

In the most basic set up of resistance spot welding, two sheets of metal are placed between two electrodes (see figure 2.5) [Del Vecchio, 1956]. The current runs between the electrodes and heats up the materials. The heat generated is not uniform, as the bulk resistivity of the electrodes and the metal sheets, the contact resistance between the sheets and the electrodes, and between the sheets, differ from each other and vary with temperature.
The electrodes are water cooled [Davies, 1986] and therefore serve as heat sinks. Additionally heat will be lost to the surrounding material of the metal sheets. This will lead to a temperature profile with the highest temperature between the electrodes. In the most basic set up, both sheets will be of the same material (same electrical resistivity, thermal conductivity and thickness) and heating will be most prominent at the interface between the two sheets. If the current is high enough the material will melt at that interface and a molten weld pool will start to form.

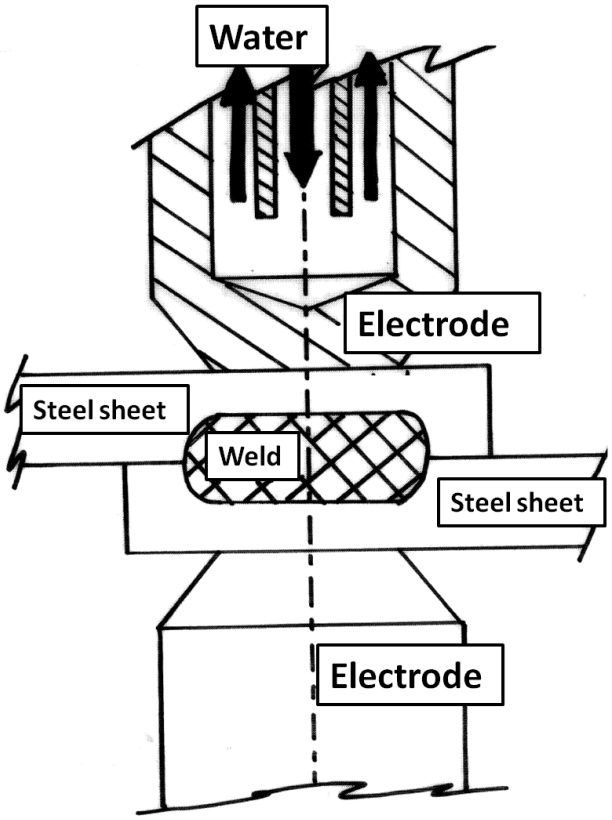

Figure 2.5: Basic set up of the resistance spot welding process; two sheets of similar material and thickness between two water cooled electrodes. The weld is formed in the centre between the two electrodes.

As soon as the current stops flowing the weld pool will start to cool (losing heat to the surrounding material and the electrodes) and eventually will solidify, forming a joint between the materials (see figure 2.6).

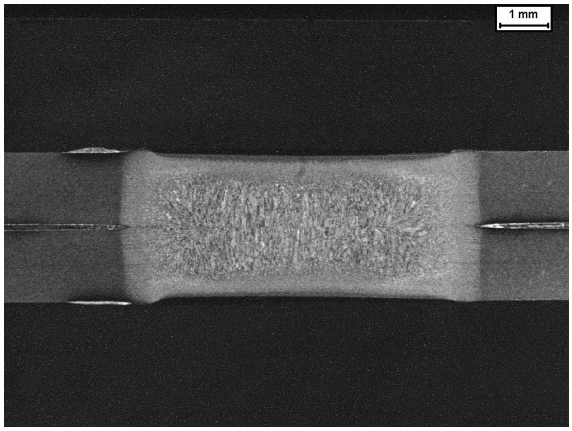

Figure 2.6: Resistance spot welded joint between two sheets of 1,0 mm thick DC01 steel. Welds made with a weld current of 8,45 kA, applied during 0,220 s. Electrode force 3,1 kN.

The process parameters set by the operator are:

- the electrode pressure,
- the welding current,
- the time the current is applied,
- the cooling time.

2.2.2 Electrode pressure

There are many classification systems for welding processes. DIN 1910 for instance distinguishes three different groups of welding processes [Krause, 1993]:

- fusion welding (*Schmelzschweißen*),
- friction welding (*Reibschweißen*),
- resistance welding (*Widerstandsschweißen*).

Within the group of resistance welding, a distinction is made between processes using pressure and those that do not. There are even more subdivisions (*e.g.* conduction or induction), before resistance spot welding is identified as a separate process.
Jackson makes a different division, recognising "*fusion welding (without pressure)*", "*surface bonding processes*" and "*welding processes which employ pressure*" [Jackson, 1967]. Here resistance spot welding is classified in the last group (as is friction welding).
Whatever the system, it is important to note that it is not just the current (in combination with the material resistance) that is a defining feature of the resistance spot welding process, but also the pressure applied by the electrodes.

The pressure applied by the electrodes clamps the materials together. The pressure determines the contact resistance between electrodes and sheets and between the sheets. A low electrode force may lead to a reduction in actual contact between the sheets of material and the contact resistance will be high. If the electrode force is increased the contact resistance is decreased. There is a limiting pressure above which the contact resistance remains uniform [Kearns, 1980].
If the pressure is too low, expulsion of molten material will occur before the weld is fully formed. If the pressure is too high indentation of the sheet material will occur as the material softens [Kearns, 1980]. Too much indentation is undesirable for cosmetic reasons and because stress concentration points may be generated as the sheet material deforms.

The electrode lifetime, *i.e.* the number of welds that can be made with an electrode before maintenance is needed to redress the electrode to ensure adequate weld quality, is an important parameter in manufacturing. The electrodes are usually made from material (copper alloys) that is softer than the sheet material. The electrode pressure causes the electrodes to deform, leading to an increase in the contact area between the electrodes and the sheet metal. As the area increases, the current density decreases. A decrease in current density leads to a decrease in heat generation. Additionally an increase in contact area leads to an increase in cooling capacity of the electrodes. Combined, the accumulation of heat will decrease, making it harder to produce welds. This puts a limit on the magnitude of the electrode force in manufacturing [Kearns, 1980 & Zhang & Senkara 2006].

2.2.3 Welding Current

The welding current can be either a Direct Current, DC, or an Alternating Current, AC. DC causes the weld pool to grow continuously. AC causes the weld pool to grow in steps as the weld pool is cooled somewhat when the current switches direction. The current can be varied during welding. The idea behind changing current profiles during welding is based on the belief that weld formation and possible expulsion of liquid material depend not only on the heat input, but also on how the heat is applied. A constant current profile, which is commonly used in resistance spot welding, provides an approximately constant heat input (or a constantly increasing heat input as the resistance increases). However, no research has demonstrated that constant heat input produces higher quality welds than other profiles [Zhang & Senkara 2006].

Expulsion of molten material (flash welding) is generally observed in the final stage of welding. The pressure in the liquid weld pool rises with increasing temperature (or the amount of heat input). Reducing the heat input at the end of welding may reduce the risk of expulsion. Weld current schemes with decreasing current levels at the end of welding have therefore been developed.
A rapid decrease in the current magnitude and a large associated heat loss, may have a negative impact on the weld quality. A more gradual decrease of the weld current magnitude and associated heat loss seems more logical to achieve large welds whilst reducing the risk of expulsion. When using half sine and sinusoidal profiles, consistent increases in weld process windows were found (up to 30% for half-sine and 70% for sinusoidal profiles respectively). No reasonable explanation has been obtained [Zhang & Senkara 2006].
Reducing current magnitudes affects process times and complicates welding operations. These considerations may limit the application of complex weld current profiles in manufacturing.

2.2.4 Welding and cooling time

The time over which the current is applied determines the size of the weld pool at a certain current. If the current magnitude is low, then welding times need to increase. If the current level is high welding times need to be reduced to avoid expulsion of liquid material. For the formation of a high quality weld, welding times need to be long enough to allow the material to melt and the weld pool to grow to its desired size. If the weld pool is not allowed to grow sufficiently (a so called stick weld) the mechanical performance of the weld is reduced [Kearns, 1980, Giroux & Deffenbaugh 1989 & Zhang & Senkara 2006].
Welding time is an important factor in manufacturing as it directly relates to costs. Especially when thicker sheets are welded it is often desirable to use multi pulsed welding schemes to form high quality welds of sufficient size. These schemes lead to increased welding times and therefore may be undesirable compared to welding schemes that lead to the formation of a weld in a single pulse.
Multi-pulsed schemes may also be used to perform a post weld heat treatment on the weld nugget. In post weld heat treatment schedules, the weld is subjected to an additional current pulse to heat up the material to temper the weld. This is generally done to soften the weld, to increase its mechanical performance. The post weld heat treatment is usually done using a lower welding current than is used to produce the weld nugget [Kearns, 1980 & Zhang & Senkara 2006].

After the current stops flowing an electrode force is still applied. During this time no more heat is generated, but heat is still conducted away from the weld pool to the water cooled electrodes. As the heat in the weld pool is reduced, the weld starts to solidify. The duration of the cooling time should be long enough to allow enough molten material to solidify to give the weld sufficient structural strength for it not to fail under thermal stresses after the electrodes are released. Often the electrodes can be released before the weld is completely solidified, allowing the remainder of the molten material to solidify by conduction of heat to the surrounding material of the construction [Giroux & Deffenbaugh 1989 & Tolf & Hedegård 2008].
When post weld heat treatments are used, the weld should be completely solidified as molten material cannot be meaningfully heat treated. To temper the weld nugget the material should be allowed to cool sufficiently for it to transform to martensite, which can then be heat treated. As martensite formation starts at temperatures considerably lower than the solidification temperature, cooling times before heat treatments can be quite long compared to the welding time and the post weld heat treatment time.

2.2.5 Challenges

In it's basic configuration, resistance spot welding is a straightforward process. In practice there are many complications. The first is splash welding. In production, manufacturers want to ensure that a joint has been formed. This may lead them to increase welding times, to ensure sufficient material has been melted [Juettner, 2011], causing molten material to be expelled, resulting in a splash weld. Although splash welds may not be a problem, they lead to smaller weld nuggets and increased indentation. Splash welds are especially undesirable if the material is coated, as the material expelled may damage the coating, thus leading to decreased corrosion protection and appearance. Splash welds caused by too long welding times or too high electrode pressure are often calculated risks (caused by the desire to be sure of the integrity of the joint formed). They can also be caused by misalignment of the electrodes (in which case they are unintentional).

Shunt welding forms a second complication. Again, when a single weld is formed between sheets the current will flow straight between the electrodes. In assembly, many welds will be made in the same sheets, and previous welds will function as short circuits between the electrodes. Part of the current will run via previously formed welds, requiring the current to be higher or the time that the current flows to be longer to form a weld of the same size [Houldcroft, 1977].
In its most basic form two sheets of similar thickness are joined together. If the thickness of the materials is not the same, the heat conducted away to the electrodes will not be equal for both sheets. This will cause the thermal profile to deviate and melting will start to occur in only one of the materials. If not enough heat is generated this may lead to a weld nugget forming in only one of the materials. Because the contact resistance between the materials is usually very high, the weld nugget will usually form at the interface, but if the difference in thickness between the materials is big enough this may not be the case.
Generally both sheets are made of the same metal. However in some instances the materials may differ considerably. The difference in thermal and electrical characteristics of the materials may lead to significant variations in the thermal profile. Thus leading to similar effects as with the variations in sheet thickness. If the materials differ in thickness and thermal and electrical characteristic, this may be even more pronounced [den Uijl, 2008].
Although two sheets are generally welded, stacks of three or more sheets may also be joined. This may complicate weld nugget formation even more [den Uijl, 2010].
The issue of springback also plays a role. If the springback of a flange after forming is too big, it is hard to press the flanges together. The sheets need to be pressed together by the electrodes to enable a current to flow, otherwise a joint cannot be formed. There may be additional complications if the strength of the sheets becomes too high.

Welds are usually formed at the interface between the sheets, because the contact resistance is higher than the bulk resistivity of the materials. The surfaces of sheet material in automotive applications are often coated. The coatings change the contact surface resistivity. If the coating has a lower melting and evaporation temperature than the melting temperature of the metal of the sheets, the thermal profile will show discontinuities. In automotive manufacturing, steel sheet is often coated with zinc. Due to the higher thermal and electrical conductivity of the zinc coating compared to an uncoated surface, and because the softer zinc surface conforms better to the electrode tip, higher current needs to be applied for a longer period of time when welding coated sheets [Madsen *et al.*, 2010]. Other coatings may decrease the electrical conductivity between the sheets (*e.g.* AlSi coatings on boron steels).
As the temperature rises, the zinc will melt and evaporate, which may not cause too much complications for the contact resistance between the two sheets, but at the electrode tip, molten zinc will be in contact with the electrodes which are (usually) made of copper. Alloying of the copper with the zinc will lead to the formation of brass which increases the resistivity at the electrode face even more. This then further raises the temperature at the electrode tip

and the material softens and deforms due to the combination of the elevated temperature and the decreased softening temperature of the alloyed electrode tip [Zhang & Senkara 2006 & Madsen *et al.*, 2010].
The wear on the electrodes causes the area of the electrode tip to increase, which gives a reduction in current density and pressure leading to undersized nugget formation and bad weld quality [Zhang & Senkara 2006 & Madsen *et al.*, 2010]. The point where weld dimensions and quality are not acceptable any more determines the electrode lifetime. Adequate electrode cooling is traditionally seen as the most effective factor to ensure optimum tip life [Davies, 1986], which has lead to the development of special electrodes with increased cooling capacity [Scotchmer & Chan, 2006].
To ensure that welds of desired dimensions and quality are produced once the electrode lifetime has passed, the electrode tips are "redressed" (*i.e.* the electrode's original geometry is restored by milling) [Chan & Scotchmer, 2010]. Redressing can be done by removing all of the affected material, but also by restoring just the side of the electrode. By leaving the brass alloy layers on the tip surface intact a "steady-state" is reached that helps to achieve consistency [Chatterjee, 2000]. This work has led to the development of special coatings to increase the electrode lifetime [Scotchmer & Chan, 2006].
The electrode lifetime is an important parameter, because the need to redress the electrode tips adds costs to the manufacturing operations. Conversely, measures to counter electrode degradation (*e.g.* increase cooling capacity or electrode tip coatings) increase the costs of consumables [Scotchmer & Chan, 2008].

Traditionally, one of the methods to counter the challenges faced by resistance spot welding has been to use multi-pulsed welding [Pfeifer, 1969]. Instead of one single pulse to melt the material, two or more pulses are used, with intermediate pauses, in which the material is allowed to cool down via the electrodes that are still in contact with the sheets. After the last pulse, there is usually a last holding stage to allow (part of) the molten weld pool to cool down sufficiently to solidify and form a joint.
The various welding stages can be denoted using "*w*" for a welding stage, "*p*" for the pauses and "*h*" for the holding stage. Before the (first) welding pulse there is usually a "*squeeze*" stage in which the electrodes are brought into contact with the sheets, this stage can be denoted using "*sq*". The duration of the different stages is given in cycles for alternating current (with the duration of a cycle dependent upon the frequency used) and milliseconds for direct current. For instance, the welding schedule for the joint shown in figure 2 would be "*5 sq 11 w 5 h*".

Finally, even the field of resistance spot welding does not escape the need to look into power consumption. With rising energy prices and possible future scarcity, optimisation of energy consumption has become a topic of interest in automotive manufacturing. Not just for the products produced, but also for the processes used. Resistance spot welding faces an extra challenge here as operations tend to interfere with the supply offered by the power grid (*e.g.* high power demand for short periods) [Weertman & Drewes, 2010]. Other factors that may play a role in future developments of resistance spot welding in automotive manufacturing are health and safety related [Boyer, 2007].

2.3 Modelling of Resistance Spot Welding

According to Zhou [2010] numerical simulation of the thermal and mechanical response to welding dates back to the 1970s [Hibbitt & Marcal, 1973]. Zhang & Senkara [2006] date early work on numerical simulation of resistance spot welding to the 1960s. Early resistance spot weld simulations were based on finite difference methods [Zang & Senkara, 2006]. Bentley *et al.* [1963] determined the temperature distribution numerically. Rice and Funk [1967] created

a simplified one-dimensional heat transfer model using the finite difference method for spot welding of composite materials used in semi-conductor fabrication. Using a similar approach Gould [1987] compared simulation results with experimentally determined weld nugget sizes.
One-dimensional numerical models lack the ability to accurately simulate local thermal gradients due to variations in current density. Two dimensional axisymmetric heat transfer models for analyzing resistance spot welding using finite difference methods were developed later. Cho & Cho [1989] modelled the electrical-thermal coupling of the process. Still a finite difference approach poses limitations to the model due to rigidity in geometry. A basic finite difference model requires that key aspects of the geometry, most notably contact areas, are pre-defined. For accurate simulation of resistance welding this is a drawback.
The use of the finite element method to simulate welding processes also dates back to the 1970s [Ueda *et al.*, 1977]. A thermomechanical model using the finite element approach was developed by Friedman in 1975. In recent years finite element analysis has become the mainstay in spot weld simulations. Using commercial finite element software packages such as Ansys, Abaqus and LS-Dyna as well as purpose built finite element models, researchers have investigated various aspects of resistance spot welding. These models are often limited in the applicability in industry as they have been purpose built to investigate the effects of set process settings and/or materials. Adjusting process parameters such as (electrode) geometry and material characteristics often requires manipulation of the model set up by an operator with extensive knowledge of finite element method theory.
Most of the early work concerned either purely academic exercises or purpose built models to investigate a specific problem. An important advance in the field was made in 1991 with the first International Seminar "*Numerical Analysis of Weldability*" [Cerjak & Easterling, 1993]. The conference has been held biannually since and has grown into the leading event in the field [Cerjak, 1993]. The conference proceedings present a comprehensive state of the art at the time of the conference . Other events also created sessions dedicated to weld modelling and simulation [Lucas & Makhnenko, 2006].
The increased interest of researchers in the use of the finite element method for simulation of resistance spot welding becomes apparent when reviewing papers in the "*Numerical Analysis of Weldability*" conference proceedings. Murukawa *et al.* [2001] investigated the influence of the gap between press formed parts in welded lap joints. Robin *et al.* [2002] investigated the numerical simulation of resistance spot welding with special attention to the contact conditions using Sysweld. It was reported that there was very little difference in using a weakly coupled approach, simulating first the complete thermal response to welding operations followed by a mechanical simulation compared to a strongly coupled approach, simulating alternatively the thermal response and the resultant mechanical effect for a set number of time steps.
This work was further elaborated upon in the next conference where the results of finite element simulations using Sysweld were transferred to another finite element software package, Pamcrash, for analysis of the behaviour of the welded joint under dynamic loading [Robin *et al.*, 2005]. It was reported that the results were promising, but the calculation effort is very high due to the use of solid elements in crash simulations. In crash simulations dedicated resistance spot weld descriptions are required for simulation of crash behaviour of parts with welded joints. Heubrandther & Akgün [2005] reported work done on coupling of pairs of special elastic Trefftz elements, that allow for the representation of the entire spot weld in a single element, connected via rigid body constraints to represent a spot welded joint in crash simulations. This work was further developed in the next conference [Heubrandtner & Ranger, 2007]. Prerequisite for this and similar approaches is a high level of predictive and repetitive behaviour of the welded joint under crash loading (*e.g.* full plug failure).
De & Dorn [2005] reported on the use of simulations of resistance spot welding to investigate electrode wear. The investigation was focussed on welding of aluminium. It was reported that the simulation of thermo-mechanical elasto-plastic behaviour was limited due to lack of mechanical material properties at elevated temperatures. Sprikunwong *et al.* [2005] reported on 2-D axi-symmetric finite element simulations using Sysweld. Comparison between

predicted and measured results showed that the model gave true thermal results at the end of the welding cycle, when the weld reaches its nominal size. However the thermal history at the beginning of the process was not as well modelled; the temperatures predicted in the first half of the welding process were lower than the temperatures actually reached experimentally. Again the importance of accurate material data at different temperatures was stressed. It was stated that enthalpy, bulk thermal and electrical conductivity play a large role. Adjusting these parameters may help to improve simulation results, but the physical justification is unclear. Even more important is contact resistance. This parameter is hard to model accurately as it is less well known and hard to measure with varying temperature.
Borhy & Szabó [2005] reported on issues concerning the use of descriptions of welded joints for assembly purposes. No finite element simulations of resistance spot welded joints were reported, but the issues concerning the representation of welded joints for large structural simulations were discussed. Robin *et al.* [2007] investigated the complexity of the electro-thermal contact modelling between sheets and electrodes of spot welding, elaborating on the work presented in the previous conference [Robin *et al.*, 2005] and proposed a technique to use finite element simulations of resistance spot welded joints for assembly of a large structure. This local-global approach allows the use of strongly coupled electrical, thermal, metallurgical and mechanical phenomena to compute local effects of welding. The results of such a simulation is used as a single input parameter in assembly simulations. Inserting these results in a mechanical assembly model allows for prediction of the direction of distortions caused in assembly by the spot welding process and the welding sequence used. The approach requires less calculation effort than a complete 3D simulation of welding. Effects such as shunt welding and degradation of the electrode tip during subsequent welding steps are not taken into account.
Over time the focus of resistance spot welding modelling in the "*Numerical Analysis of Weldability*" conferences can be seen to shift from the development of models to accurately simulate the process itself to the application of the models to simulate the effects of resistance spot welding upon manufacturing of structures, taking into account the effects of material characteristics. This more practical approach has been the focus of much work reported in another series of seminars. In 2000 the first International Seminar on Advances in Resistance Welding provided a platform for applied work simulation of resistance welding as well as experimental developments, mostly in the automotive sector. The seminar has been held biannually since and focuses heavily on applications, There is room for all kinds of simulation work [Fukui 2006; Ikeda *et al*. 2008], but due to the fact that the organisation is heavily sponsored by Swantec, most simulation work presented is done with Sorpas (of which Swantec is the supplier).
This is less of a drawback than it may seem. Westgate [2003] at the beginning of this century mentioned that a number of systems had been devised and were continually improved. At the beginning of this century there were three dedicated resistance spot weld solutions commercially available:

- Spotsim [Dilthey *et al.*, 2001],
- Sorpas [Zhang & Kristensen, 1999],
- The spot weld module in Sysweld [Robin *et al.*, 2002].

Spotsim, developed by the Tula State University, Russia, and the Aachen Welding Institute, Germany was designed for analysis of weld formation in resistance spot welding of low-carbon, non-alloy and CrNi steels with thickness of 0,5-5 mm [Spotsim, 1999]. It seems to have made virtually no impact. No scientific or engineering publication has been found using Spotsim to simulate resistance spot welding, although it may be possible that Spotsim has made some impact on the Russian market. The reason for this is probably the availability of better solutions provided by Sorpas and Sysweld. Spotsim is no longer available [Spotsim, 2012].

The resistance spot welding tool available in Sysweld initially required the user to edit input files and submit them to the solver directly. This approach requires quite some understanding of the operation of programming languages and finite element theory to vary process parameter settings and finite element parameters. Combined with the cumbersome and less than user friendly graphical user interface of Sysweld, this made it less suitable for the welding engineer on the work shop floor.
Added to that, changing the geometry of the electrode, form the given electrode geometry required even more hands-on work for the operator. In later versions a graphical user interface was supplied that made it possible for the operator to simulate process variation with more ease, but restricted the number of parameters that can be varied.
The results from simulations in Sysweld can then be used as input parameters for other ESI product such as Assembly and even PAMstamp. These are important capabilities for the engineer and designer, but not of primary concern for the weld shop floor.

Sorpas is designed in a way that it can be used by anyone that is familiar with resistance spot welding equipment. The parameters that need to be set are the same that need to be set in real life. The software comes supplied with a large database of materials, electrode geometries and equipment characteristics. It is fairly straight forward to adjust the values in the databases to simulated differences in electrode geometry and material characteristics. The software is equipped with standard options to simulate weld growth curves for different process parameters.
A drawback is that the results cannot be automatically used as input in other software platforms. In fact this requires manual intervention to feed the results of Sorpas simulations (*e.g.* weld dimensions) into other software platforms for instance to simulate mechanical loading of the weld [Den Uijl *et al.*, 2012b].

2.4 Weldability

Next to formability (important for production of parts) and strength (important for the performance of parts), weldability is an important characteristic of materials [Den Uijl & Carless, 2012]. There are two important aspects to weldability of steels [ISO 18278-1, 2004]:

- Manufacturability: the ability to produce welds, which will be discussed in sections 2.4.1 & 2.4.2.
- Performance: the quality of the welded joints, which will be discussed in section 2.4.3.

Weldability tests are a phase in every new car project. Larsson *et al.* [2009] describe such tests at Volvo Cars. "*Welding engineers receive sets of material combinations which have not been tested before and no previous test with similar sheet combinations contains information sufficient for an appropriate judgement of weldability*." [VDEh 1220-2, 2008] These weldability tests give information concerning both process and performance.

2.4.1 Weldability: Process

For automotive applications, standards for material properties, and how to determine them are issued [GMW 3032, 2002]. Welding characteristics are an important part of these standards [Larsson *et al.,* 2009]. The main focus for the welding engineer is to find welding parameters which result in a robust production process [VDEh 1220-2, 2008]. To evaluate a welding window a weld growth curve is made. A weld growth curve gives the weld nugget diameter as a function of the welding current, while the welding schedule and the electrode force are kept constant (see figure 2.7).

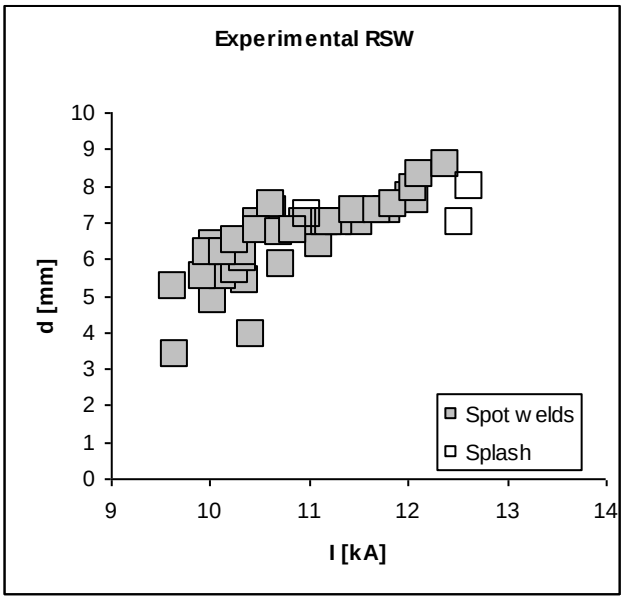

Figure 2.7: W*eld growth curve of GI-coated 1,5 mm thick DP 800 [Den Uijl & Smith, 2007].*

The welding range for resistance spot welding is often defined as the range in welding current from the point where the weld nugget reaches a required size (minimum weld size) and the onset of splash. The minimum weld size is often related to the material thickness, often $4\sqrt{t_s}$ (with t_s being the sheet thickness) is used [Larsson *et al.,* 2009], but $3{,}5\sqrt{t_s}$ or $5\sqrt{t_s}$ are also used [Zhang & Senkara, 2006]. It is also possible that a minimum weld size is defined for ranges in thickness and variations can be allowed for different applications [Zhang & Senkara, 2006, Volvo, 2005 & BMW, 2005].
Table 2.3 shows an example of minimum nugget diameters for ranges of sheet thickness for varying applications. In this example from BMW Group Standard GS 96002-2 Category A spot welds are joints that can endanger human life, as well as the function or safety, in the event of their failure. Category B spot welds are joints whose failure make the product unusable for its intended purpose or result in a loss of property, and Category C spot welds are joints whose failure has only little negative impact on the product in terms of its intended use [BMW, 2005].

Table 2.3: Example of table with minimum nugget diameter for ranges of sheet thickness and for varying applications.

Sheet thickness [mm]	**Minimum nugget diameter [mm]**	
	Category A & B	**Category C**
≥ 0,50 < 0,60	2,5	2,2
≥ 0,60 < 0,70	2,8	2,4
≥ 0,70 < 0,85	3,0	2,7
≥ 0,85 < 1,10	3,5	3,0
≥ 1,10 < 1,25	3,9	3,3
≥ 1,25 < 1,50	4,1	3,5
≥ 1,50 < 1,60	4,3	3,7
≥ 1,60 < 1,75	4,4	3,8
≥ 1,75 ≤ 1,80	4,7	4,0
> 1,80 ≤ 2,00	5,0	4,2
> 2,00 ≤ 2,25	5,3	4,5
> 2,25 ≤ 2,50	5,5	4,8
> 2,50 ≤ 3,00	6,0	5,2

The onset of splash welds is not just dependent upon the process settings, but also on factors which can be related to experimental spread, such as misalignment of electrodes and

electrode wear. Also it is possible to acquire perfectly good welds after the first splash welds have occurred. But as a rule of thumb splash welds can be expected as soon as the size of the weld nugget exceeds the electrode diameter (though they do not need to occur) [Den Uijl, 2008].
The width of the weld growth curve (referring to the welding range) gives an indication of the anticipated tolerance of a particular welding schedule in production, the aim being to maximise the welding range to achieve the greatest safety margin on weld quality [Westgate, 2004]. The welding range is dependent on various welding parameters: electrode force, welding time, *et cetera* [Weber & Göklü, 2004]. Thus, the process reliability depends on the selection of welding parameters and on additional influencing factors. Important influencing factors are the shape and material of the electrode caps, the base metal and the coating of the steel sheets as well as the static and dynamic mechanical machine properties of the welding equipment [Weber, 2002].
Another quality aspect of a weld is penetration, describing the extent of through thickness melting during welding. A small penetration may mean insufficient heating and indicate a cold weld. In general large penetration is preferred. But as penetration is directly related to the amount of heating, large penetration means softening of the material and possible large indentation by the electrodes. The requirements on penetration are generally loose, but in general large penetration is acceptable if it does not create large deformation [Zhang & Senkara, 2006].
As mentioned before a very important parameter of weldability is the electrode lifetime, *i.e.* the number of welds that can be produced within the set margins (as defined in the weld growth curve).

2.4.2 Process Considerations of Weldability

Although resistance spot welding is very well established for joining mild steels and high strength low alloyed (HSLA) steels for automotive applications, the welding process parameters are not fully developed for advanced high strength steels (and ultra high strengths steels such as Boron steels). Welding engineers face challenges to establish robust process windows for AHSS applications [Subramanian, 2008]. The lower limit for the welding current results from the requirement of a minimum spot weld diameter. The upper limit of the welding current is given by the physics of the welding process. *"The lower quality limit can in principle be optionally set by making a requirement on the spot weld diameter depending on the quality and strength demands, respectively, placed on the spot weld. Commonly used lower quality limits are spot weld diameters of* $3.5\sqrt{t_s}$ *or* $4\sqrt{t_s}$ *, whereby* t_s *is the sheet thickness."* [Weber & Göklü, 2004]
The welding range is generally narrower for high strength steels than for low carbon steels, when using a schedule suitable for the low carbon steel. A slightly lower welding current is required for the high strength steel, because of higher electrical resistance, but weld splash occurs earlier [Westgate, 2004].

Early work on high strength steels indicated that simply by increasing the electrode force, the welding range can be opened up to give a similar performance to low carbon steel [Rivett *et al,*; 2008].
Material suppliers often recommend the force levels required for different steel types and thicknesses. For high strength steels up to about 600 MPa tensile strength, this can be typically 20 to 50% higher than for low carbon steel (even greater increases are often suggested for ultra high strength steels) [Westgate, 2004].
The increased yield strength of advanced high strength steel compared to low carbon steels increases the total resistance across the electrode during the welding process and generates more heat that causes the material to melt much earlier. Therefore, time required to initiate

the melting process decreases when the material yield strength increases [Subramanian, 2008].
Weber & Göklü showed that with increasing electrode force, the upper and lower quality limits are shifted towards higher current for advanced high strength steels. The effect differed for different grades of steel, with a large increase of the width of the weld growth curve for TRIP steel, but much less effect for a complex phase steel [Weber & Göklü, 2004].
Tumuluru [2008] cautions that with the use of high force, the electrode indentation into the base material should be monitored because higher electrode force causes deeper indentation, but generally indentation at a given force will be greater in a low than in a high-strength steel.
Scotchmer [2004] mentions that the weld growth curve widens as the welding pressure is increased, and the current required for a given weld nugget diameter increases. It is also mentioned that anecdotal comments suggest that increasing welding forces at the same time as increasing heat and current are not a practical solution to increase the width of the weld growth curves of AHSS in high speed production, given equipment, time and cost constraints [Scotchmer, 2004 & Wesling *et al.*, 2004].
A higher electrode force can enable larger weld sizes to be achieved before splash and help to reduce internal porosity or shrinkage imperfections. The disadvantages are the need for higher capacity guns. [Westgate, 2004].
Dupuy [2006] carried out several welding range tests using different spot welding machines. It was found that all machines gave a similar response in spot welding, producing the same nugget diameter with a given current, although the amount of scatter varied. The welding range did vary depending on the stiffness of the construction. Increased stiffness enabled larger welding ranges as larger welds could be produced before splash occurred.
It is difficult to be precise about electrode force levels to be used, as it also depends on the weld time. Higher forces are required particularly at shorter weld times, if short sequence times are required for high production rates. However, longer weld times can also be beneficial in expanding the available welding range [Westgate, 2004]. Weber & Göklü [2004] showed that a welding time prolongation is more significant than an electrode force increase.
Subramanian [2005] also noticed that nugget formation was spontaneous with high strength grade steels. Significant variation in nugget size was found at low weld time. However, when the weld time was sufficiently large, the nugget reached its maximum size which was almost the same for all investigated grades. This could be attributed to similar high temperature stress-strain behaviour of various grades.
Weld schedules specifically for welding advanced high strength steels have been reported in the literature, using pulsed welding schedules or post weld tempering cycles [Dupuy, 2006, Peterson & Gould, 2004, Tawade *et al.,* 2004 & Auto/Steel Partnership, 2008a]. Even more complicated schedules combining variations in welding time and electrode force (adaptive welding) have been proposed [Ikeda *et al.,* 2008]. Some of the longer welding schedules would influence production rate but it might be possible to tolerate special procedures where a limited number of welds are to be made on the more difficult steels [Westgate, 2004].

The electrode shape has also been found to influence the weldability. Although advanced high strength steels can be welded with all weld tip shapes and materials [Auto/Steel Partnership, 2008b], dome shaped electrode tips (Type E, G & F) have been found to provide more consistent welds than truncated cone shaped tips (Type A & B) [Tumuluru, 2008]. Dome shaped electrode tips ensure buttons at lower currents than truncated shaped tips due to higher current densities at the centre of the electrode tip [Auto/Steel Partnership, 2008b]. However, as the material is indented by the electrode (during heating), the contact area of dome shaped electrode tips increases much faster than the truncated electrode tips [Den Uijl & Smith, 2007]. The increased contact area leads to reduced current density. As a result, dome shaped electrodes increase the current required to produce a large weld. This, in turn, increases the welding current range [Chan *et al.*,2006].

The largest welding ranges are found for uncoated steel sheets [Weber & Göklü, 2006]. But as mentioned before, the biggest influence of coatings is on the electrode lifetime. As the electrode surfaces alloy, they become more susceptible to deformation [White, 1991]. This effect becomes even more pronounced if the electrode force is increased to weld advanced high strength steels. Solutions have been proposed by changing the material of the electrodes [Craggs, 2004] or by applying advanced coatings to the electrode tips [Scotchmer, 2004 & Dong *et al.*, 2008]. Other proposed solutions encompass changing the electrode geometry and improving the cooling capacity of the electrodes [Chan & Scotchmer, 2004]. Such solutions are not preferred as electrode geometries are well defined in standards [ISO 5821, 2007] and therefore there may be reluctance to use speciality electrodes.

2.4.3 Weldability: Performance

The demands on the performance of resistance spot welded joints are related to their application. Several categories can be distinguished as described in section 2.4.1 [BMW, 2005].
It is for that reason that minimum weld nugget diameters are set for certain categories of application (see table 2.3), as the weld nugget diameter is thought to relate to the performance of the weld. Apart from the weld nugget size the performance of RSW joints is primarily a function of the chemical composition (and microstructural composition) of the materials and the thermal profile during welding (especially the maximum temperature reached during welding and the subsequent cooling rates). Three aspects in particular are important when assessing the weldability of the materials [Den Uijl *et al.*, 2008a]:

- resultant microstructure,
- post weld hardness,
- occurrence of weld defects.

Microstructure

The resultant microstructure after welding is different from the microstructure before welding, which is the key characteristic determining the strength and formability of the material. The original microstructure is destroyed and three regions can be identified after welding [Easterling, 1992 & Radaj, 1992]:

- the weld nugget,
- the heat affected zone (HAZ),
- unaffected base material.

The weld nugget consists of material that has melted during welding. After welding the material solidifies and subsequently undergoes phase transformations. Depending upon chemical composition of the material two trajectories can be identified [Porter & Easterling, 1992, Honeycombe & Bhadeshia, 1995 & Den Uijl & Smith, 2006]:

- liquid, delta ferrite, austenite, martensite and/or bainite,
- liquid, austenite, martensite and/or bainite.

Whether the resultant microstructural composition will be martensitic, bainitic or a mixture of both is dependent upon the chemical composition and cooling rate. At lower levels of alloying and/or low cooling rates the resultant microstructure will be mostly bainitic. At increased levels of alloying (with carbon being the primary alloying element) and sufficiently high cooling rates the resultant microstructure will be mostly martensitic. In general, due to the high cooling rates during resistance spot welding and the increased levels of carbon,

resistance spot welded joints in advanced high strength steels will be martensitic. Depending upon the chemical composition of material it is possible that the weld nugget contains some retained austenite after cooling (especially in TRIP steels, which after all have been alloyed to contain retained austenite) [Koistinen & Marburger 1959, Andrews, 1965, Blondeau *et al.*, 1973, Chaillet *et al*., 1976 & Porter & Easterling, 1986]
Apart from the microstructural composition of the weld nugget after welding, an important effect of welding is the size and orientation of grains, determined primarily by the solidification trajectory and the temperature gradients during cooling (see figure 2.8). Note that the voids at the centre line are caused by shrinkage due to cooling and solidification.

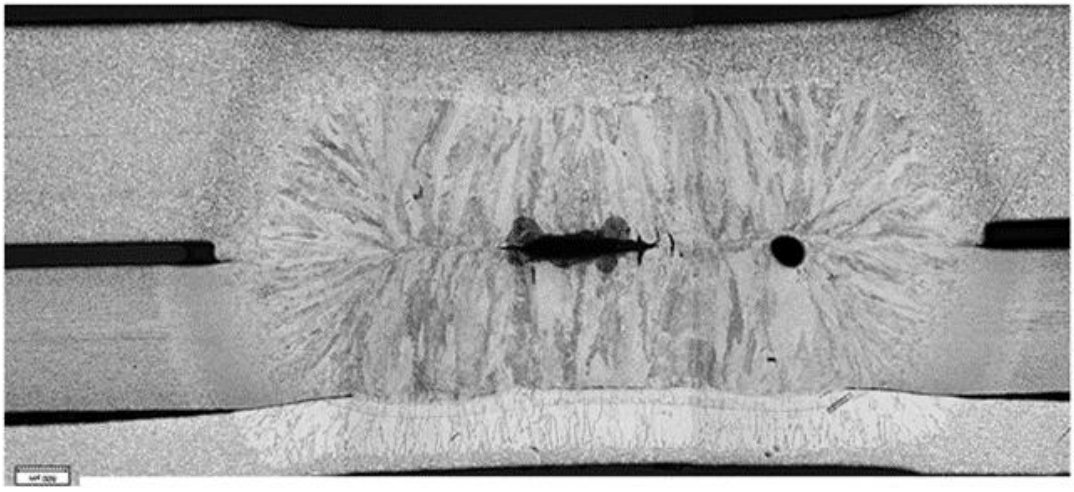

Figure 2.8: Micrograph of RSW joint of 3 sheets. The direction of the grains in the weld nugget runs along cooling lines; vertically where cooling is directed to the water cooled electrodes and horizontally along the centre line where cooling is directed to the surrounding material [Den Uijl, 2010].

The HAZ consists of material that has not been melted, but has been heated sufficiently for the material to be affected [Porter & Easterling, 1986 & Easterling, 1992]. The heat affected zone can be broadly divided into two parts:

- material heated above the austenisation temperature,
- material heated below the austenisation temperature.

Material heated above the austenisation temperature transforms to austenite during welding. After the material has been transformed to austenite the grains will start to grow. The amount of grain growth in the HAZ is determined by the maximum temperature reached and the time it has been heated above the austenisation temperature. Upon cooling the material will transform into martensite or bainite. Again, due to the high cooling rates during resistance spot welding and the levels of alloying, advanced high strength steels will predominantly transform to martensite [Den Uijl 2006b & Den Uijl *et al.*, 2007].
Material that has been heated below the austenisation temperature will be tempered during welding. Due to the microstructural compostion of advanced high strength steels (containing martensite and/or bainite) the main effect will be tempering of the martensite and bainite. This can cause significant softening of the material [Blondeau *et al*., 1975].

Hardness

Hardness is measured in a variety of ways (e.g. Vickers hardness and Rockwell hardness), but all methods measure the response of the material to indentation. [Kaluza, 2003] The

hardness is often related to the (tensile) strength of a material [Chaillet *et al*., 1976], although they are two intrinsically different properties.
Post weld hardness is influenced by three factors:

- the microstructural composition after welding,
- the chemical composition of the material,
- the cooling rate after welding.

For each microstructural phase there is a relationship between the chemical composition and the cooling rate that combine to make up the post weld hardness. [Blondeau *et al.*, 1973, Chaillet *et al*., 1976 & Den Uijl *et al.*, 2007]. The main element determining post weld hardness is carbon. To avoid high post weld hardness levels the amount of carbon in steels is often limited. This limitation also affects the strength of the base material. Therefore the steels are alloyed with other elements that increase the strength . Other elements are added to achieve the microstructural composition of the base material. These elements (e.g. molybdenum, manganese, chromium and silicon) all contribute to increased post weld hardness. Other elements significantly increasing post weld hardness are boron and vanadium [Honeycombe & Bhadeshia, 1995].

2.4.4 Weldability: Testing

Mechanical testing is an important aspect of weldability studies. Such testing is either to reveal important weld characteristics, such as weld failure mode, or to obtain quantitative measures of the strength of a weld [Zhang & Senkara, 2006].
Mechanical tests can give information on:

- **Peak load**; the maximum force measured during testing.
- **Failure mode**; a qualitative measure of weld quality. The failure mode provides information concerning whether fracture is brittle or ductile.
- **Ductility**; gives information on the energy that can be absorbed by a joint.
- **Fatigue**; a quantitative measure of the number of cycles to failure under a certain repeated loading pattern.

Procedures for testing are described in standards. Steel manufacturers use standardised test procedures to supply material data [Smith *et al.*, 2010]. Automotive manufacturers use standards to ensure that materials comply with the minimum requirements they have set for different applications [*e.g.* BMW 2002, GM 2002 & Volvo, 2005]. To streamline differences in standards, general standards have been developed. These may vary regionally (e.g. VDEh standards for Europe [*e.g.* VDEh 1220-2, 2008] or AWS standards for North America [*e.g.* AWS D8.1M, 2007]). Additionally standards are developed globally within the framework of the International Institute for Welding (IIW-IIS), which are published as ISO standards [*e.g.* ISO 10447, ISO 14270, ISO 14272, ISO 14273 & ISO 18278-1] and are subsequently often translated in national standards (*e.g.* NEN-EN-ISO 18278-2 & NEN-ISO 10447:2006). Although a wide variety of standards is available, they tend to address similar issues and set similar demands, but variations do occur.

Shop Floor Practice

To asses welding operations, welds are tested at assembly lines. Because of the limited availability of testing facilities and time, weld quality testing at the work shop floor is usually limited to evaluating the weld failure mode and measuring the weld button size. The most commonly used tests are the chisel test and the peel (roller) test [Zhang & Senkara, 2006 & ISO 10447]. These tests can be performed on parts taken form the production line or on sets

of welds made on coupons. In the latter case care must be taken that these coupons are welded using the same conditions as are used for production parts. The material should be the same (both in chemical composition and in thickness). Preceding operations, such as surface cleaning should be identical and care must be taken to prevent misleading effects from current shunting through adjacent welds [Kearns, 1980].

- **Chisel test**
  To assess the weld quality a chisel wedge is hammered between two welds. The main aim is to detect brittle weld failure and the occurrence of cold welds (joints without fusion between the sheets). The weld nugget may be measured to ensure that a set minimum is achieved. The results of chisel weld testing are strongly dependent upon the experience of the operator conducting the tests (both in consistency of applying the chisel as in evaluating the result) [Kearns, 1980, Zhang & Senkara, 2006 & ISO 10447].
- **Peel (roller) test**
  In a peel (roller) test the sheets are separated by a roller applied to one of the sheets (much like the way cans of sardines are sometimes opened). As the roller rolls over the weld the sheet is torn off at the weld and the weld is torn out if the joint is ductile, or the sheets are separated without much effort, if the joint is brittle. The test is not always suited to measure the weld nugget size, as the shape of the button can be highly irregular (especially if the base metal is torn out). Unlike the chisel test, the peel (roller) test is conducted on coupons and cannot be used for manufactured parts. Again the experience of the operator is critical in evaluating the test results [Kearns, 1980, Zhang & Senkara, 2006 & ISO 10447].

Instrumented testing

Steel manufacturers use several standardised tensile tests to assess the weldability of materials, such as (see figure 2.9):

- peel tests [ISO 14270]
- cross tension tests [ISO 14272]
- (over)lap shear tension tests [ISO 14273]

All these geometries can be loaded without much additional effort in standard tensile testing equipment.

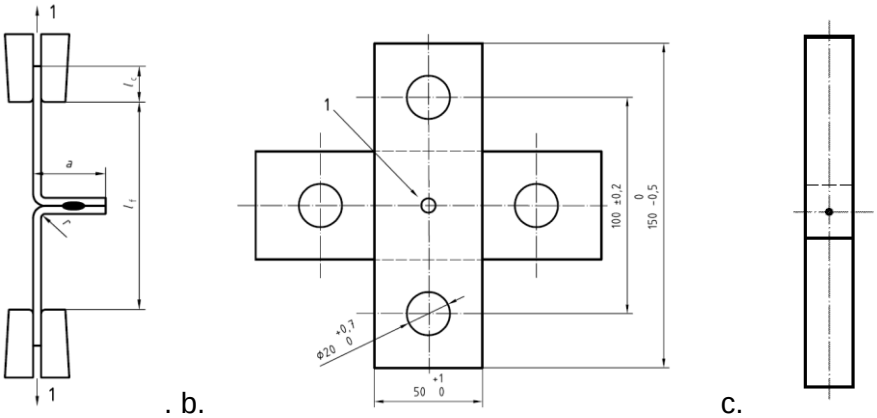

a . b. c.

Figure 2.9. (a) ISO 14270 Peel tensile testing; (b) ISO 14272 Cross tension specimen and (c) ISO 14273 lap shear specimen.

- **Peel Tests**
  This test is easy to prepare and perform as it generally does not require extra adaptations to the clamping system of the tensile testing equipment. The test is also informative because the majority of resistance spot welds will be located on flanges in an automotive structure. The test configuration provides information on the weld strength and failure mode, but not on the energy absorption because the deformation of the flanges generally absorbs most of the energy. The test results tend to show a lot of spread as the results are heavily dependent upon the location and size of spot weld.
- **Cross Tension Tests**
  This test is designed to load a weld in the direction normal to the weld interface. To achieve this care needs to be taken that the weld is positioned exactly in the centre of the test piece and does not show too much geometrical irregularity.
- **Overlap Tensile Testing**
  Overlap shear tensile testing provides data on the ultimate strength of the resistance spot welded joint and the failure mode. Compared to cross tensile tests and peel type tensile testing the results are less dependent on the exact location of the weld. Not many joints in critical areas of an automotive construction are subjected to static shear tensile loads, but because of the simplicity of the fabrication of test specimens and the test itself combined with the limited amount of experimental scatter (compared to cross tensile and peel type tensile testing) it is the most commonly used test configuration.
  The main drawback of the test is that the test specimens are asymmetric and deform during testing (see figure 2.10), this causes the spot weld to rotate and therefore the weld is not loaded in pure shear. The amount of rotation is dependent on the thickness and the size of the spot weld. Failure strength is primarily dependent upon the weld diameter [Den Uijl *et al*., 2008a].

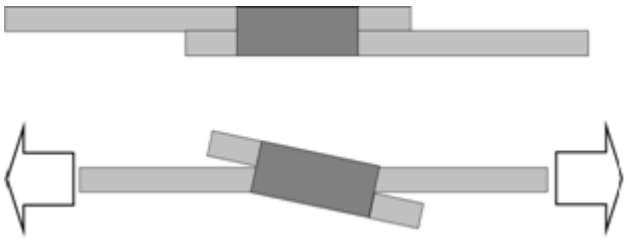

Figure 2.10: Schematic representation of the deformation of the test specimen with the rotation of the joint in tensile overlap testing.

Although the standardised test configurations supply a lot of information on the weld failure mode and failure strength of the spot welded joints, these coupon tests cannot completely simulate the complex loading conditions that occur during crash testing [Kearns, 1980].

Static and Dynamic Tensile Testing

Depending upon the application of the load, tests can be classified as:

- static tensile testing,
- dynamic tensile testing,
- crash box testing.

Static tensile tests are well known and defined [Zhang & Senkara, 2006 & AWS D8.1M:2007]. They are commonly used to test resistance spot welded joints in industry. Static tensile tests allow for clear comparison of resistance spot welded joints. They can be performed using

simple equipment that is usually available in labs, as similar equipment is also used to test unwelded materials. But resistance spot welded joints are seldom subjected to fatal static tensile loads in automotive applications. Therefore the mechanical properties of resistance spot welded joints in dynamic loading are recognised as important to assess the performance of welded structures.
Dynamic weld tests reveal trends, but the results are often difficult to quantify [Khan *et al.*, 2008]. Dynamic tests are complex (requiring specialised equipment [Den Uijl, 2010]) and tend to be not very reliable and repeatable. Therefore static tensile tests are almost exclusively used to assess weldability [Zhang & Senkara, 2006].
Figure 2.11 shows the relationship between the performance in static and dynamic shear tensile testing of several advanced high strength steels varying in strength, chemical and microstructural composition as well as in thickness. It can be seen that there is a positive relationship between the increase in strength in static tensile testing and the increase in dynamic tensile testing. Figure 2.12 shows the same relationship for static and dynamic peel type tensile testing [Den Uijl *et al.*, 2012a].

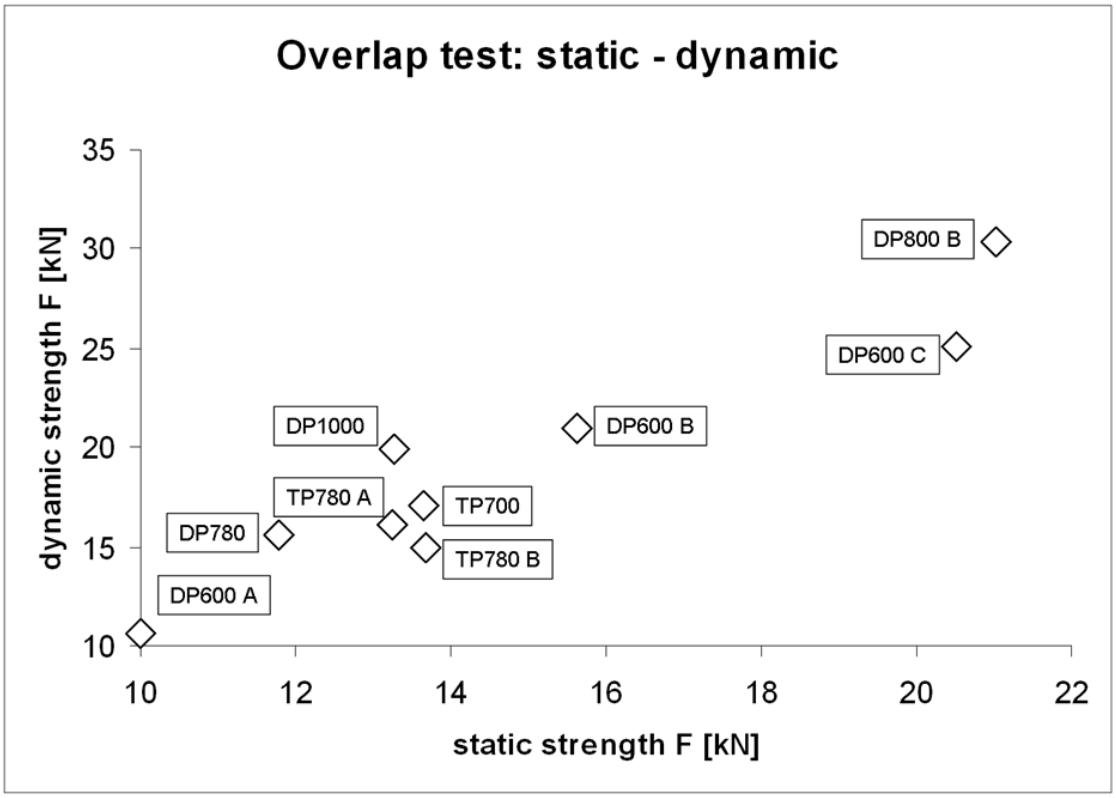

***Figure 2.11: Static and dynamic tensile strength for resistance spot welded joints in several advanced high strength steels tested in overlap tensile tests. Static test were performed with a displacement rate of 10 mm/min. Dynamic tests were performed using a standard drop weight tower* [Den Uijl *et al.*, 2112a].**

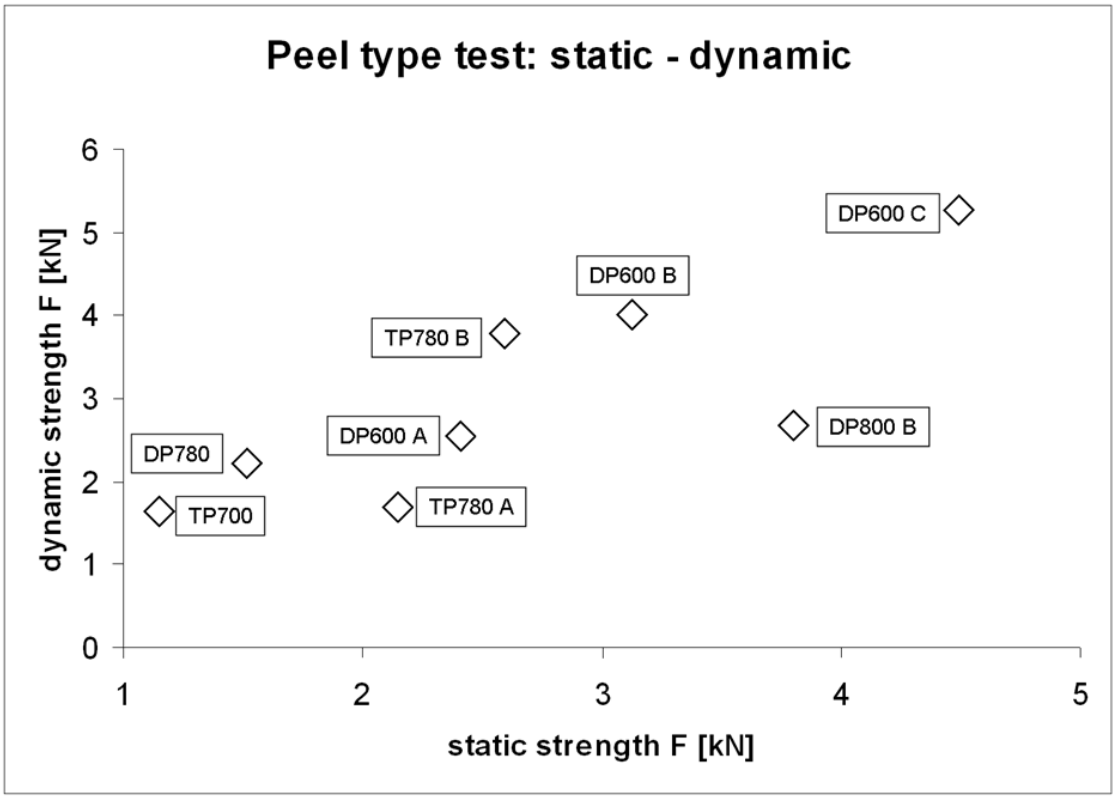

Figure 2.12: Static and dynamic tensile strength for resistance spotwelded joints in several advanced high strength steels tested in peel type tensile tests **[Den Uijl *et al.*, 2112a].**

2.4.5 Failure modes

The weld failure mode gives a qualitative assessment of the weldability of the material. Three types of weld failure mode are commonly defined to classify weld failure of RSW joints [Den Uijl *et al.*, 2008a]:

- full plug failure (see figure 2.13a),
- partial plug failure (see figure 2.13b),
- interfacial failure (see figure 2.13c).

There are gradations of (partial) plug failures which can be detailed in standards [*e.g.* AWS D8.1M:2007].
Full plug failure occurs when the RSW joint itself does not fail (see figure 2.13a). The test specimen fails either in the HAZ or in the base material. Failure in the HAZ occurs when the material strength in the HAZ has been weakened during welding or when the HAZ has grown excessively. Partial plug failure occurs when the RSW joint is affected by failure, but part of the weld nugget has remained intact (see figure 2.13b). Interfacial plug failure occurs when the weld fails along the centre line, essentially separating both sheets without leaving any part of the weld nugget intact.
If full plug failure occurs (especially when failure occurs outside of the HAZ) the weld process did not affect the ability of the material to resist the load. Partial plug failure indicates that the materials ability to resist loading has been affected. The joint has become the weakest link. Partial plug failure can often be attributed to metallurgical effects [Den Uijl & Smith, 2006]. It is often hard to quantify the results, and therefore partial plug failure should be avoided.
The influence of weld failure mode on the overall performance of test specimens with RSW joints can be seen in figure 2.13, which shows examples of cross tension full plug failure,

partial plug failure and interfacial failure. It can be seen that the overall deformation of the test specimen is dependent on the failure mode of the RSW joint. The specimen showing interfacial failure failed at low deformation, indicating decreased absorption of energy during loading. The specimen showing full plug failure failed after much more deformation of the base material, indicating increased absorption of energy before failure occurred.
The safety critical parts of cars depend principally upon their assembled properties and, as a result, welds have to meet the expected design specifications in respect of the application considered. The weld failure mode is important for design of automotive parts. Ideally the weld should not fail in crash testing. The joint should be able to resist the load. As the mechanical characteristics of the base material are often known, or can be easily determined, full plug failure allows for design based upon these characteristics of the material. With the increased use of simulation to design automotive parts, the ability to use the mechanical characteristics of the base material allows designers to accurately predict the mechanical performance of parts with RSW joints. The practice on the shop floor during spot welding quality checking is to refer to the failure type as a quality criterion: plug failure is accepted, interfacial failure is rejected [Bouzekri *et al*., 2010].

Figure 2.13a: Example of full plug failure after cross tensile testing of a RSW joint.

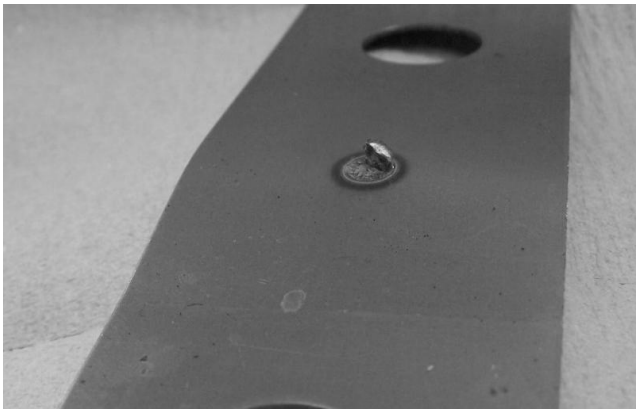

Figure 2.13b: Example of partial plug failure after cross tensile testing of a RSW joint.

Figure 2.13c: Example of interfacial failure after cross tensile testing of a RSW joint.

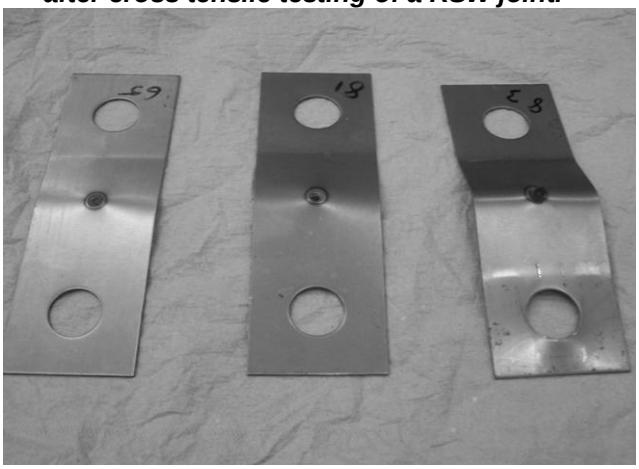

Figure 2.13d: Test specimen with different failure modes. Left interfacial failure, centre partial plug failure and right full plug failure.

2.4.6 Performance Considerations of Weldability

The introduction of advanced high strength steel (AHSS) has enabled the automotive industry to increase the crash performance of cars, without having to increase weight. Thus

contributing to increased safety on the roads and a decrease in the emission of green-house gasses. However issues have been reported on the failure mode of resistance spot welded joints in AHSS [Den Uijl & Smith, 2006, Baltazar Hernandez *et al.*, 2008, Khan *et al.*, 2008 & Lópes-Cortéz & Reyes-Valdés, 2008].

Failure mode

Spot weld failure mode is a qualitative measure of the weld quality (see § 2.4.5). Generally, spot weld failure occurs in two modes: interfacial and (partial) plug failure [Marashi *et al.*, 2008 & Pouranvari *et al.*, 2011]. In interfacial mode, failure occurs through the nugget, while in plug failure, failure occurs by complete (or partial) withdrawal of the nugget from one sheet (see figure 2.14) [*Pouranvari et al., 2007*].

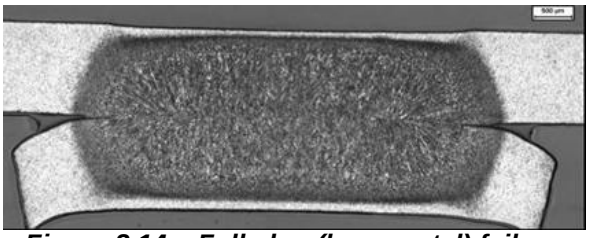

Figure 2.14a: Full plug (base metal) failure

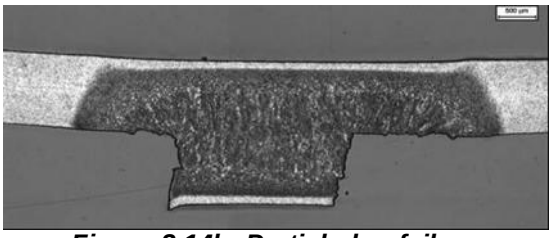

Figure 2.14b: Partial plug failure

When traditional resistance spot welding parameters are applied to advanced high strength steels, interfacial failures and (partial) plug failures can occur. Interfacial failures of spot welds are considered to be brittle and less energy absorbing than plug failures [Mimer *et al.*, 2004]. Load carrying capacity and energy absorption capability for those welds that fail under interfacial mode are much less than those which fail under plug failure mode [AWS D8.1M:2007]. The pullout failure mode indicates that the welds have been able to transmit a high level of force, thus causing severe plastic deformation in adjacent components, and increased strain energy dissipation in crash conditions [Nikoosohbat *et al.*, 2010].

Steel manufacturers perform a series of static tensile test on resistance spot welded joints before they are subjected to full size crash tests [BMW, 2005]. These static tensile tests are also used to gather information on the expected performance of welded joints, during the development stage of materials, where availability of material may be an issue (see § 2.4.4). Although the standardised tests supply a lot of information on the weld failure mode and failure strength of the spot welded joints, these coupon tests cannot completely simulate the complex loading conditions that occur during crash testing [Den Uijl *et al.*, 2008a]. It has been reported that the failure mode depends strongly on the loading mode. Especially in chisel destructive testing, as used on the shop floor of assembly plants this cannot be carefully controlled [Bouzekri *et al.*, 2010].

Figure 2.15 shows the tensile strength of resistance spot welded joints made in HSLA350 and DP600 steel sheet of similar thickness illustrating the differences in levels of strength to failure between different modes of testing [Den Uijl *et al.*, 2008a].

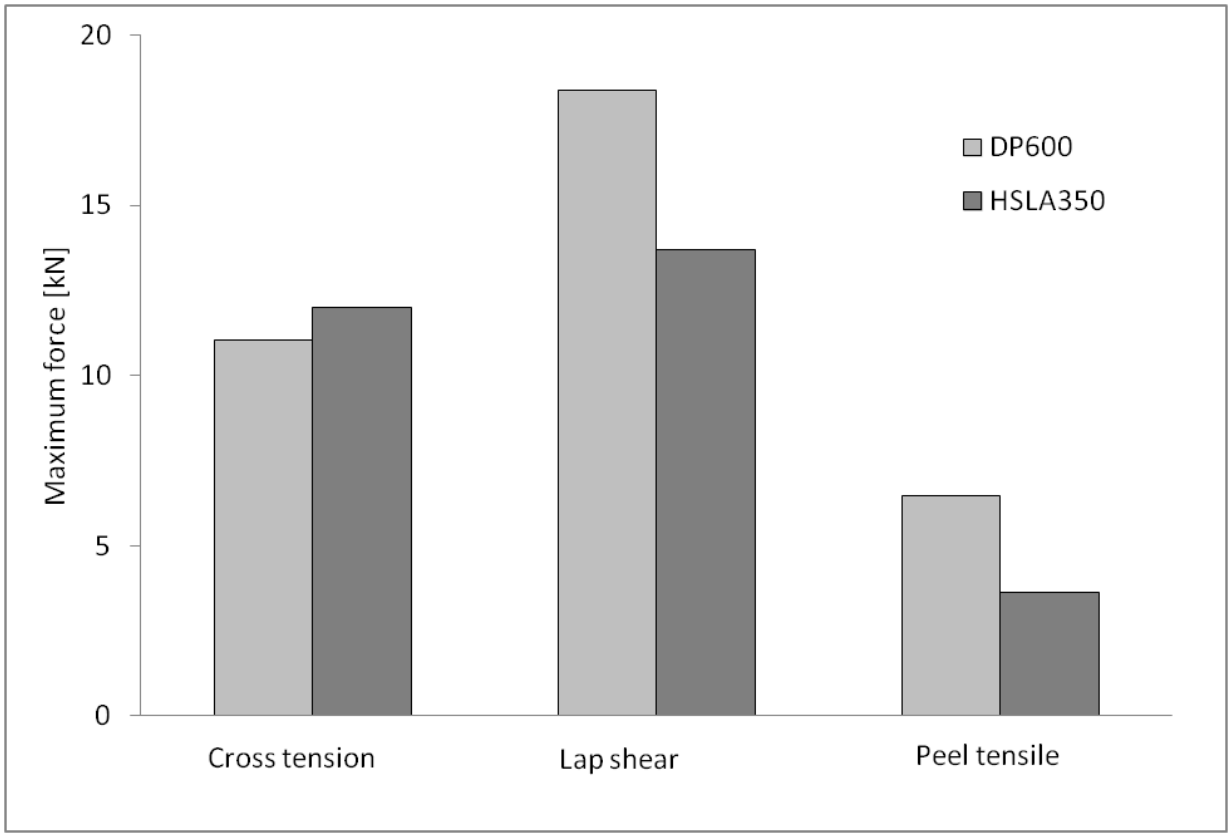

Figure 2.15: Cross tensile, overlap shear tensile and peel test results for RSW joints in 1,4 mm thick GI coated DP 600 and 1,45 mm thick GI coated HSLA 350 steel sheet [Den Uijl et al., 2008a].

Post weld hardness

Literature reports that the issue of undesirable weld failure modes is primarily related to the relatively high carbon equivalent of advanced high strength steels compared to traditional low alloyed steels, coupled with the fast weld cooling rates observed in resistance spot welding. "*The main area of concern when welding HS and UHS steels stems from their relatively high carbon equivalent, coupled with the fast weld cooling rates observed, particularly with resistance spot and laser welding. This can cause high hardness levels and brittleness of the weld, leading to unfavourable fracture modes (partial or complete interface failures) and low cross-tension strength. For resistance spot welding, plug failure is normally a quality requirement in routine destructive tests*." [Westgate, 2004]

Mimer *et al.* [2004] reported that interfacial and partial plug failures can occur when traditional resistance spot welding parameters are applied to AHSS. The interfacial and partial plug failures are considered to be brittle and less energy absorbing than plug failures. Plug failures are considered to be more favourable than interfacial failures because the tensile strength is higher. The interfacial and plug failures are attributed to the combination of fast cooling rates (10^3 to 10^5 °C/s) combined with the modified alloy content (compared to mild steels) that lead to the formation of hard and brittle martensite in the weld and parts of the heat affected zone.

Gould *et al.* [2006] state that martensite, particularly with increasing carbon contents, results in weld zones with hardness levels sufficient to fail in a brittle manner. Marya & Gayden [2005] have drawn the same conclusion. Pedersen *et al.*, 2008 stated that although martensite formation will enhance the tensile strength of the material it degrades its toughness. *"Brittle fracture due to martensite formation is unacceptable in the automotive industry where ductile failure is a safety design parameter."* It was found that hardness levels exceeding 450HV correlate with an increased tendency towards brittle failure through the nugget. This is associated with a large degree of martensite in the microstructure. *"The*

accurate prediction and modelling of the resulting microstructure after resistance welding of AHSS steels has a high priority when designing joints and evaluating the risk of brittle failure mechanisms." [Pedersen *et al.*, 2008]

Attempts have been made to relate weld failure mode directly to post weld hardness and even chemical composition. Studies on High Strength Steels in the 1980s attempted to derive a modified carbon equivalent formula to define weldability, in particular the borderline of potential interface failures, for resistance spot welds. While reasonable correlation was achieved, no universal relationship was found. In addition, there is the question whether a maximum weld hardness value could be specified to define the limit of suitable weldability. Westgate [2004] finds that although hardness levels around 400HV and above are certainly more likely to give interface failure, there appears to be no ideal answer, as material thickness and material type can also have an effect.
Mimer *et al.* [2004] state that generally, welds with hardness exceeding 400-450 HV caused unstable fractures, and interfacial failures were seen in spots with weld hardness exceeding 450 HV. Radaj [1992] even mentions a general desire to aim for degrees of hardness below 350 HV in general in welding. He states that the problem is aggravated by diffusible hydrogen in martensite hardened zones, leading to brittle fracture. In another report [Gould, 1999] undesirable failure modes are attributed to solidification-related porosity which can contribute to the formation of critical sized flaws that can eventually propagate down the faying surface. Harder microstructures then allow easier propagation of these flaws into cracks.

Carbon equivalence numbers

Carbon equivalent numbers have been used now for several decades to compare the weldability of steels with different chemical compositions. Most famous of all is probably the Carbon Equivalent number commonly referred to as the IIW CE number, published in 1967 [IIW, 1967]:

$$CE\ (IIW) = C + \frac{Mn}{6} + \frac{Cr + Mo + V}{5} + \frac{Ni + Cu}{15}, \qquad \text{(Eq. 2.2)}$$

where the element codes (*e.g.* C for carbon) denote their contribution in weight-percentage (wt %) in the chemical composition of the steel.
Over the years steels and their applications have changed considerably. As far as automotive applications are concerned, much higher strength levels are desired to enable manufacturers to reduce weight, whilst maintaining performance (fatigue and crash). The chemical composition and process routes of steels changed as applications posed new demands on the strength and formability of steels.

Carbon equivalent numbers relate the composition of a steel to its weldability, but they themselves are also dependent upon the chemical composition of the steel. The IIW CE number is usually used for steels with carbon levels exceeding 0,18 wt % C, as it was found that other carbon equivalent numbers worked better for steels with lower carbon content. In 1968 Ito & Bessyo published a paper in which a more complete relation was derived to predict post weld hardness of steels containing carbon levels of less or equal to 0,12 wt % [Ito & Bessyo, 1968]. The chemical portion of this formula (P_{cm}) is commonly used as a carbon equivalent number for steels with [C] < 0,18 wt %:

$$CE(P_{cm}) = C + \frac{Si}{30} + \frac{Mn + Cu + Cr}{20} + \frac{Ni}{60} + \frac{Mo}{15} + \frac{V}{10} + 5B, \qquad \text{(Eq. 2.3)}$$

where the element codes denote their contribution in weight-percentage [wt%] in the chemical composition of the steel.

Strictly speaking, carbon equivalent numbers cannot to be used to compare the weldability of steels with different chemical composition, but the hardenability of steels. Weldability is often defined as the inverse of hardenability [Easterling, 1992].

Sheet thickness and weld nugget size

Steel sheet thickness has also been identified as an important factor determining the failure mode, with interfacial failure becoming dominant with increasing thickness [Chao, 2003 & Marya & Gayden, 2005]. Combined with the fact that the load required to cause (interfacial) failure in very high strength materials (e.g. boron alloyed steels) [Tumuluru, 2008 & Larsson *et al.*, 2009], this has lead to the suggestion that load to failure should be considered more important in judging weld quality [Tumuluru, 2008, Larsson *et al.*, 2009 & Bouzekri *et al.*, 2010].
Tumuluru [2008] reported that the load required to cause interfacial fracture was almost 90 percent of the load required to cause button pull out fracture. Therefore it was suggested that the fracture mode should not be used as the sole criteria to judge weld integrity in high strength steels. Instead the load to failure should be considered more important in judging weld quality. For thicker gauges in shear-tension testing of advanced high strength steels interfacial fractures become the expected mode of failure.
The strength of a joint is related to the size of the weld nugget [Chao, 2003, Mimer *et al.*, 2004, Radakovic & Tumuluru, 2008]. Tumuluru [2008] reported that larger welds fail through button pull out, whereas smaller welds generally fail interfacially. Plug failure and interfacial fracture are two competing fracture modes and tensile specimens fail by the mode that requires lower load to initiate failure. Again, for thicker sheets (>1.5 mm), interfacial fractures become the expected mode of failure even at large button sizes. "*A subsized weld may present inadequate strength in overload or crash scenarios and reduced fatigue life under normal operation of the vehicle. An oversized nugget requires large scale welding machinery and is thus of higher cost to fabricate*." [Chao, 2003]
As the weld nugget size is related to the sheet thickness it is not surprising that there is a relationship between sheet thickness and weld performance. Additionally there is a relationship between sheet thickness and other weld process parameters, such as welding time, weld current and electrode geometry, which are all detailed in standards.

Weld defects

Expulsion or splash welding can lead to a decrease in performance of resistance spot welded joints. The ejection of molten material from the weld pool can lead to a lack of material to fill the weld nugget upon solidification. If the electrode force is high enough the weld nugget will be continuous and no cavities or pores will be left after cooling, but the indentation will lead to geometrical deformation. [Kearns, 1980].
Without expulsion large cavities and pores after the formation of an RSW joint can be caused by the solidification of molten material. If the electrodes are released before the weld pool has solidified completely, excessive shrinkage of the material during cooling can lead to the formation of pores. These pores are located where solidification occurs last, usually in the centre of the weld [Kearns, 1980].
It has to be noted that these pores do not need to be detrimental for the weld strength or failure mode. If the joint fails outside the weld nugget, the pores do not contribute to a reduced weld failure strength. Figure 2.16 shows a resistance spot welded joint where the weld centre has been drilled out prior to testing. It can be seen that the joint fails outside of the weld nugget, without reduction of the weld strength [Den Uijl & Smith, 2006]. But if the joint fails in the weld nugget the pores can lead to reduced weld strength.
Depending upon the chemical composition of the material, hot cracking can occur during welding. Carbon, sulphur and phosphorus are known to contribute significantly to the hot cracking susceptibility of a material. Silicon and nickel increase the hot cracking susceptibility too, but to a lesser extent. Manganese, chromium, molybdenum and vanadium reduce the

hot cracking susceptibility of a material [Porter & Easterling, 1986 & Easterling, 1992]. For hot cracking to occur tensile stresses are needed. Stresses occur due to the construction of a work piece and shrinkage due to solidification of molten material. These effects can be countered by the pressure exerted by the electrodes. Early release of the electrodes will increase the possible occurrence of hot cracks [Kearns, 1980].
Hot cracks appear between grain boundaries. If the joint fails outside the weld nugget, hot cracks do not need to be detrimental for the weld strength. During tensile testing the cracks can grow and thus increase the likelihood of joint failure in the weld nugget. Additionally the presence of (micro) cracks can serve as preferential weld failure paths [Gould, 1999].

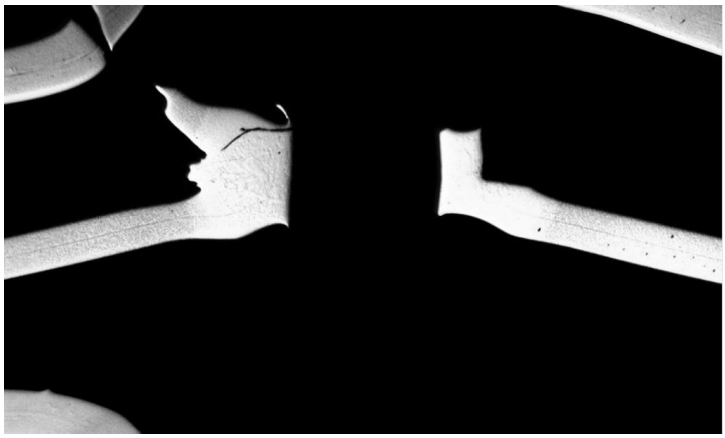

Figure 2.16: RSW joint with centre of weld removed showing failure outside the weld nugget [Den Uijl & Smith, 2006].

2.5 Summary

With the introduction of advanced high strength steels in automotive applications issues arose concerning the resistance spot weldability of these materials, both with regard to the process and on the performance. Reported process issues concern the welding range and the electrode lifetime. Reported performance issues concern the post weld hardness and the failure mode of the joints.
It has been reported that the welding range of advanced high strength steels is limited due to the increased strength levels (and hardness) making it more difficult to join materials together before welding and form a sufficiently large weld nugget. Apart from the high strength of the materials, issues have been reported concerning the electrode force and shape of the electrodes.
The performance of the joints mainly concerns the ability of the welded constructions to absorb energy upon loading. This is evaluated in tensile tests in which the welds are required to withstand a certain level of loading and are required to fail in certain desirable failure modes. Preferably resistance spot welds show full plug failure, *i.e.* the weld remains intact during testing and the surrounding material fails. From the literature it can be concluded that the main cause for the reported decreased ability of resistance spot welds to withstand loads in a desirable way is due to the high post weld hardness, leading to brittle failure.

The development of weld simulation software, specifically when aimed at resistance spot welding, offers tools to investigate the process aspects in more detail. Two software packages especially offer possibilities to support research; Sysweld and Sorpas. Sysweld offers possibilities to investigate the welding process in details such as the metallurgical response of a material on welding operations, but seems somewhat limited when reviewing production aspects such as weld growth curves, the application of multiple materials and geometries. Sorpas is limited in its metallurgical capabilities, but offers possibilities to

investigate different aspects of manufacturing such as weld growth curves, the application of different electrodes and materials and variations thereof. For the research reported in this thesis, Sysweld and Sorpas complement each other.

3. Materials, Measurements & Modelling

3.1 Materials

Standard production materials available at the Product Application Centre IJmuiden Technology Centre of Corus (now Tata Steel) in IJmuiden, The Netherlands were used, unless otherwise noted. The thickness, grade and surface condition are given with each experimental result. The variations in chemical composition for the advanced high strength steels used in this research are listed in table 3.1.

Table 3.1: Range of chemical composition of advanced high strength steels used in this research.

	C [wt%]		Mn [wt%]		Si [wt%]		S [wt%]		P [wt%]	
grade	**min.**	**max.**	**min.**	**max.**	**min.**	**max.**	**min.**	**max.**	**min.**	**max.**
DP600	0.09	0.117	1.44	1.83	0.207	0.378	0.002	0.004	0.016	0.019
TRIP600	0.07		1.46		1.53		0.001		0.160	
TRIP700	0.19	0.25	1.53	1.64	0.079	0.456	0.003	0.006	0.012	0.089
DP800	0.11	0.16	1.64	2.21	0.207	0.255	0.001	0.006	0.001	0.017
TRIP800	0.15	0.23	1.53	1.65	0.457	1.800	0.001	0.005	0.008	0.092
DP1000	0.13	0.16	1.50	2.22	0.250	0.518	0.001	0.003	0.007	0.014
TRIP1000	0.21		1.50		0.40		0.006		0.02	

The materials discussed in section 5.2.2 were cast and rolled at the Corporate Research & Development Laboratories of Sumitomo Metal Industries, Ltd. (Sumitomo Metals) in Amagasaki City, Japan. The chemical compositions of these materials are listed in table 5.1.

3.2 Measurements

3.2.1 Welding

Resistance Spot welding was done at the Joining group of the Product Application Centre of the IJmuiden Technology Centre of Corus (now Tata Steel) in IJmuiden, The Netherlands. Standard welding conditions according to the British Standard BS1140 1993 "*Resistance spot welding of uncoated and coated low carbon steel*" were chosen, as parameters of this type are typical of those used within industry. Whenever other welding conditions were used details are given with the corresponding results. The welding current was 50 Hz AC unless otherwise noted and cooling water was supplied to the electrodes at a rate of 4 l/ min.
Welding operations reported in section 5.2.2 were done at the Corporate Research & Development Laboratories of Sumitomo Metal Industries, Ltd. (Sumitomo Metals) in Amagasaki City, Japan.

3.2.2 Tensile testing

Cross tension testing was done in accordance with Work Instruction AUT JON 002 "*Cross tension testing of resistance spot and embossed projection welds*", and Lap Shear testing in accordance with AUT JON 003 "*Shear testing of resistance spot and embossed projection welds*". Chisel and peel testing was done in accordance with Work Instruction AUT JON 001 "*Chisel and peel testing of resistance spot welds*".

3.2.3 Weld Growth Curves

Weld growth curves were determined in accordance with Work Instruction AUT JON 004 "*Weld growth curve and weldability lobe*".

3.2.4 Metallography and Hardness Measurements

Metallographic investigations were done at the Metallography and Surface Analysis group in IJmuiden. Micrographs were etched with LePera, nital or picral etchant. Vickers hardness measurements were done with a 500 gram weight.
Hardness measurements in section 5.2.2 were performed at the Corporate Research & Development Laboratories of Sumitomo Metal Industries, Ltd. (Sumitomo Metals) in Amagasaki City, Japan using a 9.8 N load.

3.2.5 EPMA/WDX

EPMA (Electron Probe Micro Analysis) and WDX (Wavelength-Dispersive X-Ray Spectroscopy) was done at the Metallography and Surface Analysis group, IJmuiden.

3.2.6 Thermal measurement

The thermal profile of figure 5.16 was measured at the Corporate Research & Development Laboratories of Sumitomo Metal Industries, Ltd. (Sumitomo Metals) in Amagasaki City, Japan.

3.3 Simulations

The use of simulation software in this thesis is primarily to illustrate principles. The exact software package is not of primary importance, as similar results can be obtained from other verified software platforms, especially using multi-physics software or dedicated purpose built solutions programmed in third generation programme languages, such as FORTRAN or C++.
The focus in this thesis is on the interaction between the resistance spot welding process and the materials that are to be joined. As long as the right physical equations and mathematical rules are applied to set up a model, it is unlikely that the results of simulations will differ much, providing that the geometry is modelled correctly and the boundary conditions are applied in the correct manner.
Differences in the results of simulations are then much more dependent upon a correct representation of the materials, especially:

- electrical resistance,
- thermal conductivity,
- mechanical properties (stress-strain relations at varying temperatures),
- surface condition (contact resistance and friction).

In this thesis Sorpas is used as the primary software package. Sorpas is the principal solver in use in industry to simulate engineering problems, such as weld nugget diameter, weld growth curves, welding range and the effect of varying process parameter settings. Sysweld is more suited to simulate the mechanical response of welding operations for further

engineering, such as deformation and residual strains. These are very important for assembly operations and design, but these are not the subject of this thesis.

3.3.1 Sysweld

The spot welding modelling capability in Sysweld is an interface within the larger Sysweld set up. Sysweld itself is based upon SYSTUS, a multiphysics simulation suite for mechanics, heat transfer and electrotechnics, originally developed for use in the nuclear industry. Simulation results from Sysweld can be transported to Assembly, for mechanical analysis of the effects of welding (distortion and residual stresses) on assembly operations.
Sysweld simulations are sequential; the results of thermal simulations are used to calculate the metallurgical and mechanical response of the material to welding operations. Usually a full thermal simulation is first performed (weak coupling), but it is possible to force stronger coupling between thermal, metallurgical and mechanical simulations, in which the different simulation modules are updated after several steps, to more accurately simulate the interaction between different aspects of welding.
Though Sysweld can be used to simulate the effects of welding operations, the thermo-metallurgical and mechanical computations performed with Sysweld do not amount to true welding process simulation. It is, for instance, not possible to simulate fluid flow within the molten weld pool.
The spot welding interface does get close to simulating welding operations, as there is no arc, laser beam or filler wire that needs to be modelled for accurate welding process simulation. The interface couples the electromagnetic, thermal, metallurgical and mechanical modules available in Sysweld.
For accurate simulations it is necessary to calibrate for a specific problem. This is especially important when simulating arc and beam welding processes, where the geometry of the weld pool needs to be calibrated to accurately simulate the interaction between the arc or beam with the surface. In spot welding, this is less important, though verification of the simulation results against experimental results is always a prerequisite to ensure that the results are valid.

Sysweld provides a database in which material information is given. The material properties, as functions of temperature and phase, are grouped in two separate input files. The thermal data file contains the thermal conductivity, density and specific heat. The mechanical data file contains the modulus of elasticity, Poisson's ratio, the yield strength, stress-strain curves and thermal strains.
The thermal strains, depending on the temperature field and changes in the microstructure, serve as the input for structural simulations as performed by the Assembly module.
The material data are listed for different phases. In general, ferrite, martensite and bainite are given similar values, whilst the values for austenite are different from these. Above ~900°C the material data are considered to be more important for numerical behaviour than for physical response and values for similar steels are considered the same. At higher temperatures the material history is removed to accommodate the effects of melting.

The thermo-metallurgical simulations are based on CCT diagram curves. Phase composition is calculated as a percentage, again the simulations are not true weld process simulations and it is not possible to simulate local solidification *et cetera*. As the thermo-metallurgical computations are performed after thermal simulation, the phase transformations do not affect the thermal calculations.

The spot welding interface requires input data specific for spot welding processes. These can be divided into four groups:

- the geometry of the electrode (see figure 3.1),
- the number and geometry of the metal sheets (see figure 3.1),
- the contact resistances,
- welding process parameters.

The geometry of the electrode is defined by the electrode curvature and radius, the height of the electrode (h2 in figure 3.1), the distance between the electrode tip and the internal cooling surface (h1 in figure 3.1) and the internal and external radii. Based on the input data an electrode mesh is automatically generated. It is possible to use a user-defined electrode geometry and mesh, but this requires some effort by the operator.
The number of sheets that are to be joined is limited to four. This is sufficient for simulation of resistance spot welding operations in automotive manufacturing, which seldom exceed three sheets. If necessary the input file generated by the interface can be manually adapted to a total of nine sheets. Each sheet is defined by its thickness, which can be separately defined. It is not possible to define different lengths of sheets. Additionally two contact zones can be defined. These are automatically generated by the interface, but can be manually adapted in the input file generated by the interface. Each sheet can be defined as a separate material.
The contact resistances are defined in a function-file containing definition of the different thermal and electrical contact resistances: for the electrode-sheet contact and the sheet-sheet contact. It is not possible to define different contact resistances when multiple sheets of different materials are used.

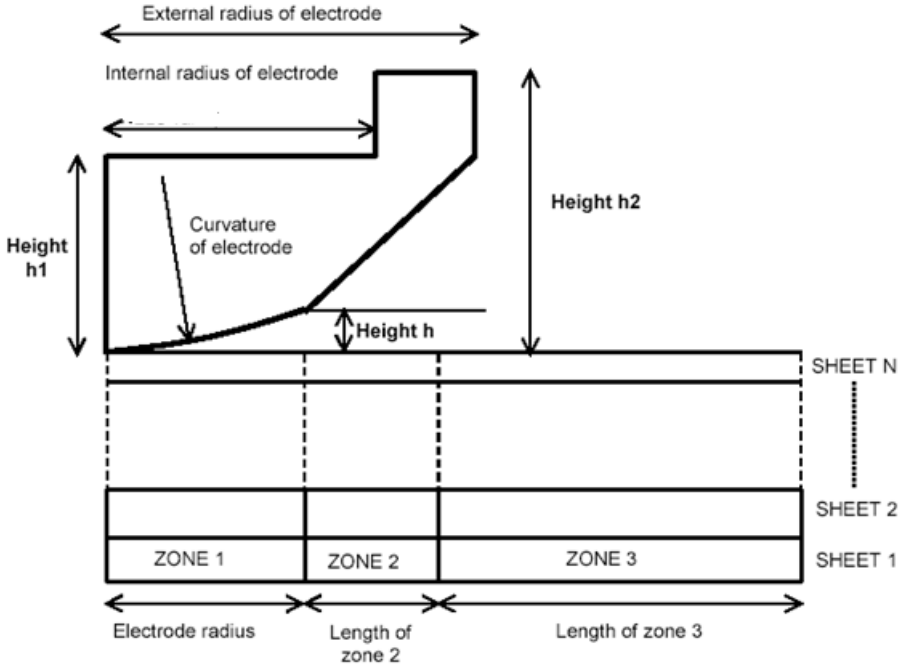

Figure 3.1: Geometrical definition of spot welding process in Sysweld [ESI, 2009].

The welding process parameters are the current, the frequency of the current, the number of current pulses, the electrode force (“squeeze force”). Additionally it can be specified whether weak or strong coupling is to be used. This is not so much a welding process parameter, but a simulation parameter. If strong coupling is selected, the coupling frequency is to be defined in the process input file.

Figure 3.2 shows the result of a Sysweld simulation. The simulation concerns a single weld made in two sheets of steel. The results give the weld pool nugget size, temperature profile,

indentation and deformation of sheets. The maximum temperature is also listed, but as soon as melting occurs (*i.e.* the temperature exceeds 1450 °C) this value is to be distrusted. Sysweld does not take fluid flow into account and therefore cannot accurately calculate the temperature in the molten weld pool.

Figure 3.3 shows the metallurgical composition varying with time, both in the weld and in the heat affected zone. These graphs are the result of the metallurgical post processing, that can be performed after the thermal computation is complete.

It is important to realize that the aim of the spot welding interface is to provide input for the Assembly module, not the simulation of resistance spot welding operations *per se*. As such there is no capacity to determine weld growth curves, or weldability lobes automatically.
The coupling between the spot welding interface and the Assembly module is based on the local-global approach, in which the local effects of welding operations, deformation and residual stresses, are transferred from the spot welding interface to the Assembly module. The metallurgical changes are not transported.

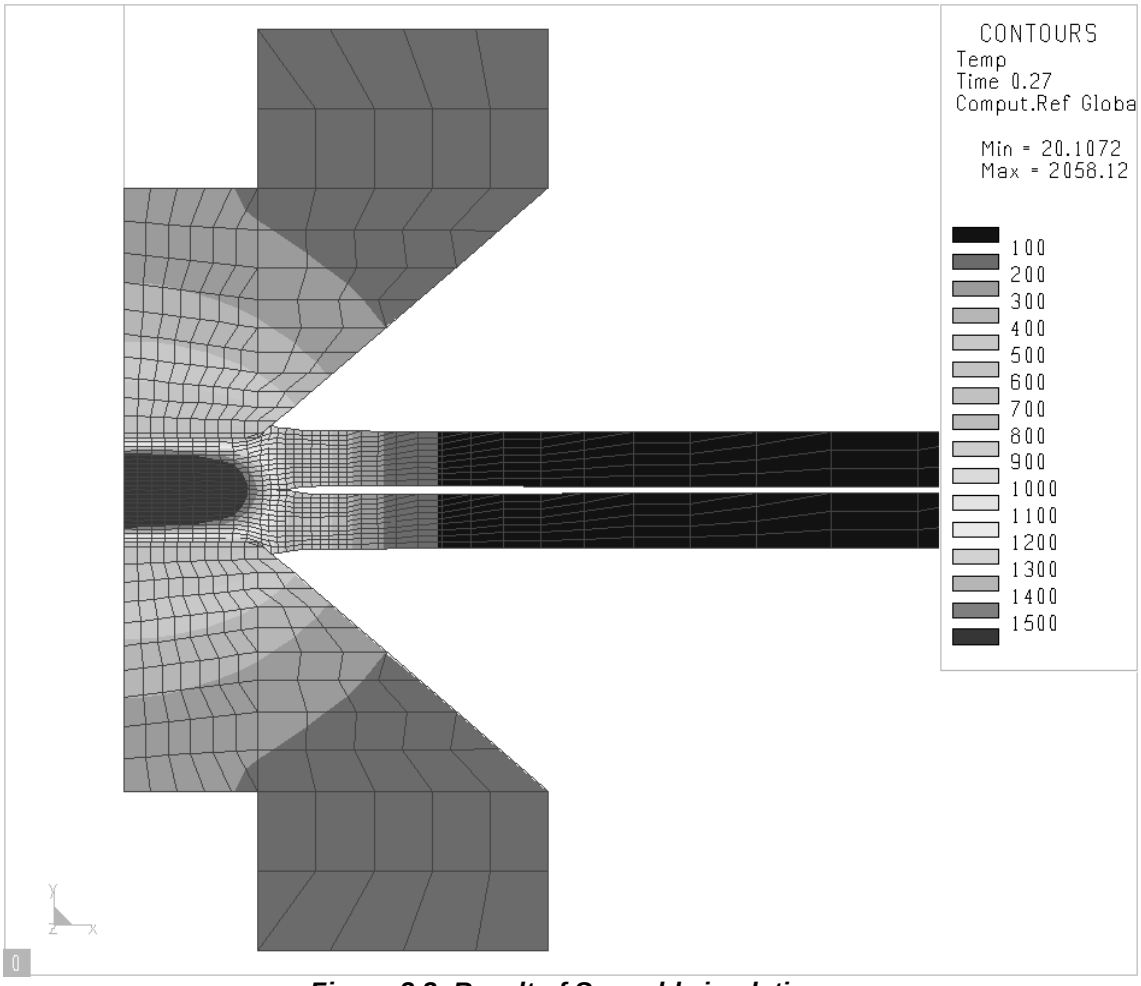

Figure 3.2: Result of Sysweld simulation.

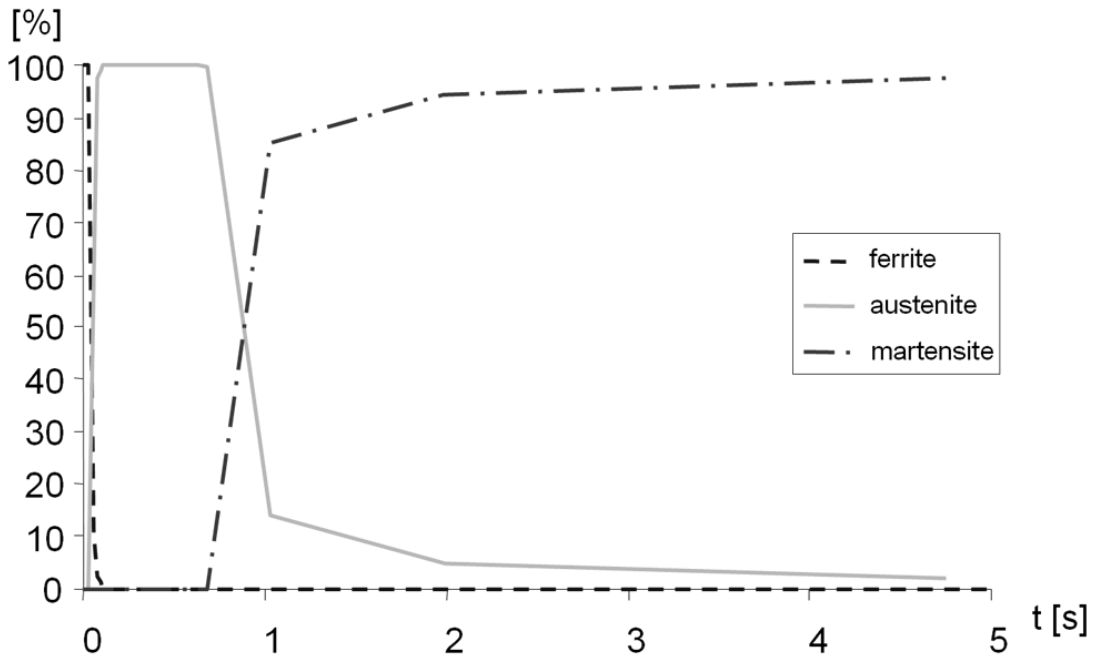

Figure 3.3a: metallurgical composition varying with time in the weld pool.

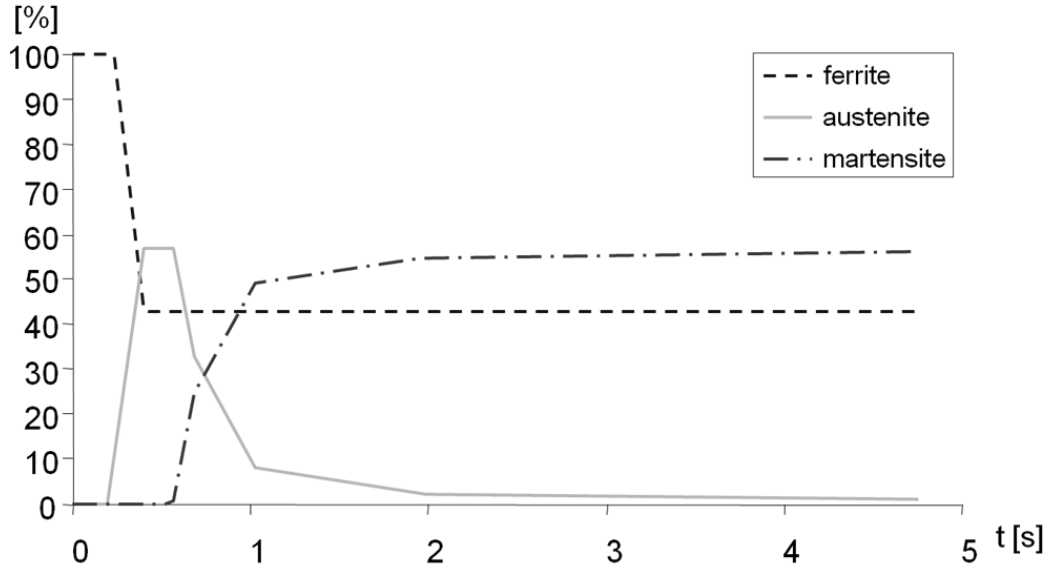

Figure 3.3b: metallurgical composition varying with time in the heat affected zone.

3.3.2 Sorpas

Sorpas has been developed based on research done at the Technical University of Denmark. Sorpas is a finite element analysis tool, used to simulate resistance spot welding and projection welding. It is tailor made for this purpose and cannot be used to simulate other welding processes.

Sorpas comes with three integrated databases: a material database, an electrode database, and a work piece database. The material database contains material properties as functions of temperature. The materials in the database are not just those for the sheets that are to be joined, but also the materials for the electrodes and the coating layers. These materials can be assigned to any distinct piece of geometry in the model set up, as they are not dedicated

to a single application. Material data can be easily manipulated and new data can be added using the graphical interface
The electrode database contains all standard electrodes as described in ISO standard 5821 [2007] (see figure 4.22). The pre-defined geometries can be adapted using the graphical interface. The interface can also be used to define user-specific geometries.
The work piece database contains predefined work piece geometries as well as the geometry of the contact layers that are numerically necessary for simulation. The work pieces are not just for resistance spot welding, but also for projection welding. Again the geometries can be manipulated using the interface and user-defined geometries can be added.

Simulations are set up using a graphical user interface that is used to define the welding process parameters. This is done in three steps for resistance spot welding:

- definition of geometry,
- definition of welding parameters,
- definition of simulation goal.

Additionally it is possible to manipulate the numerical parameters for simulation.
The definition of geometry addresses the electrodes, the sheets, and the coating layers. The electrode geometries are derived from the electrode database, and the electrode materials form the material database. It is possible to choose different top and bottom electrodes. The number of sheets that are to be joined is defined and for each sheet a thickness, a material and a possible coating layer is assigned. It is possible to vary all these parameters for each individual sheet. It is also possible to specify a different width for each sheet. The sheet geometry comes from the work piece database and the material parameters for the sheets and the coating layers come from the material database. The contact layers are automatically added by the software.
In the definition of the process parameters the number of welding steps is defined. For each step the welding current, duration and frequency (AC or DC) are specified. Between welding steps, pauses can be defined and after welding, a cooling stage, in which the electrodes are in contact with the sheets but no current is supplied, can be included. Additionally a pre-welding squeeze stage, in which the electrodes are in contact with the sheets and an additional cooling stage, in which the electrodes are not in contact with the sheets can be defined. The electrode force can be specified for each welding step individually. It is also possible to specify the welding apparatus, with different mechanical characteristics (stiffness of the construction).
In the simulation goal parameters are provided for the simulation of a single weld, a weld growth curve (varying welding current), the automated optimisation of weld current (to produce a weld of pre-defined size), or a weldability lobe (varying welding current and process time or electrode force). These parameters are used to generate a batch of input files that will be run in sequence, each serving as input for a single simulation. The batch file is then used by the software to compile a curve or graph from the individual simulations. The advantage of this approach is that each individual file can be reviewed after simulation to investigate the influence of process settings on the results of an individual weld. Additionally individual files can be manipulated to vary process parameters settings for individual simulations of welds.
Manipulation of numerical parameters requires some understanding of the finite element method, and is discouraged for “standard” simulations, as they can greatly influence the results. However it is possible to vary the number of elements and the thickness of contact layers using the graphical interface.

The output generated by the software comes primarily in the form of parameter curves and animated distributions. Parameter curves can be generated for current, power, resistance, electrode force, temperature, weld nugget diameter, weld nugget volume, displacement of

the electrodes, and weld nugget size. Resistance can be shown for different parts of the configuration and temperature profiles can be generated for different points within the configuration. These curves can be generated individually or in simulation reports.
Figure 3.4 shows a simulation report generated after Sorpas simulation. In this case the simulation is of a single weld with post weld heat treatment. The report shows the process parameters and the temperature curves for two different points in the sheets, one in the centre of the weld and one at the edge of the weld nugget. The report also shows the temperature profile after the entire cycle.

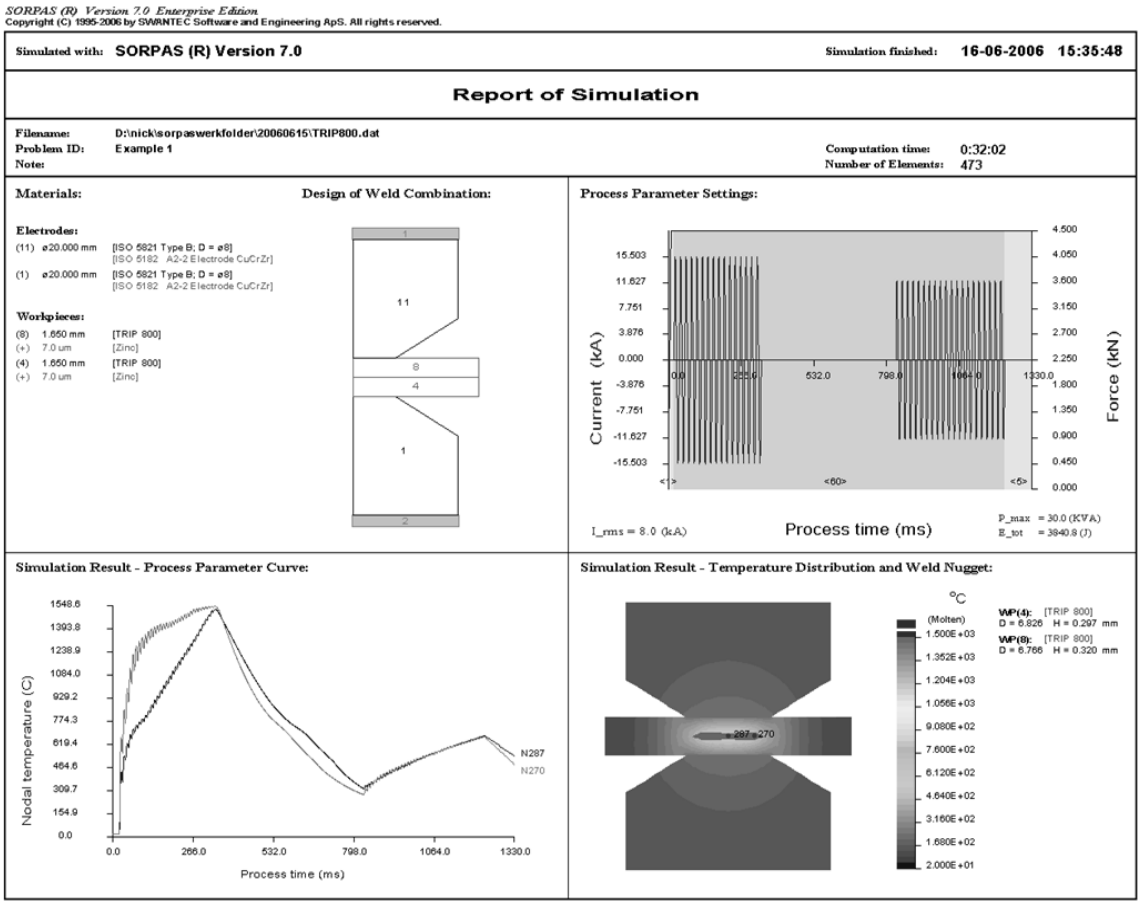

Figure 3.4: Simulation report of a weld with post weld heat treatment generated by Sorpas.

Animated distributions can be generated for the voltage/potential, current density, temperature, rate of change of temperature, mechanical strain, and mechanical stress. Individual time steps of the simulation can be investigated in more detail, producing profiles at specified times during welding.
The results of several simulations produced from a batch file can be compiled in weld growth curves and weldability lobes. These can be generated individually or in simulation reports. Figure 3.5 shows a weld growth curve generated by Sorpas.

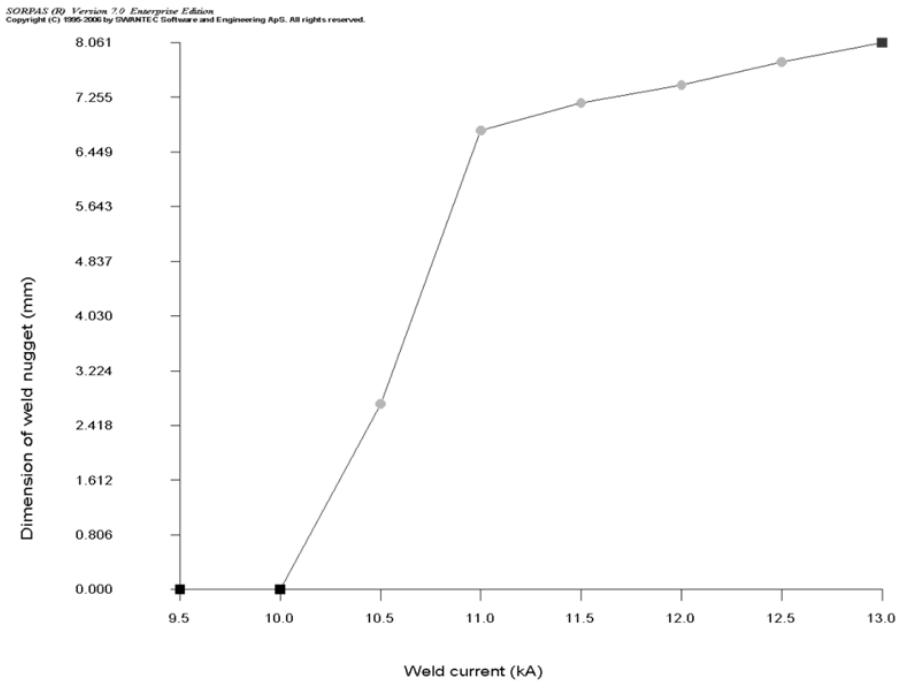

Figure 3.5: Weld growth curve generated by Sorpas.

Though both Sysweld and Sorpas have been developed to be used within the limited scope of process settings for which the software was designed, it is possible to use the software for analysis of effects of welding in a wider context, incorporating effects such as shunt welding. In the case of Sysweld it is possible to manipulate the input files for simulation generated by the interface. In Sorpas it is possible to manipulate the predefined databases and the numerical settings for this purpose. Figure 3.6 shows the results of the simulation of welding of a three sheet configuration with a shunt weld done with Sorpas. The addition of the shunt weld required manipulation of the work piece database, contact layer geometry and numerical parameters to produce a set up as shown in figure 3.7.

In this thesis the primary focus is on the formation of resistance spot welded joints in advanced high strength steels for automotive applications. It is the materials response that is the main area of interest, not the process of resistance spot welding itself.

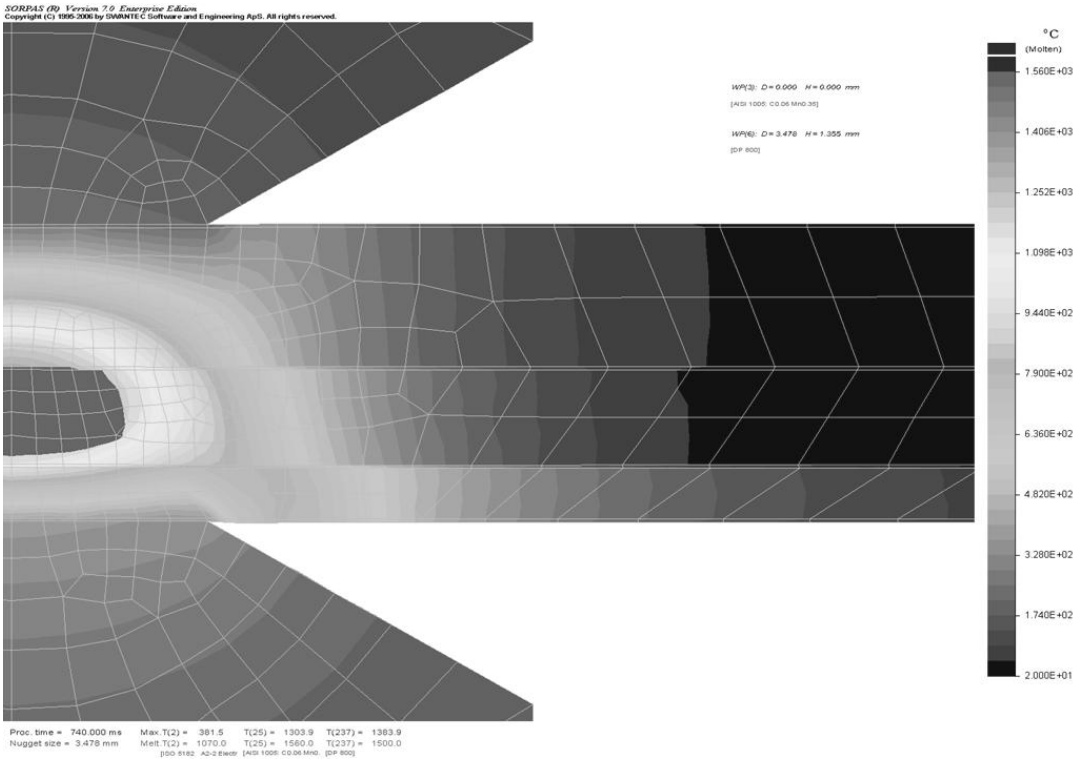

Figure 3.6: Result of simulation of resistance welding of a three sheet configuration with shunt weld [Den Uijl, 2010].

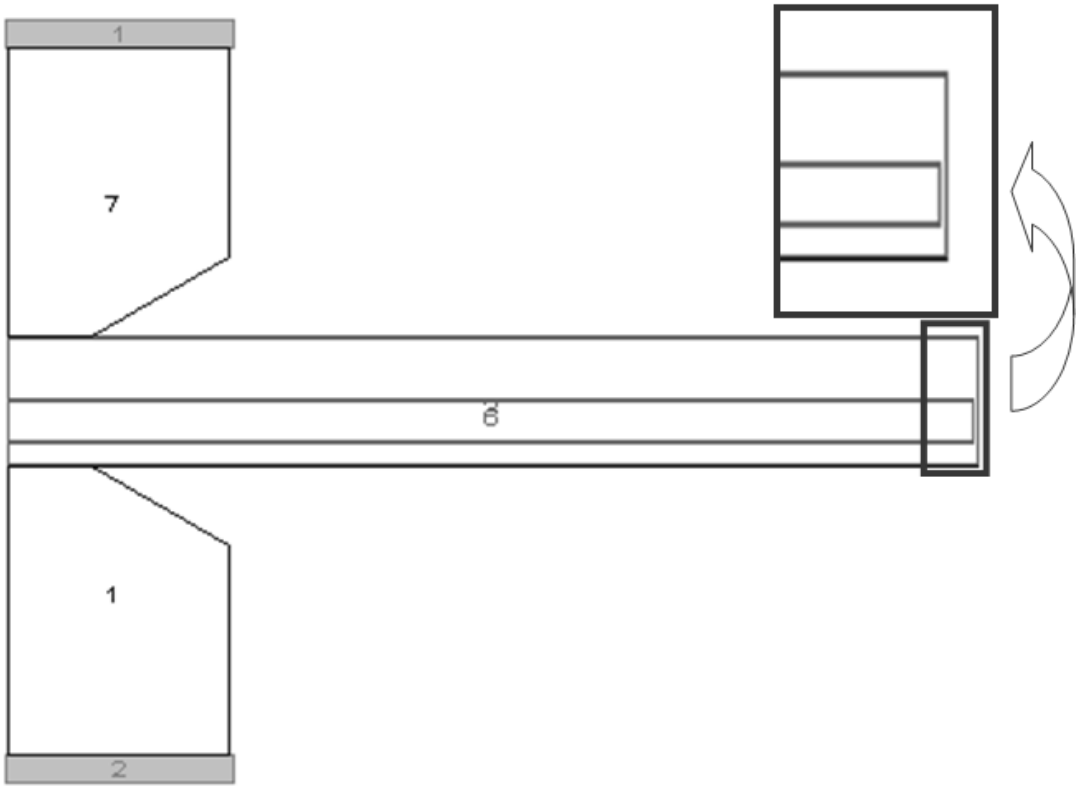

Figure 3.7: Geometrical definition of a three sheet configuration with shunt weld as used for the result depicted in figure 3.6 [Den Uijl, 2010].

4. Weldability in Manufacturing

4.1 Introduction

In this chapter manufacturing aspects of the weldability of advanced high strength steels are addressed. There are two main topics of discussion:

1. The influence of material characteristics on weldability.
2. The influence of electrode geometry on weldability.

The first topic relates to differences in the materials due to their chemical composition and thermomechanical treatment during production, the second relates to the issue of electrode types used in production and the degradation of electrodes leading to possible reduced electrode lifetime.

The data reported in this chapter has been published at various conferences and seminars. Work on the influence of material characteristics on weldability has been presented in 2008 at the 17th International "*Computer Technology in Welding and Manufacturing*" Conference in Cranfield, United Kingdom (*Thermal and electrical resistance in resistance spot welding*; Den Uijl, 2008), in 2010 at the 6th International Seminar on Advances in Resistance Welding in Hamburg, Germany (*Resistance spot welding of a complicated joint in new advanced high strength steel*; Den Uijl, 2010), and in 2010 at the M2i Conference "Materials to Innovate the Industry in Noordwijkerhout, The Netherlands (*Material data for weld modelling*; Den Uijl, 2009. Work on the influence of electrode geometry on weldability has been presented in 2007 at the 3rd JOIN Conference "*International Conference on Total Welding Management in Industrial Applications*" in Lappeenranta, Finland (*The influence of electrode geometry on resistance spot welding of advanced high strength steels for automotive applications*; Den Uijl & Smith, 2007).

4.2 Material characteristics

Simulations offer the opportunity to evaluate the influence of material parameters individually. In experiments, variations in one material characteristic cannot always be evaluated separately from others. Material strength is, for instance, coupled with the contact surface resistance, and thermal conductivity is coupled with electrical resistance. In fact the materials strength and contact resistance as well as the thermal and electrical conductivity are coupled by the chemical composition and subsequent thermomechnical treatment. Especially when commercially used materials are evaluated, as they are in this thesis, the issue becomes more complicated, as industrially applied materials vary in more than one aspect; thickness, coating layers, production routes, *et cetera*; all have an influence. The surface contact resistance for instance is not just dependent on the material strength (determining the true contact area), but additionally there are the coating layers (uncoated, GI or GA) to be considered as well as oils, passivation layers and contamination.

When evaluating the influence of material characteristics on the results of resistance spot welding operations there are also more fundamental issues to be addressed. The definition of the model in finite element terms can influence the accuracy of the predictions of the model as well. As this thesis is primarily concerned with the use of commercially available software to support the application of resistance spot welding of advanced high strength steels for automotive applications, care should be taken not to use "fiddle factors" in the model to achieve excellent simulation results that do not bare any relation to physical reality. In fact it is preferably not to change things that would not be changed in practice.

There are three main concerns with this:

- Firstly one could be tempted to use software that is not designed to be used for a specific application. Although a fitting result may be obtained, this would be meaningless, as the model was not designed for the specific application, and its use would thus be an extrapolation form its design. The resistance spot weld model in Sysweld is designed to evaluate the thermomechanical response of a material to a single spot weld operation and to evaluate the impact of resistance spot welding operations on manufacturing, especially mechanically (such as in assembly). It is therefore a comparatively crude tool to evaluate possible welding ranges for the work shop floor (for which Sorpas is better suited).
- Secondly the observed amount of experimental spread in resistance spot welding would make it possible for any simulation to fit carefully selected data. By changing the model set up for a specific situation, this would make it unusable for other situations. It is wise to distrust any result in simulation that matches an experimental result and is then used to make predictions about the expected result using different process parameters. This is especially true for resistance spot welding. The choice to use weld growth curves to validate material model representation in this thesis is specifically made to avoid this trap.
- Thirdly there are parameters that can be comparatively easily changed in the set up of a simulation, but do not have any real physical meaning. An example is manually changing the mesh density. Though changes in mesh density will affect the result of simulation (finite element theory predicts better results with increasing mesh density), this would be highly impractical, primarily because it would require the operator to adjust a non-logical parameter, but also because an increase in mesh density would lead to an increase in calculation times, making simulation a cost inefficient tool.

It is therefore advised to define materials by adjusting the properties that directly relate to material characteristics in the set up of the model. Four characteristics have been identified as playing a significant role in theory:

- material strength,
- (surface) contact resistivity,
- (bulk) electrical resistance,
- (bulk) thermal conductivity.

Admittedly other factors could also be significant; *e.g.* solidus and liquidus temperatures would play a large role in determining the size of the molten weld pool. However in the range of materials discussed here, these should not play a large role and certainly not one that would exceed the influence of the models numerical set up (especially mesh density). If the differences are considered to be large; *e.g.* comparing a low carbon steel with a stainless steel, these should be taken into account first before all other factors; however, that is not the subject of this thesis. Local solidification regimes play a role in the mechanical performance of resistance spot welds, but these cannot be captured in finite element simulations (due to the continuum requirements).

In this chapter the role of the four material parameters defined above is evaluated. In the case of the contact surface resistivity the numerical definition is related to the finite element approach, as a surface effect is represented by a volume effect; therefore an assessment of the influence of the numerical definition is significant.
The results of this chapter can be used in two main ways:

- first to evaluate the possible development of materials aimed at certain weldability aspects,

- secondly to optimise material definition for simulations without having to measure material data for each individual batch of material that is to be used (saving time and costs) by allowing the operator to adjust a verified set of material data to fluctuations in known parameters (such as variations in chemical or microstructural composition or the presence of certain surface “pollutants” such as coating layers).

Additionally the aim is to give insight into the influence of various parameters individually, that may not be separated easily in experiments.

4.2.1 Material Strength

High strength steels have been used for automotive applications for decades. They are primarily used for parts where increased strength is needed. Increased strength can be desired for several reasons:

- to improve fatigue resistance,
- to improve crash performance,
- to reduce weight.

Resistance spot welding of AHSS compared to traditional forming steels is typified by smaller welding current ranges, lower splashing currents and smaller maximum weld diameters. This relationship is shown in figure 4.1 where two GI coated automotive steels were welded using the same parameter settings; a 280 MPa interstitial free steel and a 700 MPa AHSS were compared.
If the welding current ranges are defined as in typical automotive standards, from a spot weld diameter of $4\sqrt{t_s}$ to splash, the 280 MPa steel has a welding current range of 1,10 kA and a maximum weld diameter of 6.55 mm. The 700 MPa steel has a welding range of 0.70 kA and a maximum weld diameter 5.4 mm. A further very obvious difference between the two steels is that much less current is required to weld the 700 MPa steel. Possible factors influencing this are:

1. Higher electrical resistance at all contact interfaces (electrode – sheet and sheet – sheet) as a result of the high strength materials resistance to deformation, the issue of contact is discussed in more detail in section 4.2.2.
2. The higher electrical resistance and lower thermal conductivity of the material, as a result of alloying and micro-structural factors needed to achieve the higher tensile strength. This is discussed in more detail in section 4.2.3.

Material strength also affects the electrode lifetime; *i.e*., the number of welds that can be made within an acceptable welding range before the surface needs to be restored. The electrode lifetime decreases with increased strength levels because the electrode will be deformed more by harder materials. Typically applied approaches to the welding issues posed by AHSS are usually to alter the welding process parameters such as “weld time” and “electrode force”. Very little work has been performed looking at the influence of electrode geometry. This is discussed in section 4.3.

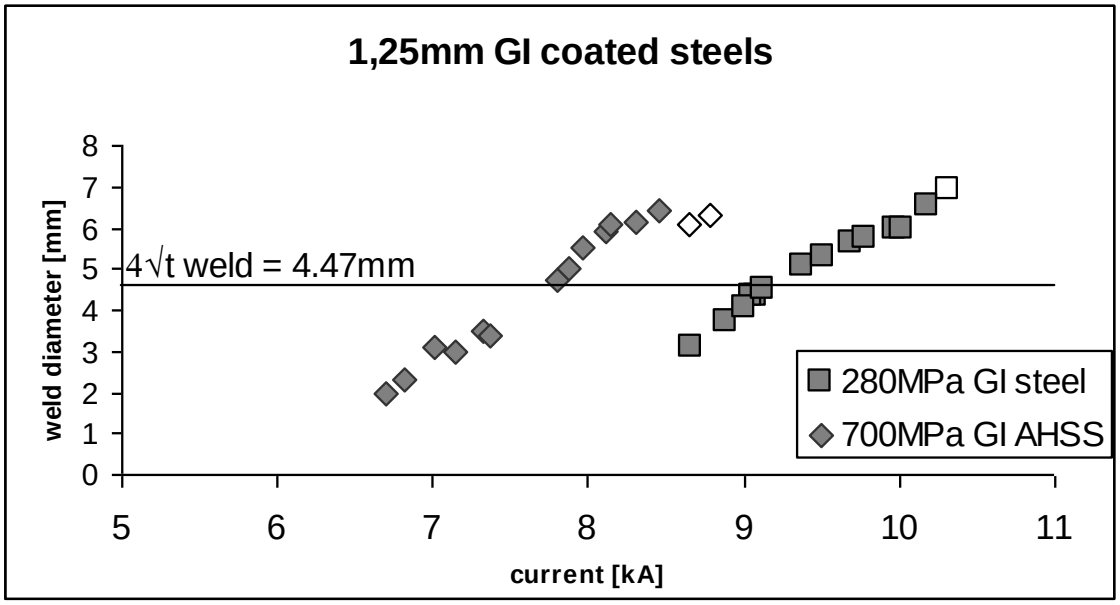

Figure 4.1: Experimental weld growth curves of 280 MPa and 700 MPa GI coated steels using identical welding parameter settings: B type electrode (5 mm tip diameter), 4.5 kN force, 20sq 10w 5h

Material strength is a complicated issue, especially in a non-static situation like resistance spot welding with varying loading conditions, deformation, changing temperatures and phase transformations. Standard available models to describe material behaviour, such as Tresca and Von Mises, are limited in their applicability to describe deformation as they do not take into account the effects of temperatures and phase transformations. More complicated models have been developed to describe material behaviour, but as they use more parameters to describe plastic behaviour of materials (*e.g.* measurement in several directions or at varying temperatures) they require extensive sets of measured data to fully utilise the descriptive power of the models. This makes them less suited for simulations in which the results of mechanical simulations are not the main aim.
For example the Bergström-van Liempt model [Van Liempt *et al.*, 2002] takes the effects of deformation rate and thermal influences into account (Eq. 4.1). The model requires a lot of parameters to be determined. However, even this model does not take into account phase transformations, thus lacking in a fundamental aspect of welding metallurgy.

$$\sigma_y = \sigma_0 + \Delta\sigma_m \left[\beta(\varepsilon + \varepsilon_0) + \left\{1 - e^{-\Omega(\varepsilon+\varepsilon_0)}\right\}^n\right] + \sigma_0^* \left[1 + \left(\frac{kT}{\Delta G_0}\right) ln\left(\frac{\varepsilon^*}{\varepsilon_0^*}\right)\right]^m, \qquad \text{(Eq. 4.1)}$$

with:

σ_0	static yield stress,
$\Delta\sigma_m$	strain hardening stress increase coefficient,
β	large strain hardening coefficient,
Ω	low strain hardening exponent,
ε_0	strain from previous deformation,
n	strain hardening exponent,
σ^*_0	dynamic flow stress coefficient,
ΔG_0	activation enthalpy,
m	strain rate behaviour exponent
k	Boltzmann constant,
T	absolute temperature,
ε^*	thermally activated strain rate.

In how far an exact representation of the mechanical response to welding is important for the results of simulations is very much dependent upon the goal of the simulations. If welding processes are simulated with the objective to use the outcome for further engineering analysis, as in the case of assembly operations, the deformation of the material around the weld is of primary importance to the applicability of the results of the simulations. If the goal of the simulation is to assess the process window of the welding process, then the importance of an exact representation of the mechanical response has to be evaluated only in so far as it has an effect on a possible larger contact area between sheet and electrode.
Further refinement of these complicated relations may give an accurate representation of the material behaviour, but may be far too cumbersome to employ for simulation. The amount of data that needs to be gathered to accurately represent a material, increases costs of the model set up, while the gain in accurate simulation results may be conceived to be limited, although this is dependent upon the stated aims of the modelling effort.

Simulations

In Sysweld, materials are described as the sum of the constituent phases. The response of bulk material is made up from the relative contributions of the different phases. The exact representation of the behaviour of the different phases is a difficult issue, as it is almost impossible to measure stress-strain curves for single phases in materials that have been specifically designed to be multi-phase materials. In fact the curves will be drawn up from approximate measurements, corrected by educated guess work. This is not necessarily a problem, as the major contributor to the overall deformation around a weld is caused by solidification shrinkage (which forms the basis of the weld planner functionality of Sysweld), and this is often found to be sufficient to describe the response to welding operations for engineering purposes.
In Sorpas a relatively simple model is therefore used to represent the material behaviour under varying loading conditions:

$$\sigma = C(B + \varepsilon)^n \left(\frac{d\varepsilon}{dt}\right)^m, \qquad \text{(Eq. 4.2)}$$

with:

- σ the stress,
- ε the strain,
- C coefficient corresponding to $\Delta\sigma_m$ in the Bergström-van Liempt model
- B constant corresponding to strain from previous deformation
- n strain hardening exponent,
- m strain rate exponent.

The values for C, B, n, and m are supplied in a table for various temperatures.

Figure 4.2 shows two different representations of the stress strain curves for TRIP 800 in the Sorpas material database. The material labelled as “old” is the representation as given in the original materials database as supplied in the Sorpas software, whereas the material labelled as “new” is the representation as offered in more recent versions of Sorpas. Both are based on measurements conducted at the laboratories supplying data for the Sorpas material database. The differences reflect developments in AHSS metallurgy and measurement and representation thereof. Both are thus valid data, but the differences in representation of measured data affect the outcome of welding simulations, as can be seen in figure 4.3.

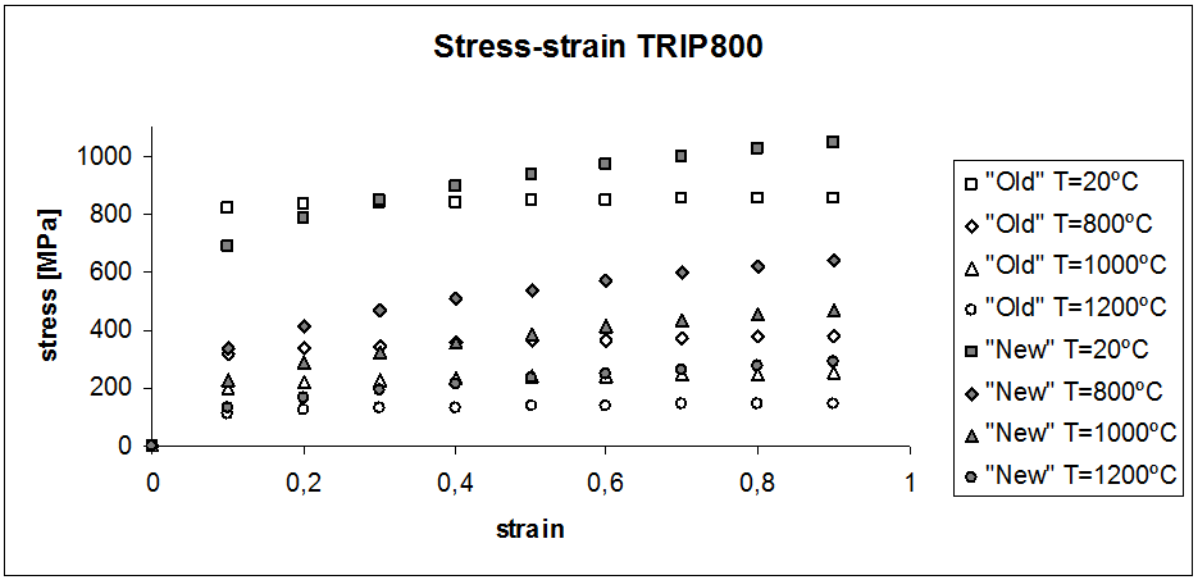

Figure 4.2: Different representations of stress strain relations for TRIP800 in Sorpas. Strain rate = 10.

Figure 4.3 shows simulation results for the weld growth curve of TRIP800, with both stress strain tables. It can be seen that there is an influence, which is predominantly apparent at lower current levels. At higher current levels the effect is limited. The variation is not so much in the weld nugget size prediction at higher welding currents but in the welding range. It is important to realise that the new representation of TRIP materials involved a change in the table for stress strain relations, but not in any other data (*e.g.*, electrical or thermal resistivity). This result shows that accurate determination of the stress strain curves at various temperatures for the assessment of weldability of materials is important.

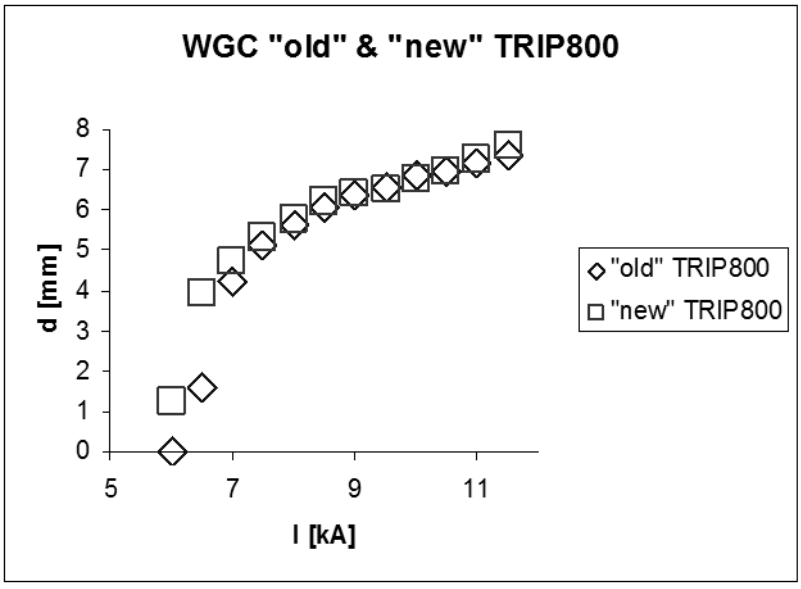

Figure 4.3: Simulation results for the weld growth curve of TRIP800 using "old' and "new" stress strain data. Simulations done with Sorpas.

If the representation of strength levels for a material of similar strength is important, this is even more pronounced when the overall strength of the material is changed. Figure 4.4 shows the simulation results of TRIP steels with varying strength levels (with other material data constant). Figure 4.5 shows similar results for DP materials (with other material data differing from the TRIP materials, but constant for the DP materials) It can be seen that

increasing strength levels shift the onset of formation of welds to lower currents. As stronger materials deform less, the contact area between electrodes and sheet material is increased less, leading to a higher current density and less heat conducted away from the material. Thus more heat is generated and accumulated, leading to material melting and weld formation.

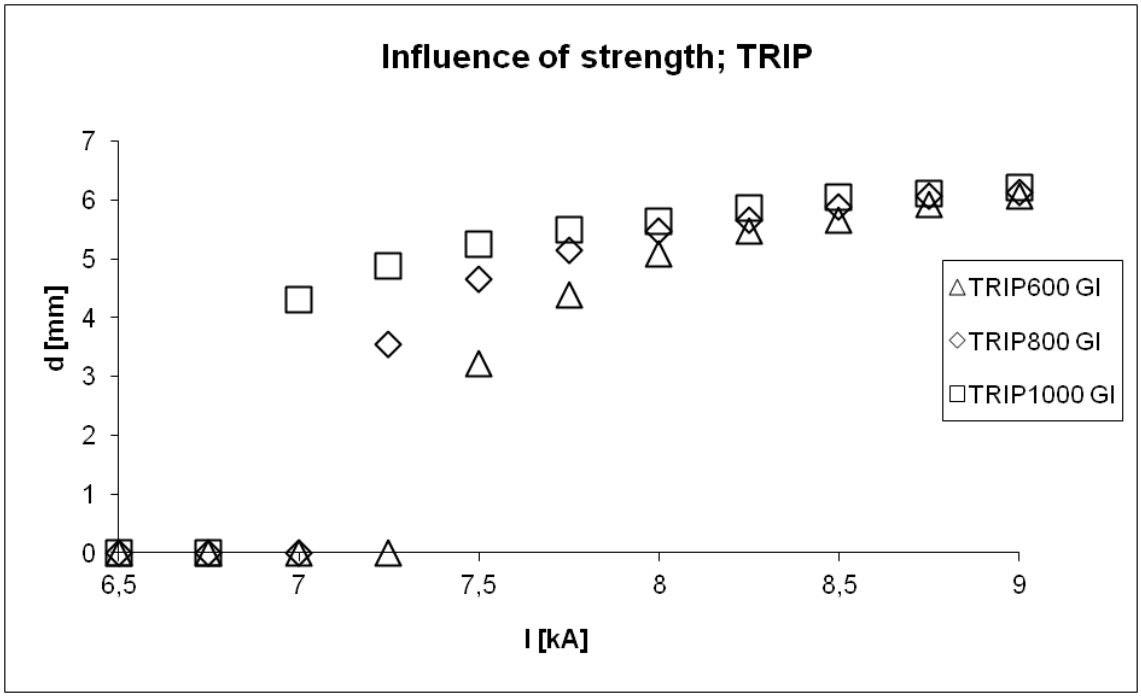

Figure 4.4: Simulated weld growth curves of varying strength 1,0 mm thick TRIP steel (6 mm B type electrode, 15 cycles 50Hz AC, 4 kN electrode force). Simulations done with Sorpas.

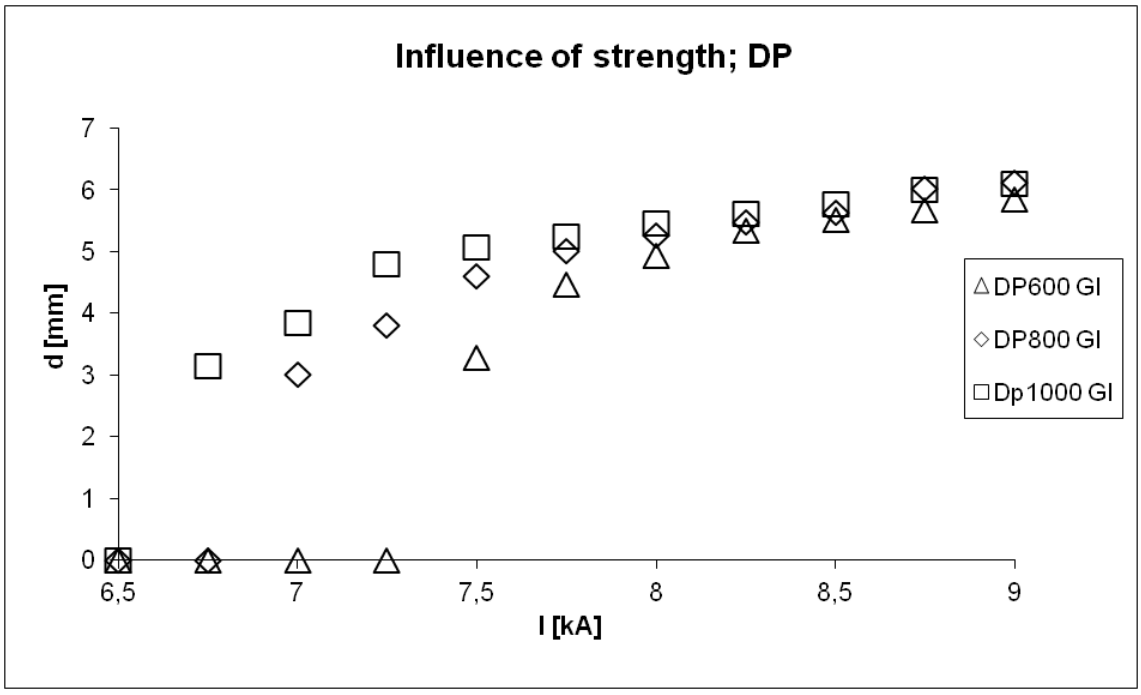

Figure 4.5: Simulated weld growth curves of varying strength 1,0 mm thick DP steel (6 mm B type electrode, 15 cycles 50Hz AC, 4 kN electrode force). Simulations done with Sorpas.

Figure 4.4 & 4.5 show that there is a difference in weld nugget formation between different grades of materials. In figure 4.6 the simulated weld growth curves of TRIP800 and DP800 are compared. Here the materials differ in chemical and microstructural composition (leading to differences in stress-strain behaviour as well as differences in thermal and electrical conductivity), but of similar strength levels. It can be seen that there is a difference in the onset of weld nugget formation, and thus in the welding range achieved, but that this difference is limited at higher currents. This can be explained by the fact that as heat is accumulated in the materials, the materials transform to austenite (and molten material) and become largely similar in their behaviour. Therefore whatever the numerical representation of the material characteristics, the response to welding operations should be the same, which is confirmed by the results shown in figure 4.6.

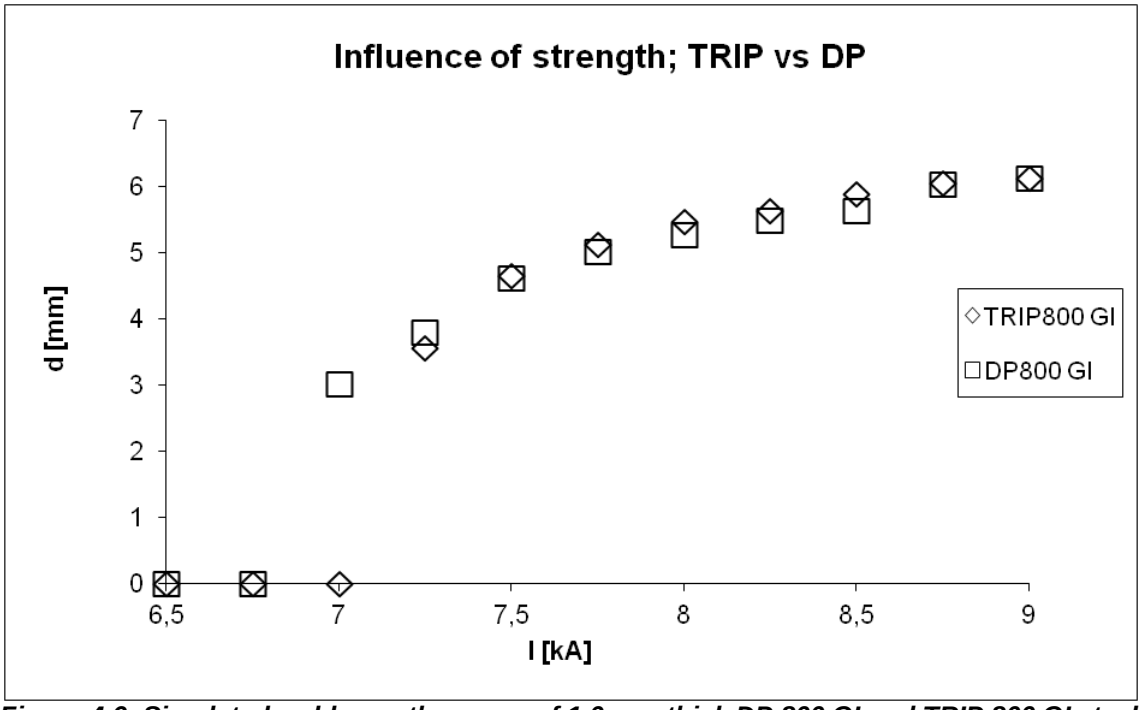

Figure 4.6: Simulated weld growth curves of 1,0 mm thick DP 800 GI and TRIP 800 GI steel (6 mm B type electrode, 15 cycles 50Hz AC, 4 kN electrode force). Simulations done with Sorpas.

4.2.2 Contact Surface Resistivity

Directly related to the material strength is the contact surface resistivity. A strong material will resist deformation more and thus have less true contact between electrode and sheet and between sheets than a softer material, leading to a higher contact resistance. Contact resistance is easily defined theoretically but less so determined experimentally, as it is basically that portion of resistance that cannot be attributed to bulk resistance. In resistance spot welding several factors play a role:

- The bulk resistance of the material.
- The amount of true contact, *i.e.* the ratio of the material surface making actual contact compared to the maximum contact area possible.
- The resistance of coating layers (galvanised, galvannealed, contamination).

In the set up of models the contact resistance can be addressed in various ways:

- One value for all factors combined, this requires determination of the resistance for each material varying in coating layers, strength levels and thickness.
- Introduction of a penalty combining all surface effects (strength, coating and contamination).
- Introduction of material data sets for substrate, coating layers, and possible contaminations, with individually defined bulk resistances.
- Introduction of a separate correction factor for true contact, combined with data sets for all other factors.

The first and the latter approach require lots of input data that need to be determined for each individual material. Although each of these approaches may give accurate results in simulation, they are only practical for an approach that models a single welding simulation. As such they are highly impractical for general automotive applications.
The second approach is used for Sysweld, which has only a limited materials database and of which the aim is not so much a determination of weldability of different materials, with varying process parameters, but an evaluation of the effects of resistance spot welding on assembly operations. This approach allows for adjustments of material characteristics to achieve overall simulation results for set process parameters (which can then be transferred to subsequent simulations).
The third approach is the one used by Sorpas. Sorpas uses the definition of bulk material resistance, combined with the definition of the resistance of coating layers, such as galvanised, galvannealed or other coating layers (e.g. aluminium, tin or nickel) and a surface contamination factor to incorporate contamination by oils, dirt, or other undefined surface effects.

Simulations

Figure 4.7 shows the influence of the type of coating on resistance spot welding of 1,0 mm thick TRIP600 sheets. Figure 4.8 shows the same for welding of 1,0 mm thick DP600 sheets. It can be seen that the influence of coating type on the weldability is negligible as far as the weld nugget diameter or welding range are concerned. Differences in coating types affect the weldability when electrode lifetime is considered, as the different coating types lead to different degradation mechanisms of the electrode tips, both in alloying, softening and deformation of the electrode tip surface. This is however not considered in these finite element simulations.

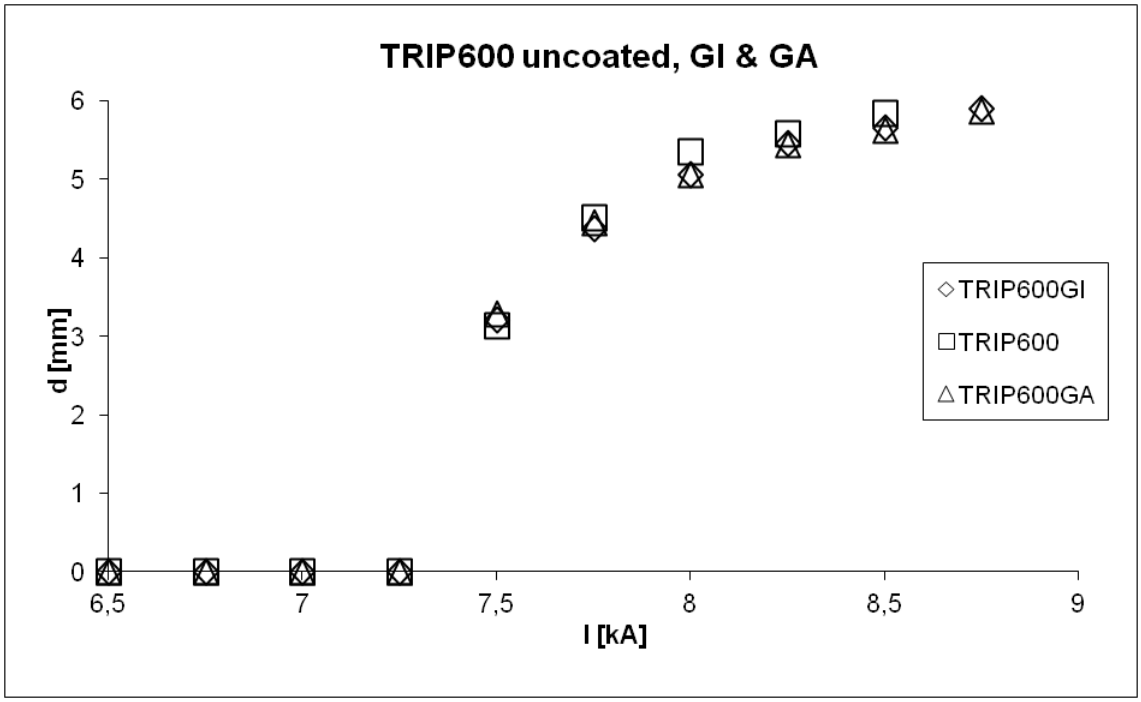

Figure 4.7: Influence of the type of coating on resistance spot welding of 1,0 mm thick TRIP600 sheets (6 mm B type electrode, 15 cycles 50Hz AC, 4 kN electrode force). Simulations done with Sorpas.

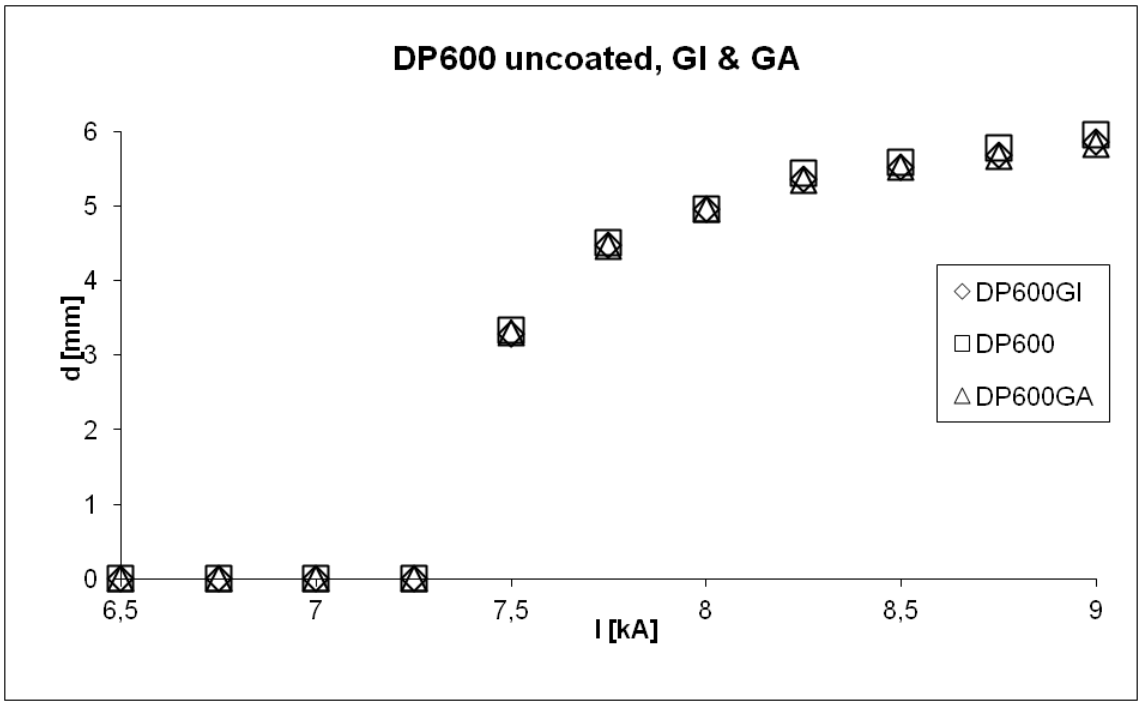

Figure 4.8: Influence of the type of coating on resistance spot welding of 1,0 mm thick DP600 sheets (6 mm B type electrode, 15 cycles 50Hz AC, 4 kN electrode force). Simulations done with Sorpas.

Figure 4.9 shows the influence of the thickness of the coating layer on the results of welding simulations for 1,0 mm thick GI-coated DP600. It can be seen that the thickness of the coating layer affects the weldability when considering weld nugget diameter and welding range. Standard GA coating layer thicknesses for automotive applications are 0,007 mm, and it can be seen that there is not much difference between this standard thickness and

uncoated material. This has already been shown in figure 4.8. The influence becomes noticeable when the thickness is increased to 0,050 mm.
It is possible that this effect should not be attributed to the thickness of the coating layer as such, but should instead be attributed to a numerical effect caused by a change in element size (as the coating layer thickness is exactly one element. Figure 4.10 shows the same effect for welding simulations for 1,0 mm thick GA-coated DP600. Here it can be seen that the effect of thickness is not as pronounced as it was for the GI coated material. This indicates that the observed effect is unlikely to be a numerical effect. It is much more likely that the effect of the differences in coating layers becomes important when the material characteristics differ substantially from those of the substrate (as is the case comparing GI with GA).
Again the influence of the thickness in coating layers is simulated without taking into account degradation of the electrode tip surface, which will affect the electrode lifetime.

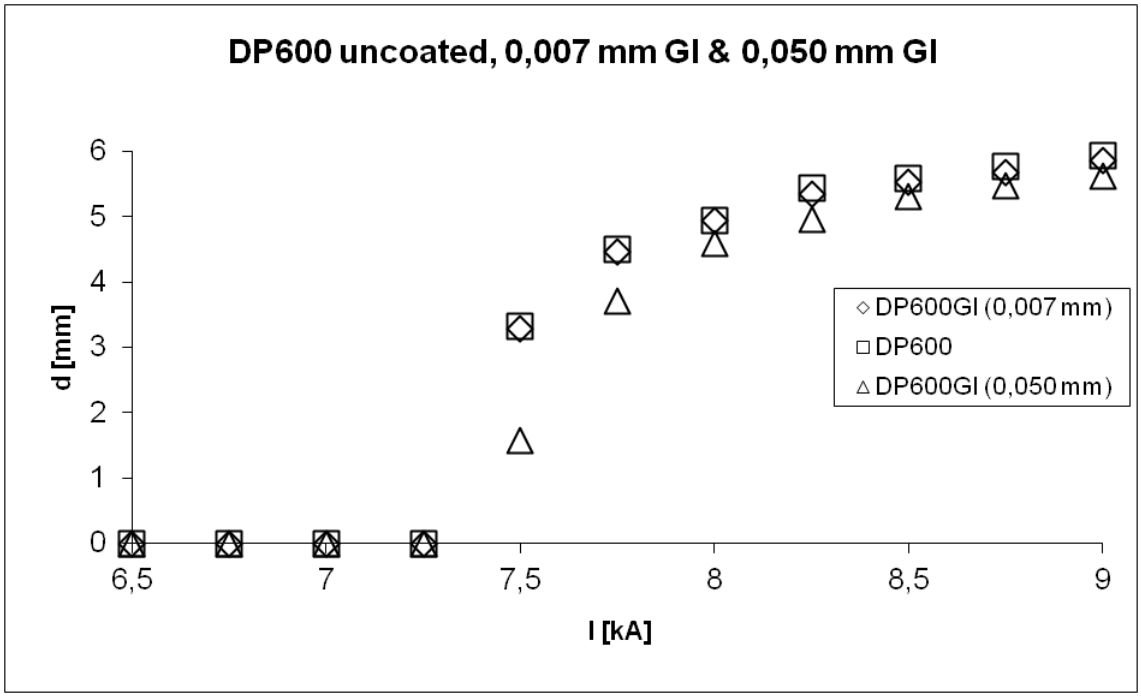

Figure 4.9: Influence of the thickness of GI coatings on resistance spot welding of 1,0 mm thick DP600 sheets (6 mm B type electrode, 15 cycles 50Hz AC, 4 kN electrode force). Simulations done with Sorpas.

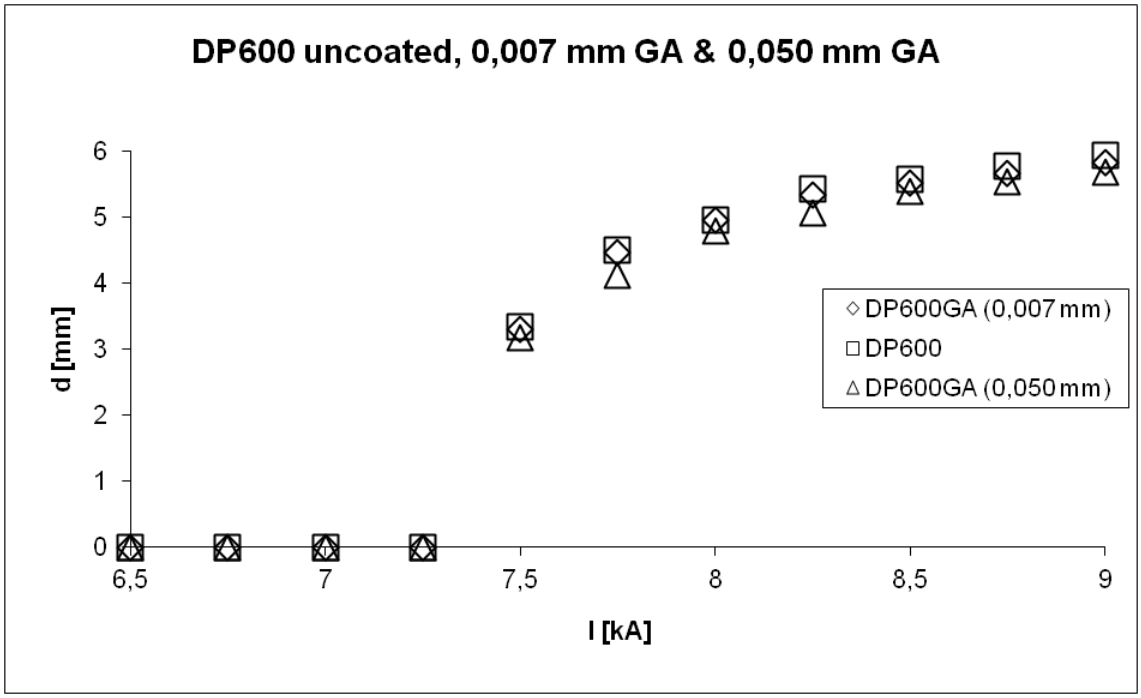

Figure 4.10: Influence of the thickness of GA coatings on resistance spot welding of 1,0 mm thick DP600 sheets (6 mm B type electrode, 15 cycles 50Hz AC, 4 kN electrode force). Simulations done with Sorpas.

The introduction of a Surface Contaminant Resistivity (SCR) factor allows simulation of the influence of surface contaminants such as lubricants (*e.g.* from forming operations), dust or excess oxidation. It can also be used to accommodate difference in surface roughness. It basically functions as a penalty added to the surface resistance. Table 4.1 gives the standard values for the SCR as given in the Sorpas material database. With increasing temperatures the value of the SCR decreases, representing evaporation of lubricants, burning off of dust and/or softening of the surface and subsequent increase of true contact area (decrease of the effect of surface roughness).
Figure 4.11 shows the effect of increasing or decreasing the value of the SCR factor on simulations of resistance spot welding of uncoated 1,0 mm thick DP600. It can be seen that the effect of changing the SCR on the results of simulations is quite significant. Although there are sound physical reasons to adjust the value of the surface contaminant resistivity, it should be done with care, as it may be used as some kind of fiddle factor to compensate for unknown variations in material data. In general it is advised not to adjust the SCR, unless there is an obvious physical reason, such as clearly visible contaminations. If the SCR is adjusted it should be justified by experimental validation against rigorously cleaned surfaces.

Table 4.1: standard values for the SCR as given in the Sorpas material database, and adjusted values for simulations of figure 4.11.

T [C]	SCR	SCR low	SCR high
20	*3,75*	*2,81*	*4,69*
60	*2,75*	*2,06*	*3,44*
120	*0,45*	*0,34*	*0,56*

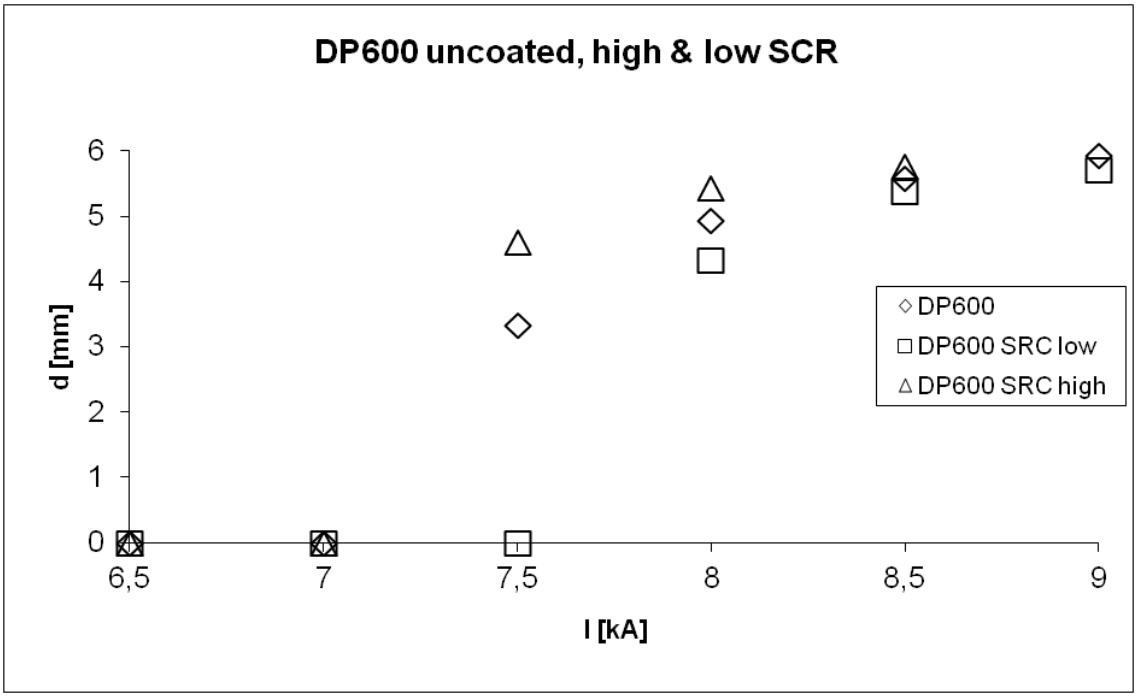

Figure 4.11: Effect of increasing or decreasing the value of the SCR factor on simulations of resistance spot welding of uncoated 1,0 mm thick DP600 (6 mm B type electrode, 15 cycles 50 Hz AC, 4 kN electrode force). Simulations done with Sorpas.

The set up of the finite element models in Sorpas requires an interface layer. This interface layer serves to allow movement between the sheets (due to possible differences in thermal expansion) and fusion between the sheets after melting and solidification. The default thickness of this layer is 0,050 mm (note; that this is bigger than the standard coating layer thickness for automotive applications). The thickness of the interface layer cannot be changed when setting up a simulation using the standard graphical user interface supplied by Sorpas, but it can be changed by manually adjusting the simulation control parameters.
Figure 4.12 shows the effect of changing the interface layer thickness for simulation of resistance welding of 1,0 mm thick DP600. It can be seen that the effect is very large. In fact, adjusting the thickness of the interface layer can be used to adjust the simulation results to fit a wide range of experimental results. It is therefore recommended to never change this parameter. In fact, as it is the ultimate fiddle factor, it is fair to state that changing the interface layer thickness renders the results of comparative simulations with this software invalid.

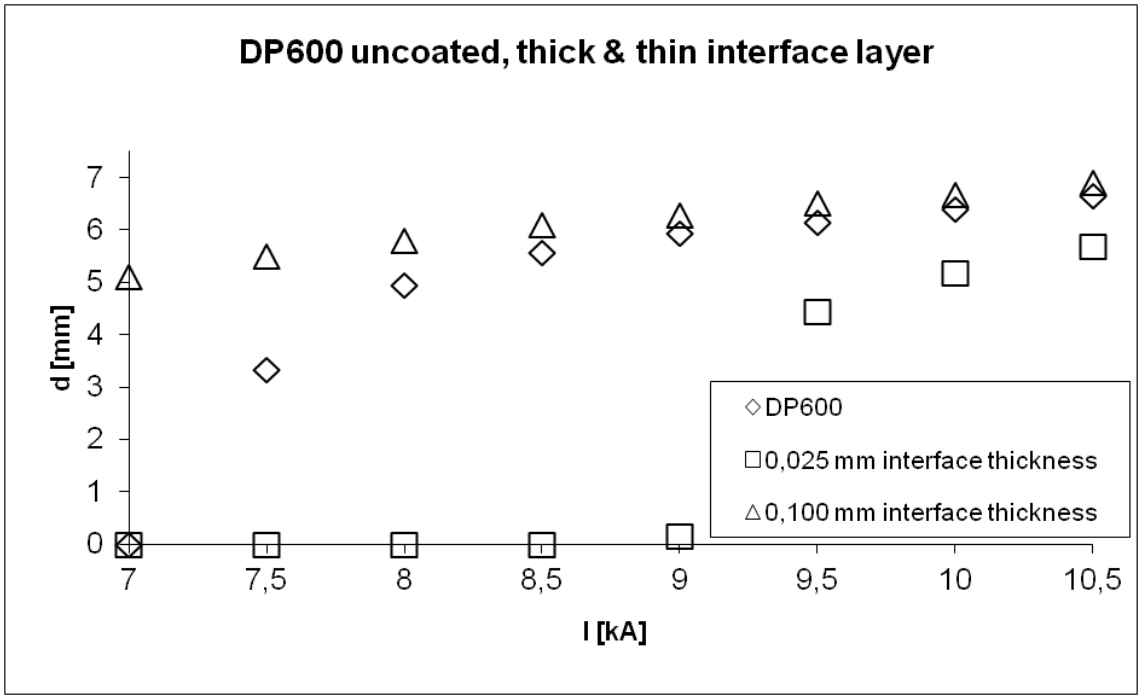

Figure 4.12 : Effect of changing the interface layer thickness for simulation of resistance welding of 1,0 mm thick DP600 (6 mm B type electrode, 15 cycles 50Hz AC, 4 kN electrode force). Simulations done with Sorpas.

4.2.3 Thermal Conductivity and Electrical Resistivity

The electrical resistance, R, of a work piece is defined by Ohm's law, relating the current, I, passing through a material with the voltage, V, applied across it:

$$V = IR. \qquad \text{(Eq. 4.3)}$$

The value of R is dependent on the geometry of the work piece. The electrical resistivity, ρ, is independent of geometry:

$$\rho = \frac{RA}{L}, \qquad \text{(Eq. 4.4)}$$

with L being the distance between two points across which the voltage is applied and A the cross-sectional area perpendicular to the direction of the current I.
Combining equation 4.3 with equation 4.4 the electrical resistivity can be expressed as:

$$\rho = \frac{VA}{IL}. \qquad \text{(Eq. 4.5)}$$

The electrical resistivity has the dimensions of Ωm.
The electrical conductivity, σ, of a material is defined as the reciprocal of the electrical resistivity:

$$\sigma = \frac{1}{\rho}. \qquad \text{(Eq. 4.6)}$$

The electrical conductivity is a measure of the ease with which a material can conduct an electrical current. An electrical current results from the motion of electrically charged particles caused by forces that are applied from an electric field. In metals the flow of electrons is hindered by so called “frictional forces” which result from scattering of the electrons by imperfections in the crystal lattice (such as impurities, vacancies, interstitial atoms, dislocations) and the thermal vibrations of the atoms. Each scattering event causes an electron to lose kinetic energy and to change its direction of motion. The overall movement of the electrons is directed opposite to the field, resulting in an electric current.

The strength levels in steels are based upon chemical composition and thermo-mechanical treatment during production. These increase the electrical resistivity of the material. When welding these steels, the electrical resistivity is further increased due to the rise in temperature, increasing thermal vibrations of the atoms and creating vacancies. With increasing temperature the increase of the thermal component of the thermal resistivity becomes the dominating factor. At around 800 °C the base material transforms to austenite. In this transformation the effects of cold work, created vacancies and some impurities are lost, changing the slope of the electrical resistivity as a function of temperature curve. Further increase of electrical resistivity with increasing temperature is due to increased thermal activity of the atoms and renewed creation of vacancies. Figure 4.13 shows the electrical resistivity of a dual phase (DP600) steel with increasing temperature.

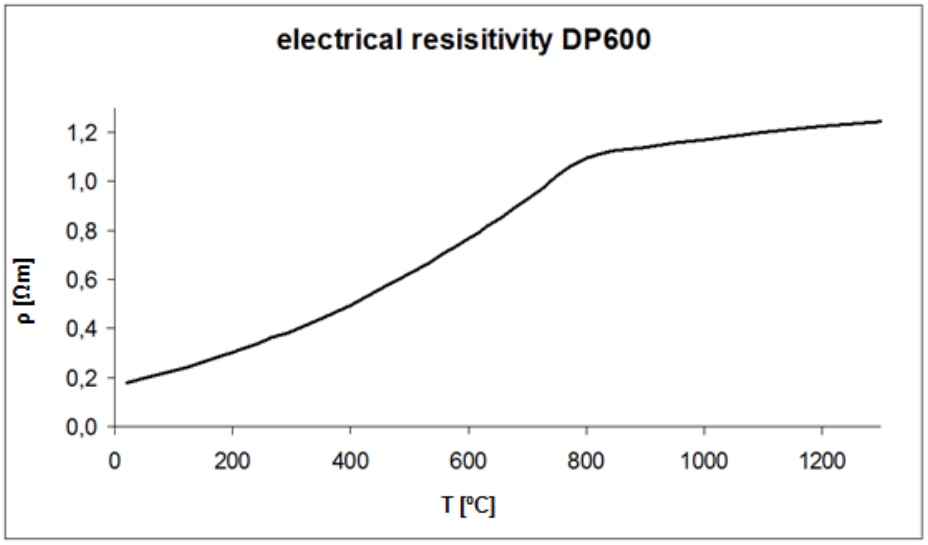

Figure 4.13: Electrical resistivity of DP600, as provided in the Sorpas material database.

The thermal conduction, k, of a material characterises the ability of a material to transfer heat. Heat is transported in solids by both lattice vibration waves (phonons) and free electrons. The total thermal conductivity is the sum of both these two contributions:

$$k = k_l + k_e. \qquad \text{(Eq. 4.7)}$$

where k_l represents the contribution of lattice vibrations and k_e the contribution of moving electrons. The k_l contribution comes from a net movement of phonons along a thermal gradient form regions with higher temperature to regions with lower temperature.
Free electrons in a region of higher temperature gain in kinetic energy. If there is a thermal gradient they migrate to regions of lower temperature where kinetic energy is transferred to atoms (as vibrational energy) by collisions with phonons or other imperfections in the crystal.
In high purity metals heat transport by electrons is much more effective than heat transport by phonons, because electrons are not as easily scattered and have higher velocities than phonons. The fact that metals have large numbers of free electrons makes them good

thermal conductors. Scattering events cause a decrease in thermal conductivity in the same way as they reduce the electrical conductivity.
In the austenite transformation the effects of cold work, created vacancies and some impurities are lost, changing the slope of the thermal conductivity curve. Further decrease of thermal conductivity with increasing temperature is due to increased thermal activity of the atoms and renewed creation of vacancies. Figure 4.14 shows the thermal conductivity of a dual phase (DP600) steel with increasing temperature.

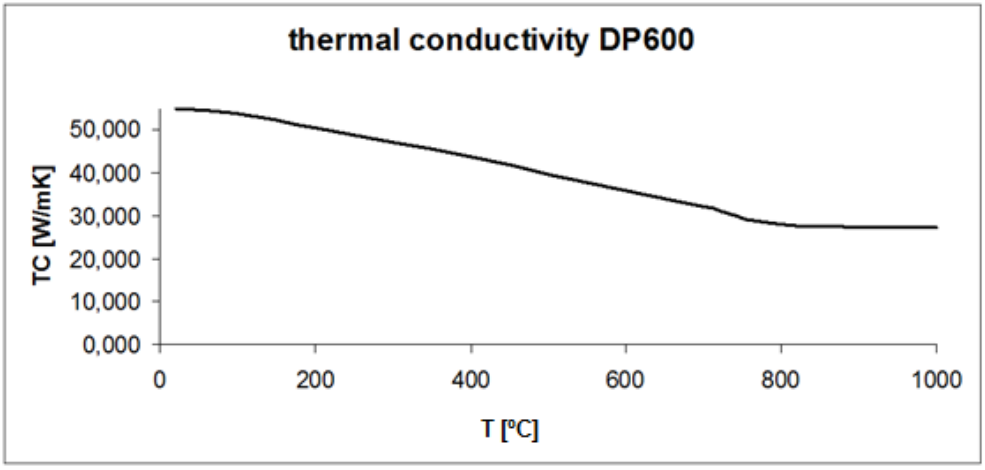

Figure 4.14: Thermal conductivity of DP600, as provided in the Sorpas material database.

The thermal conductivity of a material is usually defined by Fourier's law:

$$q = -kA\left(\frac{dT}{dx}\right), \qquad \text{(Eq. 4.8)}$$

where q is the heat flux (heat flow per unit time), A is the cross-sectional area perpendicular to the direction of flow and dT/dx is the thermal gradient. The dimensions of q are W/m^2. The minus sign indicates that the direction of heat flow is down the thermal gradient, from hot to cold. Fourier's law is only valid for steady state heat flow, *i.e.* when the heat flux does not change with time.
In welding the steady state requirement is not satisfied, although it can be assumed that it is satisfied locally in time and space, which calls for a finite element approximation to the problem. The effects of changes in thermal conductivity on the distribution of heat during welding are considered here using numerical simulations.

The fact that electrons are responsible for both electrical as well as thermal conduction in metals is expressed in the Wiedemann-Franz law:

$$\frac{k}{\sigma T} = constant, \qquad \text{(Eq. 4.9)}$$

where T is the absolute temperature in Kelvin, σ the electrical conductivity and k the thermal conductivity. The theoretical constant value is 2,44 · 10^{-8} ΩW/K^2, and should be independent of temperature and the same for all metals if heat is transported by electrons exclusively. The experimentally derived value for iron is 2,71 · 10^{-8} ΩW/K^2, which indicates that some thermal transport by phonons takes place.

Simulations

For simulations use was made of Sorpas, the material data used to represent the materials was taken from the Sorpas materials database incorporated in the software. Verification of the welding model set up was done using weld growth curves. Two examples of verified simulations are shown here. First a GI coated DP600 of 1,0 mm thickness, welded with a 6 mm B-type electrode. Welds were made using 300 cycles (300 ms) of 1000 Hz AC current and the electrode force was 4 kN.
Figure 4.15 shows the experimental weld growth curve and splash welds, as well as the simulated welds and splash welds. Note the experimental spread in weld size and onset of splash welds. Though Sorpas is not very suited to predict the occurrence of the splash welds, as these are highly dependent on irregularities and the geometry in Sorpas is always regular, the occurrence of the first splash weld is predicted satisfactorily (at 9,75 kA).

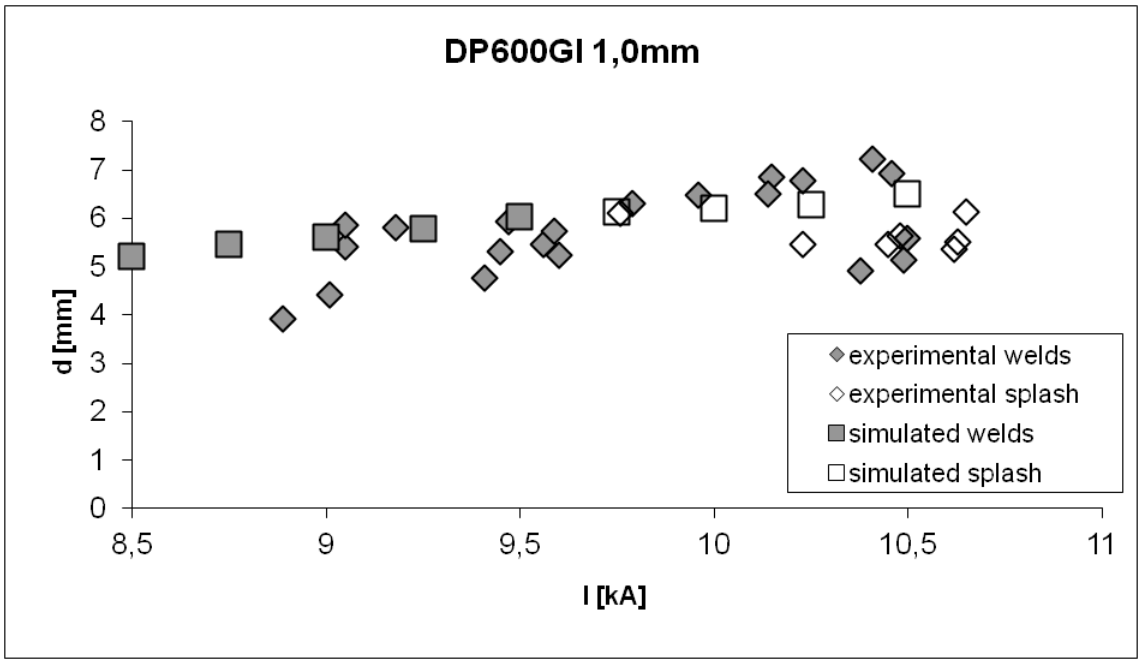

Figure 4.15: Experimental and simulated DP600 weld growth curve using a 6 mm B-type electrode. Welds made with 300 cycles of 1000 Hz AC current and 4 kN electrode force.

Figure 4.16 gives the experimental and simulated weld growth curve of 1,5 mm thick uncoated DP1000 steel welded with 8 mm G-type electrodes. Welds were made using two pulses of AC current, the first one lasting 20 cycles (400 ms) and the second one lasting 15 cycles (300 ms). Between each pulse was a pause of 20 cycles (400 ms). The electrode force was 5,5 kN.

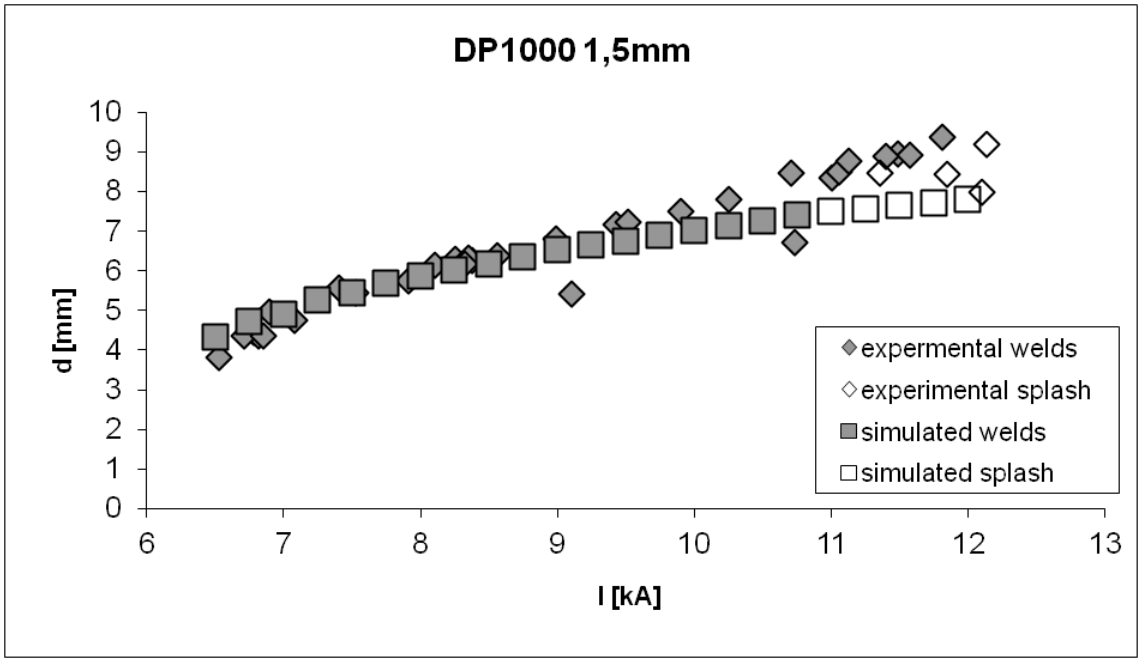

Figure 4.16: Experimental and simulated DP1000 weld growth curve using an 8 mm G-type electrode. Welds made with two pulses of 20 and 15 cycles of AC current with an intermediate pause of 20 cycles and 5,5 kN electrode force.

It can be seen that the software simulates welding behaviour of dual phase steels satisfactorily, independent of electrode types, electrode force, material thickness and welding currents. This is important because all of these parameters influence welding behaviour and therefore the software should be able to simulate the response to welding operations well for a variety of settings.

To rule out all influences on results except the thermal and electrical conductivity, the simulations in the remainder of this section have been done on dual phase steels of 1 mm thickness, welded with B-type electrodes. The electrode diameter for all simulations was set at 6 mm, and simulations were conducted using 15 cycles of AC current to form the weld with a 4 kN electrode force. All materials used in simulations were GI-coated (50 gr/m^2 Zn).

The welding range for resistance spot welding is often defined as the range in welding current from the point where the weld nugget reaches a required size (often related to the thickness of the material) and the onset of splash. In experiments the onset of splash welds is not just dependent upon the process settings, but also on factors which can be related to experimental spread, such as misalignment of electrodes and electrode wear. Also it is possible to acquire perfectly good welds after the first splash welds have occurred, as can be seen in figures 4.15 & 4.16.
As a rule of thumb splash welds can be expected as soon as the size of the weld nugget exceeds the electrode diameter (though they do not need to occur). As all simulations were done using the same material thickness and the same electrode type and size the weld growth curves were calculated up to a weld nugget size of 7 mm. Between 6 and 7 mm splash welds can be expected, but non splash welds can occur.

Figure 4.17 shows the weld growth curves of DP600 with varying electrical resistivity. It can be seen that the weld growth curve shifts to lower welding currents with increasing electrical

resistivity and to higher welding currents with decreasing electrical resistivity. Similar curves were obtained for DP800 and DP1000.

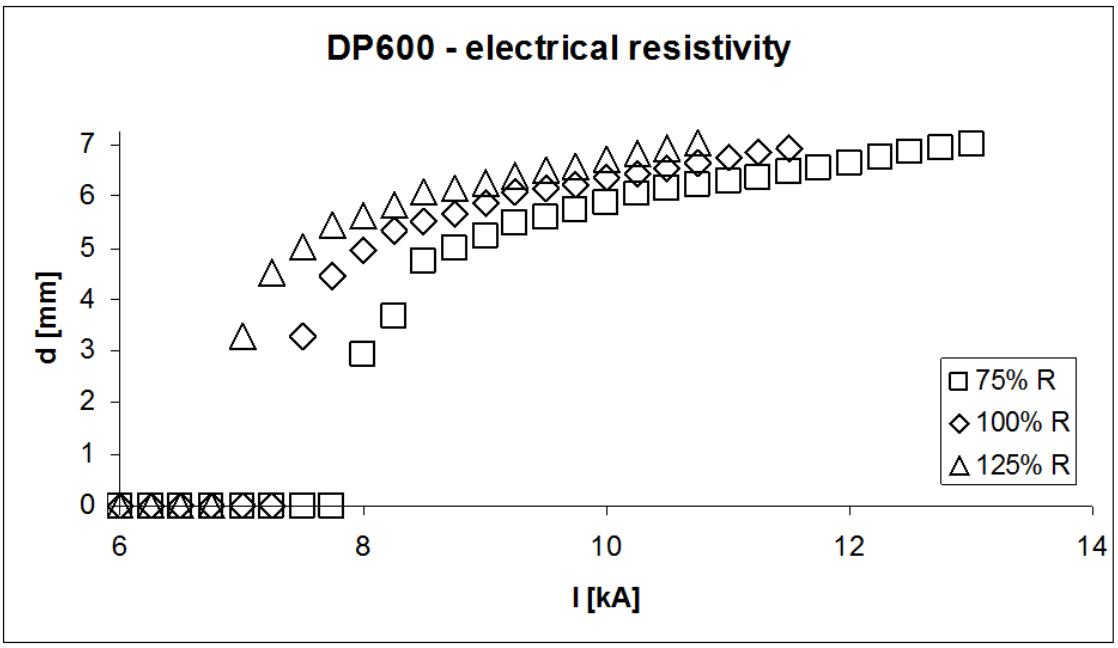

Figure 4.17: Weld growth curves for DP 600 GI with varying electrical resistivity (6 mm B type electrode, 15 cycles 50 Hz AC, 4 kN electrode force). Simulations done with Sorpas.

Figure 4.18 shows the weld growth curves of DP600 with varying thermal conductivity. It can be seen that the weld growth curve shifts to lower welding currents with decreasing thermal conductivity and to higher welding currents with increasing thermal conductivity. Similar curves were obtained for DP800 and DP1000.

Figure 4.19 shows the weld growth curves for DP600 with varying thermal conductivity and electrical resisitivity. Figure 4.20 shows the same for DP1000. It can be seen that the effects for electrical resisitivity (as shown in figure 4.17) and thermal conductivity (as shown in figure 4.18) add up to even stronger shifts of the weld growth curves. Comparing figure 4.19 with 4.20, it can be seen that the weld growth curves shift to lower welding currents for increased strength levels, but the tendencies for the effects of thermal conductivity and electrical resistivity are similar.

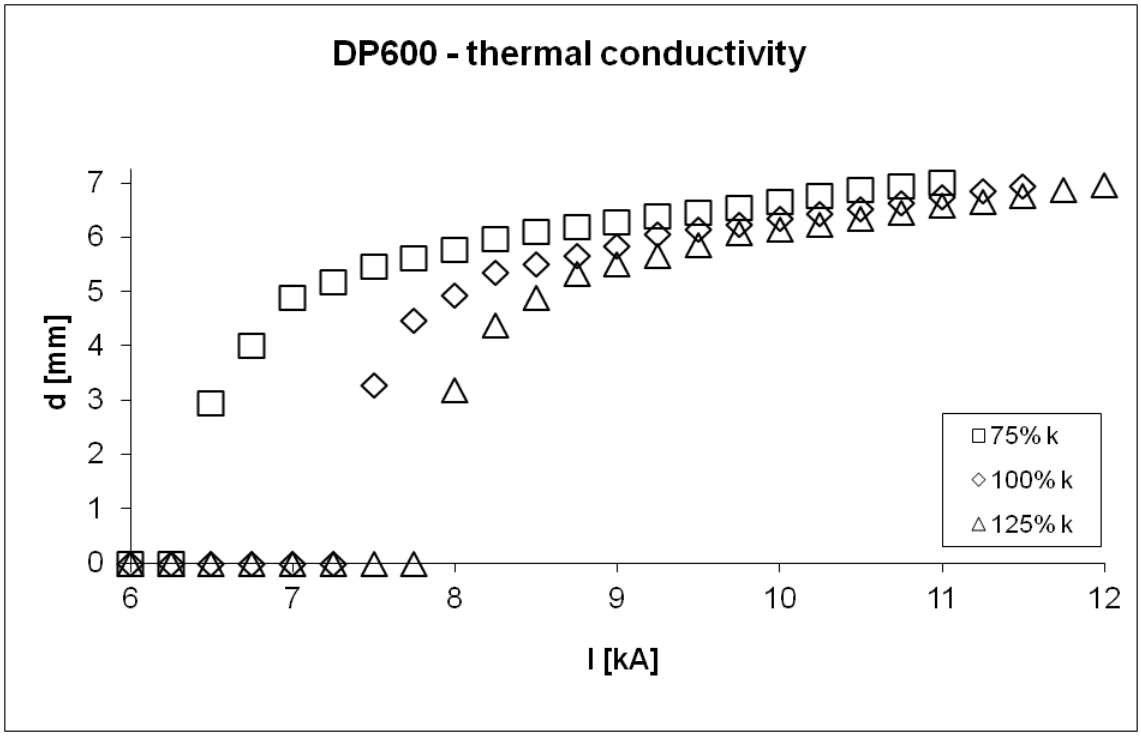

Figure 4.18: Weld growth curves for DP600 with varying thermal conductivity (6 mm B type electrode, 15 cycles 50 Hz AC, 4 kN electrode force). Simulations done with Sorpas.

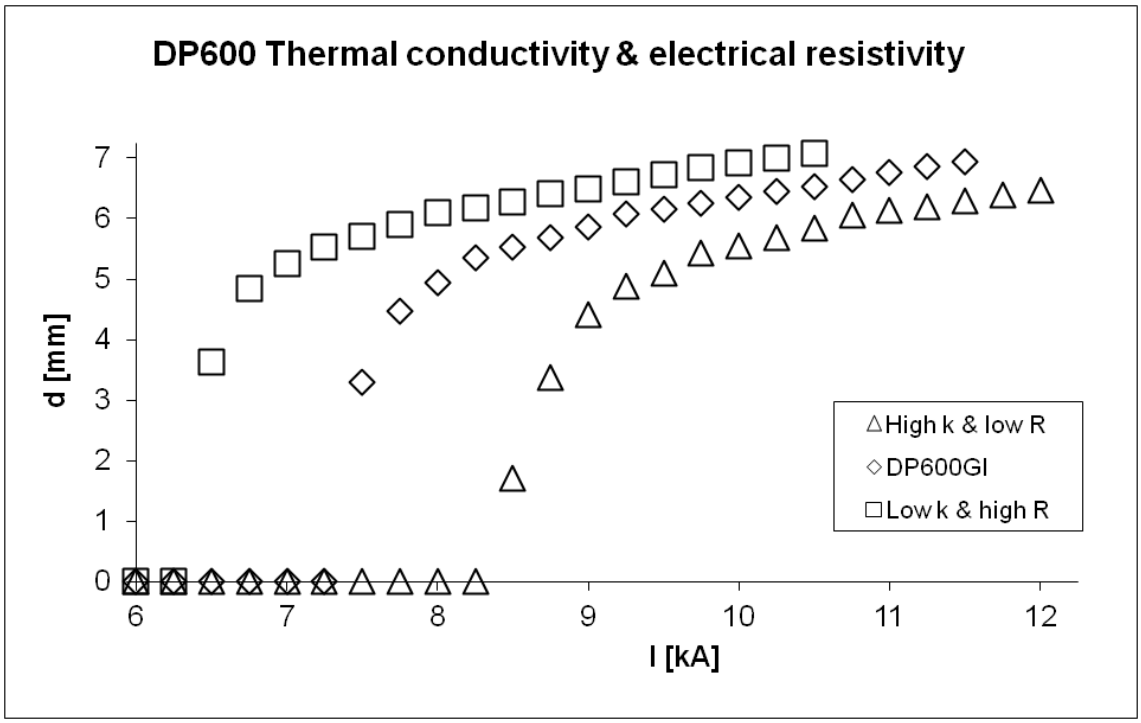

Figure 4.19: Weld growth curves for DP600 with combined variations of thermal conductivity and electrical resistivity (6 mm B type electrode, 15 cycles 50 Hz AC, 4 kN electrode force). Simulations done with Sorpas.

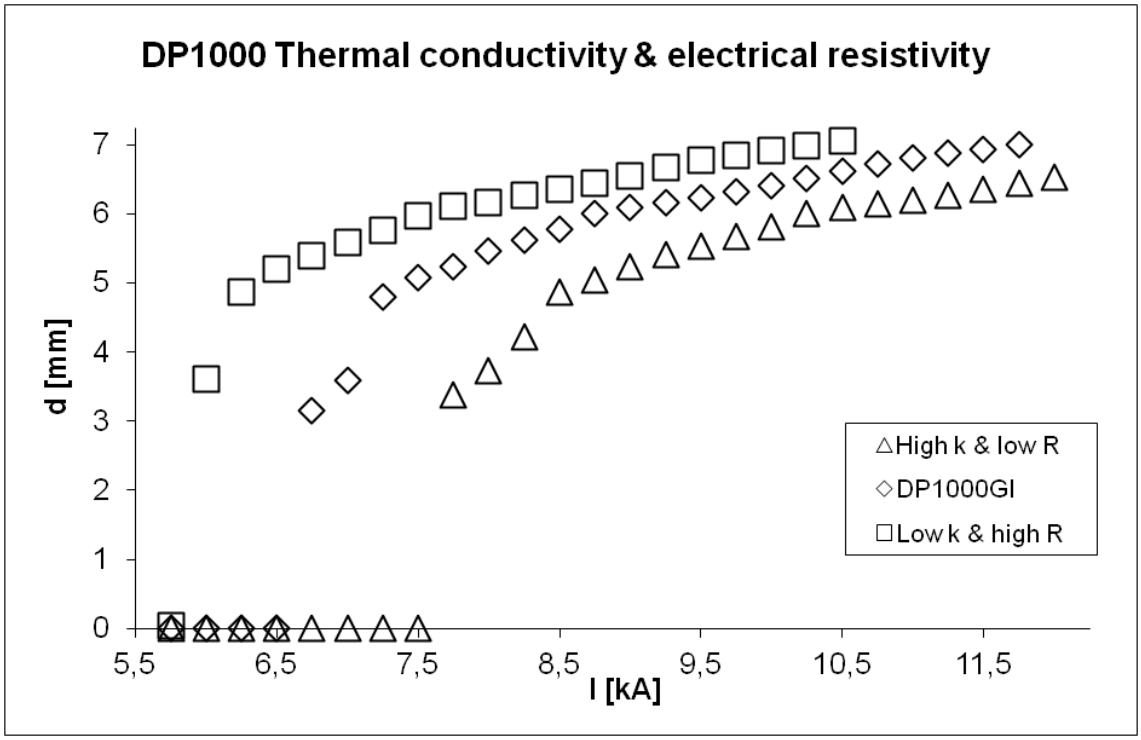

Figure 4.20: Weld growth curves for DP1000 with combined variations of thermal conductivity and electrical resistivity (6 mm B type electrode, 15 cycles 50 Hz AC, 4 kN electrode force). Simulations done with Sorpas.

Comparing the weld growth curves of DP600, DP800 and DP1000, it can be seen that with increasing strength levels the weld growth curve shifts to lower levels of welding current (see figure 4.5). This is partly due to the fact that the increased strength levels of the steels prohibit indentation of the material by the electrode. Indentation of the material leads to a decrease in weld current density, which will prevent formation of a weld nugget at lower welding currents. Another factor in the shift of the weld current is due to the increase in scattering events in steels that have been alloyed and cold worked to a greater extent to increase strength levels.

These effects can be verified experimentally when comparing materials with the same thickness and similar surface characteristics. Figure 4.21 gives the experimentally determined weld growth curves of 2mm thick DP600GI and 2 mm thick HSLA420GI. Both materials have been produced using the same production facilities, ensuring similarity in surface characteristics and cold working conditions. Welding conditions for both curves were the same. Both have been welded using 8 mm electrodes, 5,5 kN electrode force and 18 cycles (360 ms) AC current. The difference between the weld growth curves is due to alloying and thermomechanical treatment. These introduce scattering events leading to higher electrical resistivity and lower thermal conductivity for DP600GI compared to HSLA420GI.

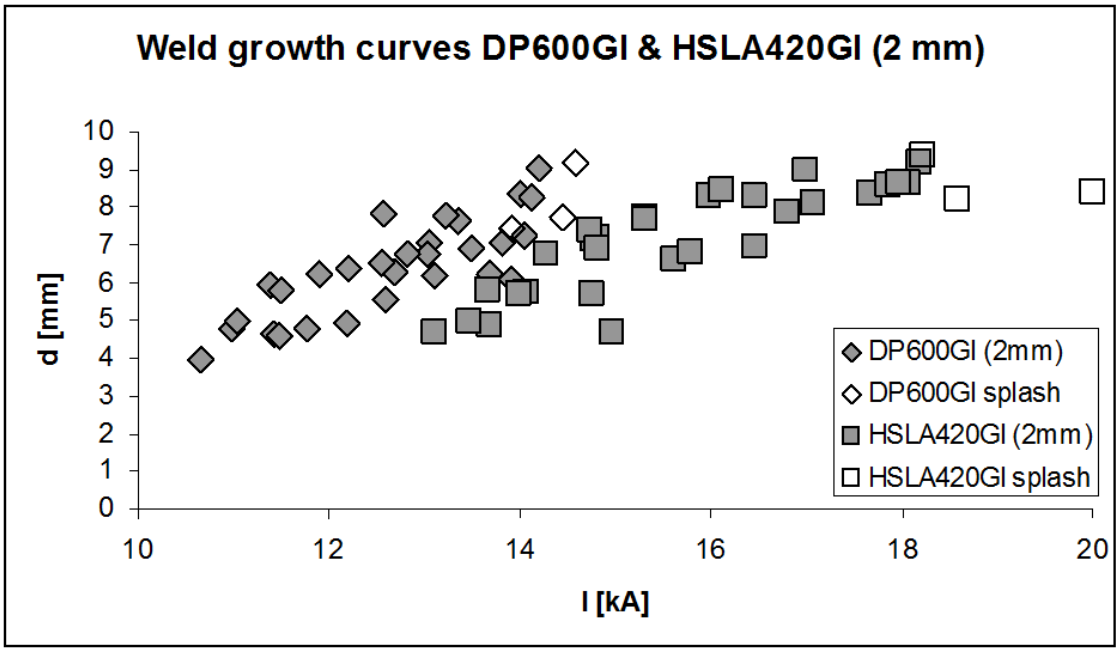

Figure 4.21: Experimentally determined weld growth curves of 2mm thick DP600GI and 2 mm thick HSLA420GI (8 mm electrode, 18 cycles 50 Hz AC, 5,5 kN electrode force).

4.3 Electrode geometry

4.3.1 Introduction

Two aspects of the impact of electrode geometry on the weldability of advanced high strength steels in manufacturing have been evaluated. The first concerns the geometry of the electrode caps as defined by standards and the second concerns the size of the contact area between the electrode and the steel sheets.

4.3.2 Electrode cap geometry

Figure 4.22 shows the standard electrode caps used in resistance spot welding according to ISO 5821. Table 4.2 gives the dimensions of these electrode caps according to the standard. These geometries are commonly used in resistance spot welding in the automotive industry, although sometimes, specially adapted geometries are used for specific applications [Chan & Scotchmer, 2004]. Figure 4.23 gives the geometries of B type electrodes (figure 4.23a) and G type electrodes (figure 4.23b), as used in simulations to compare the effect of electrode cap geometry on weldability.

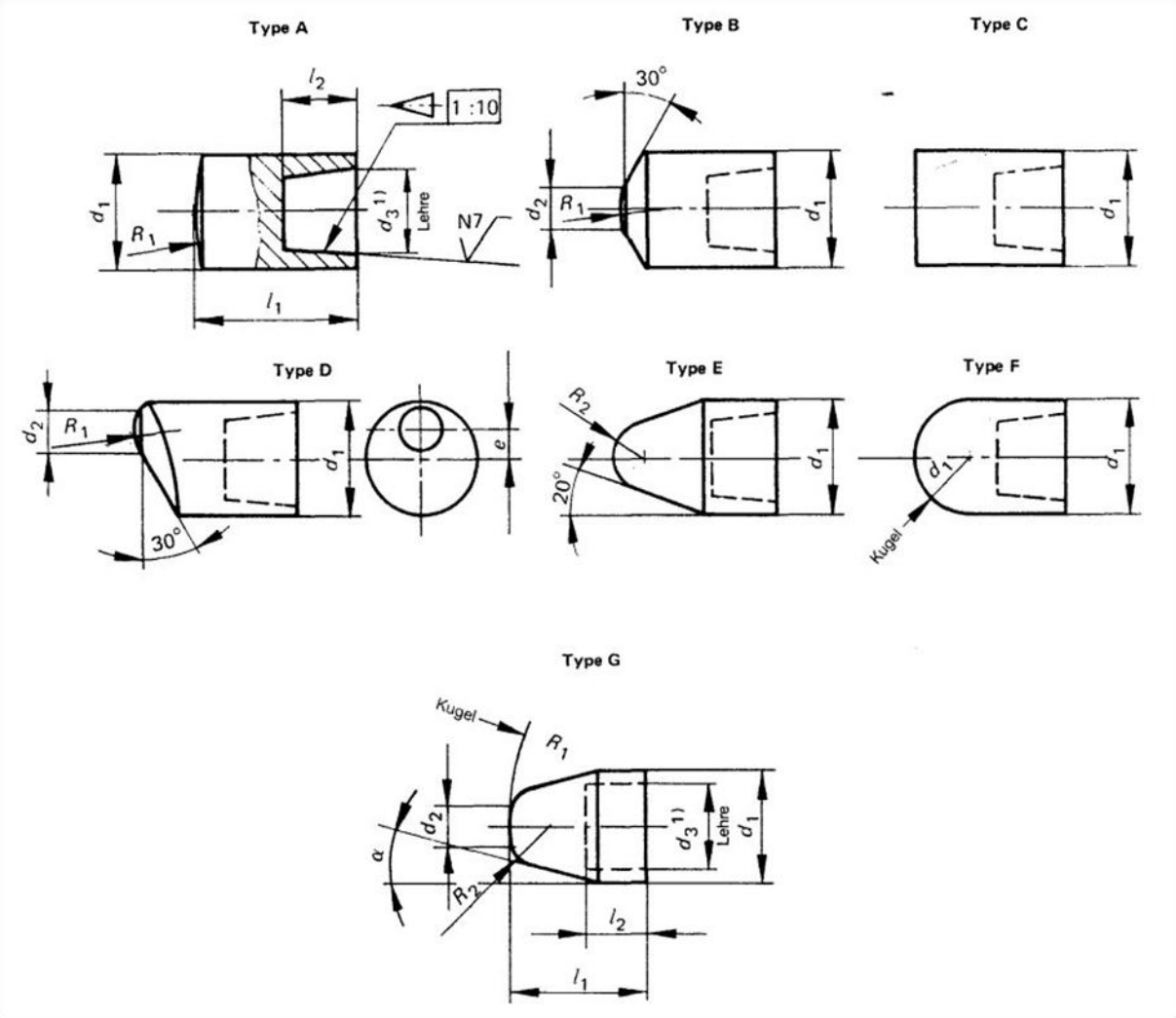

Figure 4.22: Electrode cap geometries according to ISO 5821.

Table 4.2: dimensions of electrodes with respect to ISO 5821.
The various parameters refer to geometrical properties of the electrodes as shown in figure 4.22. Electrode caps are referred to with their type and contact area diameter, d_2 in the table. Diameters d_1 and d_2 refer to the outer diameter of the electrode caps and the inner diameter that serves as the cooling water canal. l_1 refers to the length of the electrode cap and l_2 to the length of the cooling canal where the electrode cap is fixed to the welding machine. The excentricity of the contact area of a Type D electrode is given by e. R_1 is the radius of curvature of the contact area, and R_2 the radius of curvature of the electrode cap. The angle α gives the angle of the cone of the electrode cap of type G electrodes.

d_1	d_2	d_3	l_1	l_2+0,50	e	R_1	R_2	α
[mm]	[mm]	[mm]	[mm]	[mm]	[mm]	[mm]	[mm]	[°]
13	*5*	*10*	*18*	*8*	*3*	*32*	*5*	*-*
16	*6*	*12*	*20*	*9,5*	*4*	*40*	*6*	*15*
20	*8*	*15*	*22*	*11,5*	*5*	*50*	*8*	*22,5*

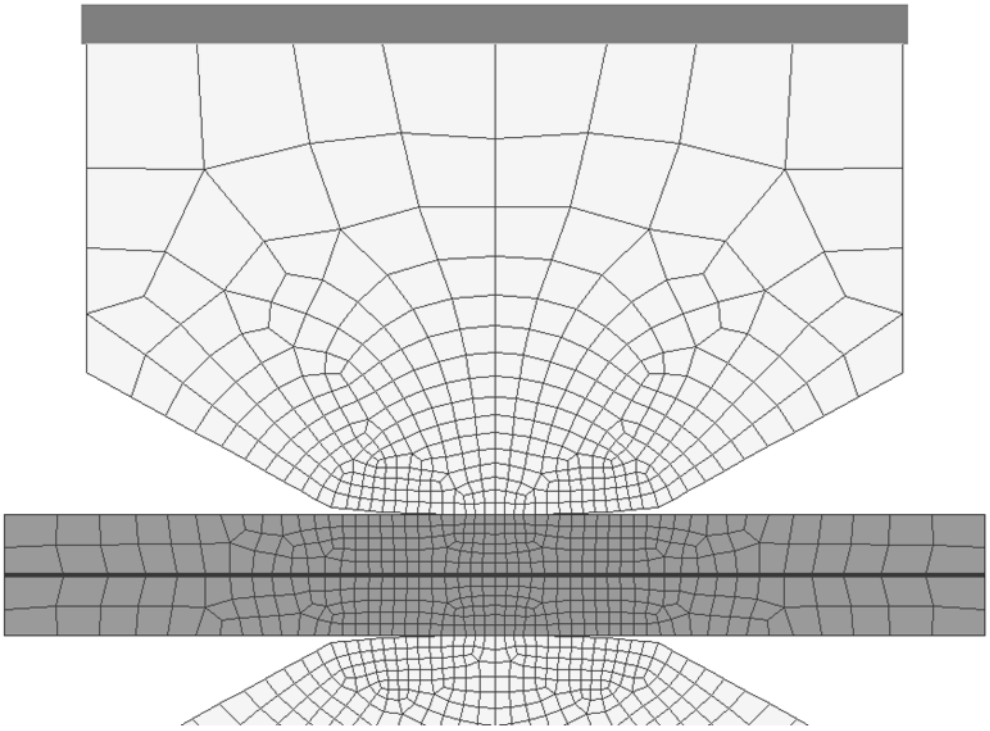

Figure 4.23a: B Type electrode geometry according to ISO 5821, as used in Sorpas simulations.

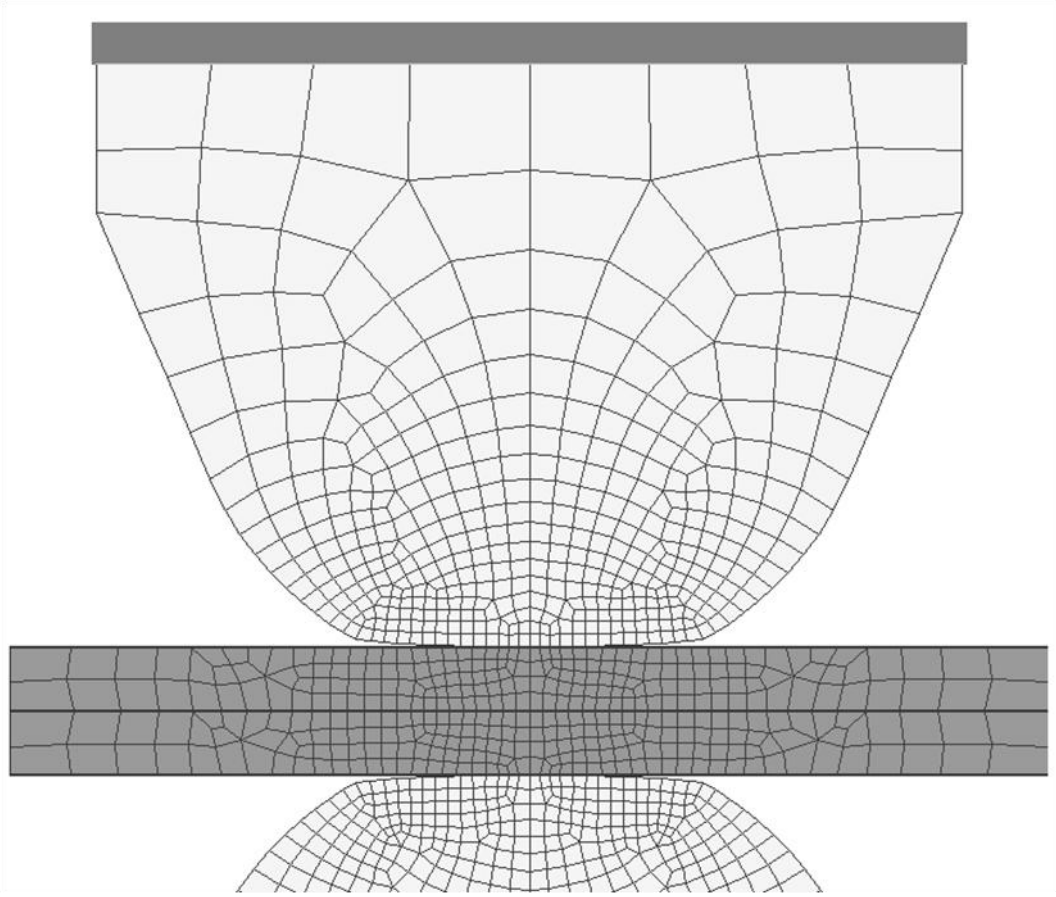

Figure 4.23b: G Type electrode geometry according to ISO 5821, as used in Sorpas simulations.

Figure 4.24a gives the weld growth curve for a 1,5 mm thick TRIP800 GI steel welded to the same material, using a type B electrode cap with an 8 mm diameter tip; the electrode force was 4,5 kN and welding time 16 cycles. Figure 4.24b gives the simulated weld growth curve for this material, using similar weld settings. It can be seen that the simulated weld growth curve corresponds reasonably well with the experimental curve (the experimental weld growth curve suggests weld nugget formation at slightly lower welding currents than the simulated curve).

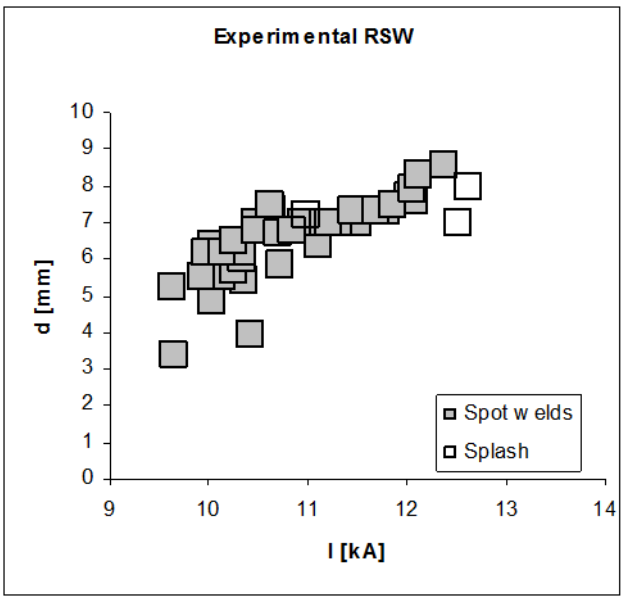

Figure 4.24a: Experimental weld growth curve for a 1,5 mm thick TRIP800 GI steel welded to the same material, using a type B electrode cap with an 8 mm diameter tip.

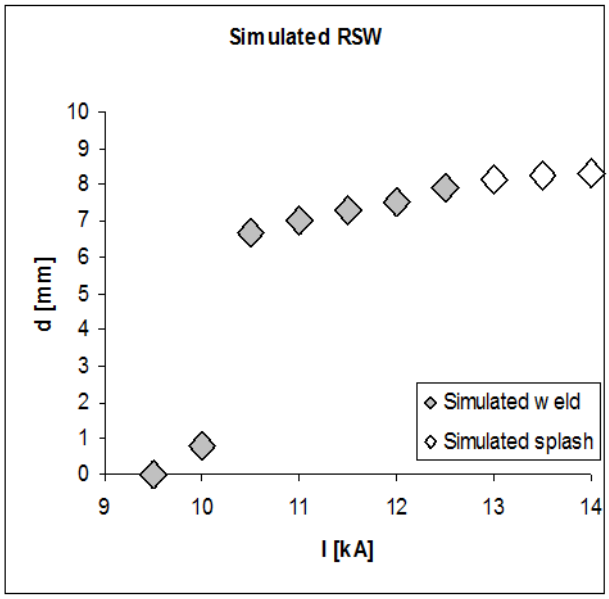

Figure 4.24b: Simulated weld growth curve for a 1,5 mm thick TRIP800 GI steel welded to the same material, using a type B electrode cap with an 8 mm diameter tip.

An advantage of simulation over experiment in resistance spot welding is that it is much easier and faster to produce weld growth curves. It is quicker to make and measure a single weld experimentally, but due to the experimental scatter many more welds are needed experimentially to produce a weld growth curve than are necessary in simulation. Therefore, once models have been verified, a range of weld growth curves can be produced. Figure 4.25, gives the simulated weld growth curves for resistance spot welded 1,5 mm thick TRIP800 GI welded to itself using a type B electrode cap with 5, 6, and 8 mm diameter tips. The difference between the curves is the contact area between the electrode and the steel sheets, which ranges from a diameter of 5 mm to 8 mm.
Similar simulations were done for type G electrode caps. Figures 4.26 gives the simulated weld growth curves for resistance spot welded 1,5 mm thick TRIP800 GI welded to itself using type G electrode caps with varying tip diameters (5, 6 & 8 mm).

Comparing figure 4.25 with 4.26 it can be seen that the weld growth curve shifts to higher current ranges with increasing tip diameters for type B electrodes but not for type G electrodes. Type B electrode tip surfaces are flat compared to the more rounded electrode tips of type G electrodes (compare figures 4.23 a & b). It can be conclude that the increase in surface contact area with increasing electrode tip diameter, and corresponding decrease in current density, is more pronounced for type B than it is for type G electrode caps.

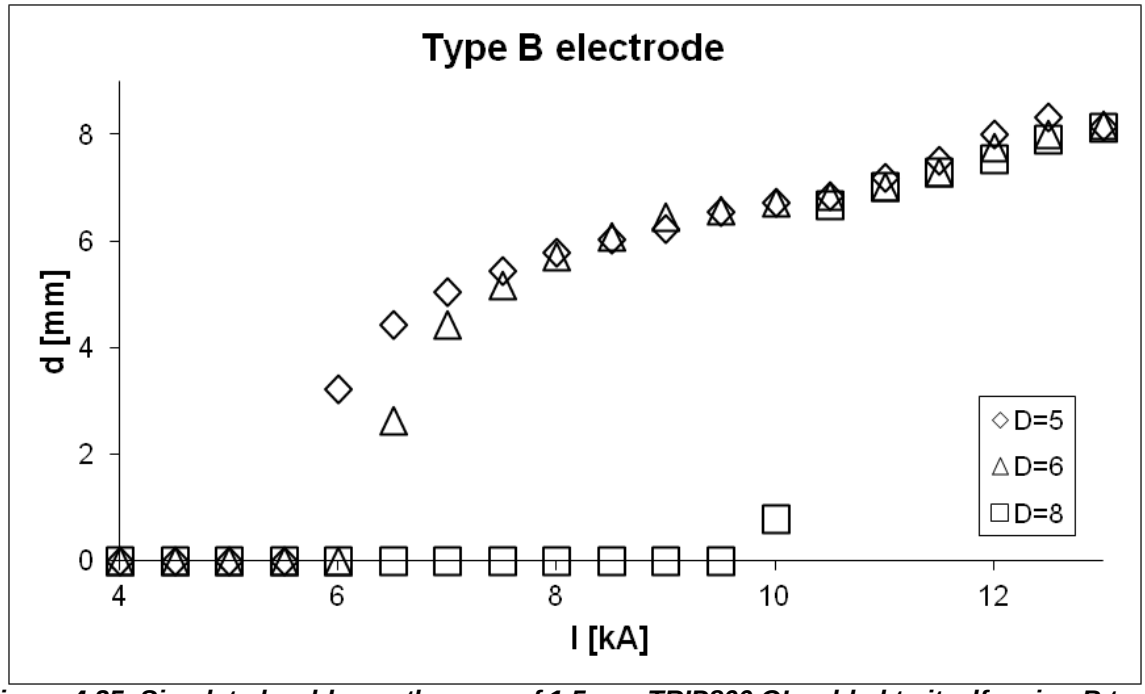

Figure 4.25: Simulated weld growth curve of 1,5 mm TRIP800 GI welded to itself, using B type electrode caps with 5, 6 & 8 mm tip diameters.

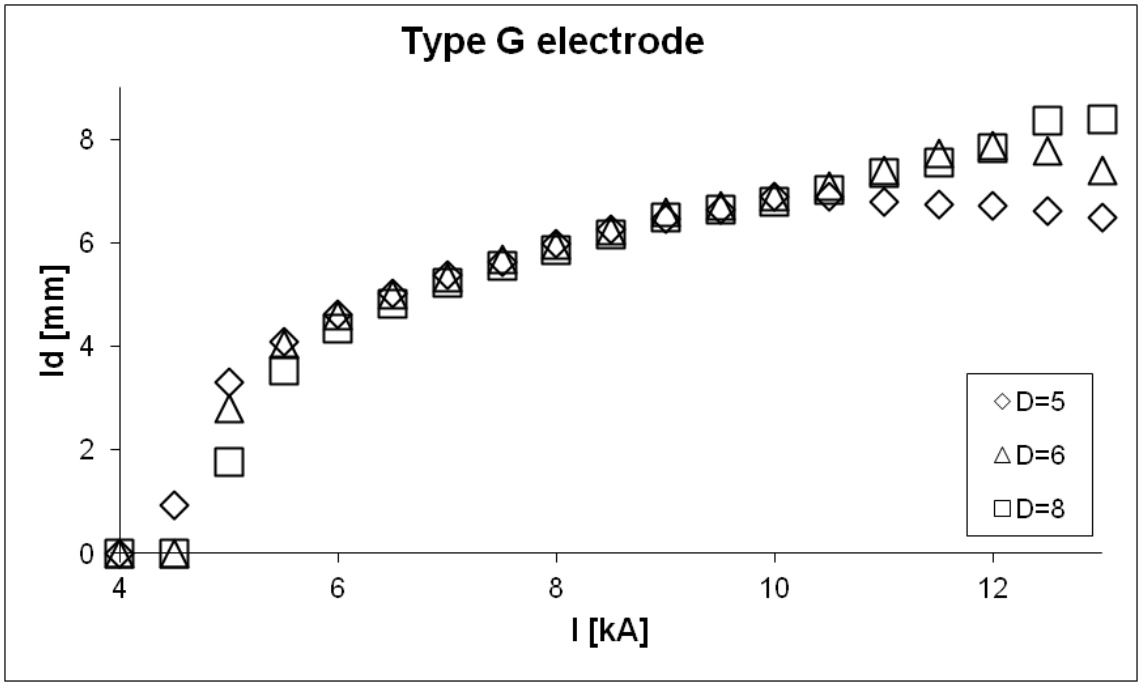

Figure 4.26: Simulated weld growth curve of 1,5 mm TRIP800 GI welded to itself, using G type electrode caps with 5, 6 & 8 mm tip diameters.

The decrease in weld nugget diameter for higher current densities for some of the weld growth curves corresponds with simulated splash welding. Comparing the weld growth curves, the onset of splash welding does not change much with increasing electrode tip diameters. For type B electrodes the first splash welds occur at a welding current of 12 kA when a tip diameter of 5 mm is used, and at 13 kA when a tip diameter of 8 mm is used. For type G electrodes the first splash welds occur at a welding current of 10,5 kA when a tip diameter of 5 mm is used and at 11,5 kA when a tip diameter of 8 mm is used. Together with the shift of the weld growth curve this leads to a decrease of the welding range for type B

electrodes when the contact surface is enlarged whilst the welding range remains almost identical for type G electrodes.

4.3.3 Electrode wear

Figure 4.27 gives the experimentally derived weld growth curves for 2 sheets of 1,25 mm TRIP700 GI using B type electrode caps with 5 and 6 mm tip diameters. The shift to higher welding currents when using larger electrode tip diameters can also be seen here, although the onset of splash welding does not occur here for the larger electrode diameter. Thus the welding range is effectively not shortened. This may be due to the difference in electrode tip surface quality that has a large impact on the shape of the weld growth curve and the size of the welding range.

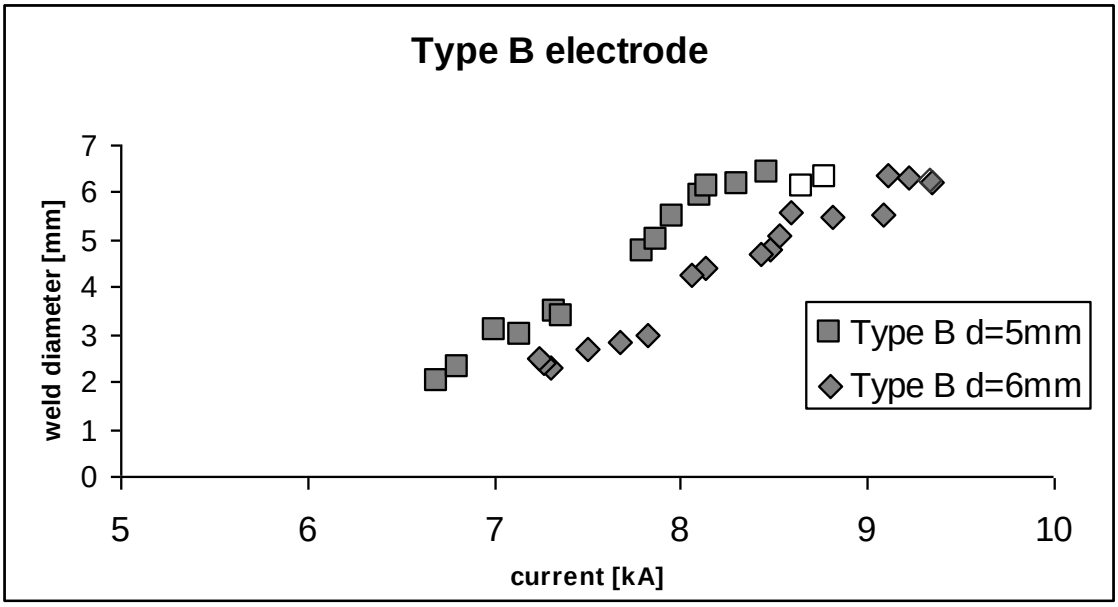

Figure 4.27: Experimental weld growth curve for two sheets of 1,25 mm TRIP700 GI using type B electrode caps with 5 mm (squares) and 6 mm (diamonds) tip diameters. Open squares and diamonds represent splash welds.

Figure 4.28 shows the weld growth curves for TRIP 700 when welded with a 6mm Type B electrode. The squares give the weld growth curve made with a fresh electrode, whilst the diamonds give the curve made with an electrode that has already produced 50 low current welds. The production of 50 low current welds is known as '*electrode conditioning*'. This is done as the fresh electrode properties change rapidly within the first 50 welds when coated steels are processed.

In the first set of welds produced, the electrode surface changes considerably; zinc is picked up and alloys onto the electrode surface and the electrode contact area roughens on a microscopic level. This leads to a reduction in real contact area and an increase in contact resistance, decreasing the welding current needed to make a weld. As more welds are made the electrode tip will deform on a macroscopic level (due to pressure at elevated temperatures) and the electrode diameter will start to grow, leading to an increase in the required welding current. In Figure 4.28 the significance of the effect of the deteriorating electrode contact surface after 50 welds can clearly be seen.

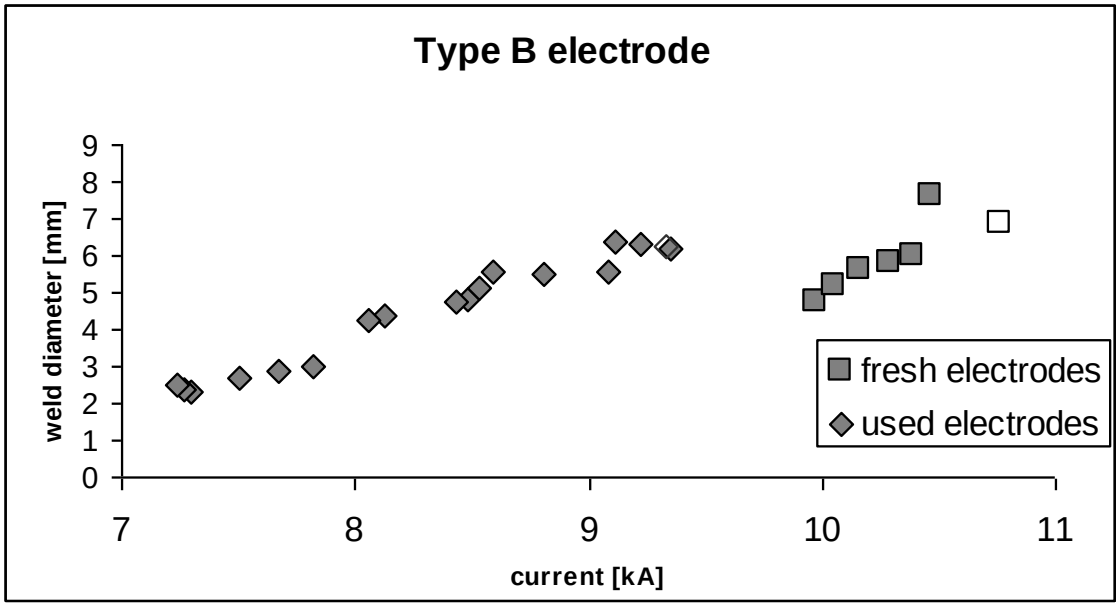

Figure 4.28: Weld growth curves for welding for 1,25 mm TRIP700 GI to itself using type B fresh electrodes (squares) and used electrodes (diamonds) with 6 mm electrode tip diameter. Opens squares and diamonds indicated splash welds.

Figure 4.29 shows the weld growth curves of TRIP800 GI steel sheet welded with constant electrode geometry and process parameters but with varying tip diameters. For each electrode size (*i.e.* tip diameter) two welding curves are shown. The first series is made up of welds made with fresh electrodes (shaded). The second series is made up of welds made with electrodes that have been used to make 50 previous welds. It can be seen that the welding ranges change as the electrode becomes conditioned (*i.e.* the surface alloys with the zinc coating and flattens somewhat due to the clamping force). Not only the welding range changes; but the shape (most notably the slope) of the welding curve changes as well.
It can be seen that the weld growth curves shift to lower currents for conditioned electrode tips, suggesting that the flattening of the electrode tip is not the main effect. It is important to notice that figure 4.29 depicts only welds made at the beginning of the electrode life; the total number of welds typically made with electrodes far exceeds 50 to 60 (depending upon the application several hundred welds will be made). When the electrodes have been used extensively the electrode tip surfaces tend to flatten more and the weld growth curve shifts to higher currents again.

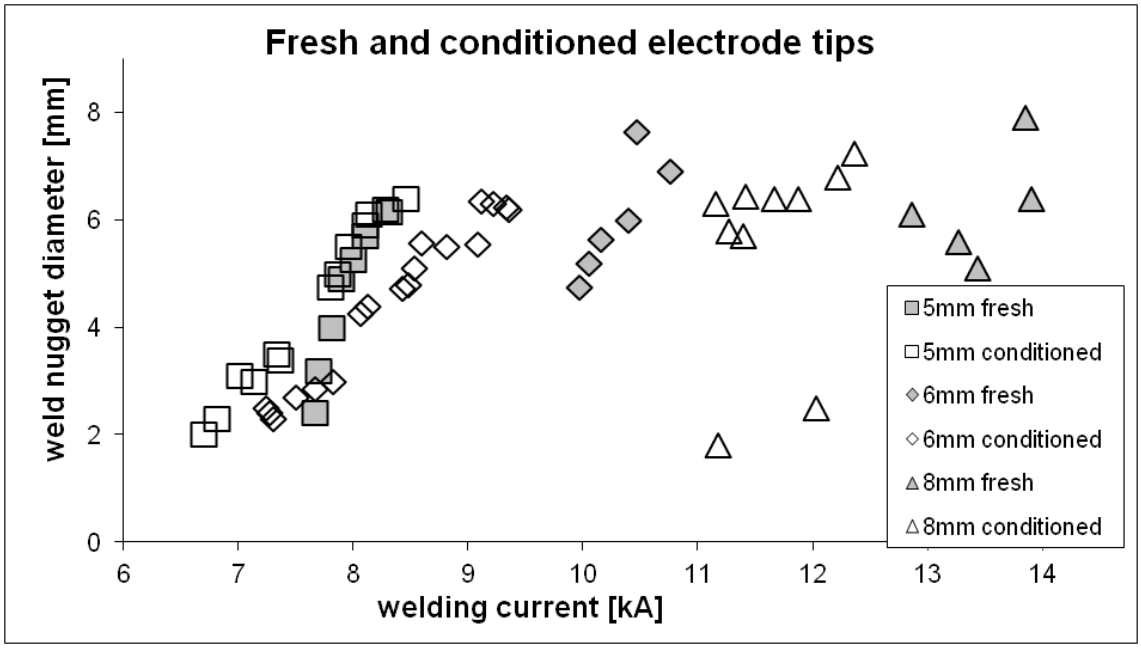

Figure 4.29: Experimentally derived weld growth curves for TRIP800 welded with electrodes with varying electrode tip diameters in two series. The first series (closed symbols) made with fresh electrodes. the second series (open symbols) made with conditioned electrodes (more than 50 welds done).

Simulations were performed to investigate the effect of electrode tip flattening. These simulations were made for two different numerical definitions of TRIP800 steel, varying in their stress-strain curves with temperature. Figure 4.30 shows the two different stress-strain curves used for these simulations. The two different material definitions are referred to as TRIP800-A and TRIP800-B, referring to the curves in figure 4.30. For type A TRIP800, stress is almost independent of strain (except for very low strains), whilst for type B TRIP800, stress increases with increasing strain.

The same electrode geometries as given in figure 4.23 were used for the simulations, To investigate the effect of severe flattening of the electrode tip surfaces, a second set of electrode geometries was defined, with a completely flat electrode tip surface for the area defined by the electrode tip diameter.

All simulations were performed using the same welding schedule: 16 cycles of current application followed by 5 cycles cooling (with electrode pressure applied). The electrode force for all simulations was 4,5 kN. Material thickness was 1,5 mm per steel sheet. For all simulations a 7 µm GI coating on all surfaces was applied, to represent AHSS steel sheets commonly used for automotive applications (at least in Europe).

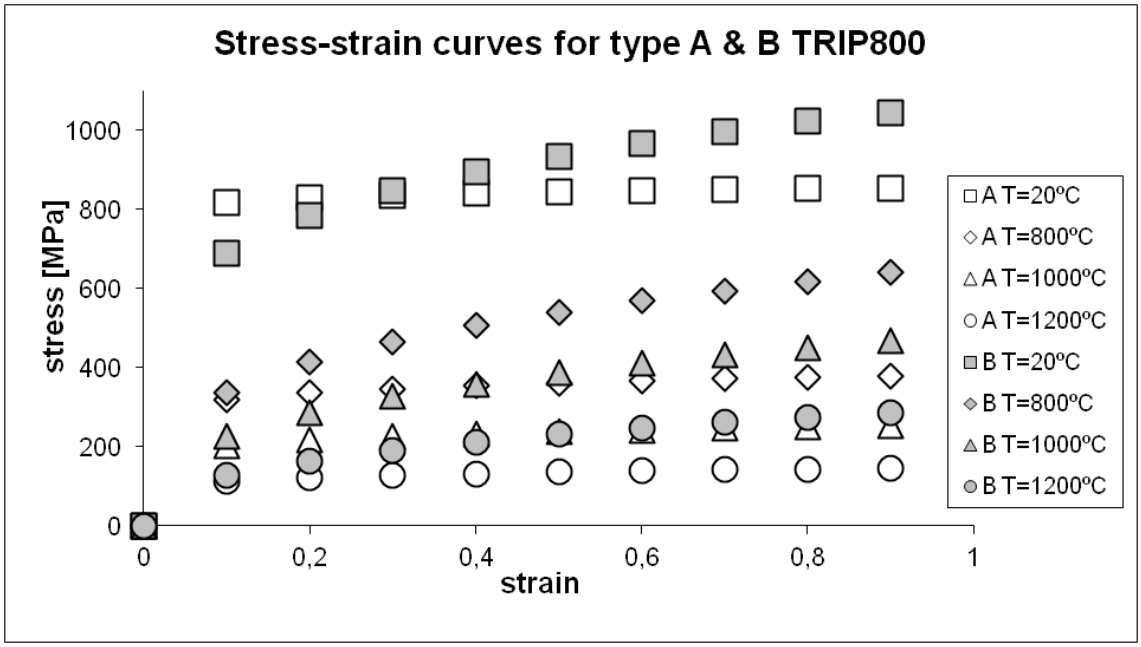

Figure 4.30: Stress-strain curves for TRIP800-A and TRIP800-B steel as used in simulations.

Two types of weld growth curves are reported as results from the simulations: weld nugget diameter as function of welding current and weld nugget volume as function of welding current. To facilitate comparison between different weld growth curves the weld sizes are normalised to the electrode tip diameter by dividing the weld nugget diameter by the electrode tip diameter for weld growth curves depicting the weld nugget diameter as function of welding current:

$$D_n = \left(\frac{D_{weld}}{D_{electrode}}\right) 100\%, \qquad \text{(Eq. 4.10)}$$

where D_{weld} is the weld nugget diameter, and $D_{electrode}$ the electrode tip diameter.

To facilitate comparison between different weld growth curves depicting the weld nugget volume as a function of the welding current, these are normalised to the maximum weld nugget volume of the electrode tip diameter over the full thickness of the steels sheet:

$$V_n = \left(\frac{4V_{weld}}{\pi t_s D_{electrode}^2}\right) 100\%, \qquad \text{(Eq. 4.11)}$$

where V_{weld} is the volume of the weld nugget, t_s the thickness of a single sheet, and $D_{electrode}$ the electrode tip diameter.

Figures 4.31 a & b show the weld growth curves for both type A TRIP800, and type B TRIP800, with figure 4.31a showing the weld nugget diameter, and figure 4.31b the weld nugget volume. All simulated with both rounded and flattened electrode tips. In all cases type G electrodes with 6 mm electrode tip diameter were used.
It can be seen that the weld growth curves shift to higher welding currents for rounded electrode tips, compared with simulations done with flattened electrode tips. It can also be seen that the weld growth curves for weld volume show a more linear growth pattern than the weld growth curves for weld nugget diameter. Note how the use of flattened electrode tips reveals a difference in weld growth behaviour for different materials that is much less apparent for rounded electrode tips.

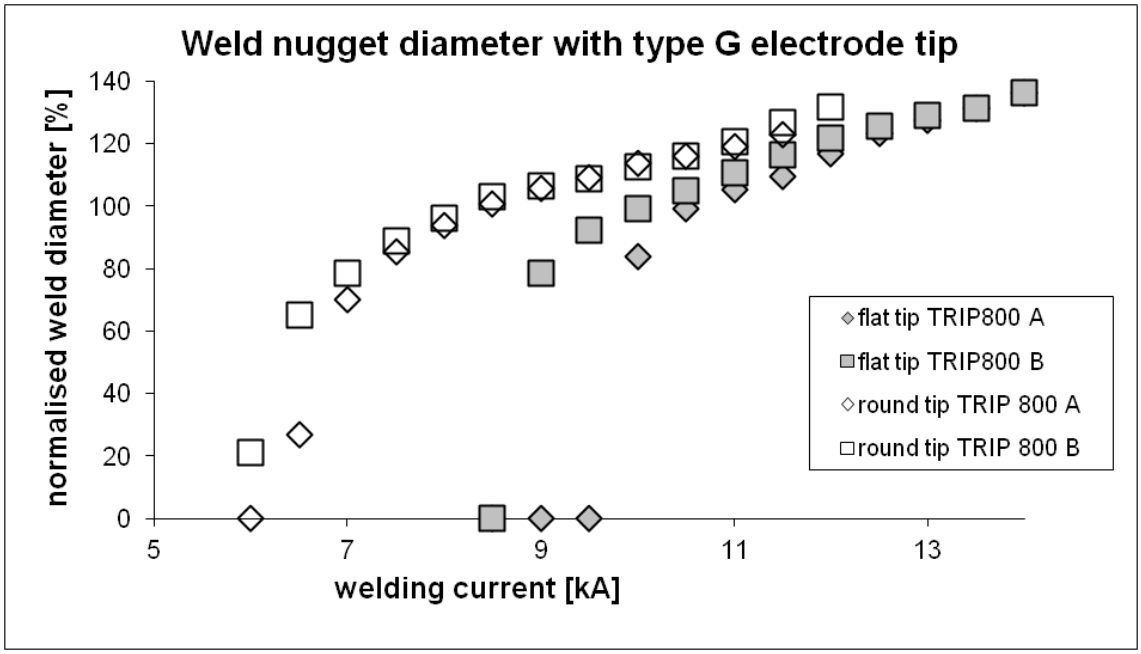

Figure 4.31a: Simulated growth curves for normalised weld nugget diameters of TRIP800, type A & B, welded with type G electrodes, ∅6 mm, with rounded (open symbols) and flattened (closed symbols) electrode tips.

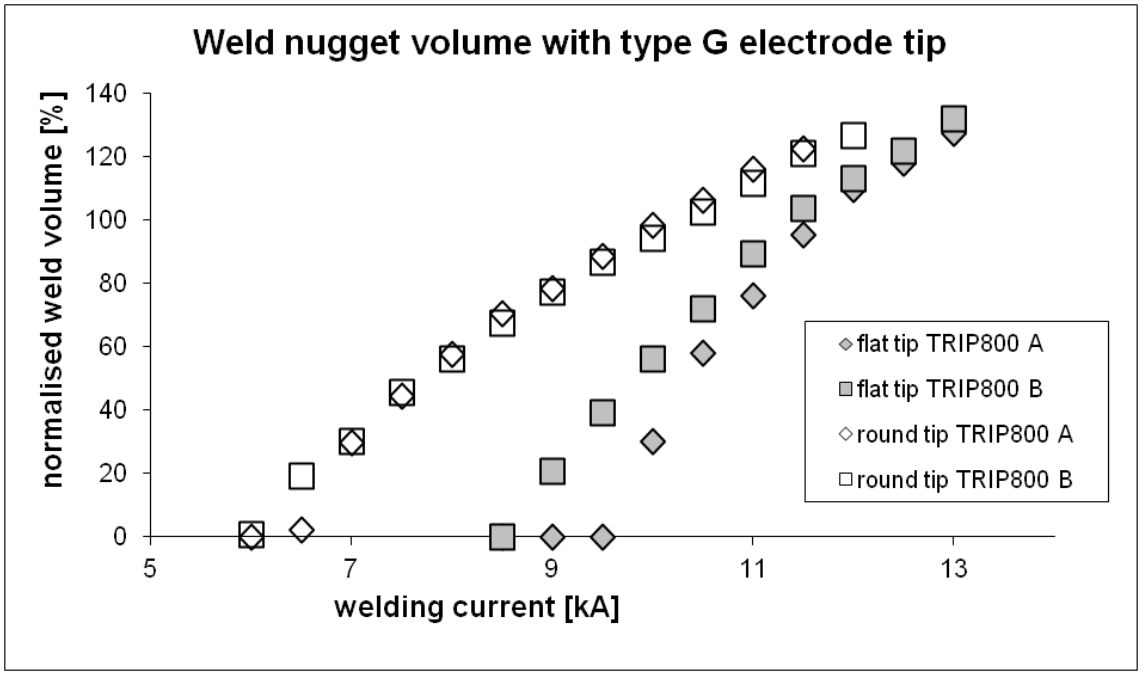

Figure 4.31b: Simulated growth curves for normalised weld nugget volumes of TRIP800, type A & B, welded with type G electrodes, ∅6 mm, with rounded (open symbols) and flattened (closed symbols) electrode tips.

Figures 4.32 a & b show the weld growth curves for normalised weld nugget diameters and weld nugget volumes for type A TRIP800 welded with type B electrode tips of various tip diameters, both rounded and flattened. Again it can be seen that the weld growth curves shift to higher welding currents for flattened electrode tips, compared with simulations done with rounded electrode tips. This effect becomes much more pronounced with increasing electrode tip diameter. Note that the weld growth curve for large flattened electrode diameters shifts to welding currents that are outside the welding current range for rounded

electrodes. Again the weld growth curves for weld volume show a more linear growth pattern than the weld growth curves for weld nugget diameter.

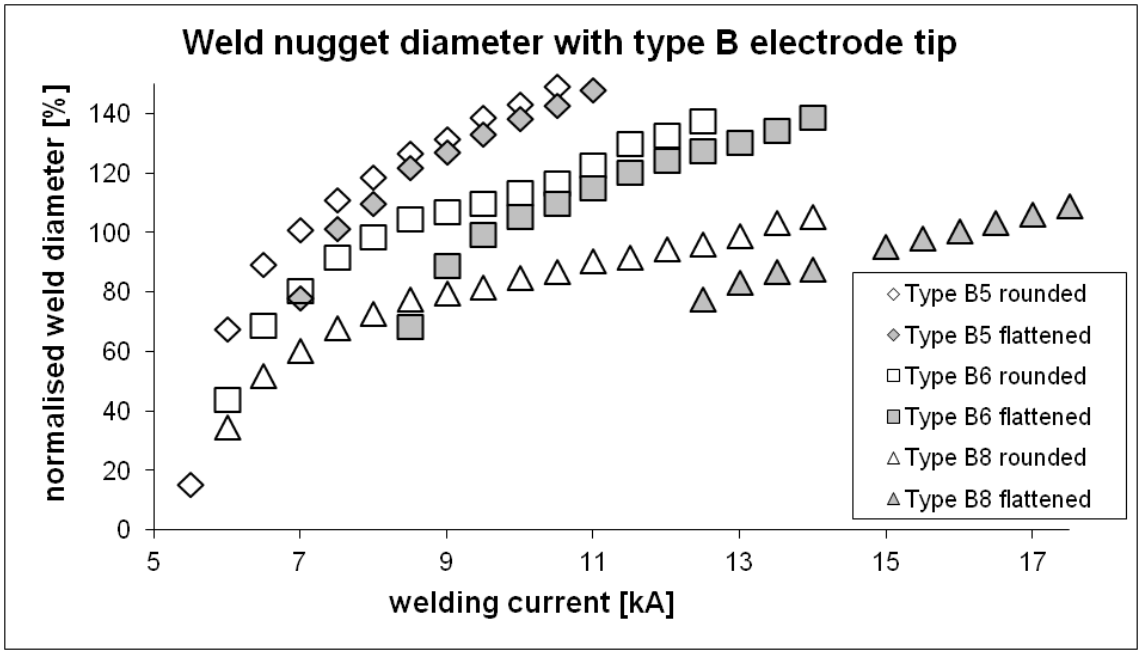

Figure 4.32a: Weld growth curves for weld nugget diameters of type A TRIP800 welded with type B electrodes of varying electrode tip diameters, both rounded (open symbols) and flattened (closed symbols).

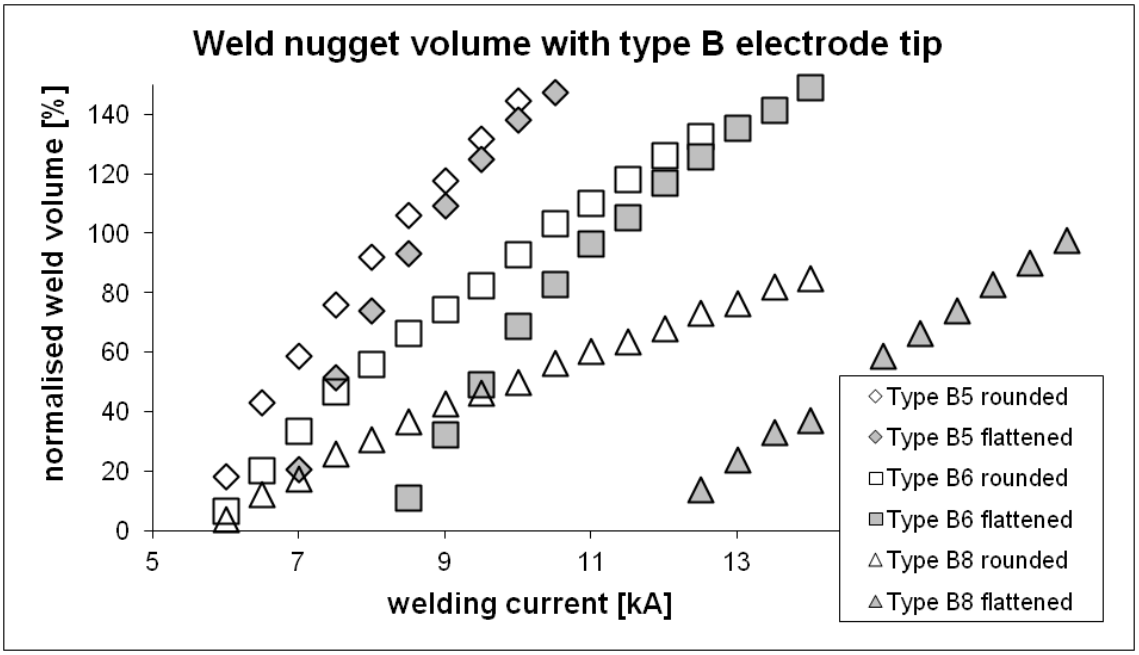

Figure 4.32b: Weld growth curves for weld nugget volumes of type A TRIP800 welded with type B electrodes of varying electrode tip diameters, both rounded (open symbols) and flattened (closed symbols).

Figures 4.33a & b show the simulated weld growth curves type A TRIP800, for both the weld nugget diameter and the weld nugget volume, for type G electrodes of various tip diameters, both round and flattened. Again it can be seen that the weld growth curves shift to higher welding currents for rounded electrode tips, compared with simulations done with flattened electrode tips. Again this effect becomes much more pronounced for increasing electrode tip diameters.

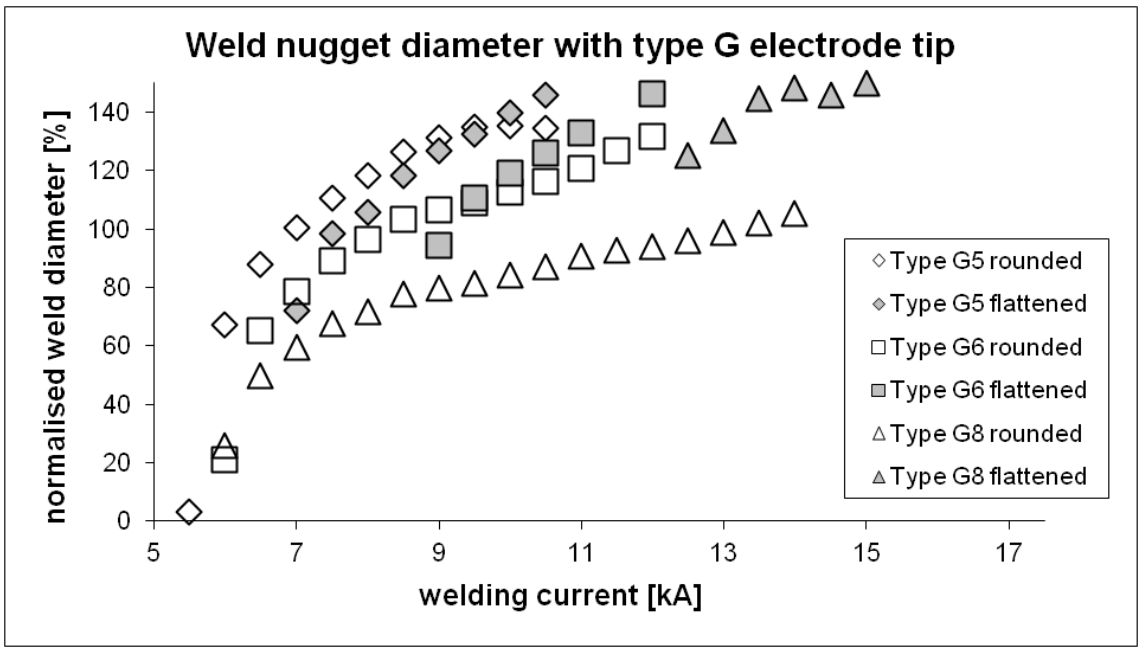

Figure 4.33a: Weld growth curves for weld nugget diameters of type A TRIP800 welded with type G electrodes of varying electrode tip diameters, both rounded (open symbols) and flattened (closed symbols).

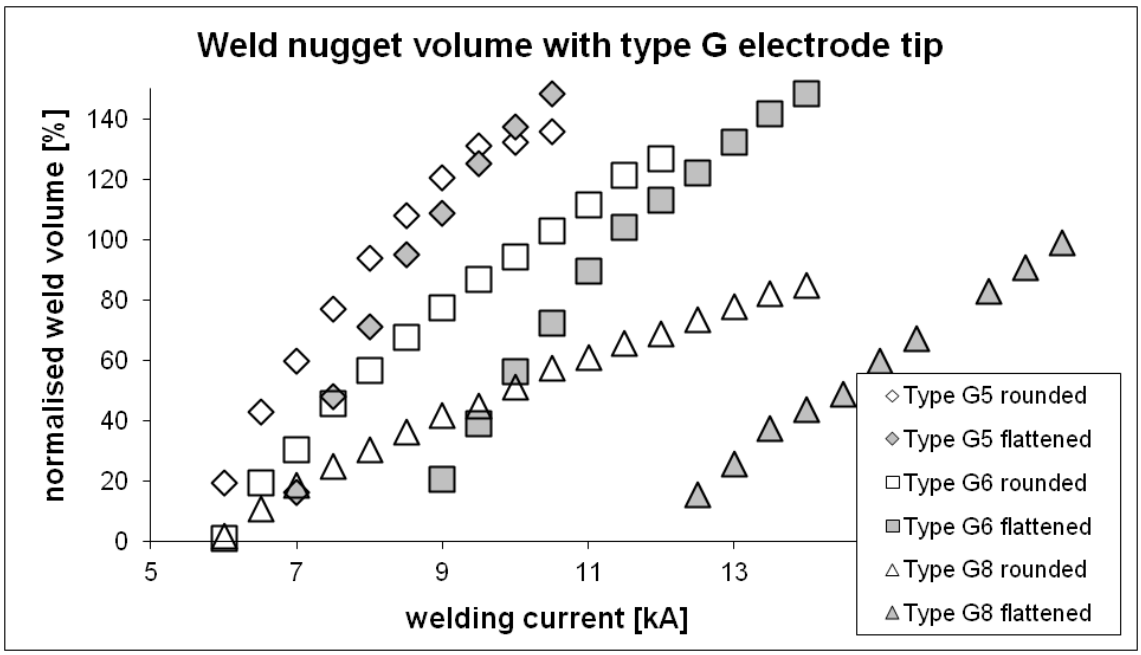

Figure 4.33b: Weld growth curves for weld nugget volumes of TRIP800-A welded with type G electrodes of varying electrode tip diameters for both rounded (open symbols) and flattened (closed symbols) electrode tips.

Note that the weld growth curve for large flattened electrode diameters also show a significant shortening of the weld current range. Again the weld growth curves for weld volume show a more linear growth pattern than the weld growth curves for weld nugget diameter.

Figures 4.34 a & b show the weld growth curves for normalised weld nugget diameters and weld nugget volumes for type A TRIP800 welded with both type B and G electrode tips of 5 mm and 8 mm tip diameters, both rounded and flattened. Note that there is little difference in

growth of weld nugget volume for welding with different electrode types, whilst there is a significant difference for the growth curves of the weld nugget diameter. There is a large difference between welds made with type B electrodes when compared to welds made with type G electrodes, especially for large electrode tip diameters

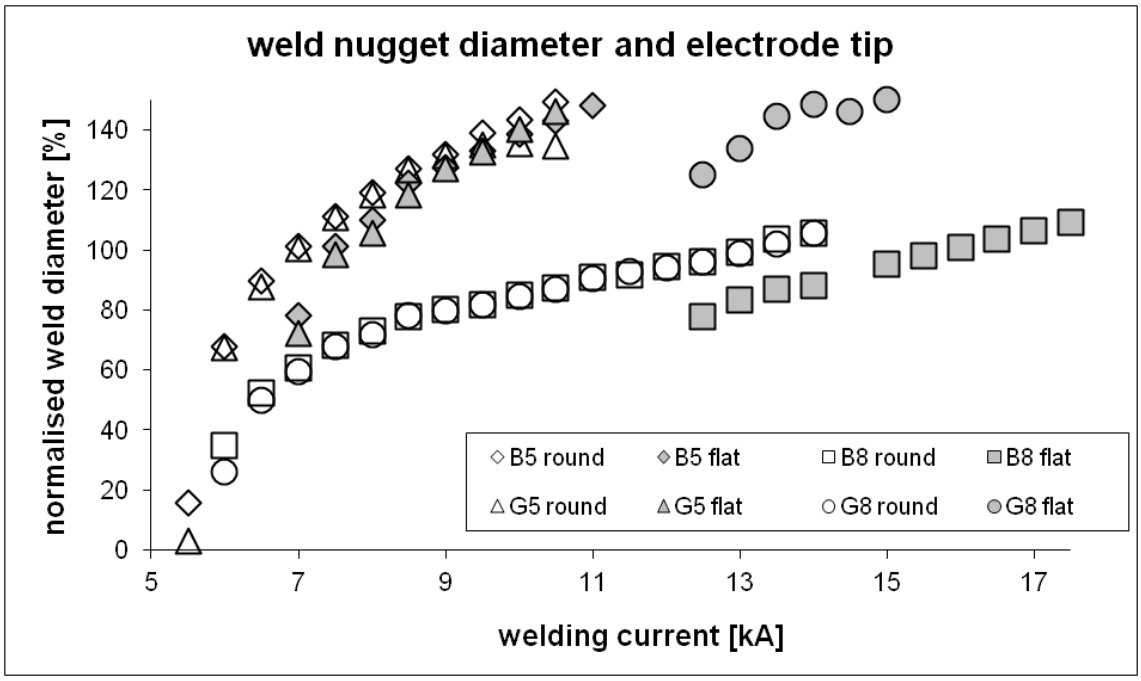

Figure 4.34a: Weld growth curves for weld nugget diameters of TRIP800-A welded with type B and type G electrodes with 5 and 8 mm electrode tip diameters for both rounded and flattened electrode tips.

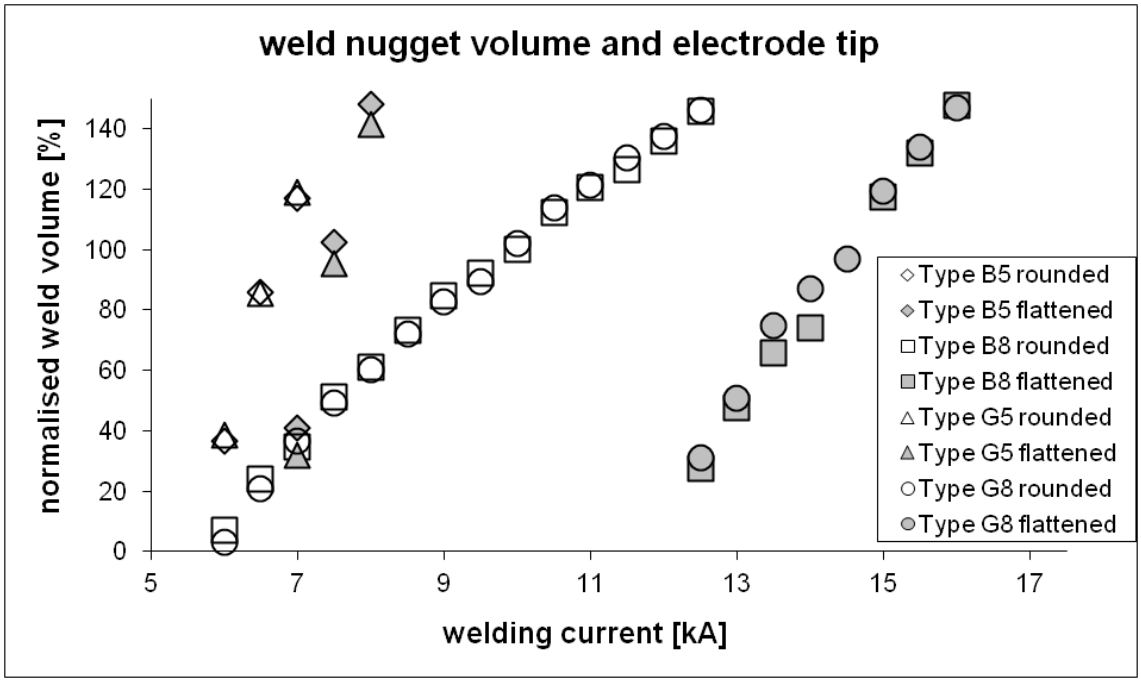

Figure 4.34b: Weld growth curves for weld nugget volumes of TRIP800-A welded with type B and type G electrodes with 5 and 8 mm electrode tip diameters for both rounded and flattened electrode tips.

The results show that the weld nugget size is dependent on the electrode geometry. The size of the weld nugget can either be described by the diameter of the weld nugget or by its

volume. The results show that the diameter is affected by the electrode type and whether the tip is rounded or flattened. This is important as electrode tips become flattened when successive welds are made. As the electrode tips become flatter, the weld growth curves shift to higher welding currents, which leads to smaller welding ranges. This affects the electrode lifetime. The results also show that although the weld nugget diameter is affected by the electrode tip flatness, the volume is not so much affected. It can be seen that the weld nugget volume is primarily dependent on the electrode type.

4.3.4 Weld nugget formation

Welding curves are drawn up using the weld nugget diameter. They do not give any information on the weld nugget volume. Figure 4.35 a & b show the simulated weld nugget cross sections for type B electrode tip with a 6 mm tip diameter (figure 4.35a) and a 8 mm tip diameter (figure 4.35b). Simulations were performed for 1,65 mm thick GI coated TRIP 700 sheets, welded with a 10,5 kA welding current, 0,32 s welding time, and 4,5 kN electrode force. It can be seen that the weld nugget volume is affected by the tip diameters. The difference in outcome can be explained by the increased contact surfaces affecting the generation of heat by decreasing the current density combined with an increased loss of heat by conduction to the water cooled electrode tips, This causes the volume of the welds to decrease, though the weld nugget diameter is essentially the same.

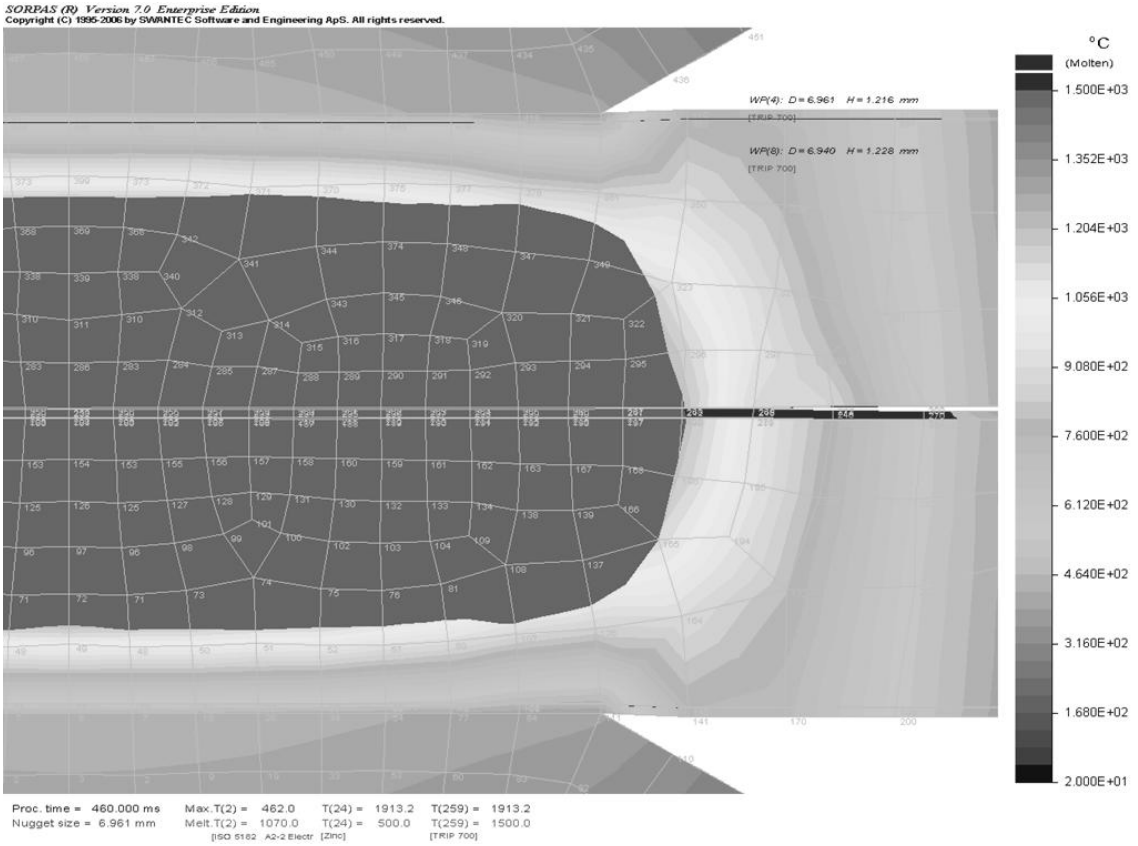

Figure 4.35a: Simulated weld nugget cross section for type B electrode with 6 mm electrode tip diameter welding 1.65 mm TRIP700 GI (welding current 10,5 kA, welding time 0,32 s, and electrode force 4,5 kN).

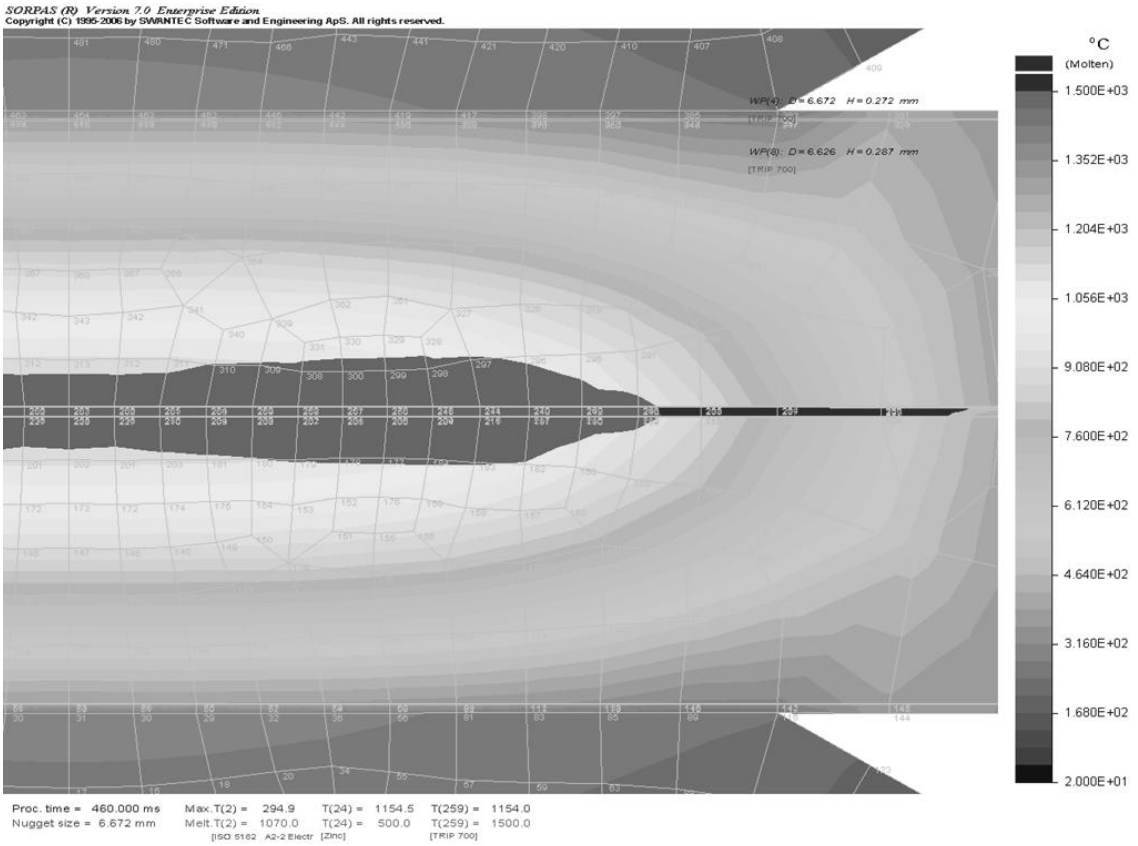

Figure 4.35b: Simulated weld nugget cross section for type B electrode with 8 mm electrode tip diameter welding 1.65 mm TRIP700 GI (welding current 10,5 kA, welding time 0,32 s, and electrode force 4,5 kN).

4.3.5 Electrode dimensions and sheet thickness

An important parameter to assess resistance spot welds is the $5\sqrt{t_s}$ weld nugget diameter (see § 4.2.1). Joining thicker sheet material obviously requires more energy, as $5\sqrt{t_s}$ welds will be larger. The increase in energy needed to form welds is also influenced by other factors. There will be more bulk material in thicker steel sheets that will conduct heat away from the weld. Also thicker sheets will mean more material between the electrodes. Therefore there is more electrical resistance between the electrodes, which will lead to more energy generated.
Simulations were performed welding TRIP700 GI for varying sheet thickness using B type electrode caps with 5 or 6 mm electrode tip diameter, aimed at $5\sqrt{t_s}$ weld nugget diameters, therefore requiring different welding currents, all other process parameters were held constant. Table 4.3 gives the welding currents used in these simulations.

Table 4.3: Welding currents used to simulate $5\sqrt{t_s}$ weld nugget diameters in TRIP700 GI sheets of varying thickness welded with 5 or 6 mm type B electrode tips.

electrode tip diameter [mm]	sheet thickness [mm]	welding current [kA]
5	0,8	7,3
	1,0	7,4
	1,2	8,4
	1,4	9,7
6	1,2	8,4
	1,4	9,0
	1,6	10,0
	1,8	11,3
	2,0	12,7
	2,2	13,5

Figure 4.36 gives the simulated weld current needed to produce a $5\sqrt{t_s}$ weld nugget diameter with varying sheet thickness for type B electrode caps with 5 and 6 mm tip diameters. It can be seen that the increase in weld current is relatively independent of the electrode geometry. This may sound contradictory to earlier results, but as can be seen in table 4.3, the weld nugget diameter may be the same, the weld nugget volume is not. To produce welds with larger volume using larger electrodes would require either longer welding times or higher weld currents. To compare the welds the weld dimensions were normalised, *i.e.* the dimensions are divided by the sheets characteristic dimensions. For the weld nugget diameter the characteristic dimension is $5\sqrt{t_s}$ (figure 4.37). For the weld height the characteristic dimension is the sheet thickness (figure 4.38). For the weld nugget volume the characteristic dimension is $19{,}6 \cdot t_s^2$ $(= \pi(5\sqrt{t_s}/2)^2 \cdot t_s)$ (figure 4.39).

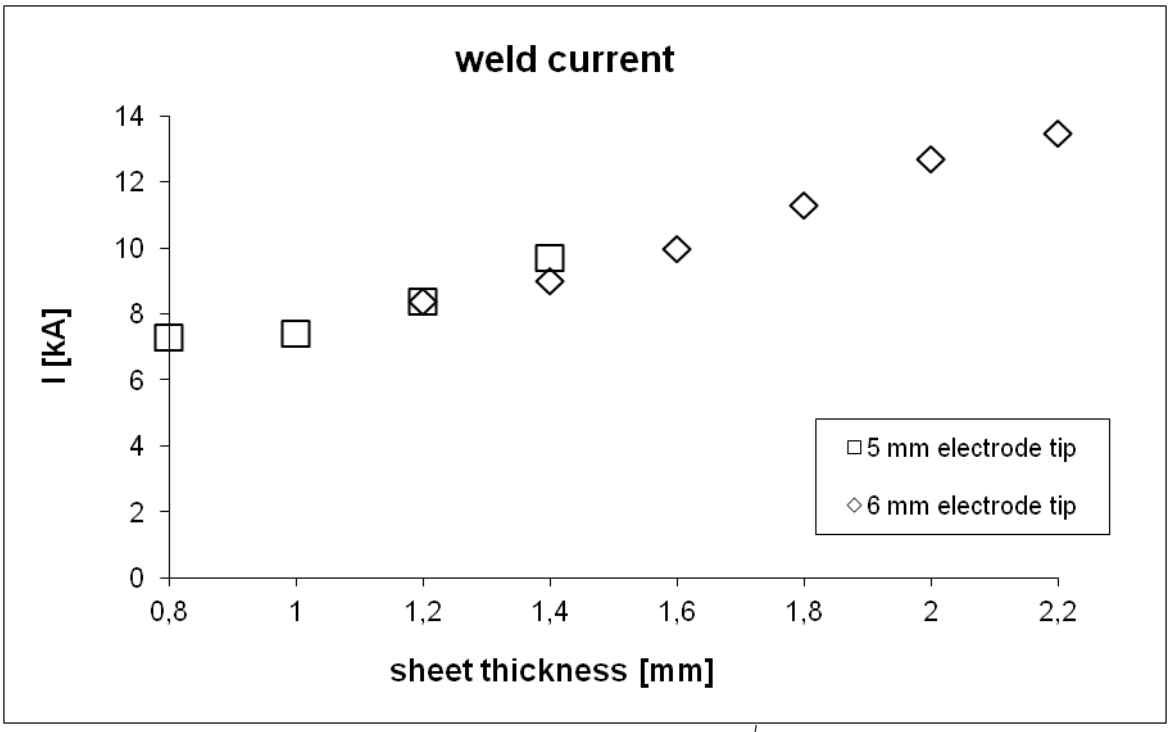

Figure 4.36: Simulated welding current needed to produce $5\sqrt{t_s}$ welds when welding TRIP700 GI sheet to itself using type B electrodes with 5 and 6 mm electrode tip diameters.

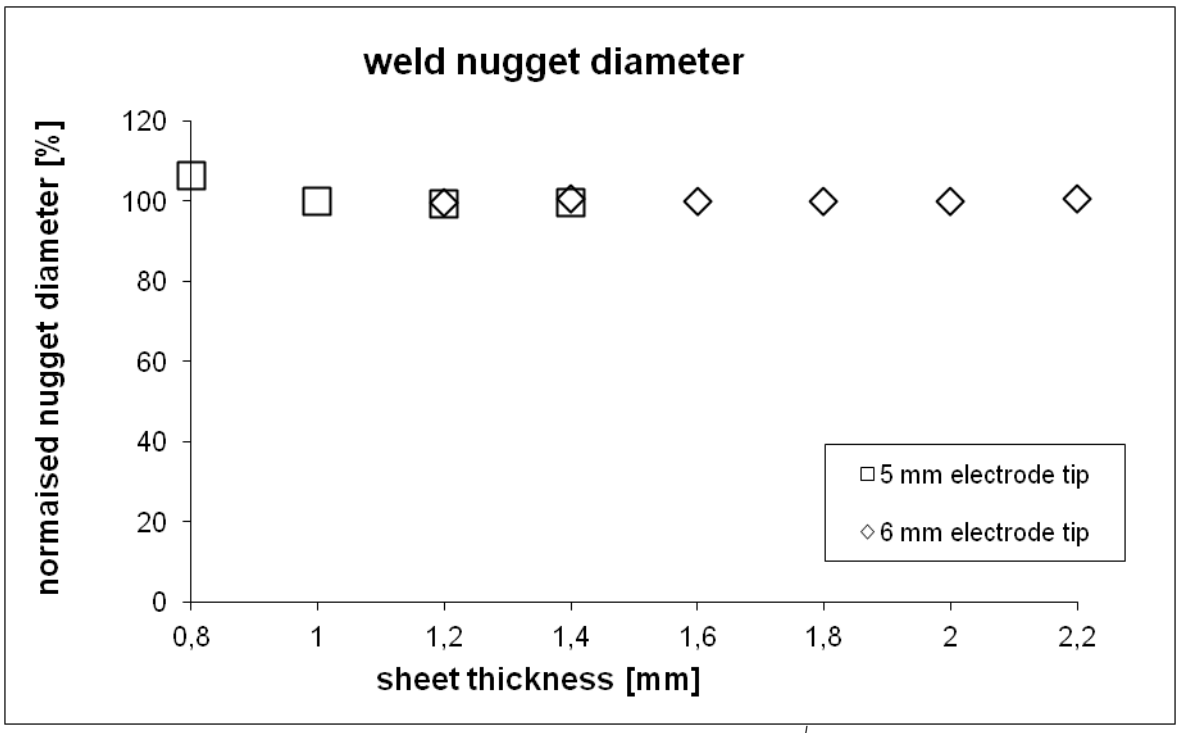

Figure 4.37: Normalised simulated weld nugget diameter for $5\sqrt{t_s}$ welds when welding TRIP700 GI sheet to itself using type B electrodes with 5 and 6 mm electrode tip diameters, for various steel sheet thicknesses.

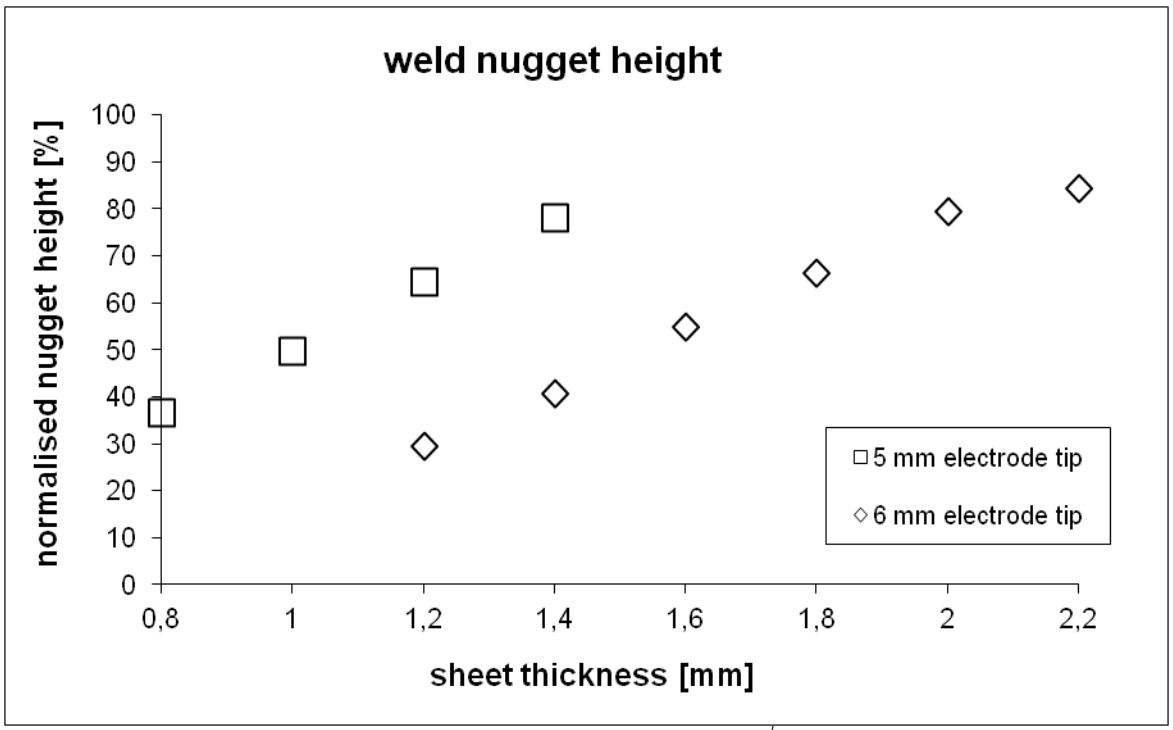

Figure 4.38: Normalised simulated weld nugget height for $5\sqrt{t_s}$ welds when welding TRIP700 GI sheet to itself using type B electrodes with 5 and 6 mm electrode tip diameters, for various steel sheet thicknesses.

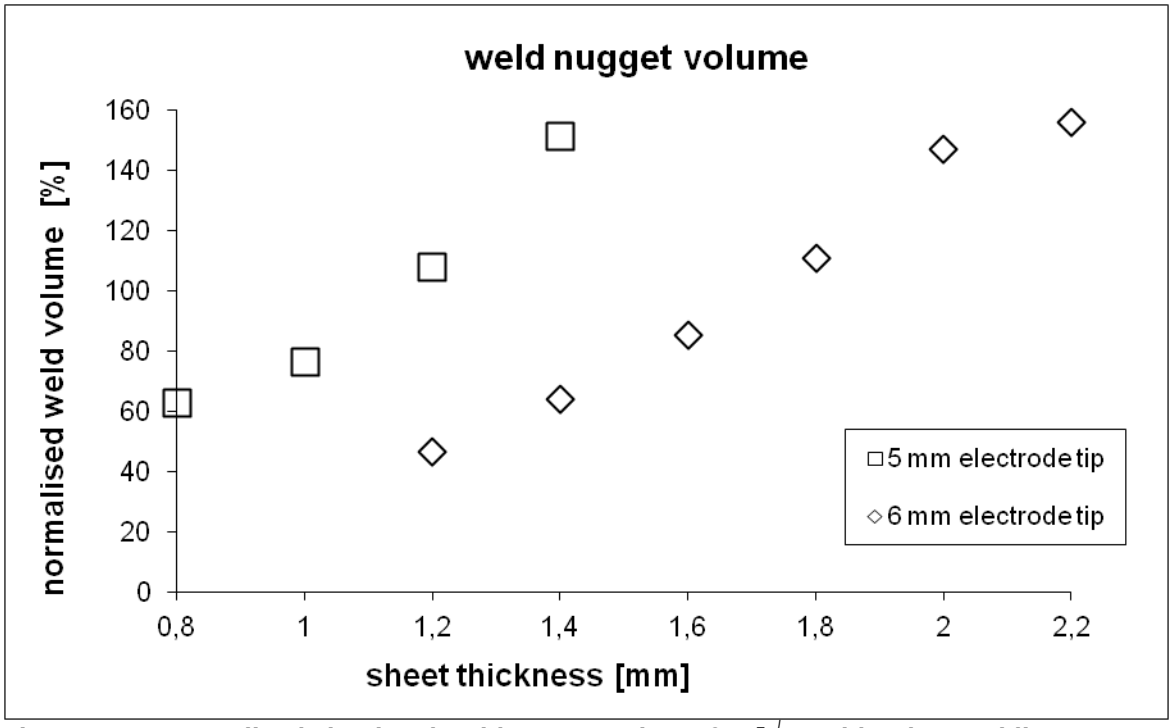

Figure 4.39: Normalised simulated weld nugget volume for $5\sqrt{t_s}$ welds when welding TRIP700 GI sheet to itself using type B electrodes with 5 and 6 mm electrode tip diameters, for various steel sheet thicknesses.

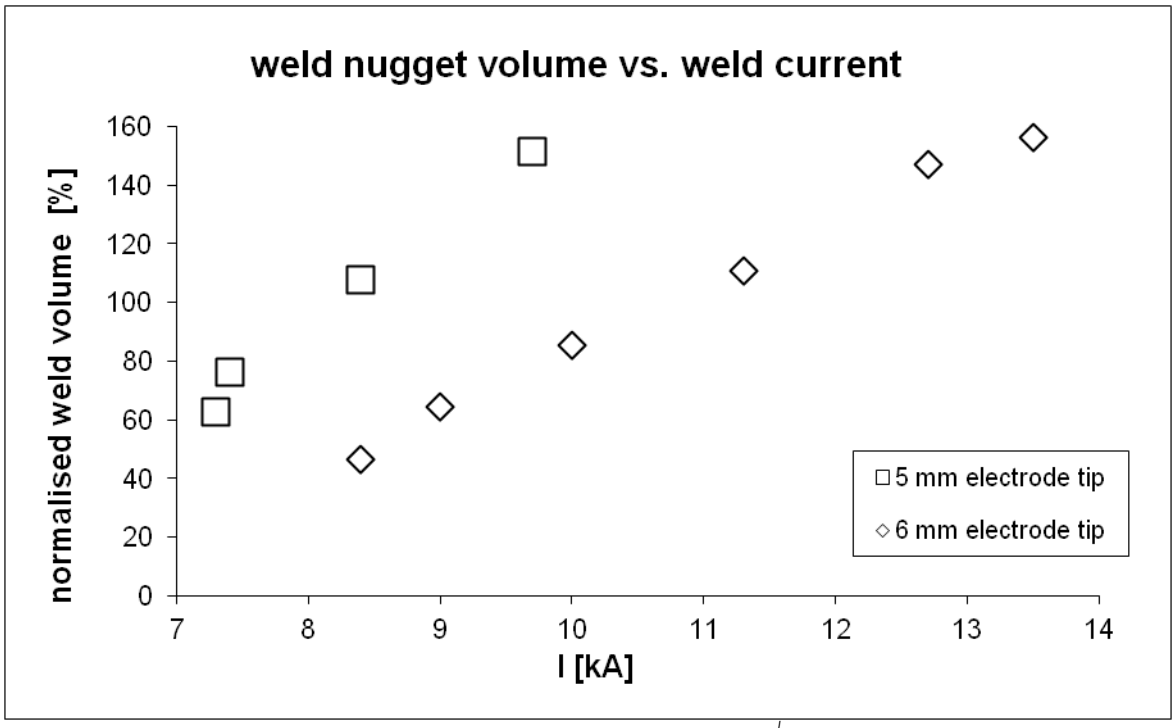

Figure 4.40: Normalised simulated weld nugget volume for $5\sqrt{t_s}$ welds when welding TRIP700 GI sheet to itself using type B electrodes with 5 and 6 mm electrode tip diameters, for various welding currents.

It is not surprising that the dimensionless weld diameter (figure 4.37) is constant with the steel sheet thickness, as the target weld diameters were directly dependent upon sheet thickness, independent of electrode geometry. The weld nugget height increases with increasing sheet thickness (figure 4.38). This is because the weld pool, as it forms, forms not on a spot but over an area along the weld interface. Further addition of heat serves to grow

the weld not just in diameter, but more so in height. The result of this is most obvious in the growth of weld volume (figure 4.39). When the weld volume is measured against the welding current used it can be seen that it takes less energy to form a certain volume weld using smaller electrodes (figure 4.40). It can also be seen that the increase in growth of weld volume decreases as the sheet thickness increases. This is because the weld diameter becomes larger than the electrode diameter, making it harder for the weld to grow and eventually leading to splash. It is interesting to note that the dimensionless height and volume can never reach a full 100% as the material between the electrodes is compressed during welding and therefore the height of the sheet locally decreases.

The results show that the primary parameter determining the welding current necessary to produce a weld nugget of sufficient size is the steel sheet thickness. It can also be seen that the relative height of the weld nugget (*i.e.* compared to the sheet thickness) increases with increasing sheet thickness. This also becomes apparent in the relative weld nugget volume, indicating that more energy is needed to produce a weld nugget of sufficient size in thicker sheets.

5. Weldability in Performance

5.1 Introduction

In this chapter performance aspects of the weldability of advanced high strength steels are examined. There are two main topics of discussion:

1. Post weld hardness
2. Post weld heat treatment

The first topic relates to the main issues identified in the literature that cause undesirable weld failure modes, the second topic relates to measures that can be taken to counter the effects of excess post weld hardness to achieve desirable weld failure modes.

The data used in this chapter has been published at various conferences, seminars, and in journals. Work on the relation between chemical composition and post weld hardness has been presented in 2006 at 3rd International Conference on Mathematical Modelling and Information Technologies in Welding and Related Processes, in Kiev, Ukraine (*Modelling the Influence of Resistance Spot Welding on Material Properties*; Den Uijl, 2006b), in 2007 at 60th Annual Assembly of the IIW-IIS, in Dubrovnik, Croatia (*Prediction Of Post Weld Hardness Of Advanced High Strength Steels For Automotive Application Using A Dedicated Carbon Equivalence Number*; Den Uijl *et al.*, 2007), and in 2008 in the November/December issue of Welding in the World (*Prediction of post weld hardness of advanced high strength steels for automotive application using a dedicated carbon equivalent number*; Den Uijl *et al.*, 2008).
The data on the performance of resistance spot welded joints and post weld heat treatment has been published in 2006 at the 4th International Seminar on Advances in Resistance Welding in Wels, Austria (*Resistance Spot Welding of Advanced High Strength Steels for the Automotive Industry*; Den Uijl & Smith, 2006), in 2008 at the 5th International Seminar on Advances in Resistance Welding in Toronto, Canada (*Failure modes of resistance spot welded advanced high strength steels*; Den Uijl *et al.*, 2008a), in 2010 at the 63rd Annual Assembly of the IIW-IIS in Istanbul, Turkey (*Performance of resistance spot welded joints in advance high strength steel in static and dynamic tests*; *Den Uijl, 2010*), and in 2012 in the July/August issue of Welding in the World (*Performance of resistance spot welded joints in advance high strength steel in static and dynamic tensile tests*; (Den Uijl *et al.*, 2012a).

5.2 Post Weld Hardness

Post weld hardness of materials has been identified as a parameter relating to weld performance. The idea is that harder welds will fail in a brittle manner; with this in mind various automotive manufacturers have set limits on the post weld hardness of resistance welded joints. If the post weld hardness of welded joints in advanced high strength steels can be related to a simple material characteristic, this would allow designers to make predictions about the performance of welded joints and would help manufacturing engineers to set up welding operations in production. It would also give steel producers a tool to design materials with increased weldability.

In this section post weld hardness of resistance spot welded advanced high strength steel sheets is reviewed. A review of different parameters influencing the post weld hardness is given. The underlying mechanisms influencing post weld hardness are discussed and a

simple relation between the chemical composition of the material and the resultant post weld hardness is derived.

5.2.1 Background

Material thickness, chemical composition (specifically carbon content) and various carbon equivalence numbers all have been proposed to predict the performance of welded joints in steel sheet [Shi & Westgate, 2003, Chao, 2003, Westgate 2004, Mimer *et al.*, 2004, Marya & Gayden, 2005, Gould *et al*., 2006 & Shi & Westgate, 2007].
The thickness of a material is related to the post weld hardness of welded joints *via* the cooling rate. First of all the size of the weld nugget is determined by the material thickness as welding operations are generally aimed at a weld nugget diameter that is a multiple of the square root of the thickness of the materials joined. Thinner materials will have smaller weld nuggets, thus less heat is accumulated in the material. The build up of heat in a material is not just dependent upon the desired size of the weld pool, it is also dependent on the chemical composition of the material, as this will influence the thermal capacity and the electrical resistance through the mechanism of Joule heating . The electrical resistance of a material is also influenced by additional scattering events caused by lattice defects such as grain boundaries and microstructural composition (thus an advanced high strength steel composed of various phases will have a higher electrical resistance than a mono-phase material of similar chemical composition). Additionally the distance between the hot material and the water-cooled electrodes is smaller, which will increase cooling rates. Thinner materials will cool faster as less heat builds up and needs to be removed. In general it can be concluded that post weld hardness will have a relation with material thickness within a certain range of material grades (taking into account chemical and microstructural make up).
The chemical composition of a material will influence the post weld hardness of a material because it affects the electrical resistance and the thermal conductivity. More important is the influence that the chemical composition of the material will have on the hardenability of the material. Increased alloying levels will change the cooling rates at which steels will form harder phases. In general it can be stated that increased alloying levels will decrease the critical cooling rates. The critical cooling rate for a steel is the lowest rate at which a steel can be quenched to give an all martensitic structure. At lower rates bainite and/or finely divided pearlite will form [Davies, 1984].
Traditionally in welding text books, $t_{8/5}$, *i.e.* the cooling time between 800ºC and 500ºC, is mentioned as an important parameter to determine post weld microstructure and corresponding post weld hardness of welded joints [Granjon, 1991]. The idea behind this is based upon standard continuous cooling transformation (CCT) diagrams. CCT diagrams show the transformations that occur during continuous cooling form a fully austenised steel to room temperature. A key feature of a CCT diagram is the inclusion of the resultant hardness values for the cooling trajectories.
Figures 5.1 a&b respectively show an experimentally determined CCT diagram for a DP600 steel with corresponding resultant hardness [Den Uijl, 2009]. It can be seen that the cooling rate between 800ºC and 500ºC is critical as there are trajectories where none of the regions giving rise to softer phases (bainite, ferrite & pearlite) are crossed. Such cooling trajectories will result in martensitic welds of high hardness. The critical cooling rate is here the trajectory that just misses these regions (“the nose”), and is a property of the steel [AWS, 1976].

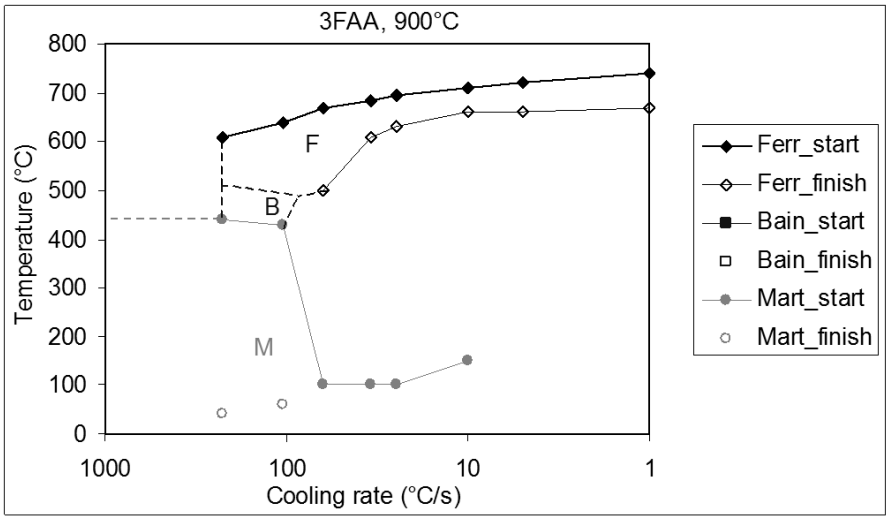

Figure 5.1 a: Experimentally derived CCT diagram for a DP600 steel (0,09 wt% C, 0,25 wt% Si, 1,65 wt% Mn, 0,03 wt% Al, 0,01 wt% P, 0,575 wt% Cr) [Kop, 2006].

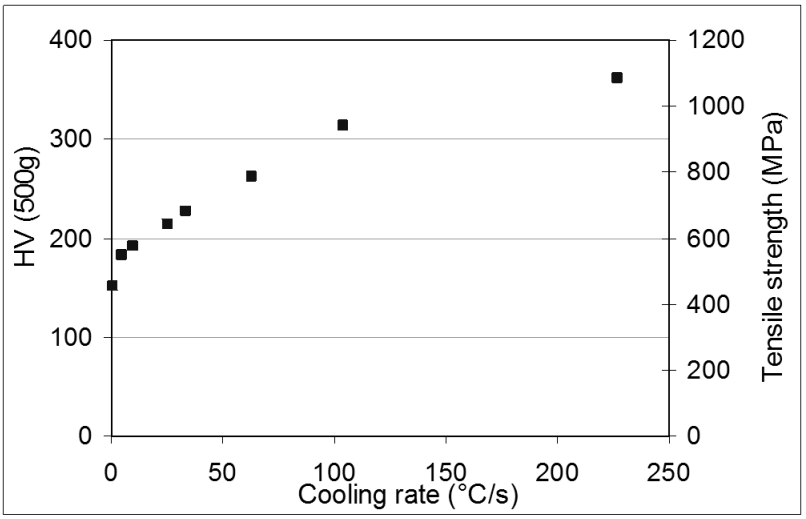

Figure 5.1 b: Measured hardness values corresponding to the CCT diagram of figure 5.1 [Kop, 2006].

The main alloying element determining the hardness of martensite is carbon. Increased carbon content will lead to increased hardness of martensite. Carbon is also the main element determining the critical cooling rate, or the width of the region in the CCT diagram that results in the formation of fully martensitic welds (see figure 5.1a). Increased carbon levels will cause martensite to form at lower cooling rates [Bhadeshia & Honeycombe, 2006]. To relate the influence of various other alloying elements, relative to the effect of carbon on the hardenability of a material, carbon equivalence (CE) numbers have been developed. The main carbon equivalence number in use within the welding community is the so-called IIW CE:

$$CE\ (IIW) = C + \frac{Mn}{6} + \frac{Cr + Mo + V}{5} + \frac{Ni + Cu}{15}, \qquad \text{(Eq. 5.1)}$$

with the alloying content of various elements in wt% [IIW, 1967].

The IIW CE number was drawn up to be used for steels with carbon levels exceeding 0,18 wt% C. Over the years steels and their applications have changed considerably. As far as automotive applications are concerned, much higher strength levels are desired to enable

manufacturers to reduce weight, whilst maintaining performance (fatigue and crash). The chemical composition and process routes of steels changed as applications posed new demands on the strength and formability of steels.

Carbon Equivalence numbers relate the type and composition of a steel to its weldability, but they themselves are also dependent upon the chemical composition of the steel. In 1967 Ito & Bessyo published a carbon equivalence number for steels with $C < 0{,}12\ wt\%$.

$$CE(P_{cm}) = C + \frac{Si}{30} + \frac{Mn + Cu + Cr}{20} + \frac{Ni}{60} + \frac{Mo}{15} + \frac{V}{10} + 5B, \qquad \text{(Eq. 5.2)}$$

with the alloying content of various elements in wt%.

5.2.2 Post Weld Hardness and Welding Processes

A batch of laboratory steels was cast to examine the influence of various chemical compositions on weldability . All steels were hot and cold rolled to a thickness of 1,4 mm. The tensile strength of all these steels was approximately 900 MPa. As the focus of the experiments was on the post weld hardness in the weld; the steels did not undergo any further heat treatment (*e.g.* annealing) prior to welding. Samples of the material were welded using different welding processes: resistance spot welding (RSW), laser beam welding (LBW) and plasma arc welding (PAW) . Table 5.1 gives the chemical composition of these materials [Den Uijl *et al.*, 2007].

Resistance spot welding was done using a 5 kA AC welding current, 2,94 kN electrode force and 18 cycles welding time (60 Hz). All samples were welded with a type B electrode (d_1 = 16 mm, d_2 = 6 mm, and R_1 = 16 mm; as in figure 4.2.2). Each sample was welded with a 10 cycles (60 Hz) hold after welding as well as with a 60 cycles (60 Hz) hold, *i.e.* forced cooling, after welding . After welding the post weld hardness for both sets of samples was measured using a 9,8 N load (see table 5.1). Laser beam welding was done using a 3 kW YAG laser (focus diameter: 0,6 mm). Process speed was 3m/min and argon was used as shielding gas (15 l/min). After welding the post weld hardness was measured (see table 5.1). Plasma arc welding was done using a 120 A welding current at a process speed of 1 m/min. The plasma gas used was argon + 10 % hydrogen, with a flow of 0,5 l/min. The shielding gas used was argon + 10% hydrogen, with a flow of 10 l/min. After welding the post weld hardness was measured (see table 5.1).

Figure 5.2 shows the post weld hardness of the materials from table 5.1 against their carbon content. From this figure it can be seen that the post weld hardness relates directly to the carbon content of the material. Figures 5.3, 5.4, 5.5, and 5.6 show the relation between post weld hardness and carbon content for the materials from table 5.1 for the different welding processes. It can be seen that high cooling rates (such as experienced during resistance spot welding) increase post weld hardness. When cooling rates decrease (such as in the case of laser beam welding, but even more significantly in plasma arc welding) there is more scatter in the post weld hardness. This may be attributed to elements other than carbon increasingly influencing post weld hardness, as the material does not become fully martenistic after welding.

Table 5.1: Chemical composition of lab cast materials and post weld hardness [Den Uijl et al., 2007]. Post weld hardness given after resistance spot welding (RSW) with short cooling period (10 cycles, 0,1 s, of contact between electrodes and sheets after welding), resistance spot welding with long cooling period (60 cycles, 1,0 s, of contact between electrodes and sheets after welding), laser beam welding (LBW), and plasma arc welding (PAW).

						Post weld hardness			
Steel	**C**	**Si**	**Mn**	**Cr**	**Mo**	**RSW short cool**	**RSW long cool**	**LBW**	**PAW**
[#]	**[wt%]**	**[wt%]**	**[wt%]**	**[wt%]**	**[wt%]**	**[HV]**	**[HV]**	**[HV]**	**[HV]**
St01	0,001	0,040	1,440	0,000	0,000	165	188	156	107
St02	0,001	0,040	1,460	0,000	0,000		194	176	114
St03	0,002	0,700	1,500	0,000	0,000	202	206	158	139
St04	0,002	2,000	1,500	0,000	0,000	241	247	186	161
St05	0,050	0,060	1,470	0,000	0,000		332	259	188
St06	0,050	0,070	1,390	0,000	0,000	320	328	227	188
St07	0,050	0,700	1,500	0,000	0,000	318	336	249	220
St08	0,098	0,050	1,470	0,000	0,000	356	368	304	211
St09	0,098	0,100	1,440	0,000	0,000	345	401	298	237
St10	0,098	0,200	1,430	0,000	0,000	333	372	326	259
St11	0,099	0,050	1,490	0,000	0,000	377	351	307	210
St12	0,100	0,000	0,000	0,000	0,000	304	334	172	142
St13	0,100	0,000	1,500	0,000	0,000	337	367	266	238
St14	0,100	0,050	1,000	0,000	0,000	347	356	349	298
St15	0,100	0,050	1,000	0,000	1,000	345	338	353	335
St16	0,100	0,050	1,000	0,000	2,000	366	379	311	300
St17	0,100	0,050	1,000	1,000	0,000	350	363	326	271
St18	0,100	0,050	1,000	2,000	0,000	353	368	269	255
St19	0,100	0,700	0,000	0,000	0,000	355	355	202	179
St20	0,100	0,700	1,000	0,000	0,000		354	230	189
St21	0,100	0,700	1,500	0,000	0,000	346	367	294	250
St22	0,100	0,700	3,000	0,000	0,000	387	395		354
St23	0,100	1,500	1,000	0,000	0,000	372	415	294	259
St24	0,100	1,500	1,500	0,000	0,000	373	367	319	274
St25	0,100	1,500	3,000	0,000	0,000	374	406	379	365
St26	0,140	0,060	1,440	0,000	0,000	384	397	416	375
St27	0,140	0,060	1,450	0,000	0,000	385	403	316	229
St28	0,140	1,420	1,540	0,000	0,000		399	329	349
St29	0,150	0,060	1,430	0,000	0,000		412	343	311
St30	0,150	0,070	1,370	0,000	0,000	401	438	333	324
St31	0,150	0,700	1,500	0,000	0,000	402	420	317	289
St32	0,150	1,440	1,540	0,000	0,000	416	390	374	351
St33	0,180	0,060	1,460	0,000	0,000		417	409	372
St34	0,190	0,050	1,450	0,000	0,000	395	438	392	294
St35	0,200	0,000	1,500	0,000	0,000	423	416	421	396
St36	0,200	1,000	1,500	0,000	0,000	462	462	365	326
St37	0,200	2,000	0,200	0,000	0,000		474	397	399
St38	0,200	2,000	1,500	0,000	0,000	478	484	392	367
St39	0,200	2,000	3,000	0,000	0,000		505	345	
St40	0,300	0,000	1,500	0,000	0,000	511	521	457	442
St41	0,300	1,000	1,500	0,000	0,000		532	457	461
St42	0,300	2,000	1,500	0,000	0,000	547	589	486	464

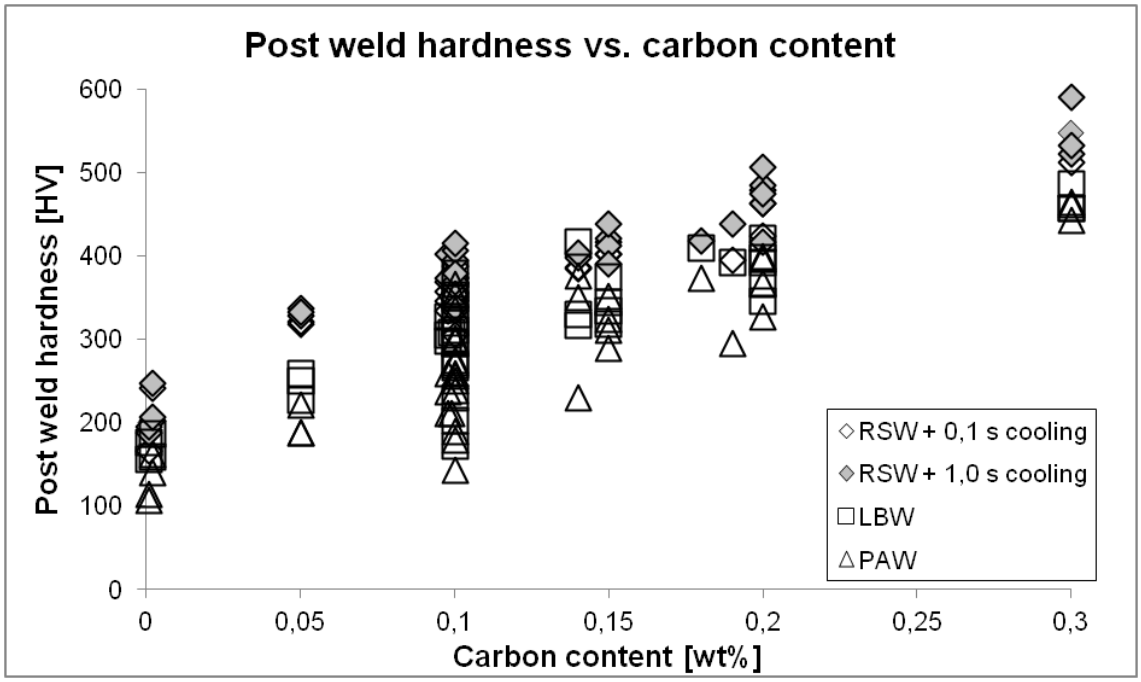

Figure 5.2: Measured post weld hardness versus carbon content of the welded lab cast materials in table 5.1.

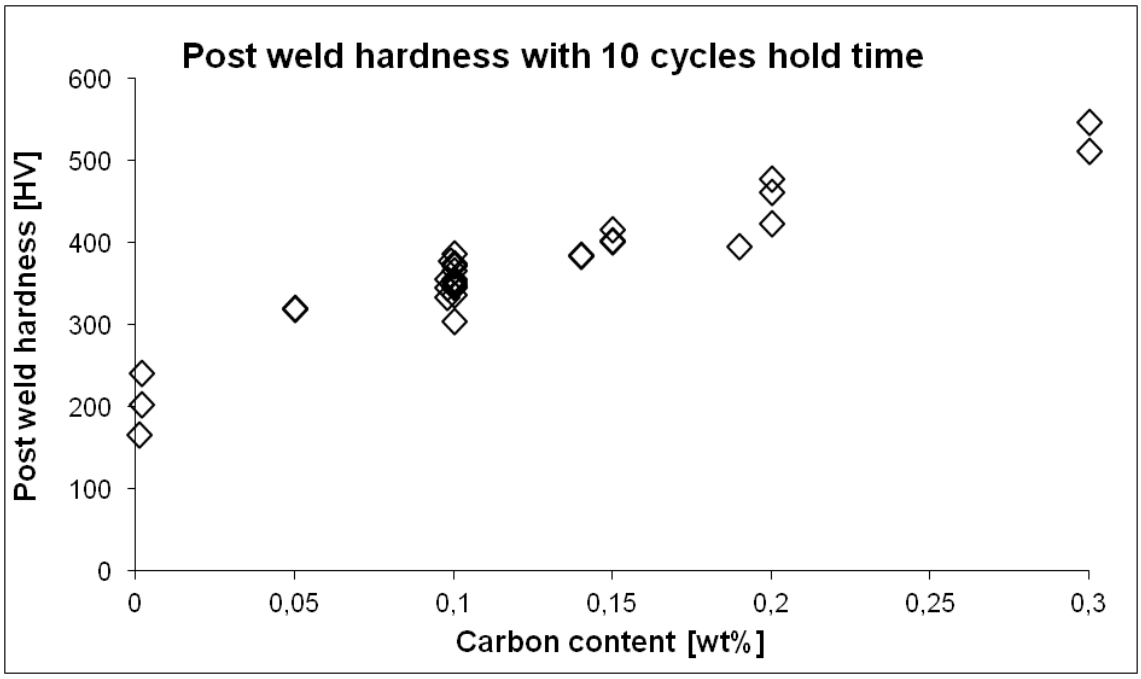

Figure 5.3: Post Weld Hardness vs. Carbon content of materials listed in Table 5.1 after resistance spot welding using a 10 cycle hold time to cool after welding before release of electrodes.

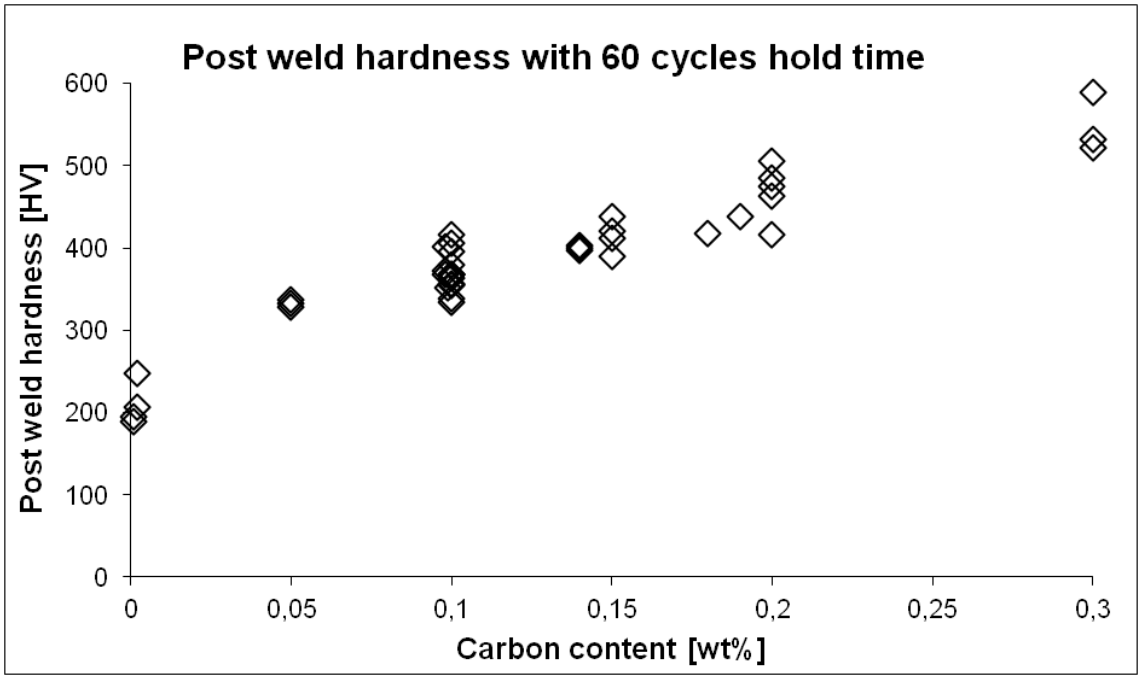

Figure 5.4: Post Weld Hardness vs. Carbon content of materials listed in Table 5.1 after resistance spot welding using a 60 cycle hold time to cool after welding before release of electrodes.

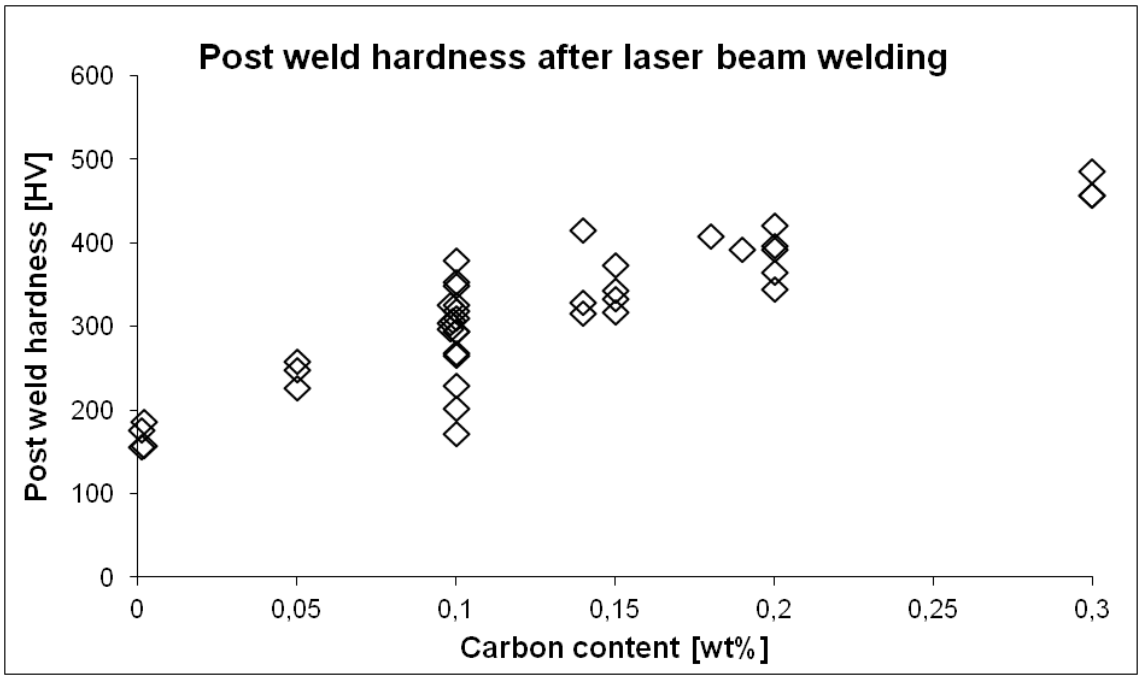

Figure 5.5: Post Weld Hardness vs. Carbon content of materials listed in Table 5. 1 after laser beam welding.

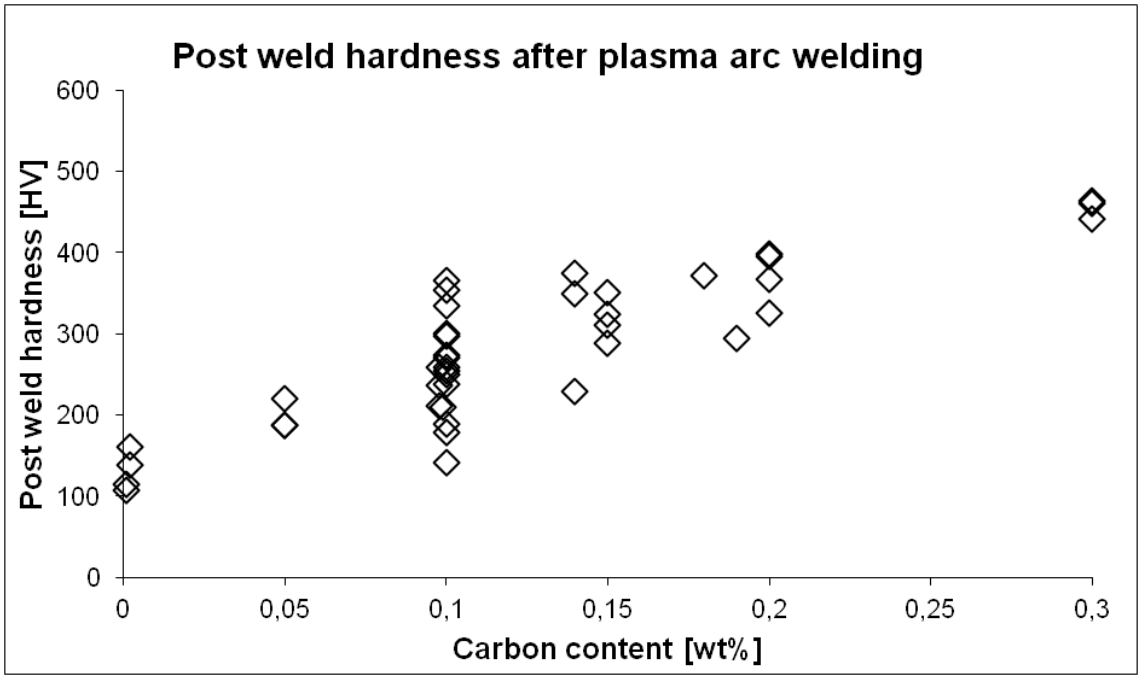

Figure 5.6: Post Weld Hardness vs. Carbon content of materials listed in Table 5.1 after plasma arc welding.

Regression analysis was used to derive relationships between the chemical composition and post weld hardness for the different welding processes and the materials in table 5.1.

For resistance spot welding with forced cooling (60 cycles, 1,0 s, hold time) the following relationship was determined:

$$HV = 229 + 1088\left(C + \frac{Si}{88} + \frac{Mn}{102} + \frac{Cr}{91} + \frac{Mo}{99}\right), \quad \text{(Eq. 5.3)}$$

with the alloying content of various elements in wt%.

For resistance spot welding without forced cooling (10 cycles, 0,1 s, hold time) the post weld hardness relation is:

$$HV = 217 + 1080\left(C + \frac{Si}{70} + \frac{Mn}{113} + \frac{Cr}{93} + \frac{Mo}{71}\right). \quad \text{(Eq. 5.4)}$$

For laser beam welding the relation is:

$$HV = 108 + 1063\left(C + \frac{Si}{77} + \frac{Mn}{21} + \frac{Cr}{28} + \frac{Mo}{30}\right). \quad \text{(Eq. 5.5)}$$

For plasma arc welding the relation is:

$$HV = 52 + 1061\left(C + \frac{Si}{44} + \frac{Mn}{24} + \frac{Cr}{20} + \frac{Mo}{17}\right). \quad \text{(Eq. 5.6)}$$

Table 5.2 shows statistical data for the regression analyses. The coefficient of determination, R^2, is over 0,9 for all welding processes. It can be concluded that the equations have high significance for predicting post weld hardness in AHSS.

Table 5.2: Statistical data for regression analysis [Den Uijl et al., 2008]. Forced cooling refers to 60 cycles (1,0 s) of hold time and free cooling refers to 10 cycles (0,1 s) of hold time.

	RSW (forced cooling)	**RSW (free cooling)**	**LBW**	**PAW**
R^2	*0,91*	*0,91*	*0,91*	*0,94*
observations	*42*	*33*	*42*	*42*

.

Table 5.3 gives the P-value (probability) for the coefficients for the various elements in all four equations, as well as the off-set value (intercept). The P-value gives an indication of the probability that the result is caused by chance. A low P-value indicates that an element is likely to be a parameter in the derived equations for the post weld hardness. Generally a P-value below 5% is seen as significant. The P-value is very low for carbon in all four cases. The P-value for the other elements varies between the different welding processes. The probability for the Mn, Cr & Mo coefficients is high for the resistance spot welding, but with decreasing cooling rates, the P-value for the Si, Mn, Cr and Mo coefficients decreases to lower levels.

Table 5.3; Coefficients and probability of the coefficients as derived by regression analysis [Den Uijl et al., 2008]. Forced cooling refers to 60 cycles (1,0 s) of hold time and free cooling refers to 10 cycles (0,1 s) of hold time.

	RSW (forced cooling)		**RSW (free cooling)**		**LBW**		**PAW**	
	coeff.	**P-value**	**coeff.**	**P-value**	**coeff.**	**P-value**	**coeff.**	**P-value**
intercept	*229*	*1,96E-19*	*217*	*8,04E-15*	*108*	*3,24E-09*	*52*	*4,35E-04*
C	*1088*	*1,85E-19*	*1080*	*2,23E-15*	*1063*	*1,49E-18*	*1161*	*3,22E-20*
Si	*12*	*6,18E-02*	*15*	*3,76E-02*	*14*	*3,77E-02*	*27*	*2,82E-04*
Mn	*11*	*1,44E-01*	*10*	*2,46E-01*	*50*	*5,58E-07*	*49*	*5,15E-07*
Cr	*12*	*3,43E-01*	*12*	*3,35E-01*	*38*	*6,65E-03*	*57*	*6,68E-05*
Mo	*11*	*3,67E-01*	*15*	*1,91E-01*	*35*	*8,72E-03*	*69*	*1,91E-06*

It can be concluded that the main element determining post weld hardness is carbon for fast cooling rates. As cooling rates decrease other elements start to play their part. Compared to resistance spot welding the influence of manganese, chromium and molybdenum on post weld hardness increases for laser beam welding. The influence of silicon increases as the cooling rate decreases from laser beam welding to plasma arc welding. It can also be seen that with decreasing cooling rates the offset hardness decreases. This should happen as the offset hardness captures the influence of cooling rate (high cooling rates lead to the formation of hard phases, increase occurrence of lattice defects, and limit auto-tempering).

Figures 5.7, 5.8, 5.9, and 5.10 show the calculated post weld hardness for the various welding processes using equations 5.3, 5.4, 5.5, and 5.6 versus the measured post weld hardness given in table 5.1.

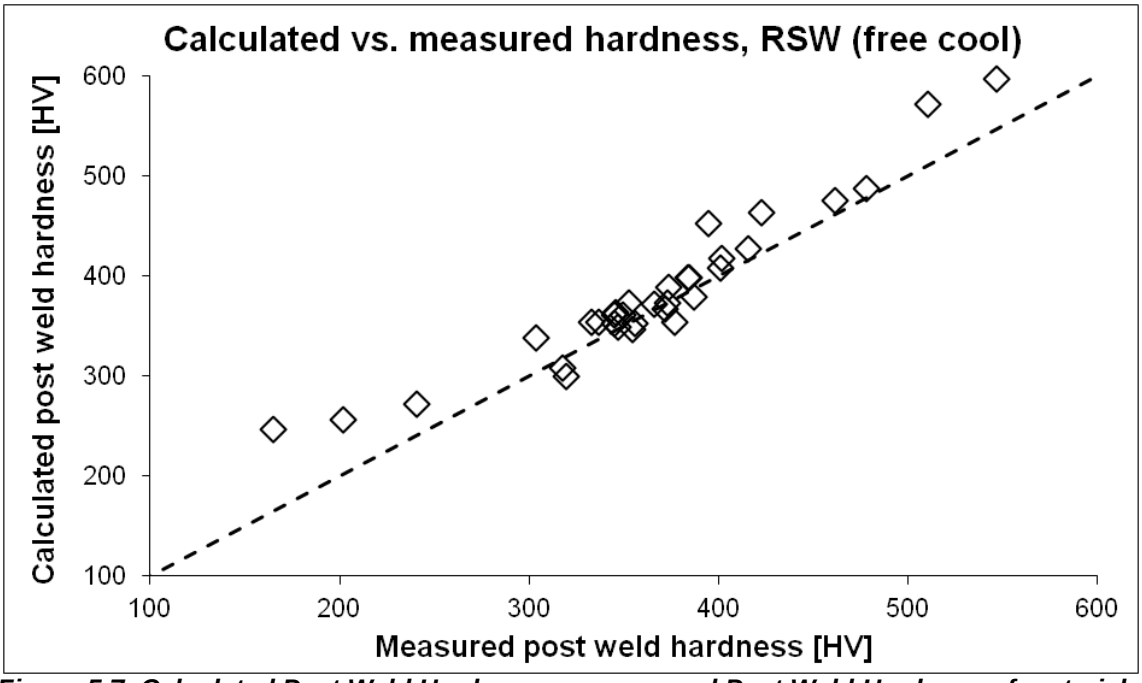

Figure 5.7: Calculated Post Weld Hardness vs. measured Post Weld Hardness of materials listed in Table 5.1 after resistance spot welding using a 10 cycle hold time to cool after welding before release of electrodes.

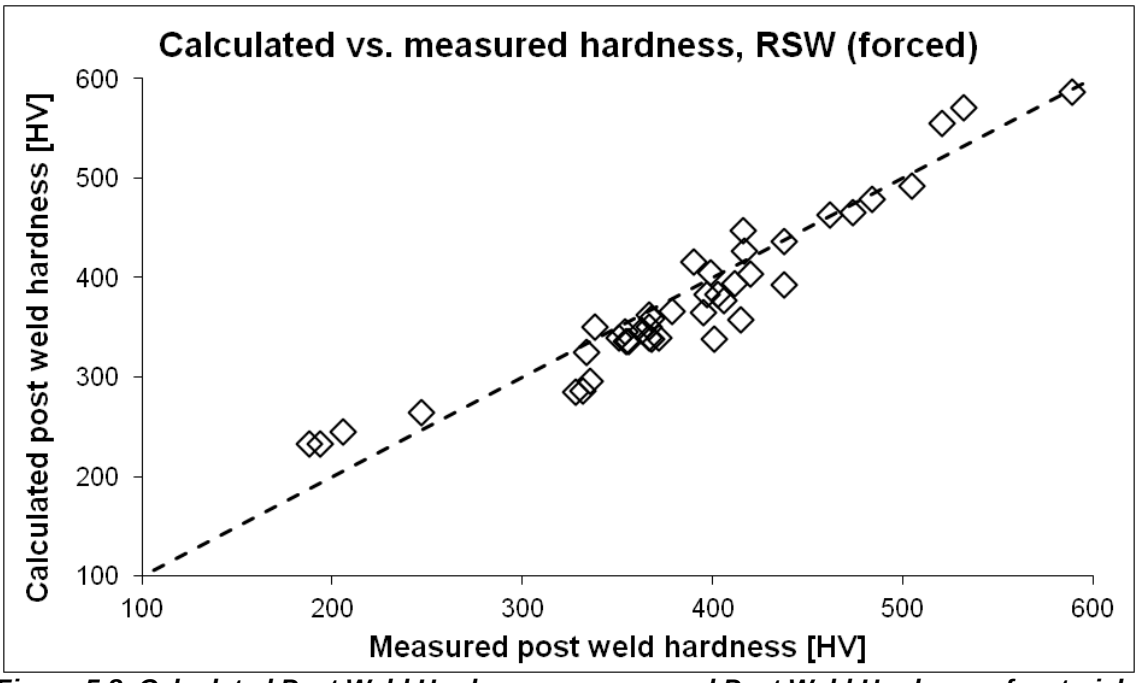

Figure 5.8: Calculated Post Weld Hardness vs. measured Post Weld Hardness of materials listed in Table 5.1 after resistance spot welding using a 60 cycle hold time to cool after welding before release of electrodes.

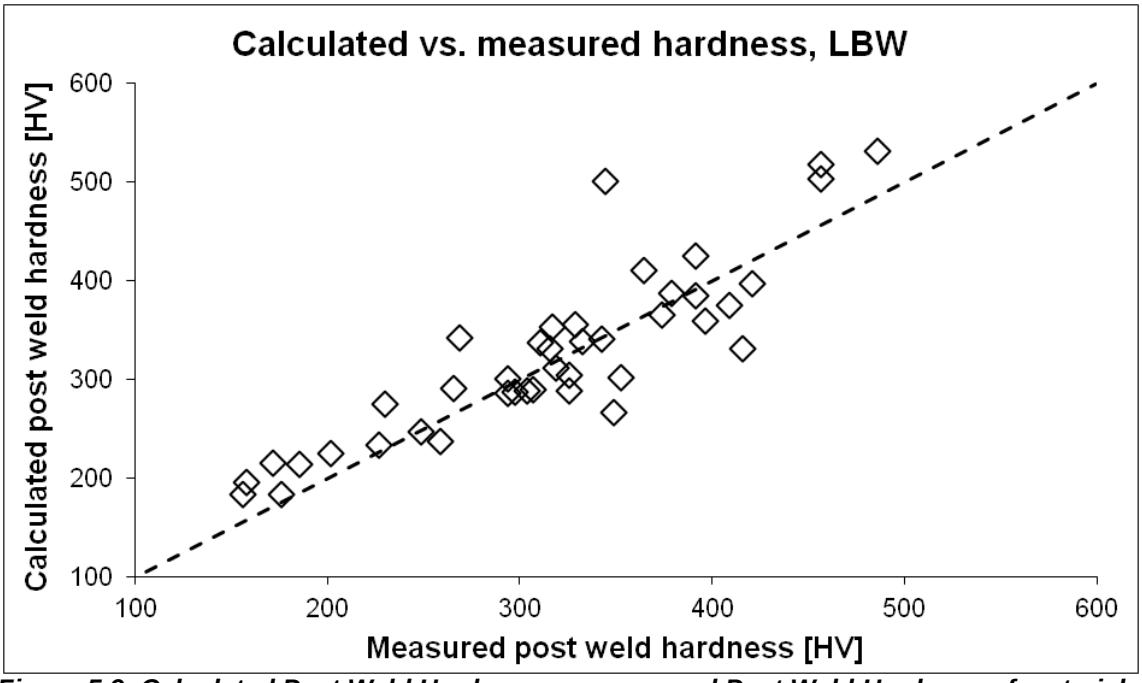

Figure 5.9: Calculated Post Weld Hardness vs. measured Post Weld Hardness of materials listed in Table 5.1 after laser beam welding.

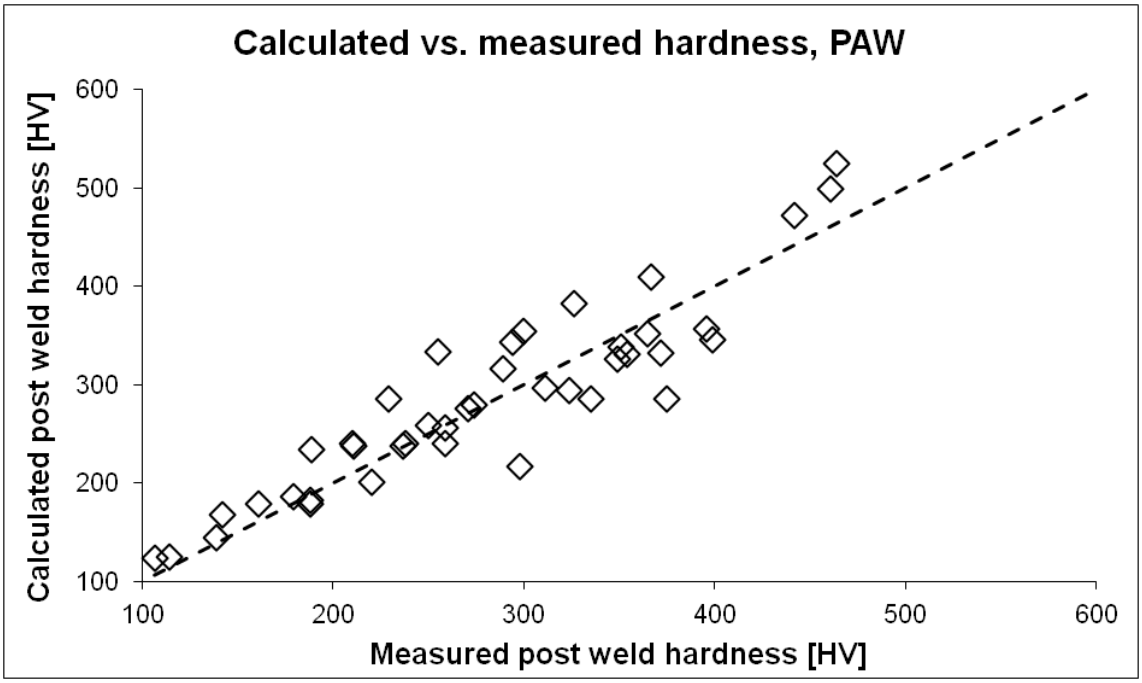

Figure 5.10: Calculated Post Weld Hardness vs. measured Post Weld Hardness of materials listed in Table 5.1 after plasma arc welding.

5.2.3 Post Weld Hardness of Resistance Spot Welded Advanced High Strength Steels

Figure 5.11 gives an experimental and simulated weld growth curve for 1,2 mm thick uncoated DC04 steel sheet welded to itself. Welding was done using 6 mm type B electrodes, with a 3,5 kN electrode force and 20 cycles (50 Hz) welding time. Figure 5.12 shows the experimental weld nugget and heat affected zone welded with a welding current of 8,5 kA

compared to the result of simulation (Sysweld). It can be seen that the result of simulation fits well with experiment. The simulations were done using Sysweld.
Having verified the weld growth curve, simulations offer a possibility to investigate the formation of a weld nugget (which cannot be achieved in experiment). Figure 5.13 shows the simulated growth of the weld pool during welding. It can be seen that the weld nugget grows fast. It should be noted that figure 5.13 is a 2 dimensional depiction of the weld nugget growth and although it appears that the weld nugget growth decreases with increasing time, the actual growth in volume is rather constant. Figure 5.14 shows the growth of the weld pool volume (simulation done with Sorpas). Note that the graph shows a stepped growth, corresponding to the step-wise nature of AC-currents.

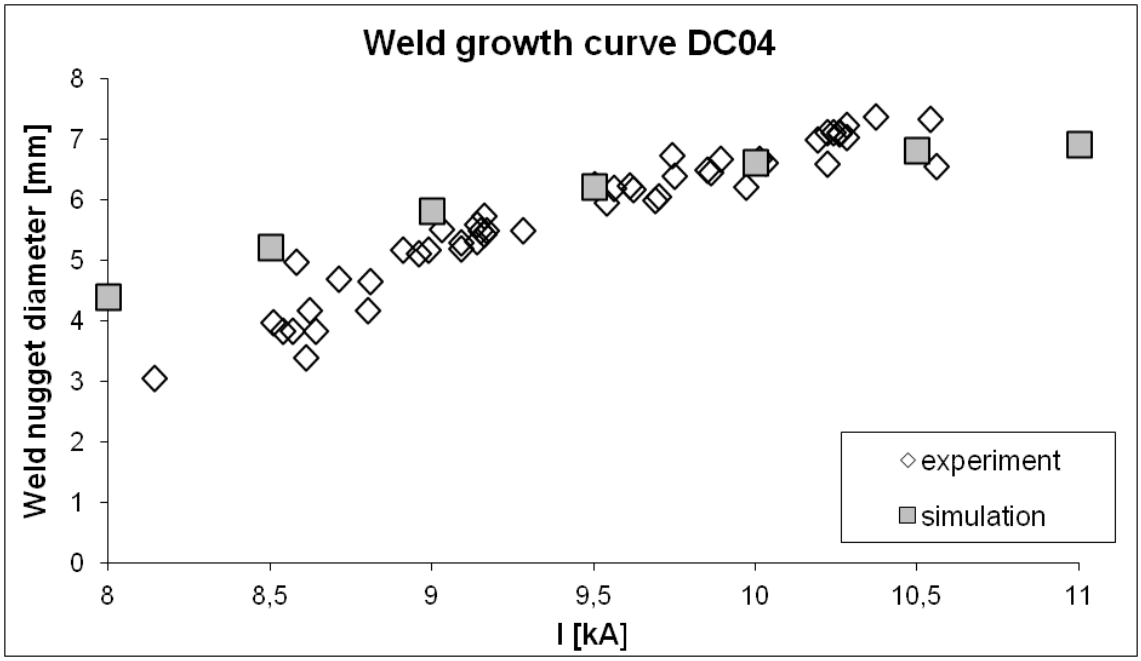

Figure 5.11: Experimental and simulated weld growth curve for 1,2 mm thick uncoated DC04 steel sheet welded to itself. Welding was done using 6 mm type B electrodes, with a 3,5 kN electrode force, and 20 cycles (50 Hz) welding time.

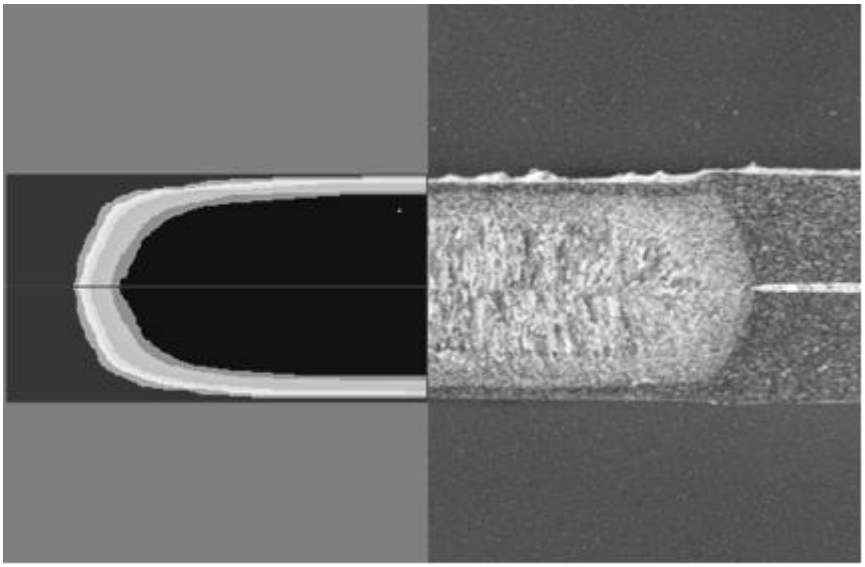

Figure 5.12: Experimental and simulated weld nugget and heat affected zone for 1,2 mm thick uncoated DC04 steel sheet welded to itself. Welding was done using 6 mm type B electrodes, with a 3,5 kN electrode force and a welding current of 8,5 kA applied for 20 cycles (50 Hz).

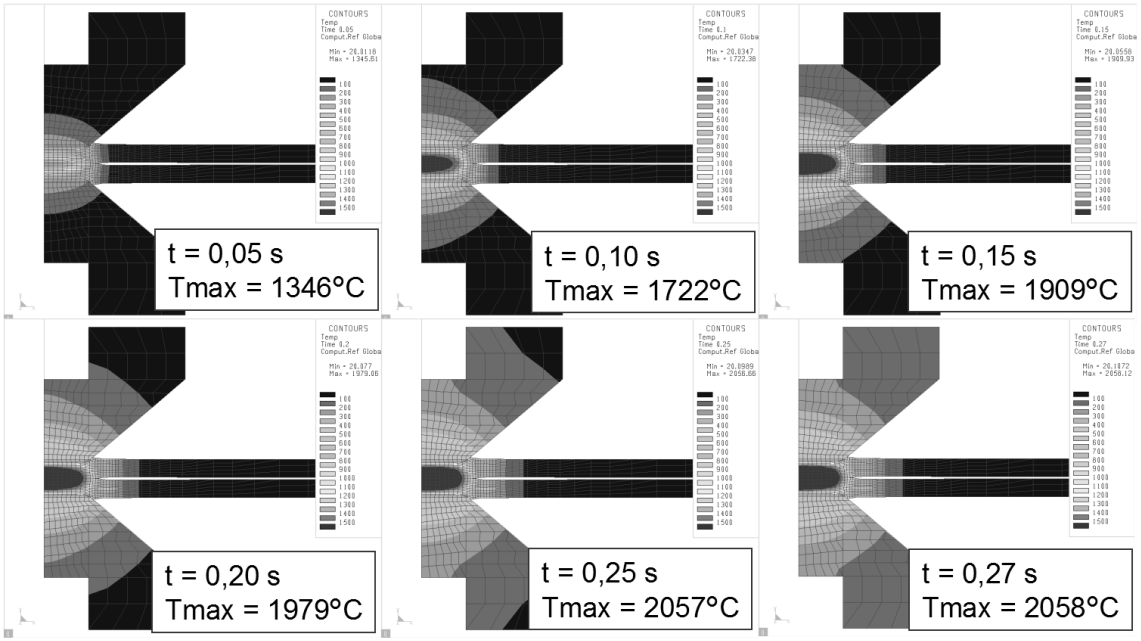

Figure 5.13: Simulated growth of the weld pool during resistance spot welding of two sheets of 1,2 mm thick DC04. Simulations done with Sysweld using 6 mm type B electrodes, with 3,5 kN electrode force, and 8,5 kA welding current applied (20 cycles;50 Hz).

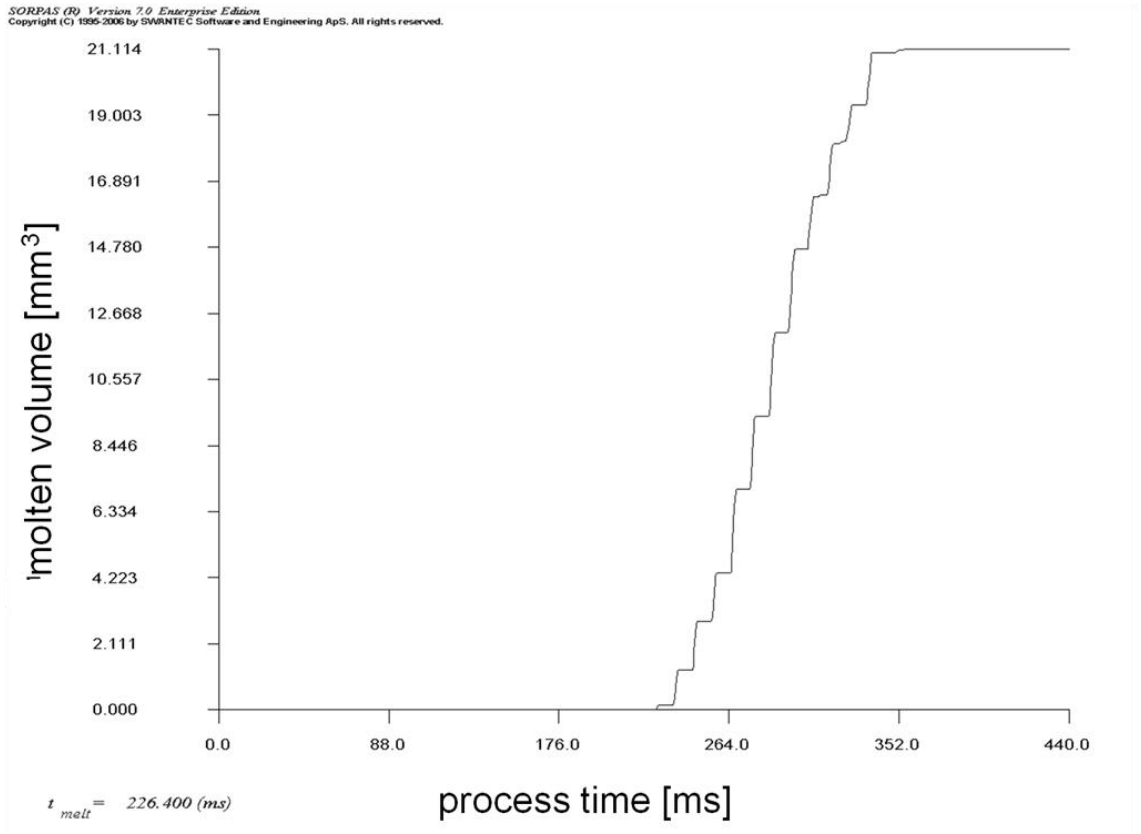

Figure 5.14: Growth of the weld pool volume during resistance spot welding of two sheets of 1,2 mm thick DC04. Simulations done with Sorpas using 6 mm type B electrodes, with 3,5 kN electrode force, and 8,5 kA welding current applied (20 cycles;50 Hz)

As soon as the weld current is stopped, the weld nugget stops growing and the materials start to cool. The main cooling mechanism is through conduction to the water-cooled electrodes. Additional heat is lost to the surrounding material through conduction and to the environment by convection and radiation. Figure 5.15 shows the simulated cooling pattern of

the weld nugget and heat affected zone. It can be seen that the heat affected zone remains at elevated temperatures even after the weld nugget has solidified. The weld nugget itself remains at elevated temperature even longer.
Figure 5.16 shows the simulated temperature profiles in the centre of the weld pool during welding. It can be seen that the shape of the temperature profile is similar for all welding currents (although start of solidification occurs later for welds made with higher welding currents because the weld pool will be larger), only varying in maximum temperature.

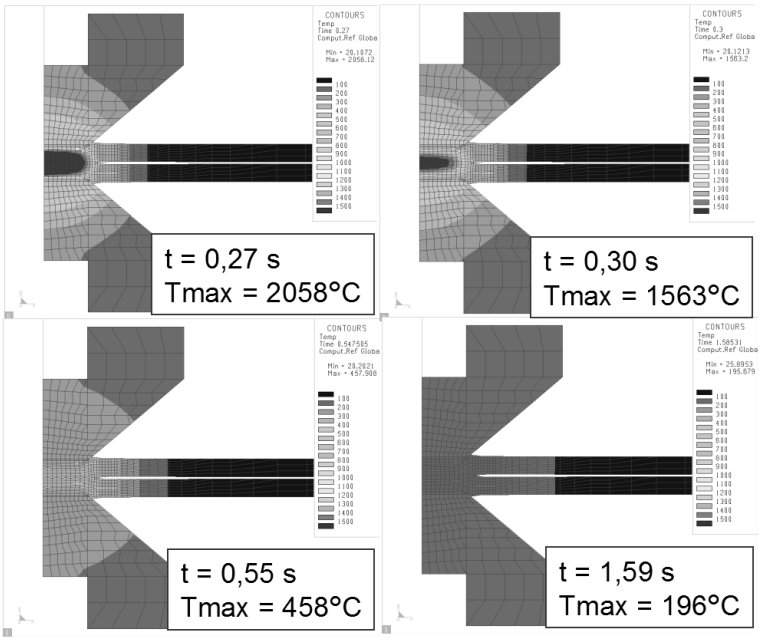

Figure 5.15: Simulated (forced) cooling of the weld and heat affected zone after resistance spot welding of two sheets of 1,2 mm thick DC04. Simulations done with Sysweld using 6 mm type B electrodes, with 3,5 kN electrode force, and 8,5 kA welding current applied (20 cycles;50 Hz).

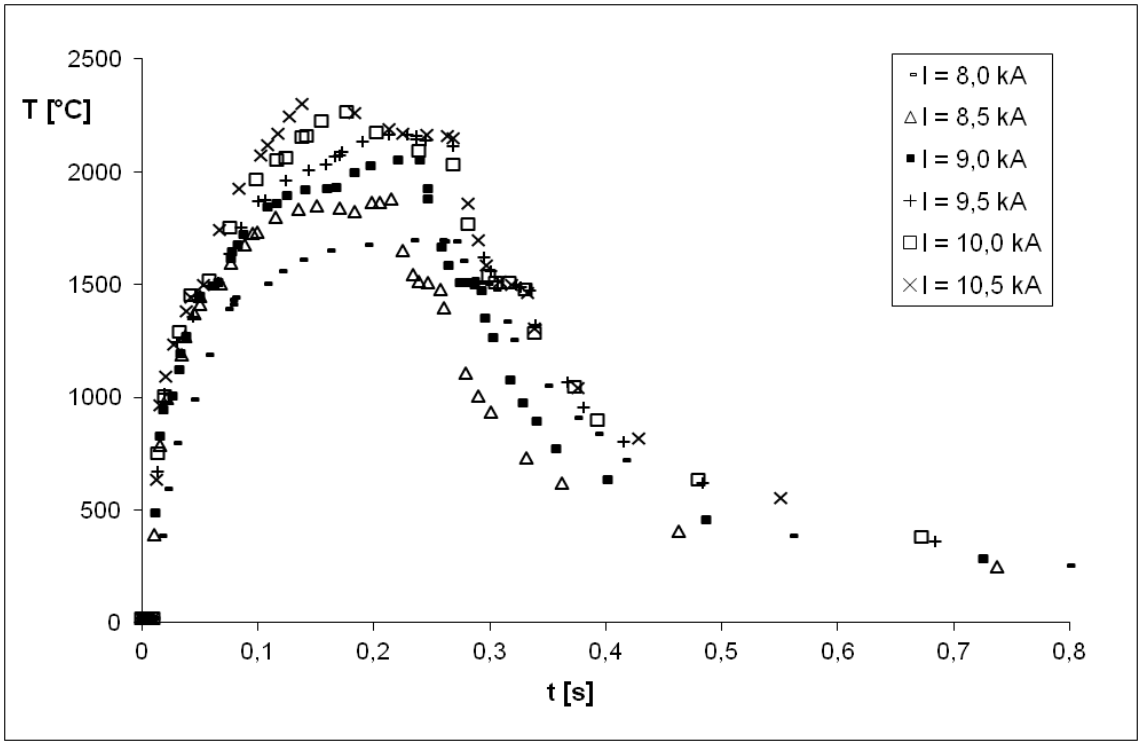

Figure 5.16: Simulated thermal profiles during resistance spot welding of two sheets of 1,2 mm thick DC04 steel made using varying levels of welding currents. Simulations done with Sysweld.

Figure 5.17 gives the simulated phase transformation of the material in the weld pool (simulations done with Sysweld). It can be seen that upon heating the material quickly transforms from ferrite to austenite. It should be noted that when the temperature exceeds the solidus, the phase composition is still given as fully austenitic. Liquid material is not taken into account as a separate phase in these post-processing results. Upon cooling the material transforms from austenite to martensite over time. The graph, generated by the Sysweld post-processor, shows the phase transformations occurring discontinuously. This is due to the time steps used by the post-processor; in reality the transformations are continuous.

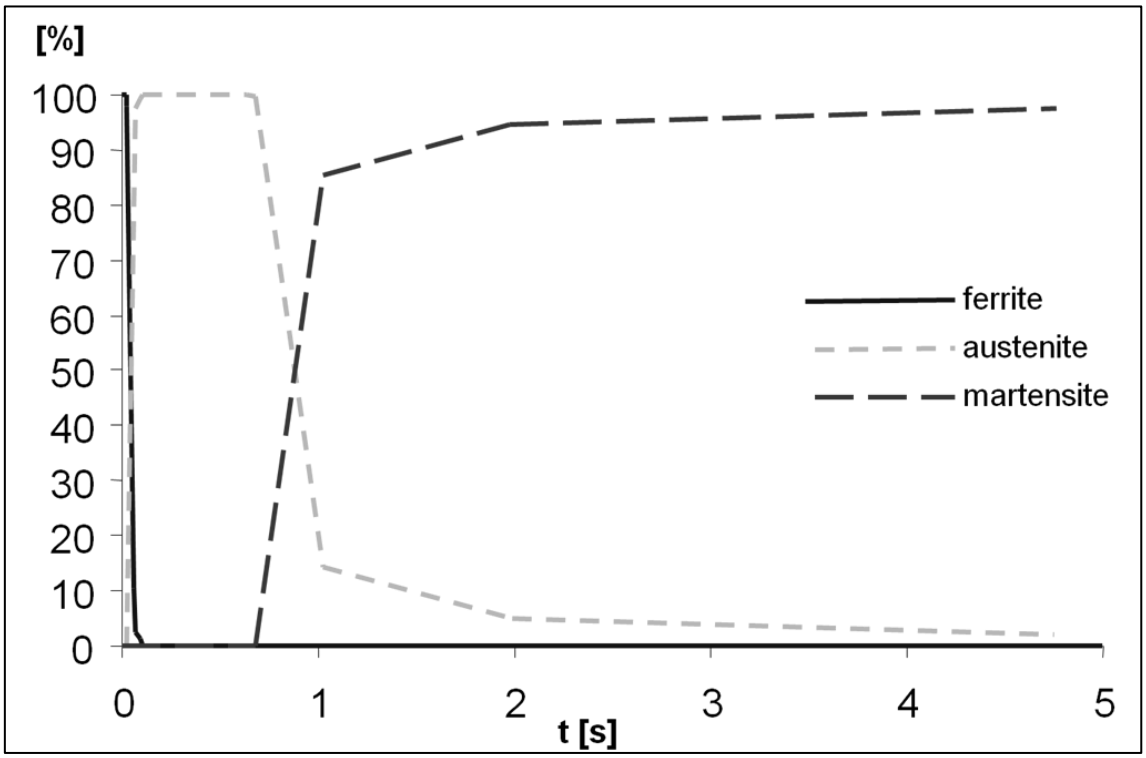

Figure 5.17: Simulated phase transformations during resistance spot welding of two sheets of 1,2 mm thick DC04. Simulations done using Sysweld.

Figure 5.18 gives the formation of martensite for various welding currents. It can be seen that there is some difference in the transformation rates depending on the welding currents, but these are minimal and all cooling rates lead to fully martensitic welds. Again phase transformations in the graph appear to be discontinuous, due to the time steps used by the post-processor, but they are continuous in reality.
Figure 5.19 shows the simulated distribution of martensite after welding and cooling (simulations done with Sysweld). It can be seen that the weld nugget is fully martenistic (>99 %), and that the heat affected zone is primarily martensitic (>75 %).

These results are important, because DC04 is a cold rolled mild (unalloyed) deep drawing steel, with C < 0,08 wt%, Mn < 0,4 wt%, and Si < 0,02 wt%. Modern HSLA steels may have lower carbon levels, but Advanced High Strength Steels (the main subject of these studies) have higher levels of alloying. It can therefore be concluded that AHSS will form fully martensitic welds after resistance spot welding.

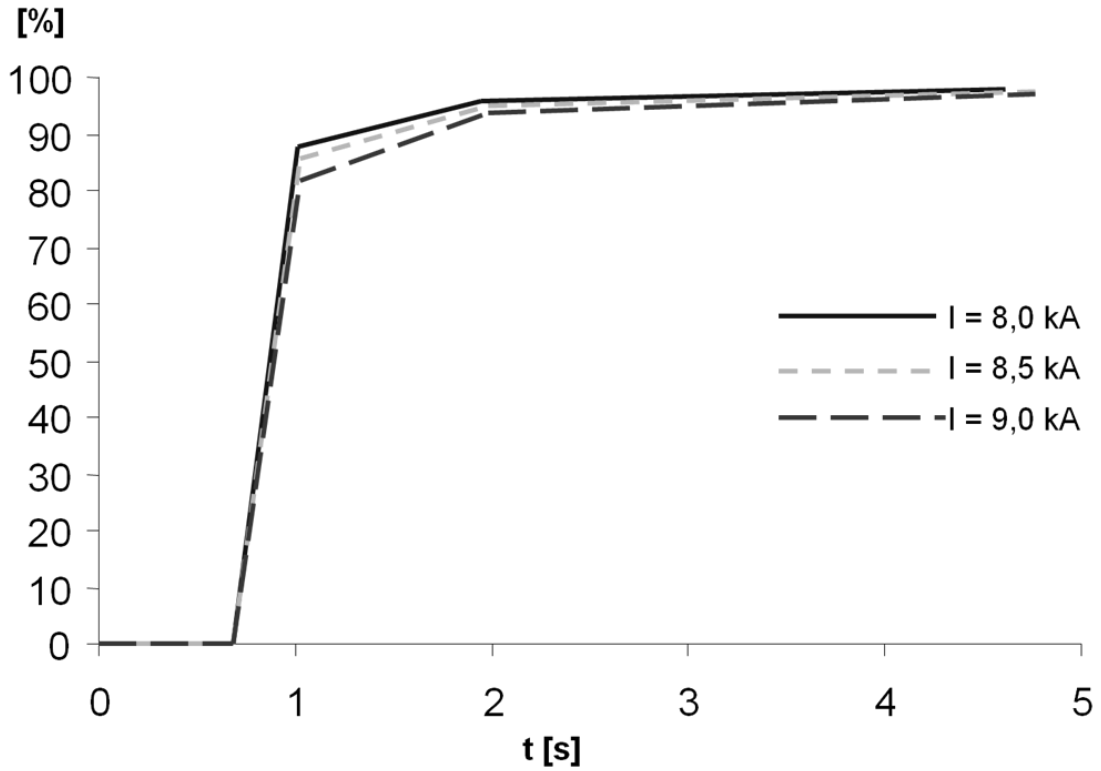

Figure 5.18: Simulated formation of martensite during cooling after resistance spot welding of two sheets of 1,2 mm thick DC04 using different welding currents. Simulations done using Sysweld.

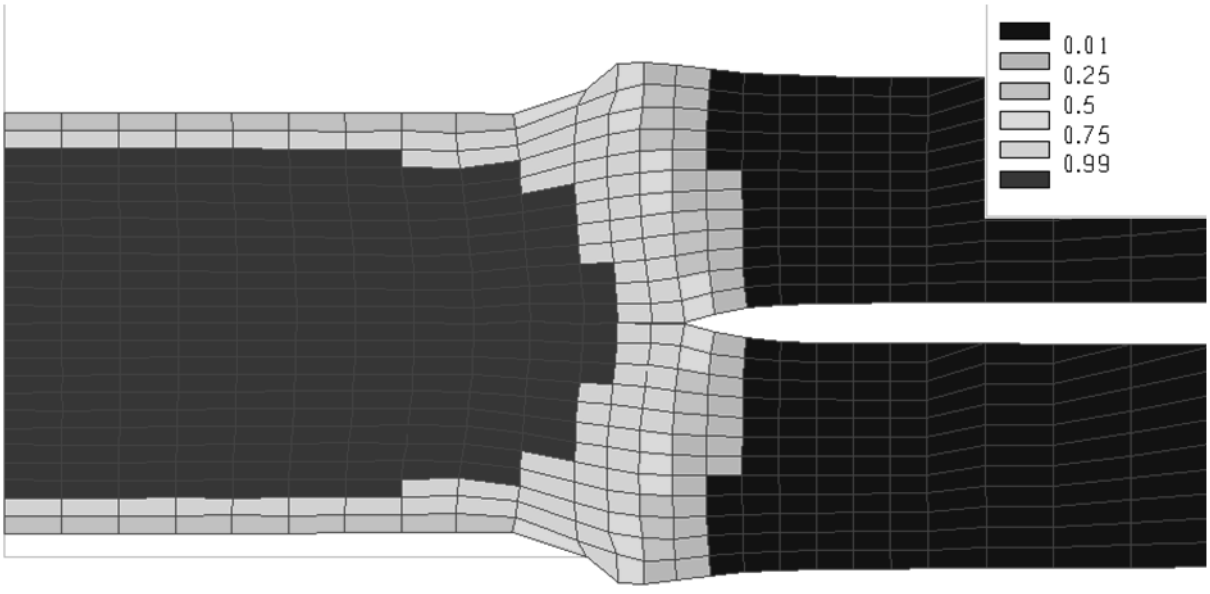

Figure 5.19: Simulated distribution of martensite after welding and cooling in a resistance spot welded joint between of two sheets of 1,2 mm thick DC04. Simulations done with Sysweld using 6 mm type B electrodes, with 3,5 kN electrode force, 8,5 kA welding current (20 cycles;50 Hz), and 50 s cooling.

A series of steels available for automotive applications have been tested. The steels were produced in various facilities and encompass a range of high strength steels: High Strength Low Alloy (HSLA), Dual Phase (DP) and Transformation Induced Plasticity (TRIP) steels. All

these steels were cold rolled. Table 5.2 lists the grades and thickness of these steels, as well as their chemical compositions.
These steels have been resistance spot welded using single pulse welding schemes. Resistance spot welding settings were chosen to ensure a $5\sqrt{t_s}$ weld diameter size, typically requiring application of a welding current of 6,8 kA for 14 cycles (50 Hz AC), using Type G welding electrodes with a 6 mm radius. After welding the post weld hardness in the weld nugget was measured for each sample (see table 5.2).
Figure 5.20 gives the post weld hardness as a function of the carbon content for these materials. It can be seen that there is a good correlation. In fact the main outlying data point ([C] = 0,077 wt%) concerns an HSLA steel. All other materials are advanced high strength steels.

Table 5.2: Production materials; grades, thickness, chemical composition, and measured post weld hardness.

steel	grade	t_s	coating	C	Mn	Si	Cr	P	S	Post Weld Hardness
		[mm]		[wt%]	[wt%]	[wt%]	[wt%]	[wt%]	[wt%]	[HV]
St43	TRIP600	1,6	EZ	0,071	1,46	1,53		0,16	0,001	375
St44	HSLA340	1,5	GI	0,077	0,515	0,005		0,008	0,007	240
St45	DP600	1	GI	0,092	1,68	0,241		0,016	0,004	390
St46	DP800	1,05		0,105	1,68	0,24	0,53	0,001	0,001	400
St47	DP800	1,05		0,11	1,69	0,25	0,54	0,009	0,006	415
St48	DP800	1,5	GI	0,149	1,83	0,207		0,013	0,002	455
St48	DP800	1,5		0,15	1,8	0,2	0,47	0,014	0,002	420
St49	DP1000	1,5		0,15	1,52	0		0,007		450
St50	DP800	1,05		0,16	1,72	0,25	0,54	0,001	0,001	460
St51	TRIP700	1,25	GI	0,185	1,61	0,352	0,02	0,089	0,003	460
St52	TRIP800	1,23		0,186	1,53	1,8		0,008	0,001	510
St53	TRIP800	1		0,205	1,52	0,38		0,077		515
St54	TRIP800	1,15		0,21	1,5	0,37		0,028		510
St55	TRIP1000	1		0,21	1,5	0,4		0,02	0,006	515

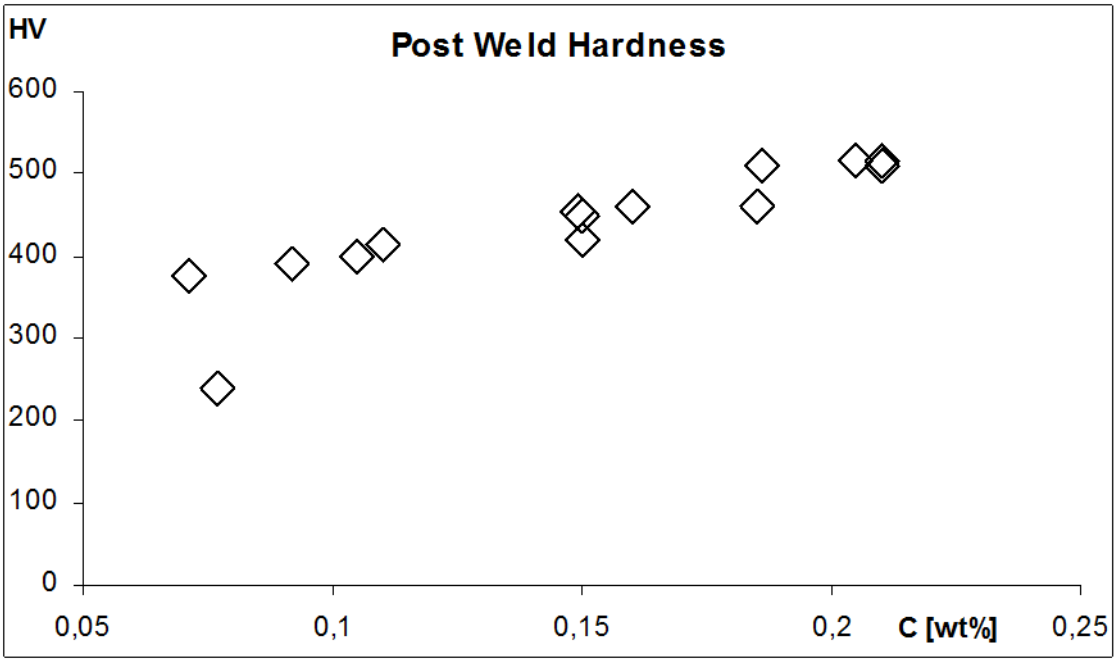

Figure 5.20: Post weld hardness against Carbon content for the materials listed in table 5.2.

5.2.4 Influence of cooling rate

Blondeau *et al.* [1973 & 1975] derived an empirical equation to calculate post weld hardness of various phases (ferrite, austenite and martensite). They predict the maximum hardness of martensite to be dependent upon composition and the cooling rate at 700ºC according to the following expression:

$$HV = 127C + 27Si + 11Mn + 8Ni + 16Cr + 21\log(t_c), \qquad \text{(Eq. 5.7)}$$

with all amounts expressed in wt% and t_c the cooling rate at 700°C (in °C/hr).
The limits for the chemical composition ranges listed by Blondeau *et al.* are given in table 5.3.

Table 5.3: Limits on chemical composition for equation 5.7, as listed by Blondeau et al. [1973 & 1975].

element	min.	max.
	[wt%]	[wt%]
C	0,1	0,5
Si	-	1
Mn	-	2
Ni	-	4
Cr	-	3
Mo	-	1
V	-	0,2
Cu	-	0,5
Al	0,01	0,05

The model by Blondeau *et al.* [1973 & 1975] has been derived for arc welded low alloyed steels. The model was tested against the measured hardness values in resistance spot welded high strength steels listed in table 5.3, for use as a tool to estimate post weld

hardness. An average cooling rate of 3500 °C/s (12,6 · 10^6 °C/hr) was used, estimated from Sysweld simulations for an average thickness of 1,2 mm, and continuous forced cooling till 700 °C.
Figure 5.21 shows the results against measured hardness levels. It can be seen that the calculated post weld hardness values correlate well with the measured values.

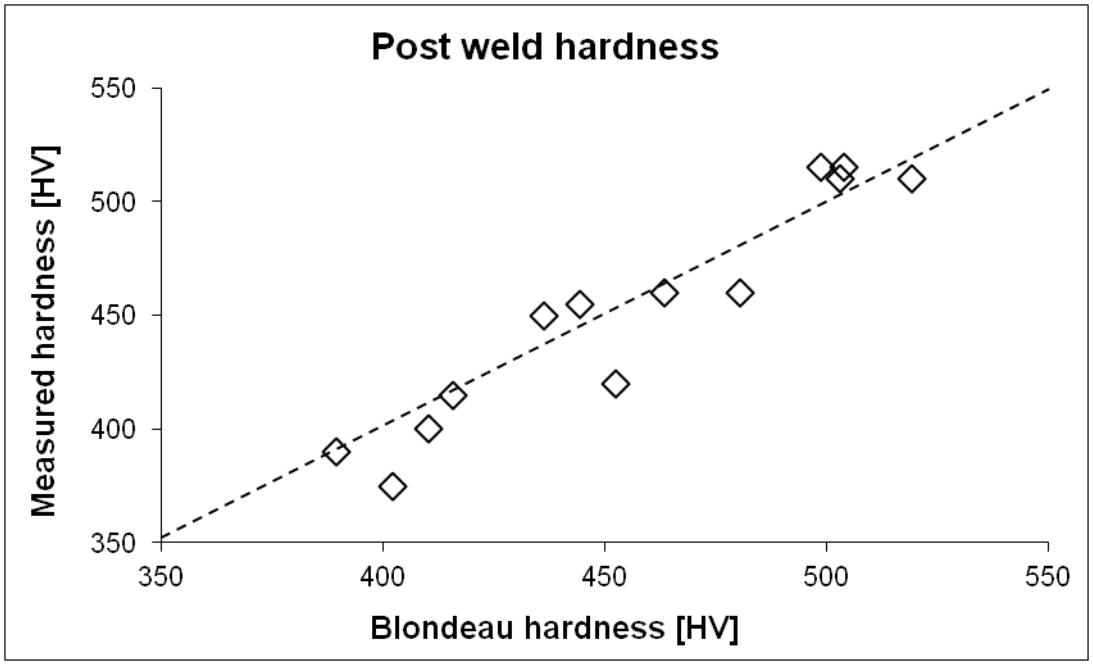

Figure 5.21: Measured hardness of materials listed in table 5.2 vs. calculated post weld hardness using Blondeau's equation.

5.2.5 A Simple Equation

The challenge in welding thin steel sheet is to keep the hardness of the resultant martensite sufficiently low to ensure ductile failure of welded joints. Undesirable failure modes have been attributed to post weld hardness exceeding 400-450 HV; unstable fractures, and interfacial failures have been reported in spot welds with hardness exceeding 450 HV [Mimer *et al.*, 2004]. Radaj [1992] mentions a general desire to aim for degrees of hardness below 350 HV in general in welding. Resistance spot welded joints with hardness exceeding 450 HV tend to show brittle failure, which is undesirable for automotive applications. Therefore models have been built to couple the carbon equivalence to actual hardness levels after welding. Generally these take one of two forms:

- chemistry dependent:
$$HV = \sum H_i(X_j) \cdot V_i \,. \qquad \text{(Eq. 5.8)}$$
- (cooling) time & chemistry dependent:
$$HV = f(H_i(X_j) \cdot t_{8/5}), \qquad \text{(Eq. 5.9)}$$

where $H_i(X_j)$ is the hardness of a certain constituent of the material, V_i is the fraction of the constituent present, and $t_{8/5}$ is the cooling time (usually between 800ºC and 500ºC).

As the chemistry dependent models do not take cooling rates into account they are generally only applicable to one welding process and for a certain range of thickness of materials. The advantage is that they are "cheap" in calculation costs. The models that take the cooling time into account are much more suited to be used for a wide range of processes and material

thicknesses. The drawback is that the user is often required to use sophisticated finite element modelling to calculate the cooling temperatures. Also these calculations have to be repeated whenever there is a significant change in the welding process or material geometry.

In general chemistry dependent equations take the shape of:

$$HV = A + B \times CE, \qquad \text{(Eq. 5.10)}$$

where A is an offset value (representing the hardness of unalloyed steel), B a coefficient (representing the impact of alloying on post weld hardness), and CE a carbon equivalence number.

Chemistry and cooling rate dependent equations take the shape of:

$$HV = P + Q \times CE + R(t), \qquad \text{(Eq. 5.11)}$$

where P is an offset value (representing the hardness of unalloyed steel), Q a coefficient (representing the impact of alloying on post weld hardness), CE a carbon equivalence number, and $R(t)$ a cooling rate function.

During resistance spot welding of advanced high strength steels the cooling rate is always high, due to the limited range in thickness of the sheets and the water cooling of the electrodes. This will always cause the formation of a martenistic weld nugget (see section 5.2.3). As long as the cooling range does not change too much, the value of $R(t)$ can be considered a constant. In that case the second equation becomes:

$$HV = \big(P + R(t)\big) + Q \times CE. \qquad \text{(Eq. 5.12)}$$

Here P represents the hardness of unalloyed steel, $R(t)$ represents the impact of cooling rate upon the hardness of martensite, Q represents the influence of alloying (itself represented in the carbon equivalence number) on the hardness of martensite.
As shown in section 5.2.4 the Blondeau model for prediction of the hardness of martensite correlates well with experimental results (material thickness ranging from 1,0 mm to 1,6 mm). In this model variations in cooling rate will lead to limited variations in post weld hardness [Den Uijl, 2006b]. The Blondeau equation can be written as:

$$HV = \Big(127 + 21log\big(t_c\big)\Big) + 949CE\ , \qquad \text{(Eq. 5.13a)}$$

where

$$CE = C + \frac{28{,}5Si + 11{,}6Mn + 8{,}4Ni + 16{,}9Cr}{1000}. \qquad \text{(Eq. 5.13b)}$$

For resistance spot welding high strength steel sheet (see figure 5.16) a cooling rate of approximately 3750 °C/s ($13{,}5 \cdot 10^6$ °C/hr) is reached, leading to a value of 150 for the term 21logtr.
Blondeau's model for spot welding steel sheet then becomes:

$$HV = 277 + 949CE, \qquad \text{(Eq. 5.14)}$$

with CE given in equation 5.13b.

To predict post weld hardness after welding, chemistry based models are much more user-friendly than models taking into account both chemistry and cooling rate. Even though they

can only be used with restrictions on process and material. The Blondeau model was originally devised for arc welding processes and the range of variations in chemical composition is much wider than needed to evaluate post weld hardness of advanced high strength steels. It was therefore decided to try and find a simple equation to derive the post weld hardness of high strength steel sheet (DP and TRIP) as used in automotive applications.

For this purpose the experimental data on the materials listed in table 5.2 were used. Linear regression of the data reveals that the most important elements in determining post weld hardness are carbon, manganese and silicon [Bain, 1939]. From the equations for Carbon Equivalence numbers and the hardness equations, a significant influence of chromium could be expected (chromium is an important alloying element in Dual Phase steels), but the influence of chromium on hardenability is primarily on the place of the "nose" in the CCT diagram [Van der Wolk, 2001]. As the cooling rates here are high enough to ensure the formation of martensite, the influence of chromium is annulled. A simple relation was derived to enable predictions of resistance spot weldability for high strength steels:

$$HV = 240 + 855CE, \qquad \text{(Eq. 5.15a)}$$

where

$$CE = C + \frac{Si}{40} + \frac{Mn}{20}. \qquad \text{(Eq. 5.15b)}$$

There is a difference in the offset value between equations 5.14 and 5.15 (277 *vs.* 240). The reason for this difference can be found in the difference in the way the two equations have been derived. Equation 5.14 has been derived using Blondeau's equation (which has originally been derived for general welding processes) combined with the results of simulations for the cooling rates. Equation 5.15 has been derived using the experimentally derived post weld hardness of a series of commercially available advanced high strength steels (see table 5.2). Both equations also use different carbon equivalence numbers.

Figure 5.22 shows the predicted post weld hardness of the advanced high strength steels listed in table 5.2 and their measured hardness using equation 5.15. The results correlate well; however the same DP800 steel (measured hardness 420 HV, predicted hardness 450 HV) that did not fit well with the Blondeau model does not fit well again (low Si, high P and high C).

It should be noted that this model has been drawn up for resistance spot welding of advanced high strength steel sheets, with varying thickness (1,0 mm ≤ t_s ≤ 1,6 mm) and welding parameters as they are used for their different applications in the automotive industry (all welds made aimed at a weld nugget diameter of $5\sqrt{t_s}$).
The limits for the chemical composition are listed in table 5.4.

Table 5.4: Limits on chemical composition for equation 5.15.

element	min.	max.
	[wt%]	[wt%]
C	0.07	0,21
Si	-	1,80
Mn	-	1,83
Cr	-	0,54

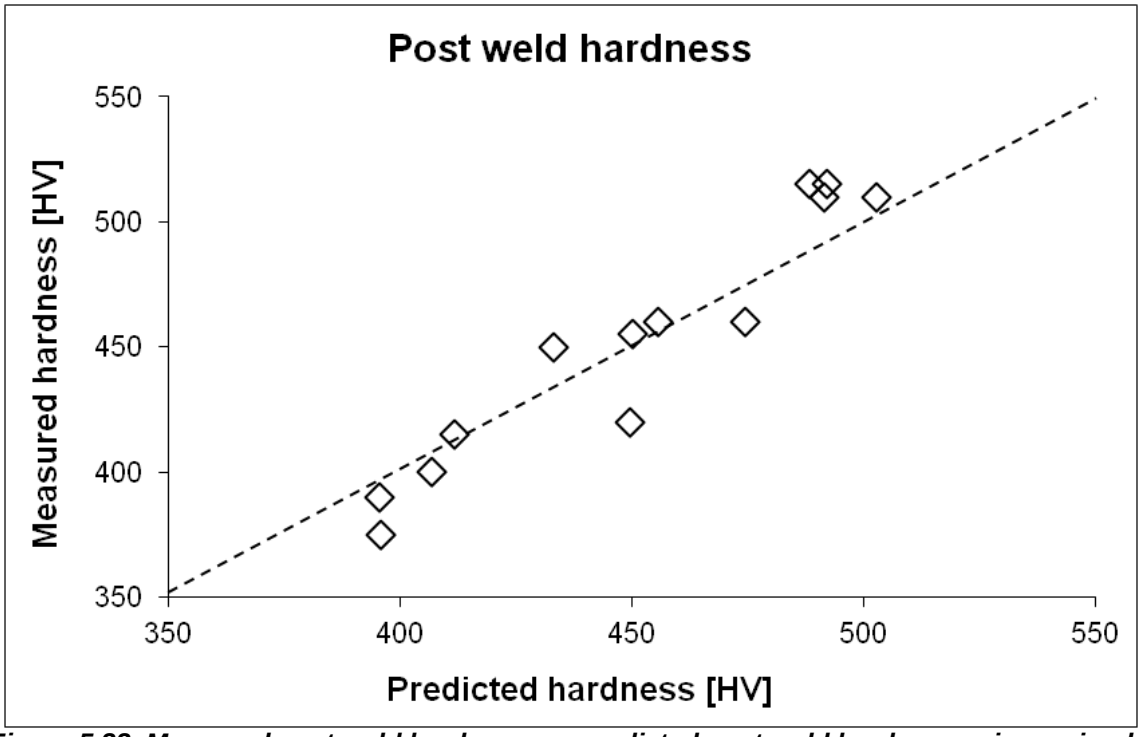

Figure 5.22: Measured post weld hardness vs. predicted post weld hardness using a simple equation for advanced high strength steels listed in table 5.2.

5.3 Post Weld Heat Treatment

Figure 5.23 shows post weld hardness of three different Dual Phase steels. It can be seen that the hardness of the weld is the same for each of the three steels. This is to be expected because the weld will be (almost) fully martensitic after welding and the carbon contents are roughly similar (approx. 0,15 wt%). Figures 5.24 a & b show cross sections of the DP 800 welds after tensile testing. It can be seen that the welds showed full plug failure. Figure 5.25 shows the weld growth curves of a 1,6 mm DP800GI. It can be seen that full plug failure occurs for all currents and a wide welding range. To improve the weld failure mode, these AHSS do not need post weld heat treatment. As can be seen from figures 5.24 and 5.25 full plug failure is achieved after a single welding step. Improvements can be made in the weld failure strength, but this is separate from weld failure mode.

There are however AHSS that show undesirable plug failure. Figure 5.26 shows the weld growth curve of a 1,25 mm thick TRIP700GI. Welding was done using a 20 cycle weld current and 4,5 kN electrode force. It can be seen that most welds fail in partial plug mode. If excess hardness is to blame for these undesirable failure modes, then a post weld heat treatment, to temper the weld should lead to improved weld failure behaviour. Figure 5.27 shows a weld growth curve of the same 1,25 m thick TRIP700Gi, with a post weld heat treatment (PWHT) consisting of a second weld current pulse of 90% of the primary weld current for the duration of 15 cycles. The cooling period between the two welding cycles was 15 cycles. It can be seen that no improvement in weld failure behaviour was achieved.
Figure 5.28 shows the combined results with and without post weld heat treatment. From these results it can be concluded that undesirable weld failure behaviour is not (necessarily) caused by excess hardness.

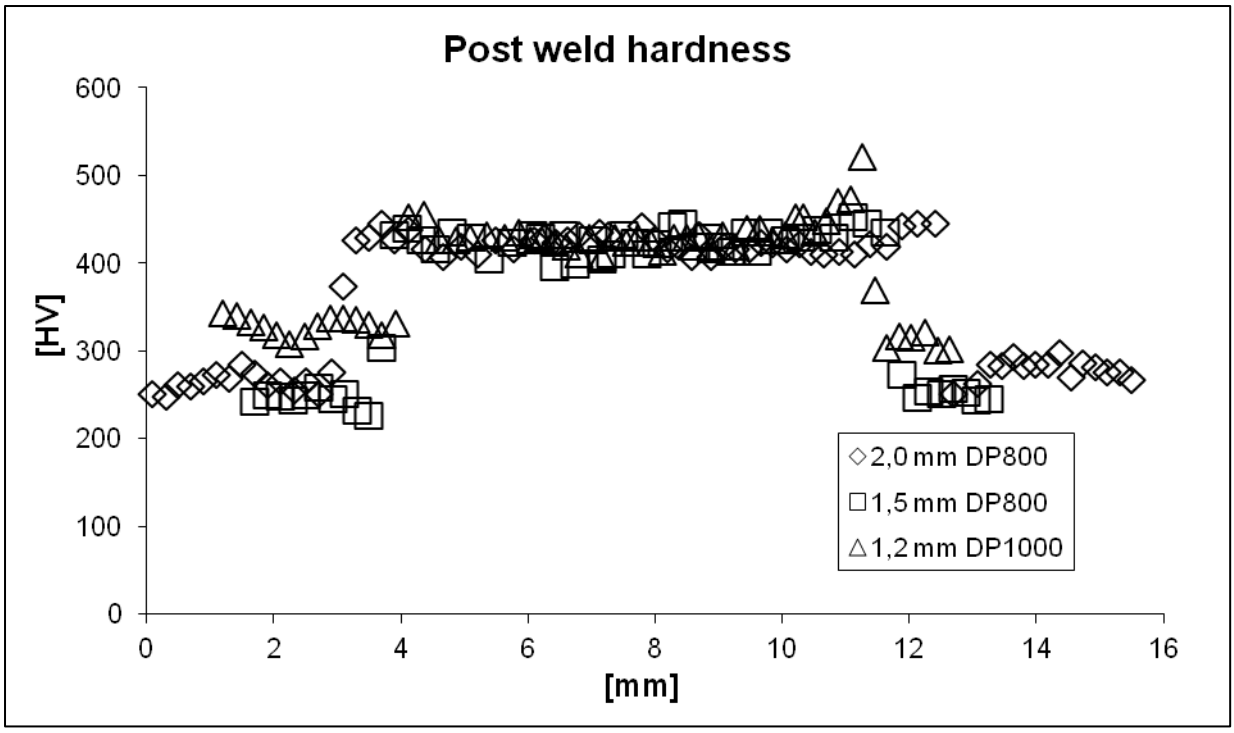

Figure 5.23: Post weld hardness of three different different Dual Phase steels.

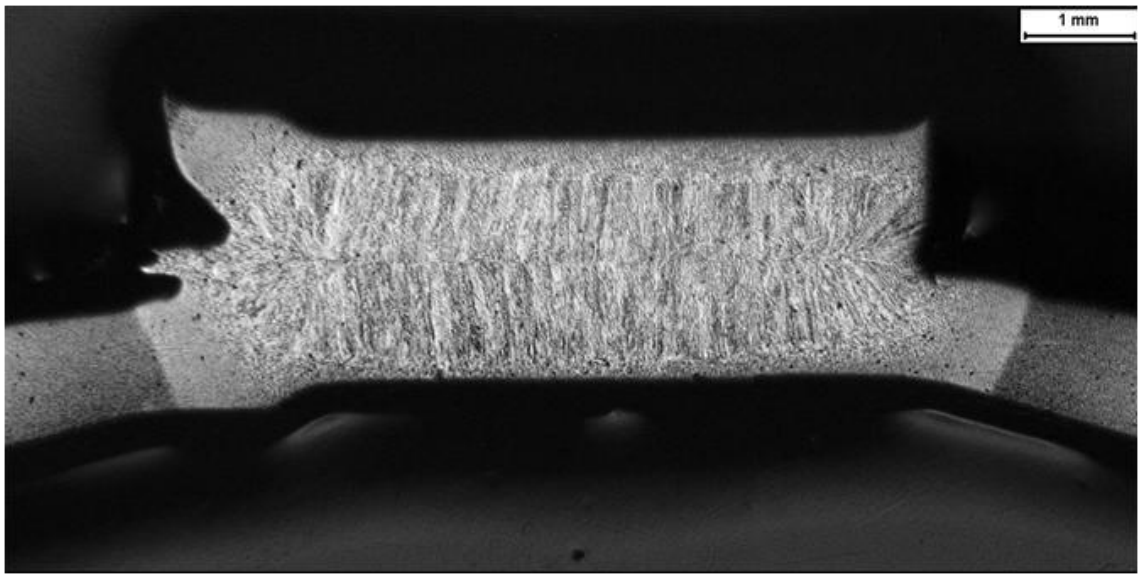

Figure 5.24 a: Plug failure in tensile tested DP800 resistance spot weld.

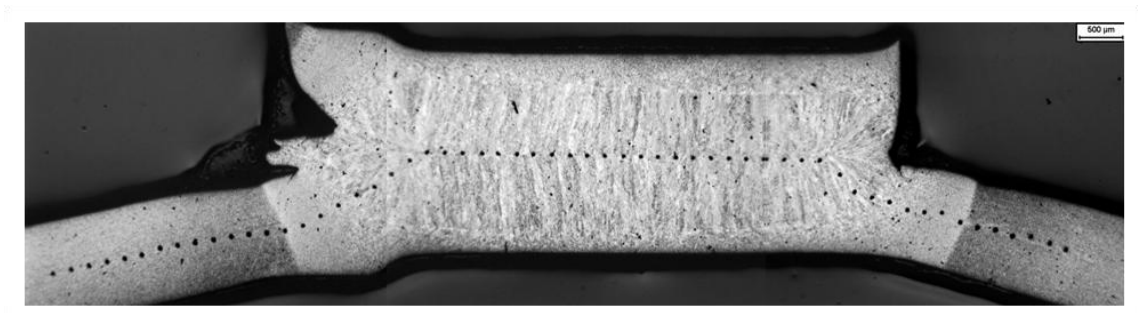

Figure 5.24 b: Plug failure in tensile tested DP800 resistance spot weld.

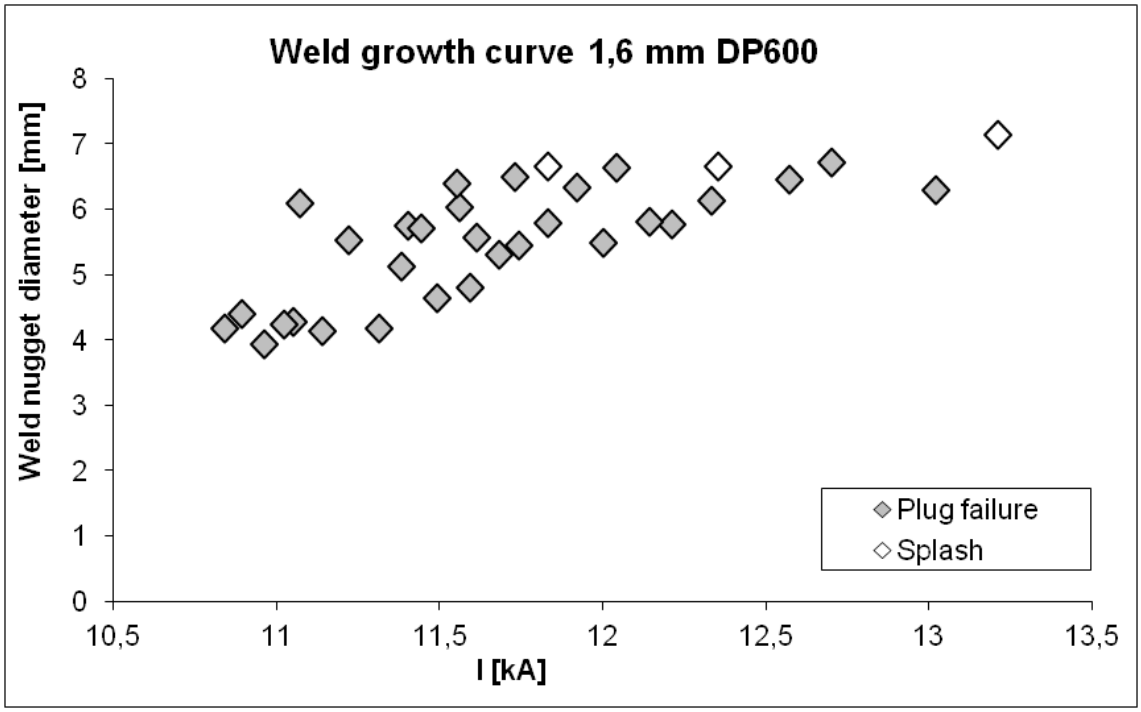

Figure 5.25: Weld growth curve of resistance spot welded 1,6 mm DP800GI.

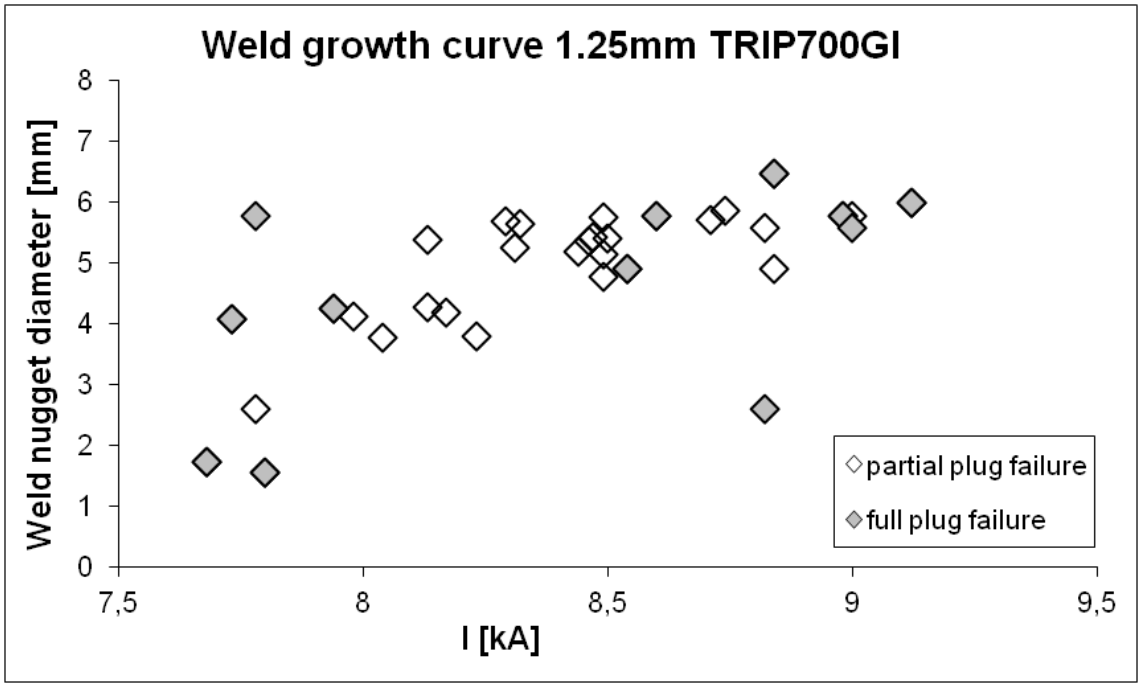

Figure 5.26 Weld growth curve of a resistance spot welded 1.25 mm thick TRIP700 without post weld heat treatment.

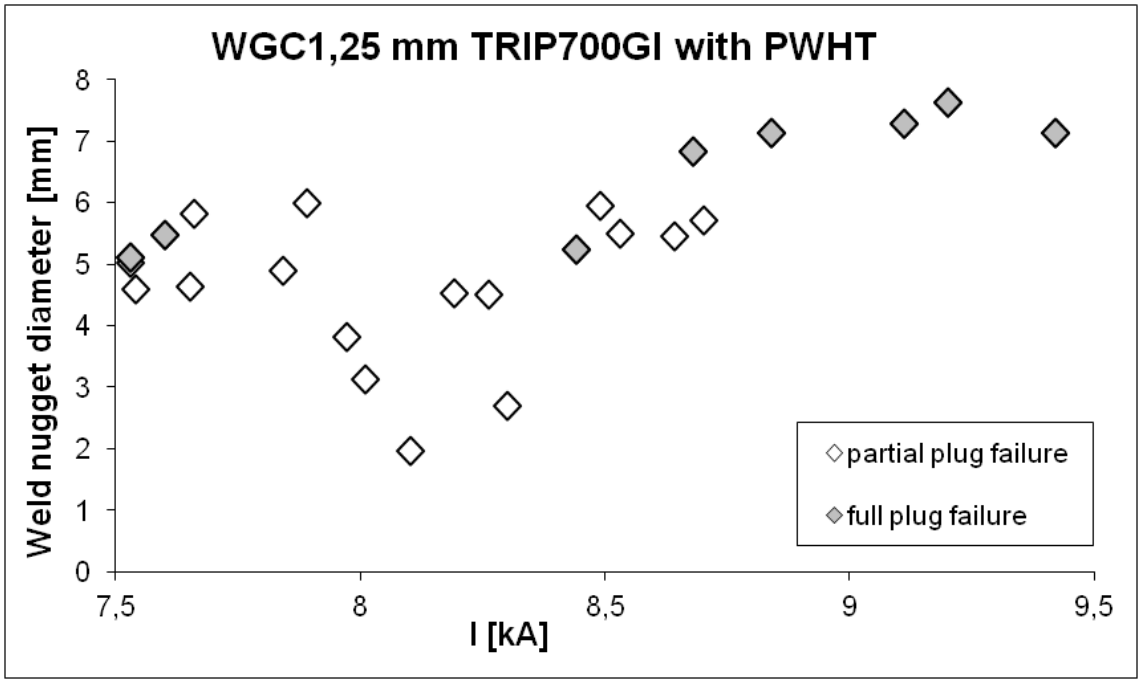

Figure 5.27 Weld growth curve of a resistance spot welded 1.25 mm thick TRIP700 with post weld heat treatment.

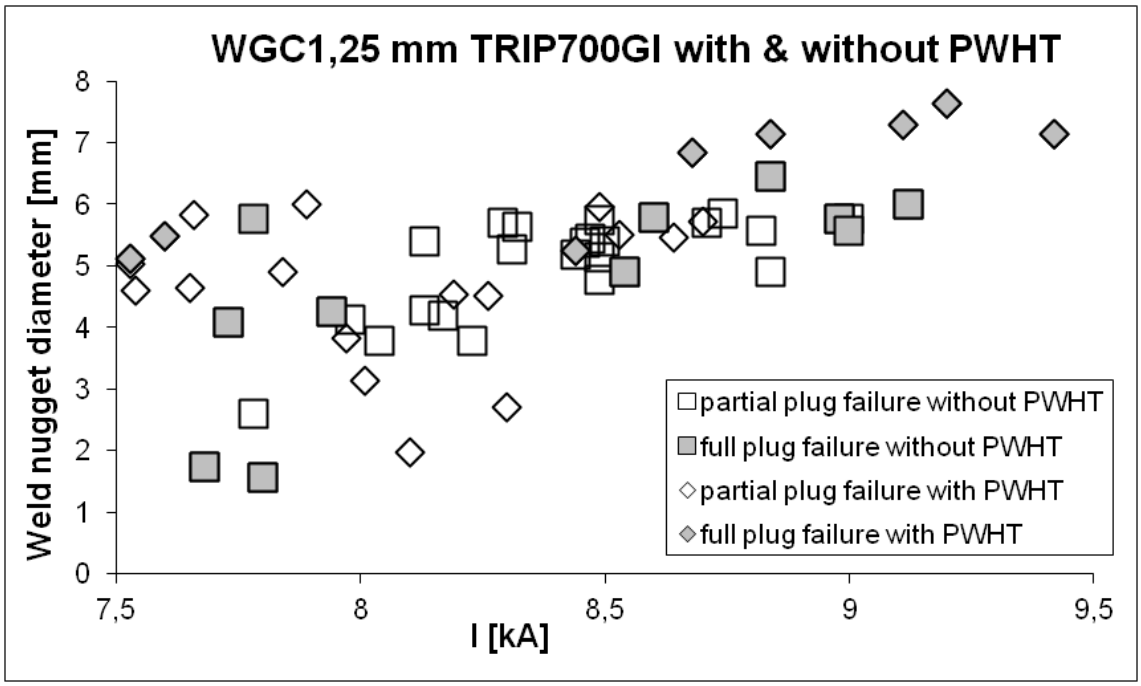

Figure 5.28 Weld growth curve of a resistance spot welded 1.25 mm thick TRIP700 with and without post weld heat treatment.

5.3.1 TRIP Steel Welding Metallurgy

The main difference between dual phase steels and TRIP steels, when considering welding metallurgy, is their chemical composition. TRIP steels often contain more carbon (to allow the formation of retained austenite), and some TRIP steels are alloyed with phosphorus to increase strength levels and to ensure that austenite is retained during production (see § 2.1).

When a carbon and phosphorus containing steel solidifies, the last liquid to solidify (as a residual eutectic) between the α-Fe dendrites, is rich in both carbon and phosphorus. The carbon rich fraction solidifies as retained austenite (as is desired in TRIP steels), and the phosphorus is segregated an the grain boundaries as the solubility of P in γ-Fe is very low (Porter & Easterling, 1992). This causes the last grain boundaries to be formed to be very high in phosphorus.
Figure 5.29 shows a mapping of phosphorus in a resistance spot weld made in a phosphorus rich TRIP steel. It can be seen that the phosphorus has indeed segregated.

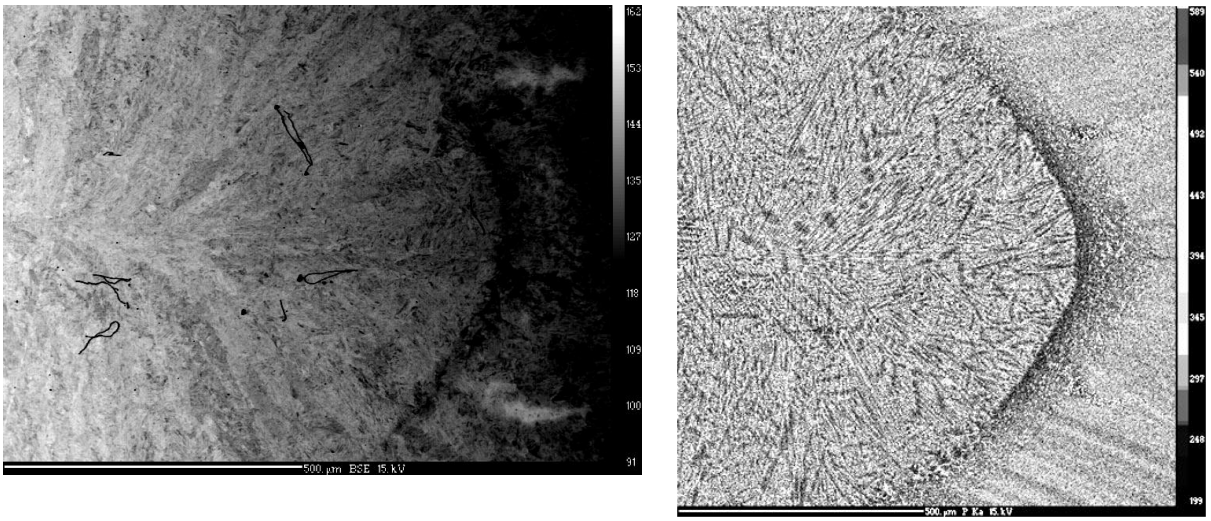

Figure 5.29 a&b: Backscattered electrons image of the edge of a resistance spot welded phosphorus rich TRIP steel (0,089 wt% P, left) and corresponding phosphorus mapping (right) (Rijkenberg, 2006).

5.3.2 Three Step Welding

Phosphorus on grain boundaries decreases the cohesive properties of the grain boundaries. This is a problem when these grain boundaries are subjected to a load perpendicular to the grain boundaries, as they are in tensile testing. The problem is aggravated by the occurrence of long elongated grain boundaries which occur at the edge of a resistance spot weld. These elongated grain boundaries originate from the cooling pattern during solidification as heat is conducted away from the edge of the spot weld to the surrounding material.
Figure 5.30 shows the notch at the edge of the weld nugget and the adjoining long grain boundaries. Failure of the weld nugget initiates at the notch between the welded sheets. Here stress concentrations peak due to geometric considerations. These increased stress levels lead to crack initiation at the notch. The crack then propagates along the long dendritic grain boundaries lateral to the weld interface into the weld nugget. In tension testing the sample is deformed so that when it becomes mechanically more favourable to propagate along a perpendicular dendritic grain boundary, the crack will propagate out of the weld nugget, causing partial plug failure (see figure 5.31). (Den Uijl & Smith, 2006).

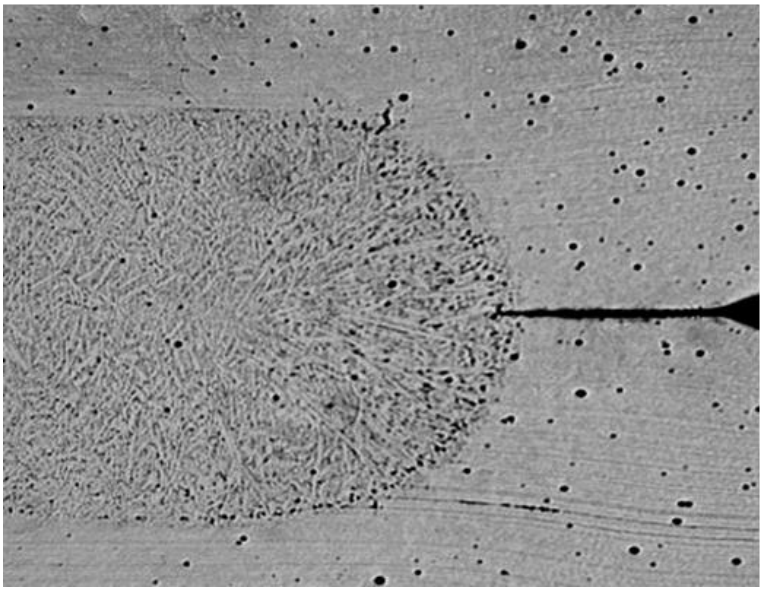

Figure 5.30: Microsection of RSW TRIP steel showing the notch where cracks initiate, and the long lateral dendritic structure along which the crack propagates (Den Uijl & Smith, 2006).

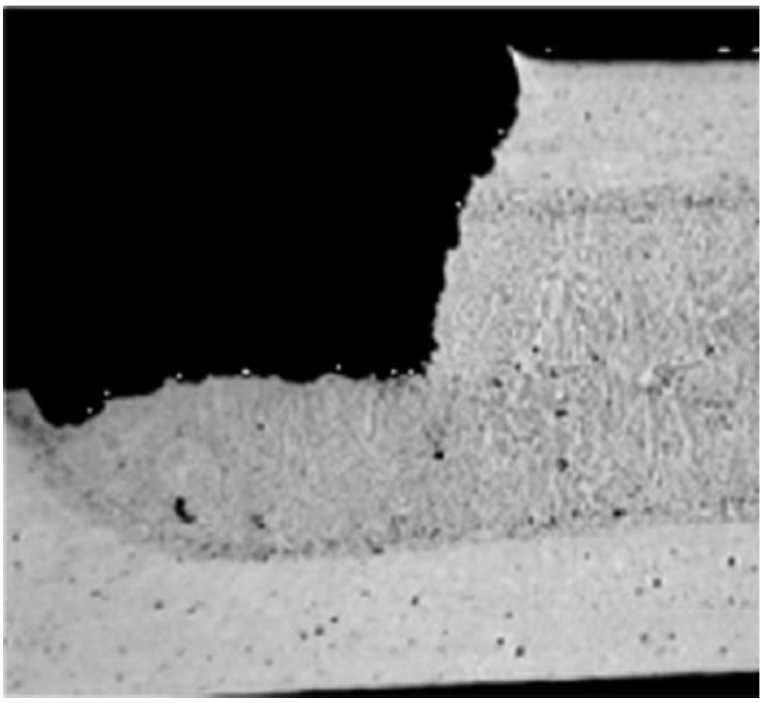

Figure 5.31: Microsection of RSW TRIP steel showing how the crack propagated from the notch along the lateral dendrites, and finally along a perpendicular denritic grain boundary (Den Uijl & Smith, 2006).

The solution is to break up the microstructure of elongated dendrites. The weld edges were therefore remelted using a second weld pulse. This pulse should follow after the edge of the weld nugget formed in the initial weld cycle has completely solidified. It is not necessary to cool the weld completely, because the problem occurs at the edge of the weld nugget. By remelting the edge of the weld the large lateral dendrites are destroyed and replaced by a more amorphous structure (see figure 5.32).

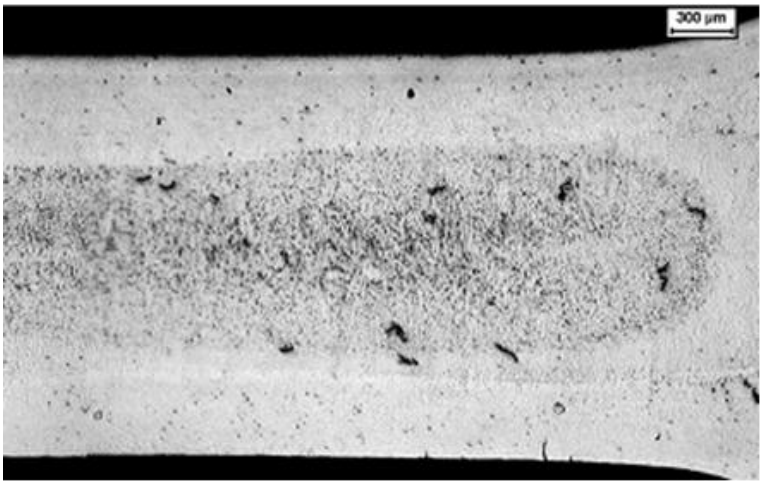

Figure 5.32 Weld nugget with remelted edge *(Den Uijl & Smith, 2006).*

When solidifying, the remelted material forms austenite. Phosphorous in the molten material will segregate on the austenite grain boundaries and after the formation of martensite, will still be present at grain boundaries. Although the remelted material still contains phosphorous grain boundaries, the effect is not so detrimental because of the absence of long columnar grains along the weld interface. Weld failure mode can thus be improved; see figure 5.33.

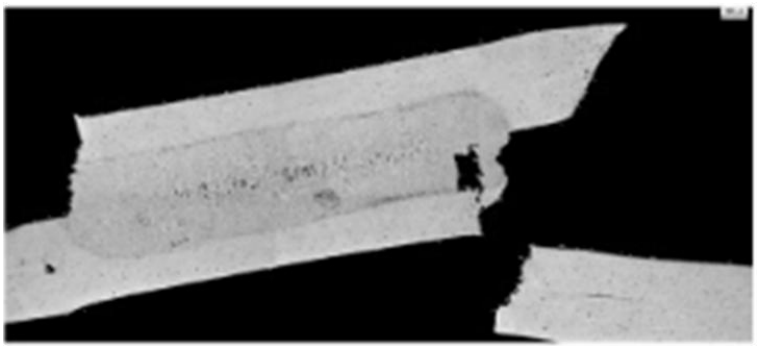

Figure 5.33: weld failure after remelting of the weld nugget edge.

Although the weld failure mode has improved, full plug failure is still not achieved. This is due to the grain boundaries still being weakened by the phosphorus, which leads to a large difference in strength between the grain boundaries in the (re)molten zone and the surrounding material. This can be addressed by tempering the surrounding material thus lowering the difference in hardness.
To temper the material it should first be cooled sufficiently for martensite to form. The temperature in the weld should therefore be lower than the martensite start temperature, M_s. It is not necessary for the weld to cool fully to room temperature, but it should be cooled sufficiently for the majority of the austenite to transform to martensite. Steven & Haynes [1956] give a M_{90} temperature at which 90% of the austenite has transformed into martensite at approximately 120 °C below M_s. When M_{90} has been reached a current can be applied to reheat the material. Care should be taken not to exceed the A_1 transformation temperature, as this would cause the material to transform to austenite again, which on subsequent cooling would transform to hard martensite.
Simulation can be used to design a welding schedule to produce a weld nugget, remelt the weld nugget edge and temper the material. Figure 5.34 shows the simulated thermal profile

for a three step welding schedule for a TRIP 700 steel. Figure 5.35 shows the simulation report with the weld process parameters.

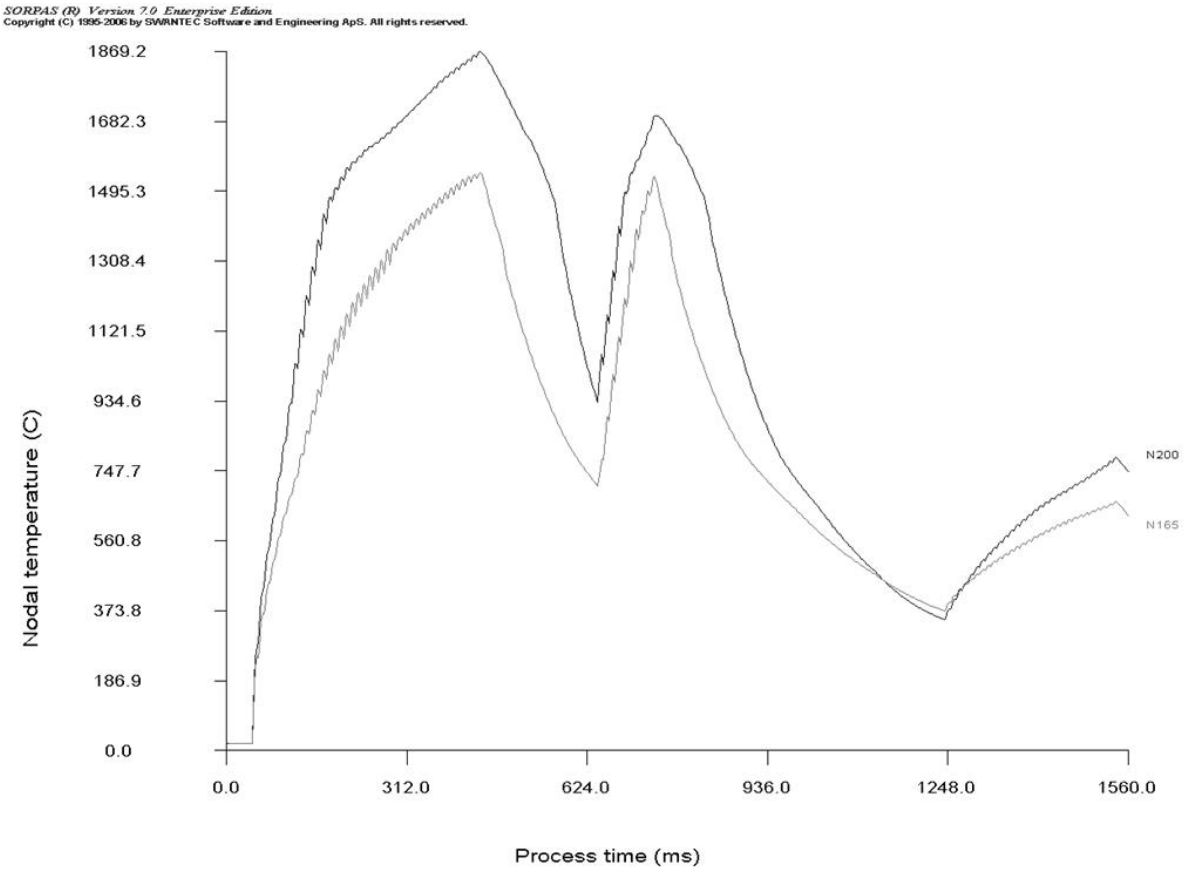

Figure 5.34: Simulated thermal profile for a three step weld schedule for a TRIP 700 steel. The top curve shows the thermal profile of the weld nugget centre and the lower curve shows the thermal profile at the weld nugget edge (simulations done with Sorpas).

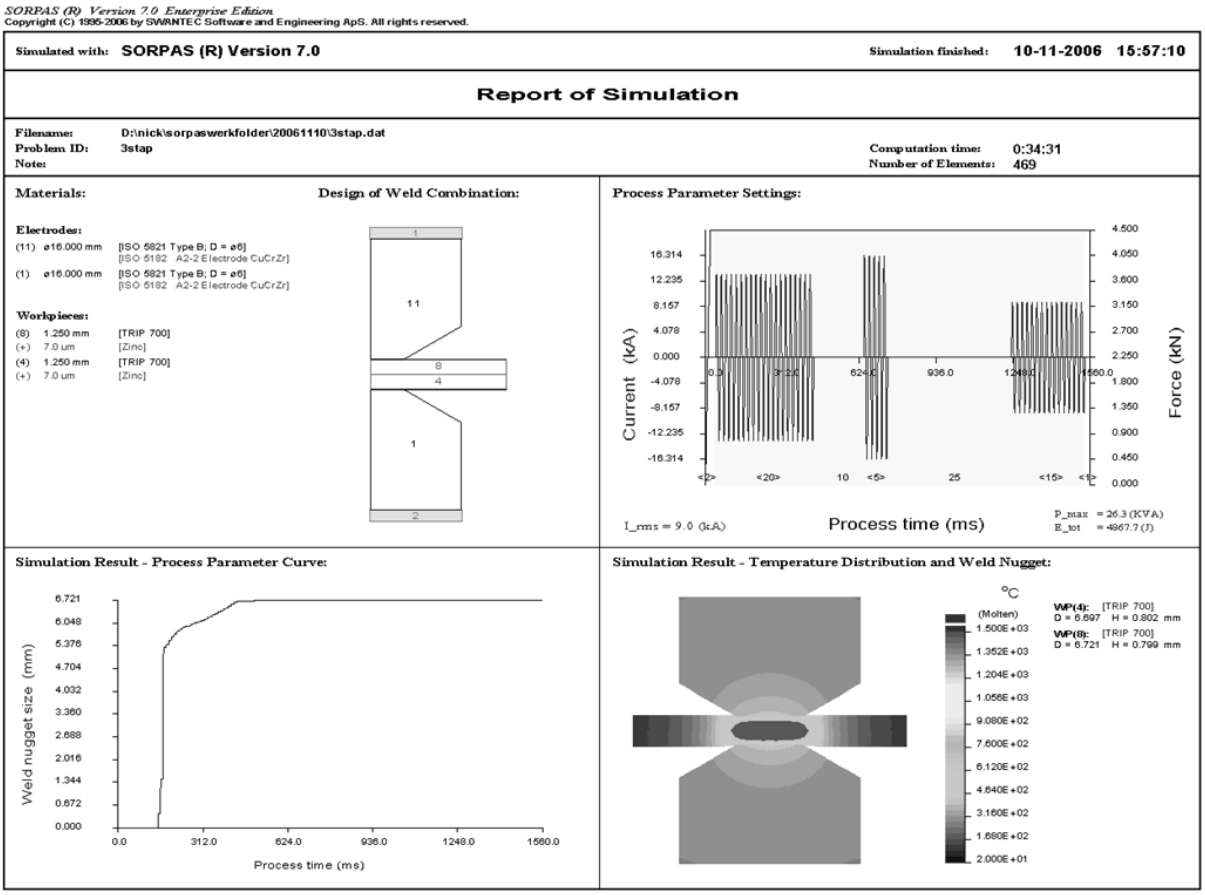

Figure 5.35: Simulation report of the parameters used for figure 5.34 (simulations done with Sorpas).

Using a three step welding approach it is possible to achieve full plug failure in high carbon, phosphorus containing, TRIP steels. Figure 5.36a shows full plug failure in a 0,187 wt% C and 0,087 wt% P TRIP 700 resistance spot welded steel, using a three step welding approach. Figure 5.36b shows a cross section in such a weld. Figures 5.37a & b show the same for a 0,216 wt% C and 0,033 wt% P TRIP 700 resistance spot welded joint, using a three step welding procedure.

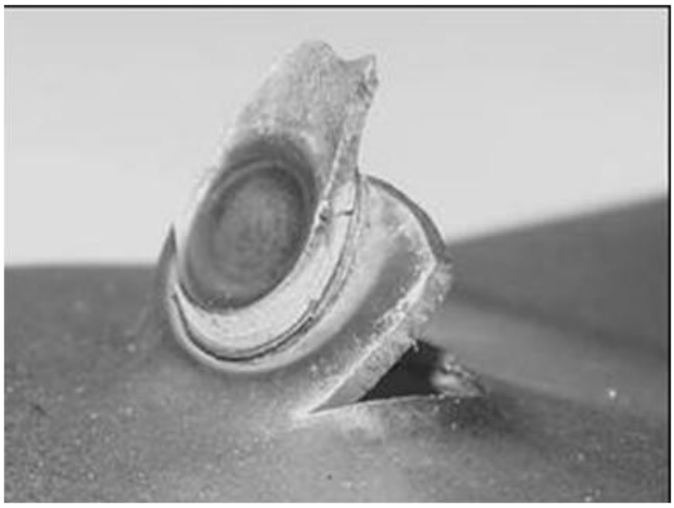

Figure 5.36a: Weld failure in the base material after three step weld scheme in TRIP700 steel containing 0.187 wt% C and 0.087 wt% P (Den Uijl & Smith, 2006).

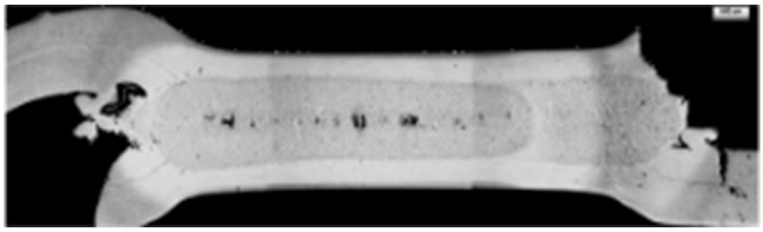

Figure 5.36b: Cross section of a tensile tested resistance spot weld using a three step weld scheme in TRIP700 steel containing 0.187 wt% C and 0.087 wt% P (Den Uijl & Smith, 2006).

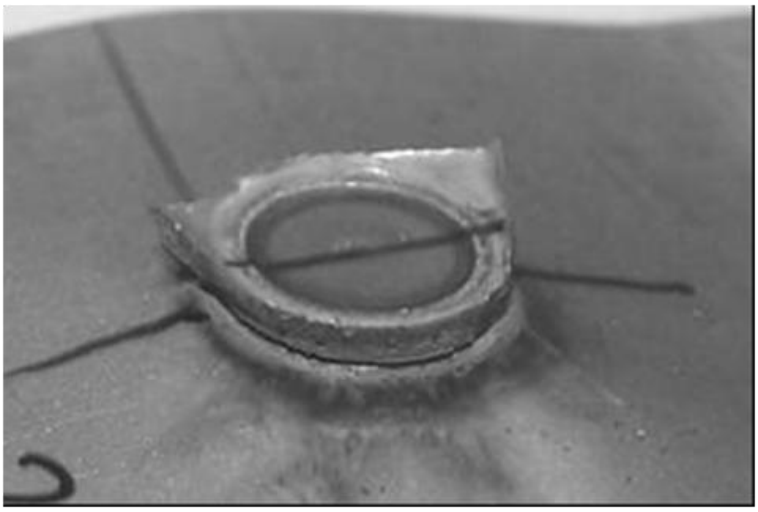

Figure 5.37a: Weld failure in the base material after three step weld scheme in TRIP700 steel containing 0.216 wt% C and 0.033 wt% P (Den Uijl & Smith, 2006).

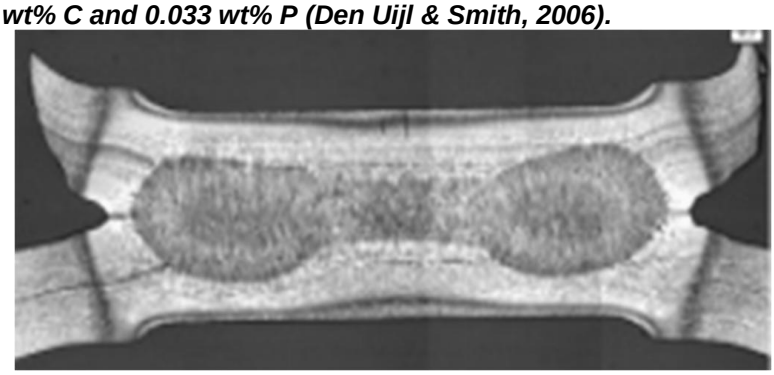

Figure 5.37b: Cross section of a tensile tested resistance spot weld using a three step weld scheme in TRIP700 steel containing 0.216 wt% C and 0.033 wt% P (Den Uijl & Smith, 2006).

Discussion

There is a strong push in automotive engineering to both reduce the fuel consumption and improve the safety of vehicles, driven by customer demand and legislative authorities. The goals are somewhat contradictory as one of the ways to improve fuel consumption is to reduce the mass of vehicles. Conversely, one of the ways to improve safety is to increase the mass of vehicles in safety critical areas, thus increasing strength and energy absorption capacity. The introduction of advanced high strength steels for automotive applications provided the industry with possibilities to simultaneously reduce the mass of vehicles whilst improving the safety.

Increasing vehicle safety requires improved performance of vehicle parts under crash loading. This can be partially achieved by design, but higher strength steels give designers more options. The combination of higher strength steels with improved design allows for better performance in crash. To allow parts with improved design to be manufactured the material needs to have good formability and weldability. AHSS combine high strength with sufficient formability and good weldability.
Improved fuel consumption can be achieved by improvements in the power supply of the vehicle. It is significant gains in the design of the power train that have led to reduction in fuel consumption, combined with reduced emission of undesirable chemical compounds (*e.g.* NO_x emission). For these gains to be effective the overall mass of a vehicle should not increase. The application of AHSS, in combination with improved design, allows for reduction of the thickness of the steel sheet used to manufacture parts designed for crash performance. This reduction of thickness contributes to an overall reduction of vehicle mass.
The reduction of thickness of materials also has a negative influence. The stiffness of parts is primarily determined by the cross section of these parts, and a reduction of thickness of materials therefore leads to a reduction in stiffness of the parts. However this can be countered by design and the application of different joining methods (*e.g.* continuous joints, such as laser welds or combinations of adhesive bonding with resistance spot welding) [Toronto, 2008].
It is not just regulations that force automotive manufacturers to improve the safety and reduce fuel consumption of vehicles. Safety can be a powerful sales argument for cars. A good example is the introduction of the Chinese manufactured Jiangling Landwind, an affordable SUV that made an impression on the European market in 2005 [Geledraak, 2005]. When it was suggested that the design did not perform well in crash tests, the initial positive reviews in the press turned negative overnight [Nu.nl, 2005], plummeting sales figures. In general automotive manufacturers strive for new designs to get a top rating in crash testing.
Similarly fuel consumption is an important sales argument. Although there is generally a large market for cars that perform well when factors like speed and power are involved, the rise in fuel costs has made fuel efficiency an important factor in car marketing. There are many factors that make a certain car design desirable to prospective buyers (looks, size, price), but fuel efficiency is often perceived to be a decisive argument when the final choice is to made [Cooper, 2008, Otten, 2008].
The possibilities that AHSS offer concerning the design of the Body In White (BIW) of a vehicle allows for addition of electronics (*e.g.* on board computers) and heat exchangers (e.g. air conditioning) that increase the appeal of a design on the automotive market. Although the addition of these extras increases the vehicle mass, the use of AHSS for the BIW allows for that without increasing the overall vehicle mass.
Other factors that contribute to the drive for automotive manufacturers to increase safety and fuel consumption can be political. Regulations can often function as effective measurements to protect domestic markets from foreign imports. Regulations also set targets for the recyclability of vehicles. Here AHSS also offer possibilities. Weight reduction of vehicle designs can also be achieved by the application of other materials than steel, *e.g.* carbon fibers, aluminium and magnesium [Cornelissen, 1993]. One argument against the use of

alternative materials can be costs, but recyclability can also be an issue [Beck, 2007]. The use of dissimilar materials to manufacture a vehicle requires joining of these materials, apart of the technological challenges this can provide, the fact that these joints will eventually need to be disassembled and the parts recycled. The use of AHSS cuts short the requirement to dissemble parts as the low levels of alloying of the materials allow for the construction to be used as scrap metal in its entirety.

Issues were reported with the resistance spot weldability (resistance spot welding still being the dominant joining method in automotive manufacturing) of advanced high strength steels. These issues concern two main points: manufacturability, and performance.

Manufacturability concerns the formation of joints by resistance spot welding. The formation of welds is dependent on two aspects: material characteristics and process parameters. These are interdependent. Changes in material characteristics requires changes in process parameters. In principle it can be stated that the relation also works the other way around, but this is less of an issue in this thesis, as a restriction in process parameters (*e.g.* equipment that cannot supply a sufficiently high welding current) will cause a manufacturer to use different materials, or use different processes.
Both material characteristics and process parameters have been investigated in this thesis, primarily using simulation. The goal of investigating the influence of material characteristics on weldability was twofold, relating to the external and the internal characteristics of materials. External characteristics in this respect relate to properties such as material thickness, surface quality and coating layers. These qualities are independent of the internal characteristics of the material, such as the chemical and microstructural composition of the material. It is for instance possible to have similar thickness HSLA and DP steels with similar coating layers that will differ in chemical and microstructural properties and therefore will differ in their weldability (see figure 4.21).
The impact of variations of external properties was investigated to directly assess their impact on weldability. These properties are usually known (or measurable without great difficulty) and are often specified in the design of a construction. The impact of variations of internal properties was investigated with the goal to assess their direct influence on weldability, but also to investigate their influence on the outcome of simulations. As these properties are not usually directly available in material data sheets as supplied by material manufacturers, they can justifiably be used to fine tune material data for simulation.
It must be noted that the division is not as strict as it may be though. The strength of a material for instance is dependent on both the chemical and microstructural composition as well as on its thickness. Also the application of a coating layer on a material may have consequences for the chemical composition of a material, such as the replacement of silicon by aluminium in TRIP steels (see § 2.1).
Reported issues with process parameters primarily concern the interaction between the electrodes and the materials, as increased strength levels were reported to lead to decreased electrode life time. Both the electrode geometry as a whole, *i.e.* the electrode type, as well as the more specific aspects of the contact surface were investigated in this thesis. Again simulations were primarily used for this goal, the advantage being that they allow specific investigations of this aspect, as simulations are not affected by experimental spread, nor variations in surface quality due to subsequent welding operations. The disadvantage is that simulations do not allow inclusion of important aspects such as alloying of the contact area of the electrode or small deformations due to subsequent welding operations.

Performance concerns the behaviour of resistance spot welds in applications. The performance is related to the demands posed by the application, and the effect failure will have on safety (see table 2.3). Some welds just need to join parts, but failure of one or more of these welds will not affect the safety of a construction or the occupants of a vehicle. Other welds may cause the construction to fail, but not affect the safety of the occupants. Finally some weld failures may affect the safety of the occupants. All weld failures are undesirable,

but there is some tolerance for the first category of failure, less so for the second category (though these may be repaired) and no tolerance for the last category of failure.
The main issue reported concerning the failure of resistance spot welded joints in advanced high strength steels falls in the last category. Advanced high strength steels are often used in safety critical situations. They should not fail, but if failure does occur, it should be outside the weld zone so that failure becomes predictable as it is then related to material properties that are known or can be tested.
Issues reported concerning the failure of resistance spot welded advanced high strength steels related to the weld failure mode; that is, welds did not fail outside the weld zone, but instead showed partial plug failure (see section 2.4). The main cause reported for the undesired weld failure mode was the post weld hardness of the resistance spot welded joints. The proposed mechanism being that excess post weld hardness caused the joints to be brittle and therefore unable to accommodate deformation. Therefore the first issue investigated in this thesis is the relationship between the chemical composition of the materials and the spot welding process. The aim being to predict the post weld hardness from the chemical composition. The chemical composition the material is usually known (at least approximately), thus the chance of undesirable weld failure can be reduced.
The second issue investigated is the possible mitigation of excess post weld hardness by post weld heat treatment. The idea being that a post weld heat treatment should lower the hardness of the joint, leading to a more favourable weld failure mode.

It should be noted that the weld failure behaviour investigated in this thesis only addresses the failure mode of welds with respect to their behaviour in crash loaded applications. Other important aspects, such as excess residual stresses due to welding operations and fatigue behaviour are not considered.

5.4 Manufacturability

5.4.1 Material Characteristics

The primary reported reason for issues with manufacturability was the material strength, which is the most striking meta-characteristic of the advanced high strength steels compared to more traditional steels used in automotive manufacturing (*e.g.* IF and HSLA steels). It was reported that AHSS showed shorter welding ranges, lower splash currents and smaller maximum weld diameters, as can be seen in Figure 4.1. The idea was that higher strength levels correspond to higher hardness and this affects contact resistance, indentation and electrode lifetime.
Because experiments in resistance spot welding tend to produce large amounts of scatter, the issues with manufacturability of advanced high strength steels were investigated using simulation. Apart from the advantage that simulation removes the experimental scatter, simulation offers the possibility to investigate the influence of changes in material characteristics and process parameters without the need to perform extensive experimental trials and without the need of actual material. Because of the large amount of experimental scatter, any variation in the input parameters of an experiment requires a lot of material and testing to obtain meaningful results. The simulation approach is valid as long as the variations are not too drastic and there are experimental verifications of the simulations.
The software used was Sorpas for several reasons:

- it is widely used in manufacturing;
- it is designed to address issues in manufacturing, such as determination of welding range;
- it contains a large database of material properties that can be manipulated to suit demands of the user.

Because Sorpas is and has been used extensively in industry, over a long period of time, it has been verified experimentally time and again. In this thesis, for example, figures 4.15, 4.16 and 4.24 give a comparison of simulated weld growth curves against experimentally derived weld growth curves.

5.4.2 Material Strength

The first issue to address is the influence of material-strength on the results of simulations. It was found that there are several factors that influence the results of simulations:

- the numerical definition of the temperature dependency of material strength;
- the material strength (*e.g.* 600 MPa tensile strength *vs*. 800 MPa);
- the grade of steel (as in DP *vs.* TRIP).

Of these is was found that the grade of steel, whether the material was a dual phase or a TRIP steel, was the least important (see figure 4.6). This is to be expected, as the software does not take into account the microstructural or chemical composition of the material and the differences in the numerical representation of the materials is solely due to differences in the shape of the tensile stress curves of the materials. As these differ, the results are affected accordingly. But because the overall shape is fairly similar for materials of similar strength (at least for the characteristics that are of importance for the numerical representation of the materials), the results of simulations are fairly similar.
As the materials behave even more alike at elevated temperatures, when the materials transformed to austenite, which is the state in which most of the plastic deformation of the material during welding will occur, the effect of differences in the tensile curves is even less at higher welding currents.
The effect of the chemical composition of the materials on the results of simulations is reflected in the melting temperature, which is lower for materials that are more highly alloyed. In the range of chemical compositions in which DP and TRIP steels differ, the influence of the changes in the chemical composition on melting temperature are not large enough to cause a noticeable difference in the outcome of simulations. This is an issue of scale. First the difference between melting temperatures compared to the total range of temperatures involved. Secondly the size of the molten weld pool compared to the distance over which the temperature gradient passes through this difference in melting temperatures. Combined this will lead to large gradients in temperature over small distances, and a relatively small variation in melting temperature is not going to make much difference on the small dimensions of the weld nugget. If the difference in melting temperatures is 50°C (a large number for the chemical compositions involved) then that would only amount to a difference of 3% in the total temperature (typically around 1450°C) and a corresponding small geometric region compared to a weld nugget diameter of 3 to 4 mm.

The second issue that influences the outcome of simulations is the numerical definition of the temperature dependency of material strength. Generic material designations such as TRIP800 may relate to materials that are quite different in their chemical composition, microstructure and thermomechanical history. The designation relates to the mechanical behaviour of the material at room temperature, but makes no claims about the material (mechanical) behaviour at elevated temperatures, let alone its weldability. These possible differences are reflected in figure 4.2, representing the stress strain relations of two TRIP800 steels in the Sorpas material database. As expected the differences affect the outcome of simulation results (see figure 4.3) but not to a significant extent in the process ranges (*i.e.* higher welding currents) that are of importance for welding operations.
The reasons for this are similar to the reasons given for the small differences in outcome when comparing a DP and TRIP steel of similar strength level; the software does not take variations in microstructural and chemical composition into account, nor does it do so for

variations in the thermomechanical history of the materials, in so far as these do not directly affect the stress strain curves.
The results show that the numerical definition of the of the temperature dependency of material strength has a bigger impact on the results of simulation than the comparison between DP and TRIP steels, especially at the onset of the formation of welds, *i.e.* at lower welding currents. This is related to the numerical representation of the materials that cannot capture all physical characteristics. In the context of Sorpas simulations, materials are represented on a macroscopic level by bulk material properties such as stress strain relationships, without taking into account the microstructural differences between DP and TRIP steels.
Therefore if the data used to define a materials stress-strain curve in the materials database is changed, *e.g.* when new test results are used, the model should be verified, even when the grade of the material has not changed. Alternatively it should be expected that if a material is changed in production, *e.g.* when material from a different supplier is used, the performance of the material in welding operations will be affected, even if the material grade is still the same. For any manufacturer it is therefore advisable to adjust the materials database to represent tested data from the material actually used in production, to maximize the value of simulations for their operations.

The third issue concerns the material strength. It can be seen from figures 4.4 and 4,5 that the material strength has a great influence on the weldability of the material. Welds are formed at lower welding currents for high strength materials compare to lower strength materials. The weld nugget size at higher weld currents is the same for all strength levels. It appears that higher strength materials actually have better welding ranges than lower strength materials.
The simulations do not take the occurrence of splash welding into account. The lowest current at which splash welding occurs is the upper limit of the welding range. So from these simulations no conclusion can be drawn on the size of the welding range. Experimentally the occurrence of splash welds is also dependent on the electrode force. This force is usually set at a higher level when welding higher strength steels. If the electrode force is too low to overcome the strength of the material, the sheets cannot be pressed together sufficiently to contain the molten weld pool and splash will occur. In the simulations the electrode force was kept constant.
The strength level directly influences the results of welding simulations in a different way. Stronger materials will not deform as much as weaker materials. This affects the contact area between the sheet material and the electrode tips. For lower strength materials the electrode tip will indent the material and thus the contact area between the electrode and the sheet material will be enlarged. A larger contact area will influence both the current density and the cooling rate. The current density will decrease, resulting in less heat being generated in the material. The cooling rate will be increased as more heat can be conducted away to the water cooled electrodes. Both lead to the formation of smaller welds, explaining the shift to higher welding currents for the weld growth curves of lower strength materials.
In the simulations the electrode force was kept constant. An increase of the electrode force will lead to increased indentation, enlarging the contact area. An increase in electrode force, which is required when welding higher strength materials to counter splash welding, will also cause the weld growth curve to shift to higher welding currents.
The occurrence of splash welding is not simply dependent on the electrode force. Other factors also play a role, such as misalignment of the electrodes or wear of the electrodes. Misalignment can occur due to poor set up of operations, but also due to insufficient stiffness in the welding apparatus. The latter is more important with increased electrode forces. Wear of the electrode tip surface can strengthen this effect, as the electrode tip may not wear uniformly, because the load may not be uniformly distributed due to (small) misalignment of the electrodes or insufficient stiffness of the welding apparatus. Additionally irregularities at the sheet surface (scratches, inclusions) may play a role. Again these effects are stronger at higher electrode forces. All of these contribute to the experimental spread.

5.4.3 Surface Quality

The strength level of the material in simulation is a bulk material characteristic. It does not affect the surface of the materials. In experiments the strength of the material affects the surface condition as well, partly due to the fact that stronger materials will resist deformation more than weaker materials and this will have an effect in the rolling operations that are part of the production process of steel sheet. The surface quality is directly related to the rolling operations that give the surface of the steel its texture. Harder materials will increase the wear of the rolls during processing and thus will affect the surface quality.
Modern steel rolling operations are well controlled and the material is closely inspected after production, so it may be expected that this effect is not very large, and probably not large enough to affect the results of welding significantly (*i.e.* any influence will be less than the experimental spread).
The material surface has texture and this means that the true contact area between the steel sheets, and electrodes and sheets is less than the contact area as defined by the electrode tip diameter and the contact area between the sheets. The electrode force presses the electrodes and steel sheets together. This increases the true contact area. As the material heats up, the material softens and the true contact area is increased. This increase of true contact is less for stronger materials as stronger materials resist deformation more.
In the simulations the effect of material strength level on the true contact area is not taken into account. This is a scale problem. The effects of material strength on true contact is on the scale of micrometers, the effects of welding operations on the formation of welds is on the scale of millimetres. In finite element models simulating the effect of material strength on the true contact area would require very small elements. To use these elements in simulations that would also predict the weld nugget size after welding, would require very large models and increase computation times accordingly.
The software used in these simulations is primarily aimed at predicting the outcome of welding operations on materials. To do this the calculations need to be fast (typically around 10 minutes for a single simulation), as several simulations varying process parameters such as welding current, electrode pressure, welding times, *et cetera*, are needed to perform a proper analysis of weldability in manufacturing.
The solution is found in a separate definition of the surface of the materials. A surface contamination factor, SCR (Surface Contaminant Resistance), is defined that allows simulation of the influence of surface contaminants such as lubricants (*e.g.* from forming operations), dust or excess oxidation. It can also be used to accommodate differences in surface roughness. It basically functions as a penalty added to the surface resistance (see Table 4.1). With increasing temperatures the value of the SCR decreases, representing evaporation of lubricants, burning off of dust and/or softening of the surface and subsequent increase of true contact area (decrease of the effect of surface roughness).

The characteristics of the material surface are not solely defined by the quality (roughness) of the surface. In automotive applications coatings are often used to improve corrosion resistance, appearance and paintability. Most important of these are zinc coatings for corrosion protection. There are several processes that can be used to coat steel sheets with a zinc layer. Most common are galvanized steels and galvannealed steels. Galvanized (GI) steels are coated with a zinc layer that consists of almost pure zinc. Galvannealed (GA) steels are first coated with an almost pure zinc layer, which is then alloyed with the steel substrate in a subsequent annealing step. The thickness of these layers is usually small (typically around 7 µm) but can be thicker for special purposes.
The effect of a thin (7 µm) zinc layer on the formation of welds is small compared to bare steel sheet in simulation for galvanized steels (see figure 4.9). The same is true for galvannealed steels (see figure 4.10). The effect of thicker zinc layers is noticeable for GI

steels (see figure 4.9), but much less for GA steels (see figure 4.10). This is likely due to the alloying in GA coatings evening out differences in material characteristics that influence welding operations (*e.g.* electrical resistivity). The effect of thicker GI coatings is mostly apparent at lower welding currents. This is likely due to the fact that the zinc will evaporate at elevated temperatures (and higher welding currents), removing the zinc layer.
The surface quality, represented by the Surface Contamination Resistance (SCR) influences the results of simulations in an important way. As can be seen in figure 4.11 the weld growth curve shifts to higher welding currents if the SCR is lowered and conversely to lower welding currents if the SCR is increased. The effect lessens at higher welding currents. This effect is likely due to the fact that the SCR decreases for higher temperatures, reflecting the evaporation of contaminants (*e.g.* lubricants) and the softening of the material increasing the true contact area.

The surface contamination resistance is used in Sorpas to calculate an overall contact surface resistance using the following model [Swantec, 2011]:

$$\rho_{contact} = 3\left(\frac{\sigma_{s\_soft}}{\sigma_n}\right)\left(\frac{\rho_1 + \rho_2}{2} + \gamma\rho_{contaminants}\right), \qquad \text{(Eq. 6.1)}$$

where $\rho_{contact}$ is the contact surface resistance, σ_{s_soft} is the flow stress of the softer material of the two materials in contact, σ_n is the contact normal pressure at the interface, ρ_1 and ρ_2 are the resistivities of the materials of the sheets in contact, $\rho_{contaminants}$ is the surface contaminants resitivity due to oxides, oil, water vapour and dirt, *et cetera* [Swantec, 2011], and γ is a factor introduced for adjustment and verification of the contact resistance.
The last factor can in Sorpas be set by adjusting a “dirty – clean” factor, that is set at a default value of 1,0. It can be varied between 0,1 and 10,0, according to the surface conditions in contact [Swantec, 2011].
The model used in Sorpas is distorted by the values for the different material properties given in the Sorpas material database. The value for the bulk resistivity, ρ_1 and ρ_2 in equation 6.1, varies between 0,182 *μΩm* to 1,247 *μΩm* for DP steels, and 0,208 *μΩm* and 1,250 *μΩm* for TRIP steels. The value for $\rho_{contaminants}$, or SCR, varies between 40 *μΩm* to 12 *μΩm* for both DP and TRIP steels. It can be said that the contribution of the bulk resistivities is negligible, and the SCR functions as the contact surface resistance, with the “dirty – clean” factor, γ, functioning as a true surface contaminants factor.

Reflecting on the primary function of the SCR to represent the increase of true contact area, although there may be good reasons to adjust the SCR to represent the effect of the strength of the material on the true contact area, the effect on welding operations may actually be limited. In the simulations reported in this work, use was made of a 6 mm B type electrode and a 4 kN electrode force. Assuming the electrode tip surface to be completely flat (which it is not) and the true contact are to be the same as the maximum contact area (which it is not) the stress in the material would exceed 212 MPa. It is easy to see that in reality the stress will be higher and exceed the flow stress in all materials used, especially as the temperature increases and the material softens.
The same is true for contaminations. Unless a severe disturbance has occurred somewhere in production, it can be expected that the steel surface is relatively clean. That is to say, it is unlikely that contaminations will affect the surface quality so much between different batches of grades of steel to justify adjustment of the SCR.

Although there may be sound physical reasons to adjust the value of the surface contaminant resistivity, or the “dirty – clean” factor, it should be done with care, as it may be used as some kind of fiddle factor to compensate for unknown variations in material data. In general it is advised not to adjust the SCR, unless there is an obvious physical reason, such

as clearly visible contaminations. If the SCR is adjusted it should be justified by experimental validation against rigorously cleaned surfaces.

The set up of the finite element models in Sorpas requires an interface layer. This interface layer serves to allow movement between the sheets (due to possible differences in thermal expansion) and fusion between the sheets after melting and solidification. The default thickness of this layer is 0,050 mm (note; that this is bigger than the standard coating layer thickness for automotive applications). The thickness of the interface layer cannot be changed when setting up a simulation using the standard graphical user interface supplied by Sorpas; it can however be change manually by adjusting the simulation control parameters.
Figure 4.12 shows the effect of changing the interface layer thickness for simulation of resistance welding of 1,0 mm thick DP600. It can be seen that the effect is very large. The weld growth curves shift to lower welding currents for thicker interfaces and to higher welding currents for thinner interfaces. The effect does not even out for higher welding currents; it is large over the entire welding range. In fact, adjusting the thickness of the interface layer can be used to match the simulation results to fit virtually any experimental result.
The interface layer is needed for numerical reasons; it serves to allow contact between different elements of the model and allows surfaces to be joined as materials melt and solidify. It does not represent any physical phenomena. It is therefore recommended not to change this parameter. In fact, as it is the ultimate fiddle factor, it is fair to state that changing the interface layer thickness renders the results of comparative simulations invalid.

5.4.4 Thermal Conductivity and Electrical Resistivity

In figure 4.17 it can be seen that with increasing electrical resistivity the weld growth curve shifts to lower welding currents and to conversely higher welding currents with decreasing electrical resistivity. This is due to the generation of heat being directly related to the resistivity of the material through the which the current runs. An increase in electrical resistivity causes increased heat generation and a lower current is therefore needed to melt the material and form a weld.
In figure 4.18 it can be seen that with increasing thermal conductivity the weld growth curve shifts to higher welding currents and with decreasing thermal conductivity to lower welding currents. With increasing thermal conductivity more heat will be conducted away to the water cooled electrodes and the surrounding material, making it harder to accumulate sufficient heat to allow the material to melt. Therefore a higher welding current is needed to melt the material and form a weld.
Simulation offers the possibility to separately investigate the effect of electrical resistivity and electrical conductivity, but they are related in reality. An increase in electrical resistivity corresponds to a decrease in thermal conductivity and *vice versa*. Figure 4.19 & 4.20 shows the effect of the combination of increased thermal conductivity and decreased electrical resistivity and the effect of decreased thermal conductivity and increased electrical resistivity in simulation; it can be seen that the effect is pronounced. With the former, the weld growth curve shifts to higher welding currents.
This is an important result. The conductivity and resistivity of a material are determined by the level of alloying and microstructure of the material. Impurities, inclusions lattice imperfections (interstitials, substitutional atoms, dislocations, *et cetera*), grain boundaries and phase transitions all function as scattering events that increase the electrical resistivity and decrease the thermal conductivity of a material. It is exactly these phenomena that are used to increase the strength of steels. So with increasing strength levels it can be expected that the electrical resistivity increases and the thermal conductivity decreases.
In advanced high strength steels it is the thermomechanical treatment that the material is subjected to after alloying that determines the strength of the material. There is quite a large

variety in which a combination of these production parameters can be used to achieve a set level of material strength. Whatever the process route, it will affect the electrical resistivity and the thermal conductivity directly. As can be seen in figure 4.19 & 4.20 these choices will have a pronounced effect on the weldability of the material.

For simulation the result is also important; when modelling a material it has been found that the material strength is an important factor in determining the outcome of simulations. The mechanical strength of a material is a set parameter, but materials of similar strength levels can still vary significantly in their electrical resistivity and thermal conductivity, depending on the choices made during production of the material. For engineering purposes it seems that adjusting the electrical resistivity and the thermal conductivity is the best way to adjust the material definition to experimental results, to ensure a sufficiently sound representation of the material in simulation (in the absence of measured material data). Care should be taken to adjust both the electrical resistivity the thermal conductivity as they are related.

5.4.5 Relationship between Weld Nugget Size and Material Properties

The weld size, in volume, WZ, is related to the heat generated during welding (see figure 4.40). The increase in weld size at any moment during welding is a function of the net heat accumulated in the material per unit time (equation 6.2), where the net heat flow, $\dot{Q}_{net}$, is the generated heat, $\dot{Q}_{generated}$, minus the heat lost, $\dot{Q}_{lost}$, to the surroundings (equation 6.3).

$$\frac{dWZ}{dt}(t) = f\left(\dot{Q}_{net}(t)\right), \qquad \text{(Eq. 6.2)}$$

where $\dot{Q}$ is the heat flow (dQ/dt), and t is time.

$$\dot{Q}_{net}(t) = \dot{Q}_{generated}(t) - \dot{Q}_{lost}(t). \qquad \text{(Eq. 6.3)}$$

The amount of heat generated, Q, is given by Joule's Law, $Q = I^2Rt$, (see equation 2.1), where I is the current applied through the conductor, and R is the resistance of the conductor. The electrical resistance in resistance spot welding is formed by a series of contact surface resistances, R_{CSR}, and bulk resistances R_{bulk}. Surface contact resistances are two dimensional properties, whilst bulk resistances are three dimensional properties. Using resistivity (equation 4.4), and incorporating the Surface Contaminant Resistivity, SCR, the total electrical resistance over a cross sectional area, dA, can be written as:

$$R = \rho \sum_{i=1}^{i=n} t_{s,i}\, dA = 2\sum_{i=1}^{i=n} [SCR_i]\rho_{CSR,i}\, dA + \sum_{i=1}^{i=n} \rho_{bulk,i}\, t_{s,i}\, dA, \qquad \text{(Eq. 6.4)}$$

where R is the resistance between the electrodes, ρ the resistivity between the electrodes, $t_{s,i}$ the thickness of individual sheets, A the cross sectional area between the electrodes, SCR_i the surface contaminants resistivity of individual sheets, $\rho_{CSR,i}$ the contact surface resistivity of individual sheets, and $\rho_{bulk,i}$ the bulk resitivity of individual sheets.

Using equation 6.4 the heat flux (heat flow per unit area) generated by Joule heating, $\dot{q}_{generated}$, can be written as:

$$\dot{q}_{generated}(t) = I^2(t)\left(2\sum_{i=1}^{i=n} [SCR_i]\rho_{CSR,i} + \sum_{i=1}^{i=n} \rho_{bulk,i}\, t_{s,i}\right). \qquad \text{(Eq. 6.5)}$$

Heat loss in resistance welding can be attributed to three mechanisms: conduction to the water cooled electrodes, conduction to the surrounding material, and radiation. Although the mechanisms differ during welding, the material that is heated is solely affected by heat being conducted away. This can be expressed in an equation using Fourier's law (equation 4.8). A factor that should be added to adjust for latent heat effects, *e.g.* due to phase transformations, dissolution of precipitates, *et cetera* is caught in a rest function, Λ. Combining these, an equation for the lost heat can be derived:

$$\dot{q}_{lost}\,(t) = \kappa\left[\frac{dT}{dx}(t)\right] + \Lambda(t), \qquad \text{(Eq. 6.6)}$$

where $\dot{q}_{lost}$ is the heat flux lost to the surroundings and by latent heat effects, κ the thermal conductivity, dT/dx the temperature gradient, and Λ the latent heat function.

Combining equations 6.3 to 6.6, adding a coefficient related to the volumetric heat capacity, $1/C$, to relate material volume to heat flux, the function for the weld size can be written as

$$\frac{dWZ}{Cdt}(t) = I^2(t)\left(2\sum_{i=1}^{i=n}[SCR_i]\rho_{CSR,i} + \sum_{i=1}^{i=n}\rho_{bulk,i}\,t_{s,i}\right) - \kappa\left[\frac{dT}{dx}(t)\right] - \Lambda(t). \qquad \text{(Eq. 6.7a)}$$

As detailed in section 4.2, the material characteristics in equation 6.7 are temperature dependent, as is the latent heat function Λ, and the volumetric heat capacity coefficient, C.

$$\frac{dWZ}{C(T)dt}(t) = I^2(t)\left(2\sum_{i=1}^{i=n}[SCR_i(T)]\rho_{CSR,i}(T) + \sum_{i=1}^{i=n}\rho_{bulk,i}(T)\,t_{s,i}\right) - \kappa(T)\left[\frac{dT}{dx}(t)\right] - \Lambda. \qquad \text{(Eq. 6.7b)}$$

It should be noted that material strength plays a role in the surface contact resistivity, as it is an important factor in determining the true contact between surfaces. This effect has been incorporated in the SCR (see § 4.2.2). Also the different effect that the bulk electrical resitivity and the thermal conductivity have on the growth of the weld size should be noted. Although both properties are related (see § 4.2.3), their effect on the weld size is different. The electrical resistivity only plays a role in combination with the weld current, whereas the effect of the thermal conductivity is independent of the welding current. This difference in effects forms the justification of the separate manipulation of these properties in modeling materials for resistance spot welding.

The difference between advanced high strength steels of similar strength levels is usually in their microstructural composition. The effect this has on the results of resistance spot welding simulations is often hard to quantify in material data used to model materials for simulation. One way to quantify this is to adjust the thermal capacity of the material, but measured data for this characteristic are often not available. As can be seen in equation 6.7b a trade off can be made between the thermal conductivity and the latent heat function. By adjusting the thermal conductivity the effect of latent heat on the results of simulations can be accounted for. This is a second justification for the individual manipulation of thermal conductivity to model material response to resistance spot welding.

From equation 6.7b it can also be seen why adjusting the surface contaminant resistivity factor has such a big impact on the results of simulations. In Sorpas simulations the SCR ($\rho_{contact}$ in equation 6.1) functions as the contact surface resistivity ($\rho_{CSR,i}$) in equation 6.7b, and the "dirty – clean" factor (γ in equation 6.1) as the SCR (SCR_i) in equation 6.7b, which

explains why changing its value has such a big impact on the outcome of simulations. The flaw in the Sorpas definition being that the contact resistivity is defined as coupled to the bulk resistivities. They work in series in reality, which is reflected in equation 6.7b.

It is therefore recommended that adjusting material properties for resistance spot welding operations should be done in a specific order. First of all material properties such as sheet thickness, coating layers and material strength, that are usually available (*e.g.* from data sheets) should be modeled correctly. Next adjustment should primarily be done by adjusting the thermal conductivity, unless there are sound reasons to adjust the electrical conductivity (such as abundant inclusions), but these would most likely also require an adjustment of the thermal conductivity, to compensate for latent heat effects. The surface contaminant resistivity should only be adjusted when there are obvious physical reasons, such as excess surface roughness or contaminations, that would justify such an adjustment. Even then the adjustments should be verified over a range of different process parameter settings.

5.4.6 Electrode cap geometry

Figures 4.25 and 4.26 compare the effects of using B type electrodes or with G type electrodes when welding 1,5 mm TRIP800 GI, varying the electrode tip diameter but keeping all other process parameters constant. It can be seen, that the electrode tip diameter has an import influence on the results when B type electrodes are used, and that the influence is negligible when using G type electrodes. All weld growth curves simulated using a G type electrode geometry start at a welding current of approximately 4,5 kA and reach their maximum size at around 10,5 kA, with larger electrode tip diameters allowing for even higher welding currents. In simulations using B type electrodes the weld growth curve started at 5,5 kA for the smallest tip diameter (5 mm) and shifted to higher welding currents for larger tip diameters (10,5 kA for 8 mm electrode tip diameter). The maximum weld current shifted from 12 kA for a 5 mm electrode tip to 13 kA for an 8 mm electrode tip. This corresponds to a substantial shortening of the welding range.
A similar effect can be observed in figures 4.32 and 4.33. The difference between these graphs and those of figures 4.25 and 4.26 may be attributed to the coating layer.
The shift to higher welding currents for the increase in electrode tip diameter of B type electrodes may be explained by the effect that a larger contact area has on the current density and cooling area. As the contact area increases the current density decreases, leading to less heat being generated (concentrated) in the material. Additionally the increased contact area leads to increased cooling area leading to more heat being conducted away from the material.
The absence of this effect in the simulations using G type electrodes may be explained by the shape of the tip. Although the shape of the tip of G type electrode caps appear to be similar to the shape of the tips of the B type electrodes (see figure 4.23), the angle between the electrode tip, outside the contact area is larger for the G type electrodes, than it is for the B type electrodes (see figures 4.23 a&b). If the angle is not too large, the sheet material will wrap around the corner of the electrode upon indentation, if the angle is too large then the material will not be able to make contact, and indentation will not lead to an increased contact area, and therefore no decrease in current density and increase in cooling area. This effect may be exaggerated by the stiffness of elements, which may not allow them to make proper contact with the curved surface of a G type electrode.

The difference in increase of contact can be calculated. The lateral surface area of an extended cone from the electrode surface onwards is given by:

$$A_{cone} = \pi r_{electrode} l_{cone}, \qquad \text{(Eq. 6.8)}$$

where A_{cone} is the lateral surface of the cone, $r_{electrode}$ the radius of the electrode tip, and l_{cone} the lateral height of the cone, with $l_{cone} = \sqrt{r_{electrode}^2 + h_{cone}^2}$, where h_{cone} is the height of the cone. After indentation the lateral surface area becomes:

$$A_{cone,indent} = \pi(r_{electrode} + \Delta r)(l_{cone} + \Delta l_{cone}), \qquad \text{(Eq. 6.9)}$$

where Δr is the increase of the radius of the base of the cone, and Δl_{cone} is the increase of the lateral height.

The increase in area:

$$\Delta A_{indent} = \pi(r_{electrode}\Delta l_{cone} + \Delta r l_{cone} + \Delta r \Delta l_{cone}). \qquad \text{(Eq. 6.10)}$$

The lateral height can be expressed as:

$$l_{cone} = \frac{r_{electrode}}{\sin\alpha}, \qquad \text{(Eq. 6.11a)}$$

where 2α is the included angle of the cone. The increase of the radius of the base of the cone as:

$$l_{cone} = \Delta h_{indent} \tan\alpha, \qquad \text{(Eq. 6.11b)}$$

where Δh_{indent} is the height of indentation. The increase of the lateral height of the cone can be expressed as:

$$\Delta l_{cone} = \frac{\Delta h_{indent}}{\cos\alpha}. \qquad \text{(Eq. 6.11c)}$$

Using equations 6.11 a, b & c, equation 6.10 then can be written as:

$$\Delta A_{indent} = \pi\left(\frac{r_{electrode}\Delta h_{indent}}{\cos\alpha} + \frac{r_{electrode}\Delta h_{indent}}{\cos\alpha} + \frac{\Delta h_{indent}^2 \sin\alpha}{(\cos\alpha)^2}\right). \qquad \text{(Eq. 6.12)}$$

If α is not too large, *i.e.* $\cos\alpha$ does not approach 0, the last term can be dismissed, as Δh_{indent} is small, and $\Delta h_{indent}^2 \approx 0$. So:

$$\Delta A_{indent} \approx \frac{2\pi r_{electrode}\Delta h_{indent}}{\cos\alpha}. \qquad \text{(Eq. 6.13)}$$

For a B type electrode, α = 60°, $\Delta A_{indent} \approx 4\pi r_{electrode}\Delta h_{indent}$. For a G type electrode, α = 22,5°, or α = 15° (see table 4.2), $\Delta A_{indent} \approx 2\pi r_{electrode}\Delta h_{indent}$. The increase in contact area for a B type electrode is approximately twice the increase in contact area for a G type electrode. Although this gives an explanation for the shift of the weld growth curve for the B type electrodes, it does not sufficiently explain the lack of a shift of the weld growth curves for the G type electrodes (there should at least be some). The effect is therefore likely to be due to the finite element model's inability to cope with curved surfaces.

The amount of indentation is of course dependent on the material hardness (strength) and the electrode force. With increasing welding currents the material softens and the electrode starts to indent the sheets, leading to an increase of the contact area. This explains why, at

higher welding currents the shape of the welding curves is similar for both electrode types and all electrode tip diameters.

5.4.7 Electrode wear

The issue of the flatness (or roundness) of the electrode tip is connected to the phenomena of electrode wear. During welding, the temperature at the interface between the electrode and the sheet material increases, largely due to the surface contact resistance. The increase in temperature is limited, because the heat is conducted away through the electrode. The increase in heat is generally not enough to affect the copper of the electrode or the steel of the sheet sufficiently to soften the material and cause the material to deform (the sheet material generally does deform, but this is due to the softening of the material around the weld nugget).
If the steel sheet is coated the coating may be affected by the increase in heat. In the case of a zinc coating (melting temperature 419.5 °C) the zinc may diffuse into the copper of the electrode forming a brass alloy. Bronze is softer than copper and may cause the electrode tip to deform, effectively flattening the contact surface. Thus wear on the electrodes causes the area of the electrode tip to increase, which gives a reduction in current density and pressure leading to undersized nugget formation and bad weld quality [Zhang & Senkara 2006]. The point where weld dimensions and quality are not acceptable any more determines the electrode lifetime. Adequate electrode cooling is traditionally seen as the most effective factor to ensure optimum tip life [Davies, 1986], which has led to the development of special electrodes with increased cooling capacity [Scotchmer & Chan, 2006].
As Advanced High Strength steels are harder than more conventional forming steels, the effect of electrode wear can be more pronounced as flattening of the softened electrode tips occurs faster and the effect is more pronounced. This then affects the electrode life time, which is a key parameter affecting weldability. As the electrode tip wears it causes the welding range to shorten. To restore the welding range the electrode tip needs to be redressed. This adds costs because of extra work, because welding operations need to be stopped to allow the electrodes to be redressed, and because electrodes eventually need to be replaced.
The alloying of the electrode tip cannot be simulated using Sorpas or Sysweld, but the effect of alloying, effectively flattening the surface (the wear) can be simulated by increasing the electrode tip diameter and flattening the electrode tip.

Figure 4.27 shows the experimental results of welding a 1,25 mm TRIP700 GI with type B electrodes of 5 mm and 6 mm tip diameters. It can be seen that the effect of the increase of the electrode tip diameter is similar to the simulated results of figure 4.25. Figure 4.28 shows the experimental results of welding a 1,25 mm TRIP700 GI with a fresh type B electrode (*i.e.* an electrode that has not been used for previous welding operations) and welding with a used type B electrode. It can be seen that the welding curve changes substantially as the electrode wears due to previous welding operations. The welding curve shifts to higher welding currents and shortens, corresponding to an increase in surface contact area as simulated in figure 4.25.
Figure 4.29 shows the experimental results of welding a TRIP 800 with three different electrode tip diameters (5 mm, 6 mm & 8 mm), each with fresh and used electrodes. It can be seen that the welding current shifts to higher welding currents and the welding range shortens when the electrode tip diameter is increased, corresponding to the results of simulation in figure 4.25. Additionally it can be seen that the welding curve shifts to higher welding currents and the welding range shortens when electrode tips wear. This effect is less pronounced for smaller electrode tips, which can be explained by the fact that a similar level of wear, causing a similar flattening effect on smaller electrode diameters results in less increase in contact area, due to electrode contact area being round.

To compare simulated results of the impact of electrode geometry, use is made of normalized weld nugget diameters and weld nugget volumes. This is done because a large electrode diameter enables the formation of a larger weld without splashing. The use of normalized weld diameters allows for a better comparison in welding ranges. As a rule of thumb, splash welds can be expected when the weld nugget diameter exceeds the electrode diameter.
Simulation offers the possibility to evaluate the weld nugget volume, which is probably a better measure for the weld quality than the weld nugget diameter, as a weld can be made without any substantial volume, but with a sufficient diameter (e.g. if the cooling effect of the electrode is large), but such a weld can be expected to be limited in its load carrying capability.

Wear of the electrodes is accelerated by the alloying and consequent softening of the electrode tips, but the amount of deformation is dependent on the hardness of the steel sheet that functions as an anvil. Figure 4.31a gives the results of simulations of two different numerical definitions of TRIP 800 steel (as depicted in figure 4.30) welded with rounded and flattened G type electrode geometries (*i.e.* the surface of the electrode has been manually adjusted for simulations). It can be seen that the welding range shifts to higher welding currents for simulations using flattened electrodes.
Additionally it can be seen that the numerical representation of the material strength affects the shift of the welding range to higher welding currents. For rounded electrodes the effect is limited, as can be expected as the results of simulations using rounded electrode geometries are less affected by changes in contact area (compare figure 4.26 with figure 4.25), as has been discussed in § 6.2.1. The effect is more pronounced for the flattened electrode tips. The material that is softer at higher temperatures (material A) shows a welding range that has been shifted to higher welding currents compared to the material that is harder at higher temperatures (material B). This can be explained by the softer material being indented more at higher welding currents, leading to an increase in contact area (with a decrease in current density and an increase in cooling).
Figure 4.31b shows the results of the same simulation depicted in figure 4.31a, but now for the weld nugget volume. The first thing that can be noticed is that the “jump” in weld nugget diameter that appears in the results for lower welding currents disappears, as does the flattening off of the welding curves at higher welding currents, making it easier to compare the weld quality of different welding curves. It can be seen that the increase in weld volume is more gradual for rounded electrodes than for flattened electrodes, an effect that is less obvious when evaluating weld growth curves for electrode diameters.
Further simulations were done with material A, as the goal of these simulations was not so much to compare the materials, but to compare the effect of electrode geometry.

Figures 4.32a&b give the results of simulation using B type electrodes with rounded and flattened electrode tips. The results for flattened tips correspond to the results shown in figure 4.25. For rounded electrodes the weld growth curves do not shift to higher temperatures with increased electrode diameter, confirming the importance of the true contact area. It can also be seen that large electrode tip diameters lead to the formation of smaller normalised weld nugget diameters; though the actual weld nugget diameter may be larger, it is not compared to the diameter of the electrode tip. When comparing the normalised weld nugget volume (figure 4.32b) it can be seen that the slope of the weld growth curves is similar for the flattened electrodes, but the slope decreases as the electrode diameter is increased. This is primarily a scale effect; the amount of heat generated is similar but the relative increase in size is less for larger electrode diameters. Additionally larger electrodes do not heat up as much as smaller electrodes and can therefore function more effectively as heat sinks than smaller electrodes.
Figures 4.33a&b show the results of similar simulations as shown in figures 4.32a&b, but now for type G electrodes. It can be seen that the results for rounded electrodes correspond well with the results shown in figure 4.26. For flattened electrodes there is a shift in the weld

growth curve for the weld nugget diameter to higher welding currents with an increase in electrode tip diameter. Again it can be seen that the effect is less pronounced than it is for B type electrodes (see figure 4.32a), and it can be concluded that the overall geometry of the electrode (*i.e.* a B or a G type electrode) affects the weld growth curve (for weld nugget diameter).
For the normalised weld nugget volume the effect is much more pronounced. In fact the results are quite similar to the results obtained for the B type electrodes (see figure 4.32b). Although the weld nugget diameter is an effective parameter to judge weld quality experimentally, because it is easy to measure and can be reproduced on the shop floor by simple chisel testing, it may not be the most efficient parameter to judge the effectiveness of the welding process. It is an important parameter if weld the weld nugget diameter is a determining parameter in judging the mechanical performance of a weld, but welds with sufficient diameter can be formed, whilst the weld volume is still small, because the quality of the weld, when measured in volume is not the same for similar weld nugget diameters. This is mostly of importance when evaluating small welds. The amount of material that needs to be melted (and therefore the amount of heat that needs to generated) to form a sufficiently large weld is dependent on the type of electrode.
This is made clear in figures 4.34a&b in which it can be seen that the results of simulated weld growth curves for weld nugget diameters vary between flattened B and G type electrodes, but not for rounded B and G type electrodes. From this it can concluded that the effect of electrode wear, as in the flattening of the electrode tip, varies between different electrode types, though there may be little difference when fresh electrodes are used. If the weld nugget volume is evaluated figure 4.34b shows that there is little, if any difference between B and G type electrodes; rounded or flattened.

Figure 6.1 shows the connections between different parameters playing a role in the life time of an electrode. Material properties that are temperature dependent have been assigned with (T), so that the figure is not obscured by relations between the heat generation, $Q=I^2Rt$, and these different properties, leaving only the connection between heat generation and electrode temperature. Still it can be seen that electrode lifetime, addressed in figure 6.1 by the factor “change electrode tip surface area”, is a complex process. In the figure it is assumed that the material of the steel sheet is harder than the electrode material (a reasonable assumption when discussing resistance spot welding of advanced high strengths steels).

Assuming that material properties are set for a certain application (*e.g.* GI or GA coating, resistivity and conductivity of the steel sheet), it can be concluded from figure 6.1, that the process parameters that can be most conveniently adapted to increase electrode life time are electrode geometry and welding time, so as to limit the increase in temperature in the electrode. As diffusion is both temperature and time controlled, the welding time seems to be the most effective process parameter to increase electrode life time. Because welding time is an important parameter in manufacturing (increasing welding times leads to a decrease in production rates), from a manufacturing point of view, choosing an optimal electrode geometry is the primary process parameter to adjust. Decreasing the electrode pressure may also be an effective parameter to increase electrode lifetime, but adjusting this process parameter may be limited by the need to make contact between sheets to ensure the formation of a welded joint.

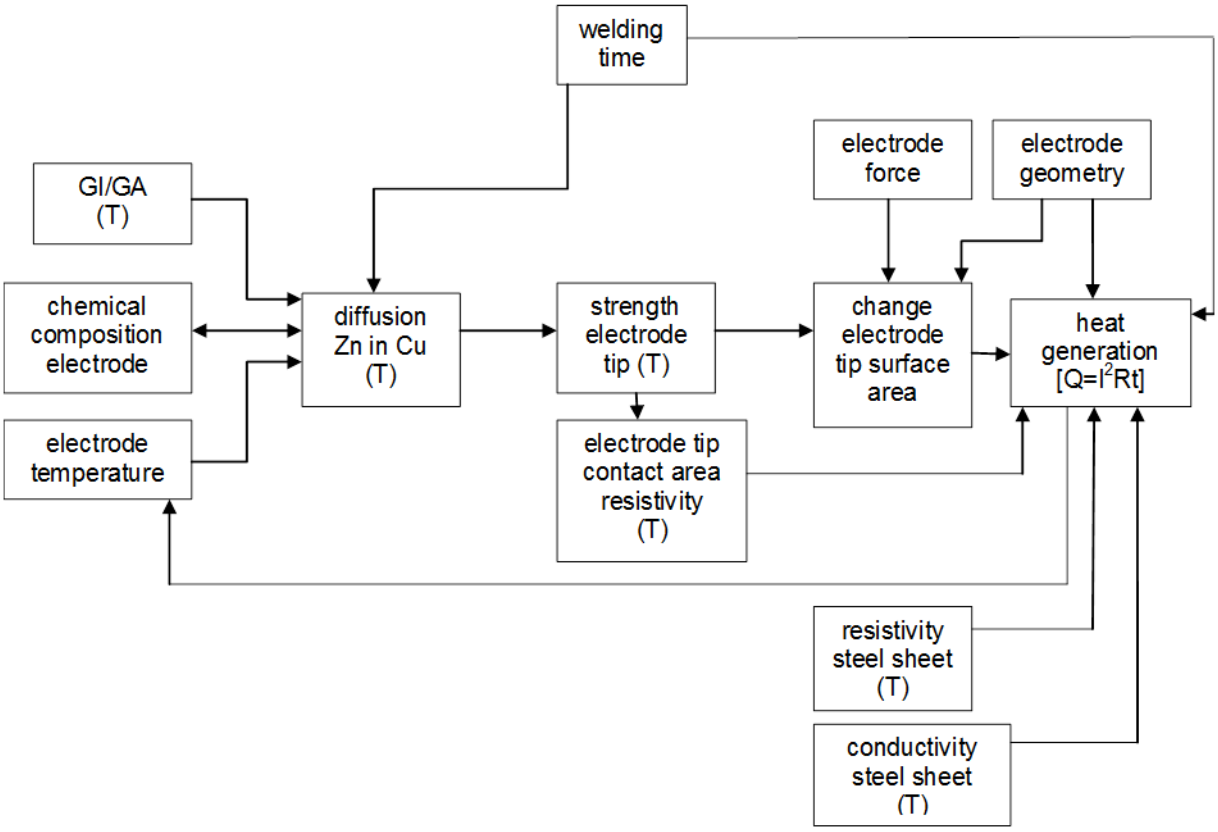

Figure 6.1: Schematic depiction of the relation between different parameters affecting electrode lifetime. Material properties that are temperature dependent have been denoted with (T).

It can be concluded that:

- The effect of electrode wear resulting in flattening of the electrode tips causes the weld growth curves for weld nugget diameters to shift to higher welding currents.
- The effect of flattening of the electrode tips on the weld growth curves for weld nugget diameters differs between electrode types.
- There is no effect of flattening of the electrode tips on the weld growth curve for weld nugget volume between B and G type electrodes.
- The weld nugget diameter may not be the only parameter suitable to evaluate weld quality.
- The numerical definition of the material strength at higher temperatures influences the results of simulation when evaluating the effect of wear on the weld quality.
- Larger electrode tip diameters may lead to larger weld nugget diameters in absolute terms but comparatively smaller weld nugget diameters in relative terms.
- The most effective process parameters to adjust to increase electrode lifetime are electrode geometry, weld time, and electrode force, although adjusting the latter two may be limited by other manufacturing considerations.

5.4.8 Weld nugget formation

The results discussed in the previous section indicate that there is a difference in the formation of the weld nugget between electrode types. Figures 4.35 and 4.36 show the simulated weld nugget cross sections for welding 1,65 mm TRIP 700 with B (figure 4.35) and G type (figure 4.36) electrodes, for varying electrode tip diameters, all other parameters kept constant. It is important to note that the weld parameters were chosen so that a good weld was produced for the intermediate 6 mm weld diameter. This explains the oversized weld

nuggets produced with the 5 mm electrode diameter. It can be seen that the effects of simulation for the smaller electrodes are similar for both the B and G types. The main difference is between the 8 mm electrode B and G types. Although the weld nugget diameter is sufficiently large for the B type electrode, the weld nugget volume is definitely undersized; conversely it is sufficient for the G type electrode.
This result seems to contradict the results discussed in the previous section. However these simulations have been performed using the electrode definition as provided by the software and therefore are more in line with the results shown in figures 4.25 and 4.26, whereas the electrode definitions in the previous sections were adjusted to compare flattened with rounded electrode tips.
The results show the effects of the more flattened geometry of the B type electrodes compared to the more rounded geometry of the G type electrodes. The 8 mm B type electrode causes decreased current density and increased cooling, leading to an undersized weld nugget, though the weld nugget diameter is sufficiently large.

It can be concluded that the weld nugget diameter can be a misleading quality indicator of a weld, and certainly in simulation, the weld nugget volume may actually be preferred to evaluate the effect of welding operations. Additionally it shows that the definition of the electrode surface (flat or rounded) significantly influences the results of simulations.

5.4.9 Electrode dimensions and sheet thickness

The normalised results of simulation do not take into account the effect of sheet thickness on the results of simulation. Thicker sheets are usually welded using larger electrode diameters. Figure 4.37 shows the weld current needed in simulation to produce a $5\sqrt{t_s}$ weld nugget diameter (see figure 4.38) for different electrode tips with increasing sheet thickness. The weld current, according to standards, is roughly independent of the electrode diameter for different sheet thickness. Although the weld nugget diameter is the same, figure 4.39 and figure 4.40 show that the weld quality expressed in height of the weld and volume of the weld varies. Smaller electrodes lead to bigger welds in similar thickness sheets, even though they are produced using the same welding current and the welds have similar nugget diameters. Figure 4.41 shows that a smaller electrode tip diameter leads to a larger weld volume at lower welding currents. Again this can be attributed to the current density and the cooling capacity.
The results show that it is advantageous, both for the quality of the weld and for the energy needed to form the weld to use as small an electrode as is possible to form a sufficiently large weld. The limiting factor is that a smaller electrode may give rise to splash welding.

5.5 Performance

Modern automotive design and engineering is heavily based on finite element modelling [Maotao et al., 2011], which is one of the reasons to investigate the impact of material properties on the results of simulations, as presented in section 6.1.
For crash simulations predictable failure behaviour (strength and failure mode) is important to enable assessment of the performance of resistance spot welded joints [Kumagai et al., 2007, Wood et al., 2009, Wolf et al., 2009 & Ueda et al., 2010]. Therefore it is desirable to link the failure behaviour of resistance spot welded joints to known material characteristics of advanced high strength steel sheet (*e.g.* chemical composition, sheet thickness or strength).
The performance of welds in this thesis is discussed in two aspects: the post weld hardness and the failure mode of welds. As reported in section 2.4.6 these could be related, as increased post weld hardness may lead to undesirable failure modes because hard welds tend to fail in a brittle manner. Therefore first the relationship between welding operations

and post weld hardness was investigated and next possible measures to improve weld failure were examined.

5.5.1 Post weld hardness

As explained in section 5.2.1 the post weld hardness of a joint is dependent on the chemical composition of the sheets that are joined and the cooling rate. This relationship can be shown in continuous cooling transformation (CCT) diagrams. Figure 5.1a shows the CCT diagram for a DP600 steel, figure 5.1b shows the corresponding hardness of the material. it can be seen that for high cooling rates (>100°C/s) the hardness exceeds 300 HV.
Figure 5.2 shows a wide variety in post weld hardnesses for various welding processes. Especially in plasma arc welding (PAW), post weld hardness not exceeding 300 HV can occur in material with carbon contents up to 0,2 wt%. The difference between PAW and resistance spot welding (RSW) is the cooling mechanism. In RSW heat is conducted from the weld to the watercooled electrodes. This mechanism of forced cooling leads to increased cooling rates that in turn lead to increased post weld hardness. Figures 5.3 and 5.4 show that the post weld hardness for resistance spot welded joints exceeds 300 HV for chemical compositions of steels with carbon contents exceeding 0,05 wt%.
After the electrodes are released cooling for all welding process can only occur via conduction of heat to the surrounding material, convection to the surrounding atmosphere, and radiation. According to the Stefan-Boltzmann law, heat loss through radiation is strongly dependent on temperature, varying with T^4. Therefore heat loss through radiation is limited when the material has been cooled before the electrodes are released. Heat loss through convection is dependent on the flow of the atmosphere (usually air) over the material. Unless a forced flow is present, this contribution is limited as well. Most of the heat loss will occur by conduction to the surrounding material. This mechanism is dependent on the temperature gradient in the material, and therefore will be affected by the build-up of heat in the material during welding.
Figure 5.16 shows the simulated thermal profile during resistance spot welding of 1,2 mm thick DC04 steel for various welding currents. It can be seen that the influence of heat generated during welding affects the temperature levels in the weld, but in all cases the cooling rates are high (>100°C/s). DC04 steels are mild steels with carbon contents not exceeding 0,08 wt%. Table 5.2 shows that advanced high strength steels (AHSS) have carbon contents similar to or exceeding that of D04 steels. It can therefore be concluded that post weld hardness of AHSS will always be high, exceeding 300 HV (see also figure 5.20).
Figure 5.18 shows the simulated formation of martensite during cooling of resistance spot welded DC04. Figure 5.19 shows the distribution of martensite in the weld after resistance spot welding. As carbon is the main element determining the formation of martensite in carbon steels, it can be concluded that the post weld microstructure of resistance spot welded AHSS will be predominantly martensitic. It is this martensitic microstructure that leads to the high post weld hardness of resistance spot welded joints in advanced high strength steels.

Carbon is the principal element, but not the only element determining post weld hardness; other elements also play a role. This is usually expressed in carbon equivalence (CE) numbers. Carbon equivalence numbers relate the chemical composition of a material to its hardenability. The hardenability of a material is not necessarily the same as the post weld hardness of a material, as the post weld hardness is also dependent on the cooling rate. Carbon equivalence numbers are however empirically derived and the standard CE numbers (Eq. 5.1 & 5.2) are derived primarily for arc welding processes. The cooling rate is of course also dependent on the thickness of the materials that are to welded, as these relate to the amount of heat generated in the material and the cooling capacity of the surrounding material.

If conditions are made more specific, limiting range of material thickness and welding process, dedicated CE numbers can be derived. For industrial applications both material thickness and welding process are set parameters, and the use of such dedicated CE numbers can be used to evaluate weldability of various materials, specifically their chemical composition, as design conditions limit choices in materials properties such as sheet thickness and tensile strength, and manufacturing options limits choices in welding processes.
Equations 5.2 to 5.6 give the relations between materials of similar thickness and varying chemical composition for different welding processes. It can be seen from the equations that the chemical composition as such plays a decreasing role in determining the post weld hardness when the cooling rate that is innate in the welding process (*i.e*. lowest for plasma arc welding and highest for resistance spot welding with elongated cooling time), as can be derived from the offset parameter in the equations (52 HV for PAW and 229 HV for RSW with forced cooling). This can be attributed to the fact that resistance spot welding will lead to the formation of martensitic structures, as discussed above.
Additionally it can be seen that the relative influence of the carbon content of the materials increases with increased cooling rates. This also corresponds well to the predominantly martensitic microstructure as a result of resistance spot welding.

Combining the influence of cooling rate and chemical composition a general equation for the post weld hardness of welding processes that lead to martenistic welds (such as resistance spot welding) was derived (Eq. 5.12). Using measured data for a range materials used in industry the equation could be simplified to an equation relating post weld hardness to the carbon, manganese and silicon levels of the advanced high strength steels (Eq. 5.15). This simplified equation is based on the assumption that welds are made in steel sheets of a limited range of thickness (which will also limit the range of cooling rates) and that the chemical composition of advanced high strength steels will vary within a limited range, with always a relatively high carbon content. Predictions of post weld hardness using equation 5.15 have been plotted against measured post weld hardness in figure 5.22. It can be seen that the predicted values correlate well with measured values, although there is some spread. As a first estimate of the post weld hardness equation 5.15 can be used to enable welding engineers to make an estimated guess of the impact of changing materials on the post weld hardness, which is an important parameter in many industrial standards.
Equation 5.15 was presented at the *3rd International Conference on Mathematical Modelling and Information Technologies in Welding and Related Processes* in Kiev, Ukraine in 2006 [Den Uijl, 2006b]. Equation 5.12 was presented at the *Sorpas User Group Meeting* in Wels, Austria in 2006 [Den Uijl, 2006c]. It was subsequently incorporated into the Sorpas software.

5.5.2 Weld failure mode

The formation of hard martensitic joints in advanced high strength steels after resistance spot welding was identified by several authors as the possible cause for undesired failure modes (see section 2.4.6). However figures 5.24 show that full plug failure can be achieved in advanced high strength steels with hard martensitic welds. Figure 5.25 shows that full plug failure can consistently be achieved. If the hard martenistic microstructure resulting from resistance spot welding of advanced high strength steels is the primary cause of undesired weld failure modes, this should not be the case.
Furthermore if the high hardness of the martensitic microstructure is the cause of undesirable weld failure modes, such as shown in figure 5.26, then a post weld heat treatment, leading to tempering of the weld should result in at least some improvement of the weld failure mode. However, figure 5.27 shows that this is also not the case. The cause of undesirable weld

failure modes can therefore not be exclusively related to the hard martensitic microstructure of the welds.

It is true that non-tempered martensite, such as is formed after resistance spot welding of advanced high strength steels has limited formability and fails in a brittle manner. The weld nugget is however not the only material that transforms into martensite after cooling. Materials in the heat affected zone, adjacent to the weld nugget has also been heated above the austenite transformation temperature. This material has transformed to austenite during welding, and during cooling it has experienced very high cooling rates. The cooling rates may have been lower than that experienced in the weld nugget, but still it has been cooled sufficiently fast for the material to form a hard martensitic microstructure. The resultant weld is therefore made up of a hard martensitic weld nugget where the sheets are fused together, and a region next to the joint where the sheets have not been joined, but the material is hard and martensitic. This can be seen in the micrograph of figure 5.12 and simulated in figure 5.19.
There is a second region in the heat affected zone of the weld adjacent to the section that has not been molten, but did transform into martensite, and that is the region where the material did not transform into austenite (and therefore not into martensite upon cooling), but where the material has been influenced by heating. Here the original microstructure has been tempered, and this region will therefore be softer than both the martensitic region and the unaffected base metal.

Upon loading during tensile testing the martensitic region of the HAZ will show limited deformation. As the sheets are pulled apart the result will be similar to a crack addressing the edge of the weld nugget. Because this crack will not open up much, due to the martensitic HAZ, the weld nugget will experience a crack tip opening with a very small diameter. This will result in high stress concentrations at the edge of the weld nugget.
Figure 6.2 gives a schematic representation of a resistance spot welded joint in a tensile test piece. The region of the heat affected zone that has been transformed into austenite during welding has been marked as HAZ1, the region of the heat affected zone that has not transformed into austenite during welding as HAZ2. Figure 6.3 shows the deformation of the test piece in tensile testing, similar to figure 2.10, if the material in HAZ2 has not transformed into hard martensite, for instance in the case of very low carbon steels (*e.g.* interstitial free steels). This region will have experience grain refinement upon cooling, which will cause some strengthening of the material. It can be seen that because HAZ1 is capable of deforming that the crack tip opening at the weld nugget edge will be large and therefore the stress concentrations will be limited. Figure 6.4 shows the same situation in a joint made in advanced high strength steels. Now HAZ1 consists of hard martensite, which will not deform. Deformation then occurs in HAZ2, and it can be seen that the crack tip opening is very limited, leading to large stress concentrations at the weld nugget edge.

If the material in the weld nugget is coherent, *i.e.* the grain boundaries are sufficiently strong, then this will have limited effect as the weld will fail in the softer material surrounding the hard martensitic material and will either fail in that part of the HAZ that has not transformed but been tempered during welding, HAZ2, or in the unaffected base material, both leading to full plug failure. If the material in the weld nugget is not coherent, *e.g.* due to weak grain boundaries, then the crack will propagate into the weld nugget and partial plug failure or even interface failure will occur.

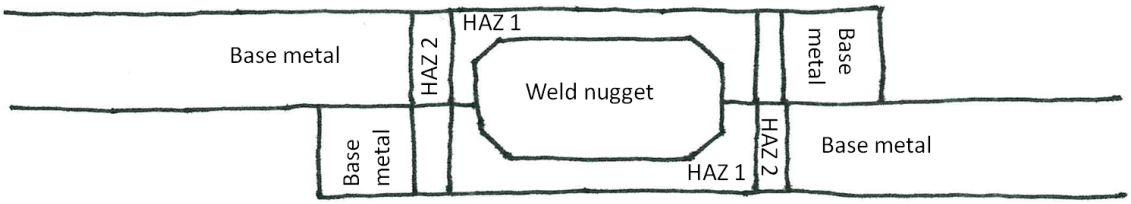

Figure 6.2: Schematic representation of a tensile test piece with a resistance spot welded joint. Indicated are the weld nugget, the region of the heat affected zone that has transformed into austenite during welding, HAZ1, and the region of the heat affected zone that has not transformed into austenite, HAZ2.

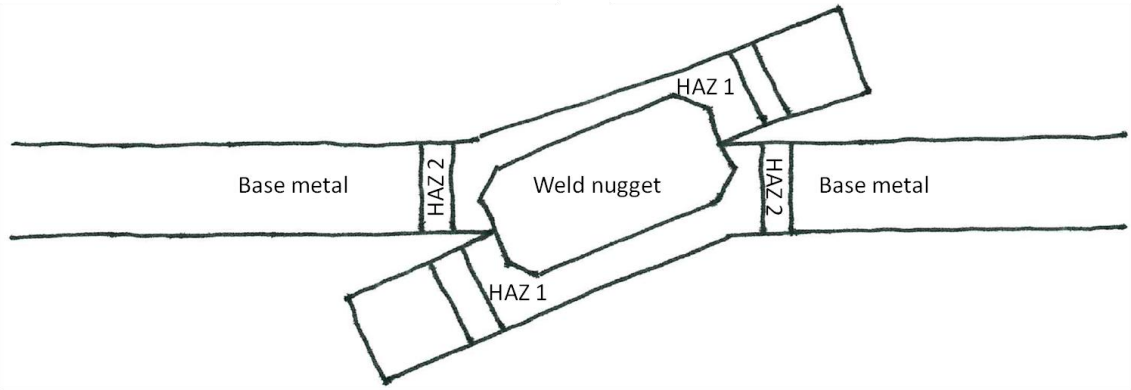

Figure 6.3: Schematic representation of a test piece with a resistance spot welded joint in material of low carbon content during tensile testing. Indicated are the weld nugget, the region of the heat affected zone that has transformed into austenite during welding, HAZ1, and the region of the heat affected zone that has not transformed into austenite, HAZ2.

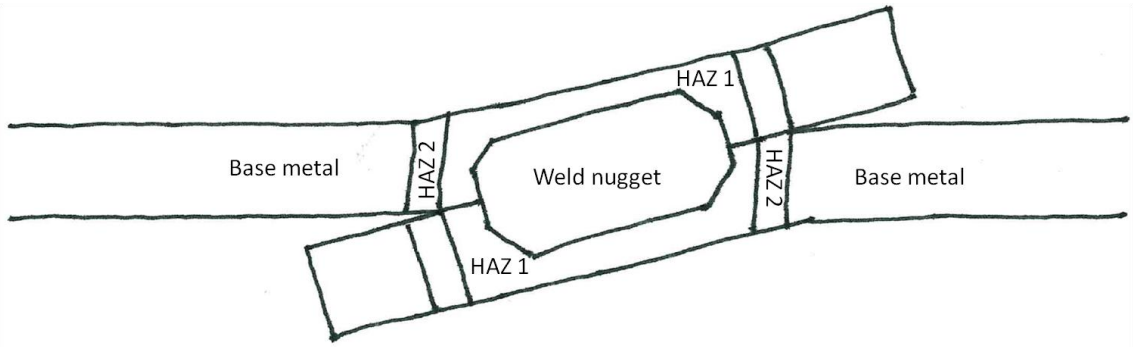

Figure 6.4: Schematic representation of a tensile test piece with a resistance spot welded joint in advanced high strength steels. Indicated are the weld nugget, the region of the heat affected zone that has transformed into austenite during welding and into martensite during cooling, HAZ1, and the region of the heat affected zone that has not transformed into austenite but has been tempered, HAZ2.

One element associated with weak grain boundaries is phosphorus. Phosphorus is a common alloying element in some TRIP steels (see section 2.1). It is these phosphorus containing materials in which undesirable weld failures are observed. After welding phosphorus segregates on the grain boundaries (see figure 5.29), and it is these phosphorus rich grain boundaries that cannot sustain the increased stresses that occur due to the limited opening of the sheets. The crack tip opening at the edge of the weld initiates a crack between grains, that propagates along the grain boundaries into the weld. The cracks can penetrate deep into the weld, because the microstructure of the welds consists of long grains that have been formed upon solidification.

Figure 6.5 gives a schematic representation of a cross section of the resistance spot welded joint. The heat affected zone has been detailed further in figures 6.2 to 6.4. The weld consists of a weld nugget which will be fully martensitic. Next to the weld nugget is the zone

of material that has been heated above the A3 temperature but has not been molten, HAZ1. This material will transform into a fully martenistic structure upon cooling. Next to HAZ1 is a region that has been heated above the A1 temperature, but not above A3, HAZ2. This material will only partially been transformed into austenite, and the resultant microstructure after cooling will consist of martensite and tempered base material (ferrite and bainite, in the case of TRIP steels). Next to HAZ2 is a region that has not been heated above A1, so no phase transformation will occur, but the base metal (ferrite and bainite in TRIP steels) will have been affected by the heat and the material will have softened due to tempering effects.
Table 6.1 gives an overview of the weld zones, the corresponding maximum temperatures reached during welding and the microstructural composition of the weld zone for welds made with a single weld pulse.

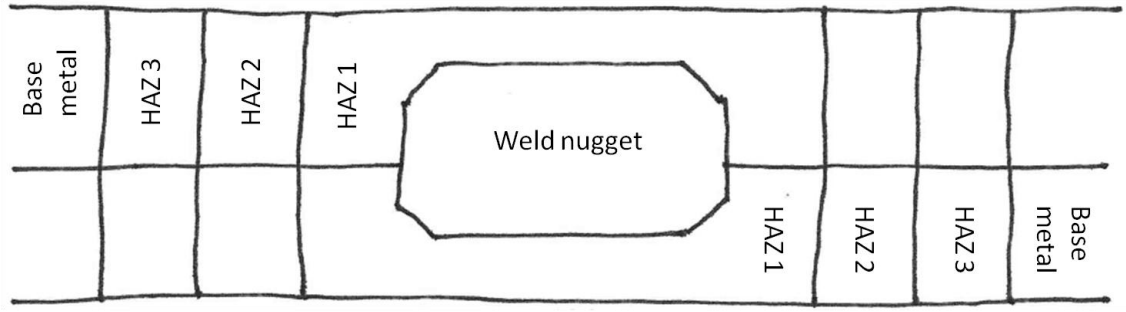

Figure 6.5: Schematic representation of a cross section of a resistance spot welded joint. Indicated are the weld nugget, the region of the heat affected zone that has been heated above A3 (HAZ1), the region of the heat affected zone that has been heated above A1 but not above A3 (HAZ2), and the region of the heat affected zone that has not been heated above A1 (HAZ3).

Table 6.1: Weld zones, corresponding maximum temperature, and microstructural composition after a single weld pulse (see figure 6.5).

Weld zone	**T_{max}**	**Microstructure**
weld nugget	$T_{max} > T_{melt}$	fully martensitic
HAZ1	$A3 < T_{max} < T_{melt}$	fully martensitic
HAZ2	$A1 < T_{max} < A3$	tempered base metal & martensite
HAZ3	$T_{max} < A1$	tempered base metal
base metal	$T_{max} < A1$	base metal

The first step to be taken to improve weld failure behaviour is to break up the elongated grains with their weak grain boundaries. This will limit the effect of the penetration of the crack formed at the edge of the weld. This is done in a first post weld heat treatment step in which the edge of weld nugget is remelted. This step will result in a finer microstructure at the edge of the weld (see figure 5.32).
The post weld heat treatment step will also affect the heat affected zone. Figure 6.6 gives a schematic representation of a cross section after the re-melt post weld heat treatment step. The weld consists of a weld nugget which will be fully martensitic. Next to the weld nugget is the zone of material that has been heated above the A3 temperature but has not been molten, HAZ1. This material will upon cooling transform into a fully martenistic structure. Next to HAZ1 is a region of material that has been heated above A1 but not A3, HAZ2a. This region consists of material that has been transformed into austenite and formed martensite upon cooling. Additionally there is material that has not transformed into austenite, but has been tempered. This material consists of martensite that was originally formed during the welding step, and has now been tempered, and material that did not transform to austenite during welding and has not been transformed into austenite during the post weld re-melt step. This material consists of base material (ferrite and bainite in the case of TRIP steel) and has now been twice tempered. Next to HAZ2a is a region that was not heated above A1 during welding, but has been heated above A1 during the post weld re-melt step but not above A3,

HAZ2b. This material has been partially transformed into austenite and after cooling into martensite. The rest of the material has been tempered during welding and did not transform into austenite during the post weld re-melt step, but has been tempered again. Next to HAZ2b is region of material, HAZ3a, that has been tempered during welding and has been tempered again during the post weld re-melt step. Next to HAZ3a, there is a region that was not affected by welding, HAZ3b, but has been tempered during the post weld re-melt step.
Table 6.2 gives an overview of the weld zones, the corresponding maximum temperatures reached during welding, and the microstructural composition of the weld zone for welds made with a remelt step.

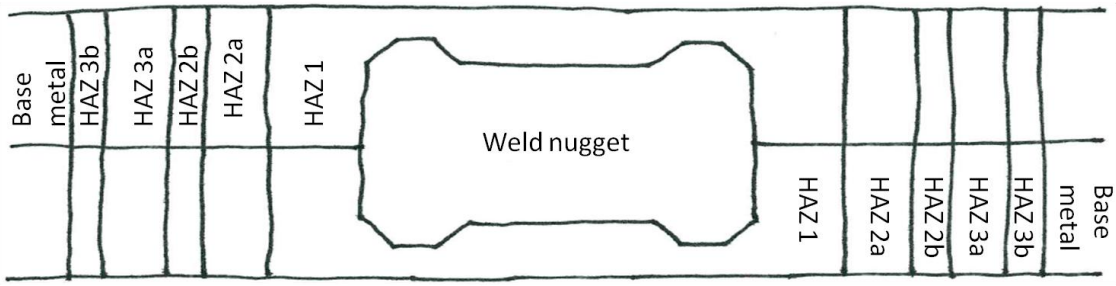

Figure 6.6: Schematic representation of a cross section of a resistance spot welded joint after the post weld re-melt step.

Table 6.2: Weld zones, corresponding maximum temperature, and microstructural composition after the remelt step (see figure 6.6)

Weld zone	**Tmax**	**Microstructure**
weld nugget	$T_{max} > T_{melt}$	fully martensitic
HAZ1	$A3 < T_{max} < T_{melt}$	fully martensitic
HAZ2a	$A1 < T_{max} < A3$	tempered base metal & martensite
HAZ2b	$A1 < T_{max} < A3$	tempered base metal, tempered martensite & martensite
HAZ3a	$T_{max} < A1$	tempered base metal
HAZ3b	$T_{max} < A1$	tempered base metal
base metal	$T_{max} < A1$	original

After the post weld re-melt step, weld failure modes in phosphorus containing TRIP steels improved, but not sufficiently. This can be explained by the fact that the post weld re-melt step broke up the easy crack propagation paths in the weld nugget, but did not address the problem of the high stress concentrations at the weld nugget edge during tensile testing. Due to the hard martensitic structure of HAZ1 the weld nugget is still affected by a narrow crack tip opening (see figure 6.4).
Using a post weld heat treatment step that caused none of the material to exceed A1, and therefore did not lead to the formation of fresh hard martensite (see figure 5.34), all of the material, and especially HAZ1, was tempered. This allows the material in HAZ1 to deform during tensile testing, widening the crack tip opening, leading to a lowering of the stress concentrations. If the material has been tempered sufficiently for the stresses at the weld nugget not to exceed the levels required to cause the grain boundaries in the weld nugget to lose coherency, whilst causing the tempered material surrounding the weld to fail, full plug failure is achieved (see figures 5.36 and 5.37). This mechanism is aided by the fact that part of the heat affected zone surrounding the weld nugget has been tempered multiple times and therefore has softened considerably.

The three step welding process has been patented: EP 2 097 207 B1 "*Method for Spot Welding, and Spot Welded Sheet Material*". The three step process adds to the process time of welding phosphorus containing TRIP steels, which is generally considered undesirable. Especially the need to cool the weld down until the martensitic transformation is complete,

necessary to allow the tempering step to be effective, adds considerable time. Simulation can help to limit the total process time, by carefully designing the welding process (see figure 5.34). Additionally it should be kept in mind that not all welds need to be welded using a three step welding process. Only those welds that need to perform in safety critical applications need to be welded using such a procedure to ensure good performance. The number of these welds, made in phosphorus containing TRIP steels in a vehicle will be limited and by carefully engineering the welding operations (again using simulations) the extra time required for the three step welding process need not increase overall production times.

6. Conclusions & Recommendations

6.1 Conclusions

In this thesis the resistance spot weldability of advanced high strength steels has been investigated. This involved an experimental approach as well as the use of dedicated weld modelling software. The research is focussed on the application of advanced high strength steel in an automotive context. Therefore use is made of materials that are used in industry, weld parameter settings according to industrial standards, and commercially available weld software.
Challenges in resistance spot welding of advanced high strength steels were reported concerning both the manufacturability and the performance of joints. According to literature issues concerning the manufacturability of resistance spot welding of advanced high strength steels are connected to the increased strength levels, making it harder to compress steel sheets and form joints. The issues concerning the performance of resistance spot welded joints in advanced high strength steels are reported to be connected with increased alloying levels, leading to the formation of hard and brittle joints that show undesirable failure modes.
The availability of dedicated resistance spot welding software for simulation is a relatively new development and therefore accurate material data for simulations are scarce. Being a relatively new research tool, methods of applying dedicated weld simulation software for research, outside direct engineering purposes to determine weld process parameters, need to be explored.

From the work reported in this thesis conclusions can be drawn on four different aspects relating to resistance spot welding of advanced high strength steels in automotive engineering. These aspects are

- The failure mode of resistance spot welded joints in advanced high strength steels.
- The post weld hardness of resistance spot welded joints.
- The use of simulation software to support engineering and research.
- The relationship between the geometry of electrodes used for resistance spot welding and weldability.

Concerning the failure mode

- Undesirable weld failure modes do not improve after post weld heat treatment for the advanced high strength steels investigated in this thesis. As post weld heat treatment should lead to some softening of the weld nugget it can be concluded that increased hardness is not the primary cause of undesirable weld failure.
- A mechanism is proposed that explains how a weld nugget is addressed by concentrated stresses upon loading. If the weld nugget is coherent, *i.e.* if the grain boundaries in the weld nugget are sufficiently strong, the weld will not show undesirable failure modes. If the weld nugget is not coherent, failure will occur along the relatively weak grain boundaries leading to undesirable weld failure modes.
- A novel mechanism was proposed to break up the microstructure of the weld nugget that is addressed by stress concentrations by a three step welding procedure. This procedure leads to full plug failure, showing that indeed the microstructure of the weld nugget, leading to incoherent welds, is to blame for undesirable failure modes in some materials (particularly phosphorus containing TRIP steels).

Concerning the post weld hardness

- Although increased post weld hardness will limit the deformability of a resistance spot welded joint, it cannot be blamed solely for undesirable failure modes, as it is possible to form hard welds that show good failure modes.
- An equation was derived and validated to link the post weld hardness of a joint to the chemical composition of the material, expressed in a carbon equivalence number, and the cooling rates during welding. A further simplified equation to make a first estimate on the post weld hardness of resistance spot welded advanced high strength steels was derived, and validated. This equation requires a very basic chemical composition (carbon, manganese and silicon) as input. The equation is only suited for a first estimate as simulations and experimental verification are needed to assess post weld hardness precisely.

Concerning the electrode geometry

- Variations of the electrode tip geometry are a primary factor affecting the results of simulations.
- The electrode geometry is an important parameter in determining the weld nugget geometry, especially in combination with the sheet thickness. Similar welding operations will lead to similar weld nugget volumes, but the diameter may vary. The weld nugget geometry and more specifically the weld nugget diameter, is an important factor determining the performance of the welded joint.
- Flattening of the electrode tip causes decreased electrode lifetime. The electrode tip geometry is an important factor in limiting a decrease in electrode lifetime.

Concerning the use of simulation software

- Sufficiently large welding ranges can be obtained with materials of increased strength levels.
- The surface quality, expressed in a surface contaminant factor, plays a major role in determining the weldability of advanced high strength steels. A mathematical model, describing the growth of the weld nugget size depending on the various material characteristics, shows the dominant role of the surface quality on the weld nugget size.
- The surface contact resistance should not be varied, unless there are sound physical reason to do so.
- Changing the thermal conductivity and electrical resistivity affects the results of simulation, by shifting the weld growth curve.
- Dedicated resistance spot weld simulation software is suited to simulate weld process parameters in a manufacturing context and can be used as a tool for research of weldability of advanced high strength steels.
- Simulation software comes with a material database. As the material data provided in the databases is not sufficient to simulate the wide variations in material characteristics, due to chemical composition and thermomechanical history of advanced high strength steels used for industrial applications the material data should be validated.
- Material databases can be expanded to represent materials that are not available in the databases. Because experimental determination of material data involves high costs and material, it is desirable to develop a method to compile material data sets that is limited in costs and material (especially as material may be limited in supply in the early stages of development). Simulations of weld growth curves using appropriate data sets, and validation of the results against experimentally derived weld growth curves is a good method to validate material data for simulations.
- A strategy to compile material data sets based on available material data, should focus first on the material strength (which is usually available) and the melting temperature

(which can be calculated). Small variations in chemical and microstructural composition will lead to a decrease in thermal conductivity and an increase in electrical resistivity, in simulation this can be represented in simulation by varying the material data accordingly.

The work reported in this thesis adds to the body of knowledge on resistance spot welding of advanced high strength steels and the use of dedicated weld software for that purpose and includes:

- A validated method to compile material data sets based on available material data sets.
- A mathematical description of the weld nugget growth.
- A validated equation linking the post weld hardness of a joint to the chemical composition of the material, expressed in a carbon equivalence number, and the cooling rates during welding. Using this equation Sorpas simulations can be used to predict post weld hardness, adding some metallurgical simulation capability to the software. The equation has been incorporated in the software.
- Proof that post weld hardness is not the primary cause of undesirable weld failure modes in resistance spot welded advanced high strength steels.
- A mechanism that explains how a weld nugget is addressed by concentrated stresses upon loading, and how undesirable weld failure modes can be attributed to incoherent welds.
- The three step welding procedure to achieve full plug failure in resistance spot welded advanced high strength steels. This method has been patented (inventors N.J. den Uijl and S.M. Smith).

6.2 Recommendations

- Accurate material data is crucial for weld simulations. The method for compiling material data derived in this thesis requires validated material data for similar materials. It is therefore desirable to have more validated material data available for weld models. A coordinated effort to measure validated material data sets, preferably according to international standards, would be beneficial for the application of weld modelling in research and industry.
- Validation of resistance spot welding models requires experimental data. It is therefore desirable to have extensive case studies of resistance spot welded materials available in literature. A coordinated effort to compile and publish case studies, preferably according to international standards, would be beneficial for the application of weld modelling in research and industry.
- The influence of electrode geometry on resistance spot weldability should be investigated in more depth, using more physically representative models than the commercially available dedicated software used in this thesis, focussing on the flow of electrical current and heat, the deformation of the electrode tip and the material in contact with the electrode, and a metallurgical model to investigate the influence of alloying on the electrode surface. This may lead to the development of more efficient electrode geometries to improve process stability.
- Additionally a more rigorous investigation on the influence of electrode geometry on resistance spot weldability could be used to develop dedicated weld models for simulations to determine the electrode lifetime.
- The development of dedicated models of standardised tests to assess the performance of resistance spot welded joints (such as cross tensile tests and crash test), that can be linked to resistance spot welding models would be beneficial for design, engineering (in manufacturing) and research.
- The mathematical equation for the growth of the weld nugget should be developed using numerical computing software, such as MATLAB, to develop simple equations that can be used to assess the response of materials to variations in welding operations, and *vice versa*.
- Combining finite element software to simulate weld modelling with metallurgical modelling software, thus joining macroscopic phenomena with microscopic phenomena, should give more insight into the factors determining the coherency of weld nuggets. Tools developed using this strategy are especially valuable in the early stages of material development.

Summary

The introduction of advanced high strengths steels enabled automotive manufacturers to simultaneously reduce weight and increase safety of vehicles. However issues were reported concerning the weldability of these steels. These issues concerned both the manufacturability as well as the performance of resistance spot welded joints. The manufacturability addresses the ability to produce joints in an industrial set up, especially the welding range and the electrode lifetime. The performance includes the post weld hardness and the failure mode of resistance spot welded joints.

Method of Research

Both aspects are addressed in this thesis using experimental data and software to model and simulate welding processes. Experimentally, use was made of weld growth curves and tensile tests. The software used was SYSWELD and Sorpas. SYSWELD is a software tool that is suited to performing simulations focussed on the metallurgical aspects of welding, Sorpas is more suited to evaluate industrial processes.
Weldability is an engineering issue; without applications there are no problems with weldability. It is the application that determines which characteristics of the materials, process, and welded joints are important. In automotive engineering these aspects of weldability are laid down in industrial standards, which specify minimum requirements to ensure manufacturability and performance of welded joints. Because of this most of the materials used in this thesis are materials that are industrially applied, and the process parameters used are primarily derived from standards. For the same reason use is made of commercially available software.
To be able to use the simulations with effect, it was first necessary to investigate the use of simulations for research. Literature reports on the use of dedicated weld modelling software for engineering purposes in manufacturing, such as determining weld process settings, but not in the use of these platforms for research. One specific point is the availability of material data. Both SYSWELD and Sorpas come with a material database, but the generic material properties available in these databases do not necessarily correspond to the materials used in this thesis. Work in this thesis therefore first focuses on the use of simulation software, the influence of material characteristics on weldability, and the compilation of validated material data sets.
Next the influence of process parameters on welding of advanced high strengths steels was investgated. Specific attention is paid to the influence of the electrode geometry, as it relates to the electrode lifetime.
Literature reports that the weldability of materials is closely linked to the post weld hardness of the welded joints. Therefore the investigation on weldability first focuses on post weld hardness, and how to predict the post weld hardness based on material characteristics that can be known with relative ease. This is important because, especially in the early stages of development of materials, relatively little material is available for testing, and being able to predict weldability without extensive testing saves time, costs and material.
Finally the weld failure modes of welded joints in advanced high strength steels were investigated in more depth. Using experimental data, a mechanism for the initiation of failure in welded joints is proposed that explains the differences in observed weld failure modes. Based on that mechanism a method is proposed to weld materials that are susceptible to undesirable weld failure modes, to counter these undesirable failure modes.

Results of Research

Issues with manufacturing can be related to material characteristics or to process parameters (or a combination of both). An obvious difference between advanced high strength steels and conventional steel is the material strength. The strength of materials was found to be an

important parameter for the weldability. The strength of a material affects the contact resistance, as it influences the hardness, and thus the amount of true contact between two surfaces that are pressed together. It was found that the contact resistance is a very important parameter affecting weldability. A mathematical model for the growth of the weld nugget was drawn up that shows the importance of the contact resistance, and thus supports this conclusion. In simulations it was also found that the definition of the contact between surfaces is an even more important factor determining the weldability of a material. This is however a characteristic of the model, not so much of the physical material.
Another characteristic of the materials that is different between advanced high strength steels and more conventional materials is the chemical and microstructural composition. This affects resistance welding through the thermal and electrical conductivity of the material. It was found that the thermal and electrical conductivity also influence the weldability of the materials.
To compile a material data set based on available material data it is first advised to evaluate the material strength. The strength of a material is relatively easy to determine using tensile tests. Data of the strength of materials is usually provided by the supplier. To adjust material data in a model to account for differences between materials (*e.g.* a DP800 and a TRIP800) it is advised to use the thermal and electrical conductivity. The contact resistance is more laborious to measure, and because the definition of the contact resistance influences the results of simulation to a high degree, it is not advised to adjust these data unless they have been measured. As the contact resistance is highly influenced by the production process of the materials, especially rolling operations (that will not differ much between material grades), this is allowable. In all instances a material model should be verified against experimental results. Weld growth curves have been found to be suited for this purpose as process conditions are varied to produce a weld growth curve.
The electrode geometry is an important process parameter determining the weldability of a material. First of all this is important because the electrode tip diameter determines the size of the contact area, which determines the current density and the amount of heat that is conducted away from the material to the water cooled electrodes. The electrode geometry is also important because subsequent welding operations lead to degradation of the electrode tip, causing it to deform and become flatter and larger.
The first aspect was investigated by varying the electrode type and the electrode tip diameter. It was found that this affects the weldability of a material and that the correct choice of the electrode type and tip diameter is key to achieving the desired weld nugget size. The degradation of the electrode tip was found to be important as it affects the weld nugget diameter (and thus the electrode lifetime). It was also found that the weld nugget volume is much less affected by the degradation of the electrode tip.
Issues with the performance of resistance spot welds in advanced high strength steels are often attributed to the post weld hardness, because the increased levels of alloying in advanced high strengths steels lead to the formation of martensitic welds. As martensite is hard it does not deform much when loaded in tension. The lack of deformability causes the material to fail, thus leading to undesirable failure modes. Using simulations it was shown that resistance spot welding indeed leads to the formation fully martensitic weld nuggets in steels with chemical compositions similar to those of advanced high strength steels.
Combining experimental data and results of simulations two models were developed to predict post weld hardness. The first model can be used in simulation software to relate the chemical composition of a material to the cooling rates (dependent on process parameter settings) to predict post weld hardness. The second model consists of a simple equation that can be used to estimate the post weld hardness, within the constraints of the application (posing limits on variation in chemical composition and cooling rates) based on a basic chemical composition. Both models are also useful for industrial applications as the chemical composition of a material can usually be obtained from the supplier.
If the post weld hardness of a material is the primary cause of undesirable weld failure modes, then a post weld heat treatment, tempering the martensite should lead to improved

weld failure modes. It was found that this is however not the case; no relation between post weld heat treatments and improved failure modes was found.
It was found that undesirable weld failure modes were primarily found in materials that had a high level of phosphorous in the chemical composition. Phosphorus can affect the coherency of the grain boundaries in the weld nugget. By breaking up these grain boundaries followed by a subsequent tempering step it was found that a weld procedure could be developed that leads to improved weld failure modes.

Conclusions

It can be concluded that the manufacturing aspects of weldability can be addressed by careful selection of the process parameters, especially the electrode type and tip diameter. Simulation software, especially Sorpas, can be a helpful tool to engineer good process settings on the workshop floor.
Modelling the material data for simulations is best done by first setting the material strength and then adjusting the thermal and electrical conductivity. Thus material data sets can be compiled based on available material data. This is useful as it saves time, costs and material. Material data sets thus compiled should be validated. It is found that weld growth curves are suited to validate material data sets for use in dedicated resistance spot weld models.
The geometry of the electrode is an important process parameter for the weld nugget diameter. Changes in the electrode diameter due to wear of the electrode tip in subsequent welding operations limit the electrode lifetime.
Two simple models, based on the chemical composition, were derived to predict the post weld hardness of welded joints. One model combines the chemical composition with cooling rates and can be used in finite element calculations. The other model consist of a very simple model relating post weld hardness to a limited chemical composition.
It was however found that the hardness of the weld nugget is not the primary cause of undesirable weld failure. Undesirable weld failure modes are most likely due to incoherent grain boundaries in the weld nugget.
A three step welding procedure was developed to improve the weldability of materials that show undesirable weld failure modes.

The work reported in this thesis adds to the existing body of knowledge on resistance spot welding of advanced high strength steels and the use of dedicated weld software for that purpose and includes:

- a patented three step welding procedure to achieve full plug failure in resistance spot welded advanced high strength steels,
- a mechanism describing how undesirable weld failure modes can be attributed to incoherent welds,
- the mechanism that explains how a weld nugget is addressed by concentrated stresses upon loading,
- proof that post weld hardness is not the primary cause of undesirable weld failure modes in resistance spot welded advanced high strength steels,
- the validated models linking the post weld hardness of a joint to the chemical composition of the material,
- a mathematical description of the weld nugget growth,
- a validated method to compile material data sets base on available material data sets.

Samenvatting

De introductie van moderne hoge sterkte stalen heeft automobiel fabrikanten de mogelijkheid gegeven om zowel het gewicht van voertuigen te reduceren als de veiligheid the verhogen. In de literatuur werden problemen met de lasbaarheid van deze materialen gerapporteerd. Deze problemen betroffen zowel de maakbaarheid als het functionaliteit van gepuntlaste verbindingen. De maakbaarheid betreft de mogelijkheid om verbindingen te maken in een industriële omgeving, met name het lasbereik en de elektrode levensduur. De functionaliteit betreft de hardheid en het falen van de puntlassen.

Onderzoeksmethode

Beide aspecten worden in dit proefschrift besproken, waarbij zowel van experimentele gegevens als van programmatuur om de lasprocessen te simuleren gebruik wordt gemaakt. De gebruikte programmatuur is SYSWELD en Sopras. Sysweld is een programma dat geschikt is voor metallurgische simulaties. Sopras is geschikter om industriële processen te evalueren.
Lasbaarheid is een kwestie van toepassing; zonder toepassingen zijn er ook geen problemen met de lasbaarheid. Het is de toepassing die bepaalt welke kenmerken van de materialen, proces, en gelaste verbindingen belangrijk zijn. In autotechnische toepassingen zijn deze aspecten van de lasbaarheid vastgelegd in industriële standaards, die de minimum eisen aan de maakbaarheid en functionaliteit van de gelaste verbindingen vastleggen. Daarom zijn de meeste materialen, die in dit proefschrift zijn gebruikt, materialen die industrieel worden toegepast. De proces parameters die worden gebruikt zijn primair afgeleid van standaards. Om dezelfde reden is gebruik gemaakt van commercieel verkrijgbare software.
Om simulaties effectief te kunnen gebruiken was het ten eerste nodig om het gebruik van simulaties voor onderzoek te onderzoeken. Literatuur over het gebruik van modelleer software voor toepassingen in fabricage, zoals het bepalen van proces parameters is beschikbaar, maar niet over het gebruik van de software voor onderzoek. Eén van de punten was de beschikbaarheid van materiaalgegevens. Zowel SYSweld als Sopras komen met een gegevensbank van materialen, maar de materialen die daarin beschikbaar zijn, gedragen zich niet noodzakelijkerwijs hetzelfde tijdens lassen als de materialen die gebruikt worden in dit proefschrift. De eerste focus ligt daarom op het gebruik van software voor simulaties, de invloed van materiaal kenmerken op de lasbaarheid, en het samenstellen pakketten van gevalideerde materiaal gegevens.
Vervolgens werd de invloed van proces parameters op het lassen van moderne hoge sterkte stalen onderzocht. Specifieke aandacht was gericht op de invloed van de elektrode geometrie, aangezien die verband heeft met de elektrode levensduur.
Uit de literatuur blijkt dat de lasbaarheid van materialen sterk verbonden is met de hardheid na het lassen van de verbindingen. Daarom richt het onderzoek naar de lasbaarheid zich eerst op de hardheid na het lassen, en hoe die kan worden voorspeld op basis van materiaal eigenschappen die met relatief gemak gekend kunnen worden. Dit is van belang omdat, vooral in de vroege stages van het ontwikkelen van materialen, nog maar weinig m,ateriala beschikbaar is voor proeven, en het kunnen voorspellen van de lasbaarheid zonder uitvoerig testen tijd, geld, en materiaal bespaard.
Tenslotte worden de wijzen van falen van gelaste verbindingen in moderne hoge sterkte stalen diepgaander onderzocht. Gebruikmakend van experimentele gegevens word een mechanisme voor de initiatie van de falen in gelaste verbindingen, dat de verschillen in waargenomen faalwijzen kan verklaren, voorgesteld. Gebaseerd op dat mechanisme wordt een methode voorgesteld om materialen, die gevoelig zijn voor ongewenste faalwijzen, te lassen waarmee ongewenste faalwijzen kunnen worden voorkomen.

Resultaten van Onderzoek

Problemen met de maakbaarheid kunnen te wijten zijn aan de materiaaleigenschappen of aan de proces parameters (of een combinatie van beide). Een duidelijk verschil tussen moderne hoge sterkte stalen en meer conventionele stalen is de sterkte van de materialen. De sterkte bleek een belangrijke factor voor de lasbaarheid. De sterkte van een materiaal heeft ook gevolgen voor de contactweerstand, omdat het de hardheid beïnvloedt, en daarmee het ware contact tussen twee oppervlakken die worden samengedrukt. Het bleek dat de contactweerstand een zeer belangrijke factor is voor de lasbaarheid. Een wiskundig model voor de groei van de laslens is opgesteld, waaruit het belang van de contactweerstand naar voren komt, en daarmee deze conclusie ondersteund. Het bleek dat de definitie van de contactweerstand in simulaties een nog belangrijkere factor is in het bepalen van de lasbaarheid van een materiaal. Dit is echter een karakteristiek van het model, niet zozeer het fysieke materiaal.
Een ander belangrijke materiaaleigenschap die verschilt tussen moderne hoge sterkte stalen en meer conventionele materialen is de chemische en microstructurele samenstelling. Dit heeft invloed op weerstandlassen door de thermische en elektrische geleidbaarheid van het materiaal. Het blijkt dat de thermische en elektrische geleidbaarheid invloed hebben op de lasbaarheid van het materiaal.
Om een set van materiaalgegevens samen te stellen op basis van bekende materiaaldata wordt eerst geadviseerd om de materiaalsterkte te bekijken. De sterkte van een materiaal is relatief makkelijk te bepalen door middel van trekproeven. Gegevens over de sterkte van materialen worden doorgaans geleverd door de leverancier van de materialen. Om materiaal gegevens in een model aan te passen om het verschil tussen materialen (bijvoorbeeld een DP800 en een TRIP800) wordt aangeraden om de thermische en elektrische geleidbaarheid aan te passen. Het is bewerkelijker om de contactweerstand te meten, en omdat de definitie van de contactweerstand de resultaten van simulaties in hoge mate beïnvloed wordt het afgeraden om deze aan te passen, tenzij men de gegevens daadwerkelijk heeft gemeten. Omdat de contactweerstand in hoge mate wordt beïnvloed door het productieproces, met name het walsen (hetgeen niet veel zal verschillen tussen verschillende materialen), is dit toelaatbaar. In alle gevallen moet een materiaal model worden geverifieerd met experimentele resultaten. Lasgroeicurven zijn geschikt voor dit doel omdat de proces parameters worden gevarieerd om een curve op te stellen.
De geometrie van de elektroden is een belangrijke parameter bij het bepalen van de lasbaarheid van een materiaal. Allereerst omdat de diameter van de punt van de elektrode de grootte van het contactoppervlak bepaald, en daarmee de stroomdichtheid en de hoeveelheid warmte die weggeleid wordt van het materiaal naar de met water gekoeld elektroden. De geometrie van de elektrode is ook belangrijk omdat opeenvolgende lassen leiden tot degradatie van de punt, waardoor die platter en groter wordt.
Het eerste aspect is onderzocht door het type elektrode en de diameter van de punt van de elektrode te variëren. Het blijkt dat dit de lasbaarheid van het materiaal beïnvloedt en dat een correcte keuze van het type elektrode en diameter van de punt belangrijk zijn om een gewenste grootte van de laslens te bereiken. De degradatie van de punt bleek belangrijk te zijn omdat het de diameter van de laslens bepaalt (en daarmee de levensduur van de elektrode). Het bleek ook dat het volume van de laslens veel minder afhankelijk was van de degradatie van de punt van de elektrode.
Problemen met de functionaliteit van puntlassen in moderne hoge sterkte stalen worden vaak toegeschreven aan de hardheid van de lassen, omdat de rijkere legering in moderne hoge stalen leidt tot de vorming van martensitische lassen. Omdat martensiet hard is vervormt het niet als het op trek wordt belast. Het gebrek aan vervormbaarheid zorgt er voor dat het materiaal faalt, leidend tot ongewenste faalwijzen. Gebruik makend van simulaties is aangetoond dat puntlassen inderdaad leidt tot de vorming van martensitische lassen in materialen met een chemische samenstelling die vergelijkbaar is met die van moderne hoge sterkte stalen.

Door combineren van experimentele gegevens met uitkomsten van simulaties zijn twee modellen opgesteld om de hardheid na lassen te voorspellen. Het eerste model kan gebruikt worden in simulatie software om de chemische samenstelling aan de afkoelsnelheden (afhankelijk van de proces parameters) te koppelen om zo de hardheid na lassen te kunnen voorspellen. Het tweede model bestaat uit een eenvoudige vergelijking die gebruikt kan worden om de hardheid na het lassen te voorspellen, binnen de grenzen van de toepassing (die grenzen stelt aan variaties in de chemische samenstelling en afkoelsnelheden) gebaseerd op een basale chemische samenstelling. Beide modellen zijn ook nuttig voor industriële toepassingen omdat de chemische samenstelling doorgaans verkregen kan worden van de leverancier.
Als de hardheid van de lassen de primaire oorzaak is van ongewenste faalwijzen, dan zou een warmtebehandeling, waarbij de las wordt getemperd, moeten leiden tot een verbetering in de faalwijze. Het bleek dat dit niet het geval is; er werd geen relatie worden gevonden tussen het toepassen van een warmtebehandeling en een verbetering in de faalwijze.
Het bleek dat ongewenste faalwijzen vooral aangetroffen werden in stalen met een hoog gehalte aan fosfor in de chemische samenstelling. Fosfor kan de samenhang tussen korrelgrenzen in de laslens aantasten. Door deze korrelgrenzen op te breken, gevolgd door een warmtebehandeling, bleek het mogelijk een lasprocedure te ontwikkelen die leidt tot verbeterde faalwijzen.

Conclusies

Het kan worden geconcludeerd dat de aspecten die te maken hebben met de maakbaarheid kunnen worden aangepakt door zorgvuldige keuze van procesparameters, met name het type elektrode en de diameter van de punt. Programmatuur voor simulaties, met name Sorpas, kan een bruikbaar stuk gereedschap zijn om goede procesparameters op de werkvloer te bepalen.
Het modelleren van materiaalkarakteristieken voor simulaties kan het beste worden gedaan door eerst de sterkte van het materiaal vast te leggen en dan de thermische en elektrische geleidbaarheid aan te passen. Daarmee kunnen sets van materiaal gegevens worden samengesteld op basis van beschikbare materiaal gegevens. Dit is nuttig omdat het tijd, geld en materiaal bespaard. Sets van materiaal gegevens die op die wijze worden samengesteld moeten worden gevalideerd. Het blijkt dat lagroeicurves geschikt zijn om materiaal gegevens te valideren voor gebruik in puntlas modellen.
De geometrie van de elektrode is een belangrijke proces parameter voor de grootte van de diameter van de laslens. Veranderingen in de elektrode diameter door slijtage van de elektrode punt door opeenvolgende lasoperaties beperken de elektrode levensduur.
Twee eenvoudige modellen, gebaseerd op de chemische samenstelling, zijn afgeleid om de hardheid na het lassen van verbindingen te voorspellen. Het ene model combineert de chemische samenstelling met de afkoelsnelheid en kan gebruikt worden in eindige elementen modellen. Het andere model bestaat uit een eenvoudige vergelijking die de hardheid na het lassen relateert aan een gelimiteerde chemische samenstelling.
Het bleek echter dat de hardheid van de laslens niet de primaire factor is die leidt tot ongewenste faalwijzen. Ongewenste faalwijzen worden meest waarschijnlijk veroorzaakt door gebrek aan samenhang in de korrelgrenzen van de laslens.
Een lasprocedure in drie stappen is ontwikkeld om de lasbaarheid van die materialen, die gevoelig zijn voor ongewenste faalwijzen, te verbeteren.

Werk in dit proefschrift dat bijdraagt aan de kennis van het puntlassen van moderne hoge sterkte stalen en het gebruik van modelleersoftware voor puntlassen is:

- een gepatenteerde procedure voor een driestapslasproces waarmee falen met intacte las kan worden bereikt in gepuntlaste hoge sterkte stalen,
- een mechanisme dat beschrijft hoe ongewenste faalwijzen kunnen worden toegeschreven aan gebrek aan samenhang in de las,
- bewijs dat de hardheid na het lassen niet de primaire oorzaak van ongewenste wijzen

van falen in gepuntlaste moderne hoge sterkte stalen,

- het gevalideerde modellen die de hardheid na het lassen relateert aan de chemische samenstelling van het materiaal,
- een wiskundige beschrijving van de groei van de laslens,
- een gevalideerde methode om sets van materiaalgegevens samen te stellen gebaseerd op bekende materiaalgegevens.

Acknowledgments

Modern industrial research is a team sport. For this thesis I was lucky to have been part of a very good team. Here I want to acknowledge their part.
First of all there are the people of Tata Steel RD&T (formerly Corus RD&T). The first person to thank is Sullivan Smith who taught me a lot about resistance spot welding and contributed to a lot of my publications. Especially the three step welding process is a joint exercise for which Sullivan's experimental work, experience and knowledge was crucial. Other people that have contributed with experimental work on resistance spot welding are Tom Moolenvliet and Ellen van der Aa.
Most of the other colleagues of the Joining Technology group of the Product Application Centre at the IJmuiden Technology Centre have been important for the work that they did, which I have incorporated in this thesis, and comments and discussions that we had over the years. Apart from the people already mentioned I should also mention Immy de Wit, Theo de Haan, Cierick Goos, Jurgen Vrenken, Arend Mennes, Henk Schipper, Johan Mosch, and Sujit Chatterjee.
Knowledge of welding and other joining processes is not sufficient for this thesis, the application of advanced high strength steels, involves aspects of forming technology, production and metallurgy. I should therefore also thank Shuwen Wen, John Droog, Theo Kop, Pieter van der Wolk, Henk Vegter, and Aad Wittebrood. A special mention here is due to Peter van Liempt with whom I spent a lot of enjoyable time in the labs, and who helped to get the picture straight in our lengthy discussions.
There were lengthy discussions on all aspects of this work with Theo de Haan, Cierick Goos, Martin Sadhinoch, and Edwin Swart, as well as on lots of other topics connected with working in an industrial research laboratory. I especially want to thank my colleague Louisa Carless, with whom I had the pleasure of sharing an office, who helped me with writing in English, general intelligent remarks, and by coping with the burden of having me in the same office.
Without support from management in Tata Steel there would have been no project, nor would there have been resources to publish results. For this I should thank, amongst others, Rob Boom and Rene Duursma.

A lot of work was done in cooperation with Sumitomo Metals Industries. It was a great pleasure to work with such knowledgeable and focussed colleagues. Thanks to Manabu Fukumoto, Hitomi Nishibata, and Kiyoyuki Fukui. Special thanks to Toru Okada and Masato Uchihara who's contributions to our joint publications have also been used in this thesis.

The last research group I should mention is the Joining group at the Materials Science and Engineering department of Delft University of Technology. Here I should mention Ian Richardson, Marcel Hermans, Murugaiyan Amirthalingam, Tobias Schenk, Masoud Pazooki, Richard Thiessen, and many others who have helped me in our discussions to understand ideas and formulate new ones.

There are probably many more people I should mention. I apologise if I forgot to mention a name which I should have. Be assured that your contribution is no less valued. All results in this thesis have been published and I have listed all the relevant publications with the results. I have taken care to make sure that all contributors to the publications have been listed. In most publications there is also a paragraph with acknowledgements to people that contributed to the work, but were not listed as authors.

List of Publications

N.J. den Uijl, R. Horn, P. van Baardwijk & J. Pauwelussen [2014] Lightweight Suspension: An Integrated Approach In Applied Sciences. Document F2014-EDU-025, FISITA 2014, Maastricht, The Netherlands, June 2 – 6 2014.

S. Celotto, T. van der Veldt, E.J. de Wit & N.J. den Uijl [2013] Method of producing a continuous metal strip; European Patent Application WO/2013/135847.

N.J. den Uijl, F. Azakane, S. Kilic, V. Docter, B. Neelis, C. Goos & E. van der Aa [2012] Performance of tensile tested resistance spot and laser welded joints at various angles. IIW document 2327-11; Welding in the World Vol. 56, 11-12, 2012.

N.J. den Uijl, T. Okada, T. Moolevliet, A. Mennes, E. van der Aa, M. Uchihara, S.M. Smith, H. Nishibata, T. van der Veldt, K. Fukui [2012] Performance of resistance spot welded joints in advance high strength steel in static and dynamic tensile tests. IIW document 2162-11 (III-1573-10); Welding in the World Vol. 56, 7-8, 2012.

N.J. den Uijl & T. de Haan [2012] Method of manufacturing a metal vehicle wheel and vehicle wheel; European patent application WO/2012/084177.

M. Amirthalingam, E.M. van der Aa, N.J. den Uijl, M.J.M. Hermans & I.M. Richardson [2012] Phosphorous and boron segregation during resistance spot welding of advanced high strength steels. 9th International Conference on Trends in Welding Research; Chicago, Illinois, USA; June 4-8 2012.

N.J. den Uijl & L.J. Carless [2012] Metal Forming Technologies. Chapter 3 of Advanced materials in automotive engineering; edited by Jason Rowe; published by Woodhead Publishing Ltd. ISBN 978-1-84569-561-3; 2012.

N.J. den Uijl, S. Kilic, F. Azakane, V. Docter, B. Neelis & C. Goos [2011] Performance of tensile tested resistance spot welded joints at various angles. IIW document SC-Auto-47-11; Presented at the 64th Annual Assembly of the IIW-IIS (Chennay, India), 2011.

N.J. den Uijl [2010] Advanced Joining and Disassembly. Poster at the M2i Conference "Materials to Innovate Industry and Society", Noordwijkerhout, The Netherlands, December 13 & 14, 2010.

N.J. den Uijl [2010] Resistance spot welding of a complicated joint in new advanced high strength steel. Proceedings of the 6th International Seminar on Advances in Resistance Welding (Hamburg, Germany); W. Zhang, K. Pedersen, R. Bothfeld & J. Eggers (ed.); pp. 40-54.

N.J. den Uijl [2010] Performance of resistance spot welded joints in advance high strength steel in static and dynamic tests. IIW document III-1213-02. Presented at the joint meeting of C-III and SC-AUTO at the 63rd Annual Assembly of IIW-IIS (Istanbul, Turkey), 2010.

T. Okada, M. Uchihara, K. Fukui, S.M. Smith, N.J. den Uijl & T. van der Veldt [2010] The effect of paint baking cycles on the spot weld strength of advanced high strength steel. Preprints of the National Meeting of JWS, Tokyo, Japan; Vol. 2010s (pp. 50-51).

S.M. Smith, N.J. den Uijl, T. van der Veldt, T. Okada, M. Uchihara, F. Fukui [2010] The effect of ageing on the spot weld strength of AHSS and the consequences for testing procedures. IIW document 1976-08; Welding in the World, p.p. R12 – R26, Vol. 54, no.1 / 2, 2010.

N.J. den Uijl [2009] Material Data for Weld Modelling. Presentation at the M2i Conference "Materials to Innovate Industry and Society", Noordwijkerhout, The Netherlands, December 7 & 8, 2009.

T. Okada, M. Uchihara, K. Fukui, S.M. Smith, N.J. den Uijl & T. van der Veldt [2009] Effect of time between welding and tensile testing on the spot weld peel strength of AHSS. National Meeting of JWS, Tokyo, Japan, 2009.

I.M. Richardson, M. Amirthalingam, M.J.M. Hermans, N.J. den Uijl & M.K. Wibowo [2009] The influence of welding on advanced high strength TRIP and dual phase steels. Proceedings 9th International Seminar on Numerical Analysis of Weldability, Schloss Seggau, Graz, Austria, September 28-30, 2009; H. Cerjak & N. Enzinger (Eds.); (pp. 185-214).

S.M. Smith, T. Okada, N.J. den Uijl, T. van der Veldt, M. Uchihara, & K. Fukui [2009] Influence of the paint baking cycle on the mechanical properties of AHSS welded structures in automotive assemblies. Proceedings International Automotive Body Congress (IABC), Global Powertrain Congress (GPC), June 23-24, 2009, Vaals, The Netherlands (pp. 1-15).

N.J. den Uijl & S.M. Smith [2008] Method for spot welding and spot welded sheet material; International Patent Application WO2008/058675.

N.J. den Uijl, S.M. Smith, T. Moolevliet, C. Goos, E.M. van der Aa, & T. van der Veldt [2008] Failure modes of resistance spot welded advanced high strength steels. Proceedings 5th International Seminar on Advances in Resistance Welding, Toronto, Canada, September 24-26, 2008. W. Zhang & N. Scotchmer (Eds.), (pp. 78-104).

T. Okada, M. Uchihara, K. Fukui, S.M. Smith, N.J. den Uijl & T. van der Veldt [2008] The effect of paint baking cycles on the spot weld strength of advanced high strength steel. Preprints of the National Meeting of JWS, Vol. 2008f (2008) pp.101-102.

N.J. den Uijl, S.M. Smith, T. van der Veldt, H. Nishibata, T. Okada, M. Uchihara & K. Fukui [2008] Prediction of post weld hardness of advanced high strength steels for automotive application using a dedicated carbon equivalent number. IIW document 1873-07; Welding in the world, 52 (11/12), pp. 18-29.

N.J. den Uijl, H. Nishibata, S.M. Smith, T. van der Veldt, T. Okada, M. Uchihara & K. Fukui [2008] Prediction of post weld hardness of advanced high strength steels for automotive application using a dedicated carbon equivalent number. IIW document III-1444-07: Presented at the meeting of commission III "Resistance welding, solid state welding and allied joining processes" of the Annual Assembly of the IIW, University of Dubrovnik, Dubrovnik, Croatia, July 2-4, 2007 (pp. 1-14).

N.J. den Uijl [2007] Post weld heat treatment of advanced high strength steel for automotive joining. Mathematical Modelling of Weld Phenomena 8; H. Cerjak, H.K.D.H. Bhadesia & E. Kozeschnik (Eds.); Verlag der Technischen Universitat Graz, Graz, Austria, (pp. 217-234).

N.J. den Uijl & S.M. Smith [2006] Resistance Spot Welding of Advanced High Strength Steels for the Automotive Industry; 4th International Seminar on Advances in Resistance Welding; Wels, Austria.

N.J. den Uijl [2006] Using Sorpas to support weldability research at Corus; Sorpas User Group Meeting; 4th International Seminar on Advances in Resistance Welding; Wels, Austria.

N.J. den Uijl [2006] Modelling the influence of resistance spot welding on material properties. Proc. Joint Int. Conf. "16th Int. Conf. Computer Technology in Welding and Manufacturing" and "3rd Int. Conf. Mathematical Modelling and Information Technologies in Welding and Related Processes"; W. Lucas & V.I. Makhnenko (Eds.); E.O. Paton Electric Welding Institute of the NAS; Kiev, Ukraine; pp. 306-313.

N.J. den Uijl & M.A. Anwar [2006] Laser weld induced microstructural changes in automotive bodysheet; Mathematical modelling of weld phenomena 7; H. Crejak, H.K.D.H. Bhadeshia & E. Kozeschnik (Eds.); Verlag der Technischen Universitat Graz, Graz, Austria; pp. 309-326.

Curriculum Vitae

Nick Johannes den Uijl
born on 7th July, 1969 in Dordrecht, The Netherlands.

Present	Lecturer and researcher, HAN University of Applied Science, Arnhem, The Netherlands.
2000 – 2012	Principal Researcher, Tata Steel RD&T, IJmuiden, The Netherlands.
1995 – 1999	IT Specialist, ING Group, Amsterdam, The Netherlands.
1995	Programmer, TAS Informatica, Baarn, The Netherlands.
1995	Teaching Assistant, University of Twente, Enschede, The Netherlands.
1988 – 1998	University of Twente, Enschede, The Netherlands, Master of Science (ingenieur) in Mechanical Engineering, section Materials Science.
1986 – 1988	Atheneum, Van Maerlantlyceum, Eindhoven, The Netherlands.
1983 – 1986	Atheneum, Stedelijk Scholengemeenschap Middelburg (SSGM), Middelburg, The Netherlands.
1981 – 1983	Atheneum, Van Maerlantlyceum, Eindhoven, The Netherlands.

References

AISI [2008] Anatomy of a Crash: The most important 100 miliseconds of your life; Poster American Iron and Steel Institute; 2008.

Amirthalingam M., Hermans M.J.M. & Richardson I.M. [2005] Literature review report on the development of microstructure in welded DP and TRIP steels; Netherlands Institute for Metals Research; 2005.

Andrews K.W. [1965] Empirical Formulae for the Calculation of Some Transformation Temperatures; Journal of the Iron and Steel Institute, 203, Part 7, 1965.

Auto/Steel Partnership [2008] Advanced High-Strength Steel Application Guidelines - A Special Edition of In-Depth AHSS Case Studies; Auto/Steel Partnership, Southfield, Michigan, April 2008.

Auto/Steel Partnership [2008] Starting Resistance Spot Welding Schedules for AHSS; Auto/Steel Partnership (www.a-sp.org); 2008.

AWS [1976] Welding Handbook; Seventh Edition, Volume 1; Fundamentals of Welding; American Welding Society; 1976. ISBN 0871711265

AWS D8.1M:2007 [2007] AWS D8.1M:2007 Specification for Automotive Weld Quality – Resistance Spot Welding of Steel; 2007

Bain E.C. [1939] Functions of the Alloying Elements in Steel"; American Society for Metals; Cleveland, Ohio; 1939.

Baltazar Hernandez V.H., Kuntz M.L., Khan M.I. & Zhou Y. [2008] Influence of Microstructure and Weld Size on the Mechanical Behaviour of Dissimilar AHSS Resistance Spot Welds; Science and Technology of Welding and Joining; Vol. 13 No. 8; 2008.

Barralis J. & Maeder G. [1982] Métallurgie Tome I: Métallurgie Physique; Collection Scientifique ENSAM, 1982, 270 p.

Beck M. [2007] EU richtlijn bedreigt auto- en staalschrootrecycling; Recycling Magazine Benelux; nr. 4; juni 2007

Bentley K.P., Greenwood J.A., Knowlson P.M. & Barker R.G. [1963] Temperature distribution in spot welds; British Welding Journal, Vol. 10 (1963) pp. 613-619.

Blondeau R., Maynier Ph. & Dollet J. [1973] Prévision de la dureté, de la résistance des aciers au carbone et faiblement alliés d'après leur structure et leur composition; Mem. Sci. Rev. Métallurgie 70, No. 12 1973.

Blondeau R., Maynier Ph., Dollet J. & Vieillard-Baron B. [1975] Prévision de la dureté et de la résistance des aciers au carbone et failblement alliés d'après leur composition et leur traitement thermique; Mémoirs Scientifiques Revue Métallurgie, Novembre 1975.

BMW [2005] BMW Group Standard GS 96002-2: "Widerstandspunktschweissen, punktschweissen, Qualitaetsanforderung, Fehlerklasse, Toleranz"; 2005.

BMW 3032 [2002] High Strength Sheet Steel (180 MPa…550 MPa Yield Strengths); General Motors Worldwide Engineering Standards; 2002.[2008] Stahl-Eisen-Prüfblätter (SEP) des Stahlinstituts VDEh 1220-2: "Prüf- und Dokumentationsrichtlinie für die Fügeeignung von Feinblechen aus Stahl; Teil 2: Widerstandspunktschweißen"; 2008.

Bonte E. & Deren T. [2004] The new PSA 407 Car Body; 6th International Car Body Benchmarking Platform „EURO CAR BODY 2004“; Bad Nauheim/Frankfurt, Germany; October 2004.

Borhy I. & Szabó P. [2005] Topical issues in the development of expert systems for use in the process planning of resistance spot welded railway vehicle structures; Mathematical Modelling of Weld Phenomena 7; Cerjak H., Bhadeshia H.K.D.H. & Kozeschnik E. (eds.); Verlag der Technischen Universität Graz; ISBN 3-901351-99-X; 2005; pp. 1099-1109.

Bouzekri M., Dancette S., Dupuy T., Lens A., Nait Oultit B., Massardier V. & Fabrègue D. [2010] An Investigation of Failure Types in High-Strength Steel Resistance Spot Welds; IIW-1973-08; Welding in the World; Vol. 54, no. 3/4; 2010.

Boyer J.N. [2007] Exposure Electromagnetic Fields During Resistance Welding Operations; III-1449-07; IIW-IIS Annual Assembly; Joint Workshop on "Health, Safety and Quality in Welding" by C-III, C-VIII and C-XII; Dubrovnik, Croatia; 2007.

Brunies F., Heinl E. & A. Schmitt A. [2004] The new Mini Cabrio Body Car; 6th International Car Body Benchmarking Platform „EURO CAR BODY 2004“; Bad Nauheim/Frankfurt, Germany; October 2004.

Campestrini P. [2014] Lightweight solutions research at Flanders DRIVE; Trends in Automotive Lightweight Solutions; Bornhem, Belgium; May 27, 2014.

Cerjak H. & Easterling K.E. (eds.) [1993] Mathematical Modelling of Weld Phenomena; The Institute of Materials; ISBN 0-901716-16-2; 1993.

Cerjak H. (ed.) [1995] Mathematical Modelling of Weld Phenomena 2; The Institute of Materials; ISBN 0-901716-63-4; 1995.

Cerjak H. (ed.) [2002] Mathematical Modelling of Weld Phenomena 5; IOM Communications Ltd.; ISBN 1 86125 115 7; 2002.

Cerjak H., Bhadeshia H.K.D.H. & Kozeschnik E. (eds.) [2005] Mathematical Modelling of Weld Phenomena 7; Verlag der Technischen Universität Graz; ISBN 3-901351-99-X; 2005.

Cerjak H., Bhadeshia H.K.D.H. & Kozeschnik E. (eds.) [2007] Mathematical Modelling of Weld Phenomena 8; Verlag der Technischen Universität Graz; ISBN 978-3-902465-69-6; 2007.

Chaillet J.M., Chevet F., Bocquet P. & Dollet J. [1976] Prediction of the Microstructure and Tensile Properties of Weld Metal Deposits; Welding of HSLA (Microalloyed) Structural Steels; Proceedings of an International Conference; 9-12 November 1976; Rome, Italy p.p.298-321.

Chan K., Scotchmer N., Bohr J.C., Khan I., Kuntz M. & Zhou N. [2006] Effect of Electrode Geometry on Resistance Spot Welding of AHSS, 4th International Seminar on Advances in Resistances in Resistance Welding, November 14-16, 2006, Wels, Austria.

Chan K.R. & Scotchmer N. [2006] The PARACAP™ - Longer Electrode Life from a New Geometry, an Innovative Multilayer Coating, and Internal Cooling Fins; Proceedings of The 4th International Seminar on Advances in Resistance Welding; W. Zhang & A. Eder (eds.); Wels, Austria; November 2006.

Chan K.R. & Scotchmer N. [2010] Predicting Electrode Life with FEM Software; Proceedings of the 6th International Seminar on Advances in Resistance Welding; W. Zhang, K. Pedersen, R. Bothfeld & J. Eggers (eds.); Hamburg, Germany; September 2010.

Chao Y.J. [2003] Failure Mode of Spot Welds: Interfacial versus Pullout; Science and Technology of Welding and Joining; Vol. 8, no 2; 2003.

Chatterjee K.L. [2000] Extending electrode life by tip design and dressing; Welding and Metal Fabrication; Vol. 68, no. 8, pp. 12-14; September 2000.

Cho H.S. & Cho Y.J. [1989] A study of the thermal behaviour in resistance spot welding, Welding Journal, 68 [1989] 236-s.

Compton K. T. [1939] Biographical Memoir of Elihu Thomson 1853 - 1937; National Academy of Sciences of the United States of America; Biographical Memoirs; Volume XXI - Fourth Memoir; Presented to the Academy at the Autumn Meeting, 1939

Cooper R. [2008] Current Comments on the Global Automotive Industry; 5th International Seminar on Advances in Resistance Welding; Toronto, Canada; 2008.

Cornelissen R.L. [1993] Materialensubstitutie in de automobile – Een case-studie naar de aluminium auto; IVEM-studentenrapport no. 63; Interfacultaire Vakgroep Energie- en Milieukunde; Groningen; 1993.

Craggs J. [2004] Welding High Strength and Ultra-High Strength Steels; Electrodes, Wear and Parameters; Proceedings of The 3rd International Seminar on: Advances in Resistance Welding; W. Zhang & P. Xu (eds.); Berlin, Germany; November 2004.

Cretteur L., Koruk A.I., & Tosal-Martinez L. [2002] Improvement of Weldability of TRIP Steels by Use of In-Situ Pre- and Post-heat Treatments; Steel Research 73 (2002), No.6.; 2002.

CSPIJ [2008] Product Range 2008; Corus Strip Products Ijmuiden; CSPY:1.750;NL:01/2008 (www.cspij-productrange.nl)

Davies A.C. [1984] The science and practice of Welding, Volume 1 – Welding science and technology; Eight edition; Cambridge University Press; 1984. ISBN 0521278392.

Davies A.C. [1986] The science and practice of welding, volume 2, The practice of welding; Cambridge University Press; ISBN 0 521 27840 6; 1986.

De A. & Dorn L. [2005] Computer simulation of resistance spot welding process; Mathematical Modelling of Weld Phenomena 7; Cerjak H., Bhadeshia H.K.D.H. & Kozeschnik E. (eds.); Verlag der Technischen Universität Graz; ISBN 3-901351-99-X; 2005; pp. 895 – 923.

Del Vecchio E.J. (ed.) [1956] Resistance Welding Manual, 3rd edition, volume 1; Resistance Welder Manufacturer's Association; Philadelphia Pa., U.S.A.; 1956.

Delhommeau M. & Hoareau C. [2004] Renault Modus; 6th International Car Body Benchmarking Platform „EURO CAR BODY 2004“; Bad Nauheim/Frankfurt, Germany; October 2004.

Den Ouden G. & Korevaar B.M. [1992] Metaalkunde, deel 1; Delftse Uitgeversmaatschappij; ISBN 90-6562-117-2; 1992.

Den Uijl N., Okada T., Moolevliet T., Mennes A., Van der Aa E., Uchihara M., Smith S., Nishibata H., Van der Veldt T., Fukui K. [2012a] IIW-2162-11 (III-1573-10) Performance of resistance spot welded joints in advance high strength steel in static and dynamic tensile tests. Welding in the World 7/8, 2012.

Den Uijl N., Smith S., Moolevliet T., Goos C. Van der Aa E.M., Van der Veldt T. [2008a] Failure modes of resistance spot welded advanced high strength steels; Proceedings 5th International Seminar on Advances in Resistance Welding; Zhang W. & Scotchmer N. (Eds.); Toronto, Canada, 24-26 September 2008 (pp. 78-104).

Den Uijl N.J. & Anwar M. [2005] Laser Weld Induced Microstructural Changes in Automotive Bodysheet; Mathematical Modelling of Weld Phenomena 7; Cerjak H., Bhadeshia H.K.D.H. & Kozeschnik E. (eds.); Verlag der Technischen Universität Graz; ISBN 3-901351-99-X; 2005.

Den Uijl N.J. & Carless L.J. [2012] Metal Forming Technologies; Advanced Materials in Automotive Bodies, Chassis and Interiors; J. Rowe (ed.); Woodhead Publishing Ltd.; ISBN 978-1-84569-561-3; 2012.

Den Uijl N.J. & Smith S. [2006] Resistance Spot Welding of Advanced High Strength Steels for the Automotive Industry; Proceedings of the 4th International Seminar on Advances in Resistance Welding; W. Zhang & A. Eder (eds.); Wels, Austria; November 2006.

Den Uijl N.J. & Smith S. [2007] The influence of electrode geometry on resistance spot welding of advanced high strength steels for automotive applications; Proceedings of the 3rd JOIN Conference "International Conference on Total Welding Management in Industrial Applications”; J. Martikainen (ed.); Acta Universitatis Lappeentantaensis 274; ISBN 978-952-214-413-3; Lappeenranta, Finland; August 21-24, 2007.

Den Uijl N.J. [2006a] Microstructure Control during the Galvannealing Cycle of TRIP-aided Steel Sheet - Visit TUD, May 15 2006; Corus internal report; reference source: 120969; 2006.

Den Uijl N.J. [2006b] Modelling the Influence of Resistance Spot Welding on Material Properties; 3rd International Conference on Mathematical Modelling and Information Technologies in Welding and Related Processes; Kiev; 2006.

Den Uijl N.J. [2008] Thermal and electrical resistance in resistance spot welding; Proceedings of the 17th International ‘Computer Technology in Welding and Manufacturing Conference’; Cranfield, UK; TWI Ltd; ISBN 13-978-1-903761-07-6; 2008.

Den Uijl N.J. [2009] Material data for weld modelling; M2i Conference: Materials to Innovate the Industry; Noordwijkerhout; December 7 & 8, 2009.

Den Uijl N.J. [2010] Performance of resistance spot welded joints in advance high strength steel in static and dynamic tests; IIW document III-1213-02. Presented at the joint meeting of C-III and SC-AUTO at the 63rd Annual Assembly of IIW-IIS (Istanbul, Turkey); 2010.

Den Uijl N.J. [2010] Resistance spot welding of a complicated joint in new advanced high strength steel; Proceedings of the 6th International Seminar on Advances in Resistance

Welding; W. Zhang, K. Pedersen, R. Bothfeld & J. Eggers (eds.); Hamburg, Germany; September 2010.

Den Uijl N.J., Azakane F., Kilic S., Docter V., Neelis B., Goos C. & Van der Aa E. [2012b] IIW-2327-11 Performance of tensile tested resistance spot and laser welded joints at various angles. Welding in the World 11/12 2012.

Den Uijl N.J., Nishibata H., Smith S., Okada T., Van der Veldt T., Uchihara M. & Fukui K. [2007] Prediction Of Post Weld Hardness Of Advanced High Strength Steels For Automotive Application Using A Dedicated Carbon Equivalence Number; IIW-IIS document III-1444-07; Dubrovnik 2007.

Den Uijl N.J., Nishibata H., Smith S., Okada T., Van der Veldt T., Uchihara M. & Fukui K. [2008b] Prediction of post weld hardness of advanced high strength steels for automotive application using a dedicated carbon equivalent number; IIW-1873-07; Welding in the world; Vol. 52 No. 11/12 2008.

Den Uijl, N.J. [2006c] Using Sorpas to support ; 2006.weldability research at Corus; Sorpas User Group Meeting; Wels, Austria; 2006.

Dilthey U. et al. [2001] MAGSIM and SPOTSIM – Simulation of GMA and spot welding for training and application; Proceedings of the 7th International Conference of the Japan Welding Society, Kobe November 2001; pp. 143-149.

Dong S., Luo C., Luo P. & Zhou Y. [2008] Effect of TiB2 Coating in Electrode Tip Surface on Electrode Degradation during Resistance Spot Welding of Coated Steels; Proceedings of The 5th International Seminar on Advances in Resistance Welding; W. Zhang & N. Scotchmer (eds.); Toronto, Canada; September 2008.

Dupuy T. [2006] Influence of the mechanical characteristics of a pedestal spot welding machine; Proceedings of The 4th International Seminar on Advances in Resistance Welding; W. Zhang & A. Eder (eds.); Wels, Austria; November 2006.

Easterling K. [1992] Introduction to the Physical Metallurgy of Welding 2nd ed.; Butterworth Heinemann; ISBN 0 7506 0394 1; 1992.

Ebert F. (publisher) [2006] Proceedings European Automotive Laser Application (EALA) 2006; 7th European Conference with Exhibition; Bad Nauheim/Frankfurt, Germany; January 2006.

Ebert F. (publisher) [2007] Proceedings European Automotive Laser Application (EALA) 2007; 8th European Conference with Exhibition; Bad Nauheim/Frankfurt, Germany; January 2007.

Ebert F. (publisher) [2008] Proceedings European Automotive Laser Application (EALA) 2008; 9th European Conference with Exhibition; Bad Nauheim/Frankfurt, Germany; January/February 2008.

ESI [2009] Spot Welding Wizard; ESI Group; 2009.

Friedman E. [1975] Thermomechanical analysis of the welding process using the finite element method; Journal of Pressure Vessel Technology 97 (1975) pp. 206-213.

Fukui K. [2006] State of the art of resistance spot welding for high tensile strength steel sheets in Japan; Presented at The 4th International Seminar on Advances in Resistance

Welding; 15 November 2006, Wels, Austria; Paper not in Proceedings but distributed seperately.

Garcia-Gonzalez J.E. [2005] Fundamental study of the austenite formation and decomposition in low-Si and Al added TRIP steels; PhD thesis; University of Pittsburg; 2005.

Geledraak [2005] Landwind: eerste Chinese auto in Nederland; www.geledraak.nl/html/showarticle.asp?id=232; September 14, 2005; last accessed July 10, 2012.

Giroux D. & Deffenbaugh J.F. (eds.) [1989] Resistance Welding Manual; Fourth Edition; ISBN 0-9624382-0-0; Resistance Welder Manufacturers Association (RWMA); 1989.

GM [2002] High Strength Sheet Steel (180 MPA...550 MPA Yield Strengths); GMW3032; World Wide Engineering Standards; Maerials Specification Metals; 2002.

Gould J.E. [1987] An examination of nugget development during spot welding, using both experimental and analytical techniques; WeldingJournal, 66 [1987] 1-s.

Gould J.E. [1999] Weld Process Effects Cracking – Hold Time Sensitivity and RSW of High Strength Steel; Welding Design and Fabrication, (8): 48-49; 1999

Gould J.E., Khurana S.P. & Li T. [2006] Predictions of Microstructures when Welding Automotive Advanced High Strength Steels; Welding Journal; Vol. 50; May 2006.

Grange R.A. & Stewart H.M. [1945] The temperature range of martensite formation; Transactions AIME, Vol. 167, pp. 467–494; 1945.

Granjon H. [1991] Fundamentals of welding metallurgy; Woodhead Publishing; 1991. ISBN 1855730197.

Heim G., Mengel C. & Wolf C. [2008] The All New Insignia; Euro Car Body 2008; 10th International Car Body Benchmark Platform; Bad Nauheim, Germany; October 2008.

Heubrandther T. & Akgün T. [2005] Trefftz finite element formulation of a spot weld in dynamic crash calculations; Mathematical Modelling of Weld Phenomena 7; Cerjak H., Bhadeshia H.K.D.H. & Kozeschnik E. (eds.); Verlag der Technischen Universität Graz; ISBN 3-901351-99-X; 2005; pp. 483 – 517.

Heubrandtner T. & Ranger G. [2007] Modelling of plastic deformation of a spotweld based on the Trefftz-method; Mathematical Modelling of Weld Phenomena 8; Cerjak H., Bhadeshia H.K.D.H. & Kozeschnik E. (eds.); Verlag der Technischen Universität Graz; ISBN 978-3-902465-69-6; 2007; pp. 573-584.

Hibbitt H. & Marcal P. [1973] A numerical thermo-mechanical model for the welding and subsequent loading of a fabricated structure; Computer Strucures, Vol 3 (1973) pp. 1145-1174.

Honeycombe R. & Bhadeshia H.K.D.H. [1995] Steels – Microstructure and properties; 2nd Edition; ISBN 0340-58946-9; Edward Arnold; 1995.

Houldcroft P.T. [1977] Welding Process Technology; Cambridge University Press; ISBN 0 521 21530 7; 1977.

IISI [2006] Advanced High Strength Steel (AHSS) Application Guides; Prepared by International Iron & Steel Institute; Committeee on Automotive Applications; Section 3 – Joining; Auto/Steel Partnership (www.a-sp.org); September 2006.

IIW [1967] IIW Technical Report, IIW doc. IX-535-67, 1967

Ikeda R., Okita Y., Ono M. [2008] Development of New Resistance Spot Welding Process for Three Sheets Joint Using Electrode Force Control; Proceedings of The 5th International Seminar on Advances in Resistance Welding; W. Zhang & N. Scotchmer (eds.); Toronto, Canada; September 2008.

ISO 10447 [2006] Welding-Peel and chisel testing of resistance spot, projection and seam weld; 2006.

ISO 14270 [2000] Specimen dimensions and procedure for mechanized peel testing resistance spot, seam and embossed projection welds; 2000.

ISO 14272 [2000] Specimen dimensions and procedure for cross tension testing resistance spot and embossed projection welds; 2000.

ISO 14273 [2000] Specimen dimensions and procedure for shear testing resistance spot, seam and embossed projection welds; 2000.

ISO 18278-1 [2004] Resistance Welding – Weldability; Part 1: Assessment of weldability for resistance spot, seam and projection welding of metallic materials; 2004.

ISO 5821 [2007] ISO 5821 Resistance Spot Welding Electrode Caps; 2007.

Ito H., Izutsu M., Ishizono M. & Kozasa N. [2008] New Jazz; Euro Car Body 2008; 10th International Car Body Benchmark Platform; Bad Nauheim, Germany; October 2008.

Ito Y. & Bessyo K. [1968] Cracking Parameter of High Strength Steels related to heat affected zone cracking, Journal of Japanese Welding Society, 1968, 37, 9, pp. 938-991.

Jackson M.D. [1967] Welding, Methods and Metallurgy; Griffin London; 1967.

Janota M. & Neumann H. [2008] Share of spot welding and other joining methods in automotive production; IIW-1856-07; Welding in the World; Vol. 52, No 3/4; 2008.

Jonsell St., Olsson A. & Edbäck S. [2004] The new Volvo V50; 6th International Car Body Benchmarking Platform „EURO CAR BODY 2004“; Bad Nauheim/Frankfurt, Germany; October 2004.

Josefson B.L. [1993] Prediction of residual stresses and distortions in welded structures; ASME J Offshore Mech Arct Eng 115 (1993) pp. 52-57.

Juettner S. [2011] Comments at the IIW SC-AUTO intermediate meeting; IJmuiden, The Netherlands; April 2011.

Kaluza W.M. [2003] Modellierung der medchanischen Eigenschaften und der lokalen Dehnungen von Dualphasen-Stählen; Dissertation RWTH Aachen; Berichte aus dem Institut für Eisenhüttenkunde; Shaker Verlag; ISBN 3-8322-1505-0; 2003.

Karlsson C.T. [1989] Finite element analysis of temperatures and stresses in a single-pass butt-welded pipe – influence of mesh density and material modelling; Eng Comput 6 (1989) 113-141.

Karlsson R.I. & Josefson B.L. [1990] Three-dimensional finite element analysis of temoperatures and stresses in a single-pass butt-welded pipe, Journal of Pressure Vessle Technology 112 (1990) pp. 76-84.

Kearns W.H. (ed.) [1980] Resistance and Solid-State Wedling and Other Joining Processes, Welding Handbook, Seventh Edition, Volume 3; American Welding Society; ISBN 0-87171-188-5; 1980.

Khan M.I., Kuntz M.L. & Zhou Y. [2008] Effects of weld microstructure on static and impact performance of resistance spot welded joints in advanced high strength steels; Science and Technology of Welding and Joining; Vol. 13 No. 3; 2008.

Khan M.I., Kunz M.L., Biro E. & Zhou Y. [2008] Microstructure and Mechanical Properties of Resistance Spot Welded Advanced High Strength Steels; Materials Transactions; Vol. 49 No. 7; 2008.

Koistinen D.P. & Marburger R.E. [1959] A general equation prescribing the extent of the austenite-martensite transformation in pure iron-carbon alloys and plain carbon steels; Acta Metall.; vol. 7, pp. 59–60; 1959.

Kop T. [2006] Transformation kinetics of 3FAA DP600GI; CRD&T reference source: 132312.

Krause M. [1993] Widerstandspreßschweißen, Grundlagen – Verfahren – Anwendung; Die Schweisstechnische Praxis Band 25; Verlag für Schweisstechnik; DVS; ISBN 3-87155-531-2; 1993.

Kumagai K., Shirooka M., Ohachi J. & Ogawa T. [2007] Rupture Modeling of Spot Welds Suitable for Crash FE Analysis in Vehicle Development Process; 6th European LS-DYNA Users' Conference; Gothenburg, Sweden; 2007.

Larsson J.K., Lungren J., Asbjörnsson E. & Andersson H. [2009] Extensive Introduction of Ultra High Strength Steels Sets New Standards for Welding in the Body Shop; IIW-1972-98; Welding in the World; Vol. 53, No 5/6 – 2009.

Lassl G., Nedic S., Ljungquist H. & Hollander E. [2008] The New Volvo XC60 Car Body; Euro Car Body 2008; 10th International Car Body Benchmark Platform; Bad Nauheim, Germany; October 2008.

Le Floch B. & Barbier M. [2008]: La Nouvelle Citroën C5; Euro Car Body 2008; 10th International Car Body Benchmark Platform; Bad Nauheim, Germany; October 2008.

Lee A. [2014] Trends and market developments in lightweight solutions; Trends in Automotive Lightweight Solutions; Bornhem, Belgium; May 27, 2014.

Lee S.-J. & Lee Y.-K. [2005] Effect of Austenite Grain Size on Martensitic Transformation of a Low Alloy Steel; Materials Science Forum Vols. 475-479 (2005) pp. 3169-3172

Liesenfelder B., Gall C. & Weber M. [2008] The New Ford Fiesta; Euro Car Body 2008; 10th International Car Body Benchmark Platform; Bad Nauheim, Germany; October 2008.

LLewellyn D.T. & Hudd R.C. [2000] Steels: Metallurgy & Applications, 3rd Edition; Butterworth Heinemann; ISBN 0 7506 3757 9; 2000.

Lópes-Cortéz V.H. & Reyes-Valdés F.A. [2008] Understanding Resistance Spot Welding of Advanced High-Strength Steels; Welding Journal; Vol. 87; December 2008

Lucas W. & Makhnenko V.I. (ed.) [2006] Proceedings of Joint International Conference Computer Technology in Welding and Manufacturing (16th International Conference) & Mathematical Modelling and Information Technologies in Welding and Related Processes (3rd International Conference); E.O. Paton Electric Welding Institute; Kiev; 6-8 June 2006; ISBN 966-95847-8-7.

Madsen A., Pedersen K.R., Friis K.S. & Bay N. [2010] Analysis and Modelling Electrode Wear in Resistance Spot Welding; Proceedings of the 6th International Seminar on Advances in Resistance Welding; W. Zhang, K. Pedersen, R. Bothfeld & J. Eggers (eds.); Hamburg, Germany; September 2010.

Maotao Z., Zhong W. & Weiwei Z. [2011] Static Strength and Fatigue Analysis of the Automobile Sub-Frame by FEA Simulation Method and Fatigue Test; Advanced Materials Research Vols, 179-180; 2011.

Marashi P., Pouranvari M., Amirabdollahian S., Abedi A. & Goodarzi M. [2008] Microstructure and failure behavior of dissimilar resistance spot welds between low carbon galvanized and austenitic stainless steels; Material Science and Engineering A 480 (2008) 175-180.

Marchal P. & Zwetsloot R. [2002] Lassen van dual phase staal; Corus RD&T internal report; Reference Source: NUMMER; 2002

Marya M. & Gayden X.Q. [2005] Development of Requirements for Resistance Spot Welded Dual-Phase (DP600A) Steels; Part 1 – The Causes of Interfacial Fracture; Welding Journal; Vol. 84; November 2005.

McGannon H.E. (ed.) [1971] The Making, Shaping and Treating of Steel; United States Steel; 9th Edition; 1971.

Michiura Y., Morita Y. & Sakamoto H. [2008] Teana; Euro Car Body 2008; 10th International Car Body Benchmark Platform; Bad Nauheim, Germany; October 2008.

Mimer M., Svensson L-E. & Johansson R. [2004] Possibilities to Improve Fracture Behaviour in Resistance Spot Welds of EHSS and UHSS by Process Modifications; Proceedings of the 3rd International Seminar on Advances in Resistance Welding; W. Zhang & P. Xu (Eds.); Berlin, Germany; 2004.

Murakawa H., Zhang J. & Minami H.: FEM investigation on effect of initial gap upon nugget formation and expulsion in spot welding; Mathematical Modelling of Weld Phenomena 5; ; Cerjak H. (ed.); IOM Communications Ltd.; ISBN 1 86125 115 7; 2001; pp. 983-995.

Muraki T, Bryan J. & Masubuchi K. [1975] Analysis of thermal stresses and metal movement during welding; ASME Journal of Engineering Materials Technology 96 (1975) pp. 81-84.

NEN-EN-ISO 18278-2 [2004] Resistance welding - Weldability - Part 2: Alternative procedures for the assessment of sheet steels for spot welding (ISO 18278-2:2004,IDT); 2004

NEN-ISO 10447:2006 en [2006] Lassen - Pel- en splijtbeproeving van puntlas-, doordruklas en rolnaadlasverbindingen; 2006

Nied H.A. [1991] The finite element modelling of the resistance welding process; Welding Journal 70 (1991) p. 339-s.

Nikoosohbat F., Kheirandish S., Goodarzi M., Pouranvari M. & Marashi S.P.H. [2010] Microstructure and failure behaviour of resistance spot welded DP980 dual phase steel; Materials Science and Technology; Vol. 26 No. 6; 2010.

Nu.nl [2005] ANWB: Chinese terreinauto levensgevaarlijk; www.nu.nl/news/591752/10/ANWB%3A_Chinese_terreinauto_levensgevaarlijk.html; September 14, 2005; last accessed July 10, 2012.

Orsbeck C. [2002] The New Volvo XC90 Car Body; 4. Europäische Karosserie Forum, „EURO CAR BODY 2002"; Bad Nauheim, Germany; September, 2002.

Otten R. [2008] Fabrikanten zetten massaal in op kleine auto's; NRC Handelsblad; October 3, 2008.

Payson P. & Savage C.H. [1944] Martensite reactions in alloy steels; Transactions ASM, Vol. 33, pp. 261–281; 1944.

Pedersen K.R., Harthøj A., Friis K.L., Bay N., Somers M.A.J. & Zhang W. [2008] Microstructure and Hardness Distribution of Resistance Welded Advanced High Strength Steels; Proceedings of the 5th International Seminar on Advances in Resistance Welding; Toronto, Canada; W. Zhang & N. Scotchmer (Eds.); 2008.

Perrot P., Roussineau L. & Trognot P. [2004] Citroën C4; 6th International Car Body Benchmarking Platform „EURO CAR BODY 2004"; Bad Nauheim/Frankfurt, Germany; October 2004.

Perrot Ph., Combemore C.& Vincenti R. [2002] Development of the PEUGEOT 307 Space Wagon (SW) body in white and platform 2; 4. Europäische Karosserie Forum, „EURO CAR BODY 2002"; Bad Nauheim, Germany; September, 2002.

Peterson W. & Gould J.E. [2004] Development of Spike Tempering Diagrams for a Range of Advanced High-Strength Steels; XI SMWC Conference, Sterling Heights, MI, 2004.

Pfeifer L. [1969] Fachkunde des Widerstandsweißens; Verlag W. Girardet; Essen; 1969.

Pickens J.W., Abraham J.K., Mintus R.E. & Thomas M.H. [1984] Batch annealed dual phase steels; US Patent, No-4437902, 1984.

Plaideau P., Cousseau S. & Lannes A. [2008] Laguna III Coupé; ; Euro Car Body 2008; 10th International Car Body Benchmark Platform; Bad Nauheim, Germany; October 2008.

Porter D.A. & Easterling K.E. [1992] Phase Transformations in Metals and Alloys; 2nd edition; Chapman & Hall; ISBN 0-412-45030-5; 1992.

Pouranvari M., Asgari H.R., Mosavizadch S.M., Marashi P.H. & Goodarzi M. [2007] Effect of weld nugget size on overload failure mode of resistance spot welds; Science and Technology of Welding and Joining; Vol. 12 No. 3; 2007.

Pouranvari M., Mousavizadeh S.M., Marashi S.P.H., Goodarzi M. & Ghorbani M. [2011] Influence of fusion zone size and failure mode on mechanical performance of dissimilar resistance spot welds of AISI 1008 low carbon steel and DP600 advanced high strength steel; Materials and Design 32 (2011) 1390-1398.

prEN 10336 [2006] Continuously hot-dip coated and electrolytically coated strip and sheet of multiphase steels for cold forming - Technical delivery conditions; European Standard (draft); 2006.

Quidort D. [2006] Microstructure Control during the Galvannealing Cycle of TRIP-aided Steel Sheet; lecture at the TU Delft; May 15, 2006.

Radaj D. [1992] Heat Effects of Welding. Temperature Field, Residual Stress, Distortion; Springer Verlag; ISBN 3-540-54820-3; 1992.

Radakovic D.J. & Tumuluru M. [2008] Predicting Resistance Spot Weld Failure Modes in Shear Tension Tests of Advanced High-Strength Automotive Steels; Welding Journal; Vol. 87; April 2008.

Rebele M., Hahn T. & Weiß R. [2008] The Audi Q5, a New Member of the Audi B Model Range; Euro Car Body 2008; 10th International Car Body Benchmark Platform; Bad Nauheim, Germany; October 2008.

Rice W. & Funk E.S. [1967] An analytical investigation of temperature districbutions during resistance welding; Welding Journal, 46 [1967] 175-s.

Rijkenberg, A. [2006] EPMA/WDX mappings of [...] TRIP steel welds; MSA 2060492; Corus RD&T internal document; 16062006; 2006.

Rivett R.M., Murch M.G. and Westgate S.A. [1983] 'Welding high strength steel sheet for the mass production industry'. Proc. of the International Conference on 'The effects of residual, impurity and micro-alloying elements on weldability and weld properties'. London, November 1983, pp.P47-1 to P47-20.

Robin V., Bernauer G., Akgün T. & Heubrandtner T. [2005] Spotweld performance under high strain rate loading conditions; Mathematical Modelling of Weld Phenomena 7; Cerjak H., Bhadeshia H.K.D.H. & Kozeschnik E. (eds.); Verlag der Technischen Universität Graz; ISBN 3-901351-99-X; 2005; pp. 419-434.

Robin V., Feulvarch E., Masters I., Fan X. & Dry D. [2007] A local spotweld model to predict large assembly distortions; Mathematical Modelling of Weld Phenomena 8; Cerjak H., Bhadeshia H.K.D.H. & Kozeschnik E. (eds.); Verlag der Technischen Universität Graz; ISBN 978-3-902465-69-6; 2007; pp. 585-602.

Robin, V. Sanchez, A. Dupuy, T. Soigneux, J. Bergheau, J. M. [2001] Numerical Simulation of Spot Welding with Special Attention to Contact Conditions; Mathematical Modelling of Weld Phenomena 6; Cerjak H. (ed.); Maney Publishing ; ISBN 978 1 902653 56 3; 2001.

Saito Y. & Nakamura A. [2004] Inspired Design, Everyday Functionality, Superior Drivability; 6th International Car Body Benchmarking Platform „EURO CAR BODY 2004"; Bad Nauheim/Frankfurt, Germany; October 2004.

Scotchmer N. & Chan K. [2006] The PARACAP™ - Longer Electrode Life from a New Geometry, an Innovative Multilayer Coating, and Internal Cooling Fins; Proceedings of the

4th International Seminar on Advances in Resistance Welding; W. Zhang & A. Eder (eds.); Wels, Austria; November 2006.

Scotchmer N. & Chan K.R. [2008] A Multi-Disciplinary Approach to Optimizing the Resistance Welding Process; Proceedings of The 5th International Seminar on Advances in Resistance Welding; W. Zhang & N. Scotchmer (eds.); Toronto, Canada; September 2008.

Scotchmer N. [2004] Widening the Welding Lobe of Advanced High Strength Steels in the Resistance Spot Welding Process; Proceedings of The 3rd International Seminar on: Advances in Resistance Welding; W. Zhang & P. Xu (eds.); Berlin, Germany; November 2004.

Sekyr P. [2004] Skoda Octavia - II. Generation - Teil 2; 6th International Car Body Benchmarking Platform „EURO CAR BODY 2004“; Bad Nauheim/Frankfurt, Germany; October 2004.

Shi G. & Westgate S.A. [2003] Resistance spot welding of high strength steels; JOM – Eleventh International Conference on the Joining of Materials; May 25-28, 2003; Helsingor, Denmark.

Shi G. & Westgate S.A. [2007] TRIP steel – better weldability using resistance spot welding; TWI bulletin; 2007.

Simon P. & Senkyr P. [2008] Skoda Superb; Euro Car Body 2008; 10th International Car Body Benchmark Platform; Bad Nauheim, Germany; October 2008.

Smith S., Den Uijl N.J., Okada T., Van der Veldt T., Uchihara M. & Fukui K. [2010] The effect of ageing on the spot weld strength of AHSS and the consequences for testing procedures; Welding in the world, 54 (1/2), 1-24; 2010.

Sourmail T. & Garcia-Mateo C. [2005a] Critical assessment of models for predicting the Ms temperature of steels; Comp. Mater. Sci., 2005:34, p323-334

Sourmail T. & Garcia-Mateo C. [2005b] A model for predicting the Ms temperatures of steels; Comp. Mater. Sci., 2005:34,p213-218 Critical assessment of models for predicting the Ms temperature of steels; Comp. Mater. Sci., 2005:34, p323-334

Spotsim [1999]: ISF Aachen Direct 19; April 1999.

Spotsim [2012] Question about SPOTSIM; e-mail correspondence with Prof. Dr.-Ing. Prof. h.c. Ulrich Dilthey of Institut für Schweißtechnik und Fügetechnik, Rhein.-Westf. Technische Hochschule Aachen

Sprikunwong C., Dupuy T. & Bienvenu Y. [2005] Influence of electrical-thermal physical properties in resistance spot welding model; Mathematical Modelling of Weld Phenomena 7; Cerjak H., Bhadeshia H.K.D.H. & Kozeschnik E. (eds.); Verlag der Technischen Universität Graz; ISBN 3-901351-99-X; 2005; pp. 999 – 1022.

Steven W. & Haynes A.G. [1956] The Temperature of Formation of Martensite and Bainite in Low Alloy Steels; Journal of the Iron and Steel Institute, 183, 1956, 349-359.

Subramanian S. [2008] Influences of Material Yield Strength on Resistance Spot Welding Process; Proceedings of The 5th International Seminar on Advances in Resistance Welding; W. Zhang & N. Scotchmer (eds.); Toronto, Canada; September 2008.

Svensson L.E. & Larsson J.K. [2006] Welding and joining in high performance car bodies; III-1397-06; IIW-IIS Annual Assembly; Dubrovnik, Croatia; 2006.

Swantec [2011] Sopras Version 10,6 User Manual; SWANTEC Software and Engineering ApS; March 2011.

Tawade G., Lee A.J., Boudreau G.D. & Bhole S.D. [2004] Robust Schedules for Spot Welding Zinc-Coated Advanced High Strength Automotive Steels; XI SMWC Conference, Sterling Heights, MI, 2004.

Thomson E. [1890] Method of Electric Welding; United States Patent 451345; Patented Apr. 28, 1891.

Thomson E. [1909] Electrical Welding of Sheet Metal; United States Patent 1078225; Patented Nov. 11, 1913.

Tolf E. & Hedegård J. [2008] Influence of Reduced Cooling Time on the Properties of Resistance Spot Welds; Welding in the World, March 2008, Volume 52, Issue 3-4, pp 43-53

Toronto [2008] Remarks made during the 5th International Seminar on Advances in Resistance Welding; Toronto, Canada; 2008.

Trost W., Betker J. & Kellernann H. [2004] Die Rohbaukarosserie des neuen Mercedes Benz SLK; 6th International Car Body Benchmarking Platform „EURO CAR BODY 2004“; Bad Nauheim/Frankfurt, Germany; October 2004.

Tsai C.L., Jammal O.A., Paritan C & Dickinson D.W. [1992] Modelling of resistance spot welding nugget growth; Welding Journal 71 (1992) p.47-s.

Tumuluru M. [2008] Some Considerations in the Resistance Spot Welding of Dual Phase and TRIP Steels; Proceedings of The 5th International Seminar on Advances in Resistance Welding; W. Zhang & N. Scotchmer (eds.); Toronto, Canada; September 2008.

Ueda H., Okamura K., Nakayama E., Fujimoto H., Okada T., Ushihara M. & Fukumoto M. [2010] Evaluation of Crash Performance in Steel Sheet Parts Coupled with Fracture Prediction of Spot Welded Joints; F2010-C-128; FISITA 2010 World Automotive Congress; Budapest, Hungary; 2010.

Ueda Y., Fukuda K. & Nakacho K. [1977] Basic procedure in analysis and measurement of welding residual stresses by the finite element method. International Conference ofn Residual stresses in Welded Construction and Their Effects; 15-17 November 1977; The Welding Institute; UK.

Van der Wolk P.J. [2001] Modelling CCT-diagrams of Engineering Steels using Neural Networks; thesis Technical University Delft; DUP Science; 2001. ISBN 9040722005.

Van Liempt P., Onink M. & Bodin, A. [2002] Modelling the influence of dynamic strain ageing on deformation behaviour; Advanced Engineering Materials, 2002, 4.4; 225-232.

VDEh 1220-2 [2008] VDEh 1220-2 Stahl-Eisen-Prüfblätter (SEP) des Stahlinstituts VDEh 1220-2: "Prüf- und Dokumentationsrichtlinie für die Fügeeignung von Feinblechen aus Stahl; Teil 2: Widerstandspunktschweißen"; 2008.

Verstraeten B. & Feyaerts J. [2006] Weerstandslassen van hogesterkte staalsoorten; Lastechniek; December 2006.

Volvo [2005] Volvo Coporate Standard STD 8631,14: "Weldability of sheet metal, spot welding".

Wang, L, Liu, Y. & Qiao X. [2014] Design of BIW light weight base on positive development process; F2014-LWS-020; FISITA 2014 World Automotive Congress; Maastricht, The Netherlands, June 2-6, 2014.

Wang, L. & Weijun, F. [2011] Development and Application of Q&P Sheet Steels; Advanced Steels; ISBN 978-3-642-17664-7; Springer-Verlag Berlin Heidelberg and Metallurgical Industry Press; 2011; pp. 255 - 258.

Waterschoot T., Kestens L. & De Cooman B.C. [2002] Hot rolling texture development in CMnCrSi dual-phase steels; Metallurgical and Materials Transactions A; Volume 33, Number 4, 2002; pp. 1091-1102.

Weber G. & Göklü S. [2004] Resistance Spot Welding of High-Strength Multi-Phase Steels; Proceedings of The 3rd International Seminar on: Advances in Resistance Welding; W. Zhang & P. Xu (eds.); Berlin, Germany; November 2004.

Weber G. & Göklü S. [2006] Resistance Spot Welding of Uncoated and Zinc Coated Advanced High-Strength Steels (AHSS) – Weldability and Process Reliability-Influence of Welding Parameters; IIW-1722-05; Welding in the World; Vol. 50, no 3/4 – 2006.

Weber G. [2002] Weldability lobes in resistance spot welding; IIW-Dok. III-1207-02, Kopenhagen 2002.

Weertman A.C. & Drewes E.J. [2010] Weld applications in market and practice; Proceedings of the 6th International Seminar on Advances in Resistance Welding; W. Zhang, K. Pedersen, R. Bothfeld & J. Eggers (eds.); Hamburg, Germany; September 2010.

Wesling V., Rekersdrees T., Keitel S., Winkler R., Schreiber S. [2004] Investigations into the Resistance Spot Welding of Newly Developed Sheets Made of Higher Strength and Super-High-Strength Steels; Welding and Cutting, DVS, Düsseldorf, March 2004.

Westgate S. [2004]: The Resistance Spot Welding of High and Ultra-high Strength Steels; Proceedings of The 3rd International Seminar on: Advances in Resistance Welding; W. Zhang & P. Xu (eds.); Berlin, Germany; November 2004.

Westgate S.A. [2003] Resistance welding – State of the art; Welding and Cutting 55 (2005) No. 5; pp. 256-261.

White C. [1991] “Metallurgical Effects of Zinc Coated Steels on Electrode Wear of Dispersion Strengthened Copper Resistance Welding Electrodes”. International Lead and Zinc Research Organization. 1991.

White M. [2006] The new Jaguar XK car body - Car Body development and production; Automotive Circle International Confernce; Bad Nauheim/Frankfurt, Germany; May 2006.

Wilde H., Hunger H., Erbe R. & Feust H. [2004] Die Korosserie des neuen Audi A6; 6th International Car Body Benchmarking Platform „EURO CAR BODY 2004“; Bad Nauheim/Frankfurt, Germany; October 2004.

Wolf K., Schilling R., Lütjens J., Wallmersperger T., Jankowski U., Sihling D., Wiegand K. & Heuse M. [2009] Coupled FEM Calculations - A CAE Tool to Improve Crash-Relevant

Automotive Body Components by Local Hardening; 7th European LS-DYNA Users' Conference; Salzburg, Austria; 2009.

Wood P.K.C., Schley C.A., Beaumont R., Walker B., Dutton T. & Buckley M.A. [2009] Modelling and Predicting Spotweld Failures in Automotive Crash Structures; 7th European LS-DYNA Users' Conference; Salzburg, Austria; 2009.

WorldAutoSteel [2009] Advanced High Strength Steel (AHSS) Application Guidelines; Version 4.1; June 2009.

Yaghi A. & A.A. Becker A.A. [2005] State of the art review – Weld simulation using finite element methods; ISBN 18743760108; NAFEMS (2005).

Yang H.-S. & Bhadeshia H.K.D.H. [2009] Austenite Grain Size and the Martensite–Start Temperature; Scripta Materialia 60 (2009) 493–495

Young J.F. [1954] Materials and Processes; 2nd Edition; Modern Asia Edition; Charles E. Tuttle Company; Japan; 1954.

Zhang H. & Senkara J. [2006] Resistance welding: fundamentals and applications; CRC Press; ISBN 0-8493-2346-0; 2006.

Zhang W. & Kristensen L. [1999] Finite element modelling of resistance spot and projection welding processes; NIST Special Publication 949; Proceedings Ninth International Conference on Computer Technology in Welding; Detroit 28-30 Sept. 1999; pp. 15-23.

Zhou D. [2010] Review of recent advances in computer-based prediction of weld distortion; TWI November 2010 971/2010.